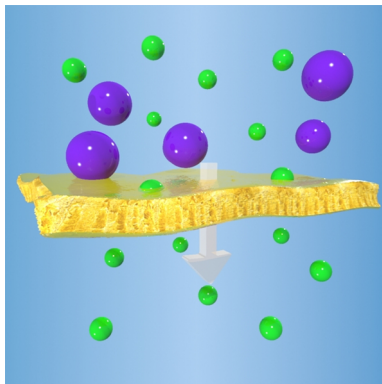


Molecular Separation with Organic Solvent Nanofiltration: A Critical Review

Patrizia Marchetti, Maria F. Jimenez Solomon, Gyorgy Szekely, and Andrew G. Livingston*

Department of Chemical Engineering and Chemical Technology, Imperial College London, Exhibition Road, London SW7 2AZ, United Kingdom



CONTENTS

1. Introduction	10736
2. Membranes and Membrane Characterization	10741
2.1. Membrane Functional Characterization	10741
2.2. Membrane Materials and Preparation	10742
2.3. Polymeric Membranes	10742
2.3.1. Integrally Skinned Asymmetric (ISA) Membranes	10742
2.3.2. Thin Film Composite (TFC) Membranes	10746
2.4. Mixed Matrix Membranes (MMM)	10751
2.4.1. Research Work on ISA Mixed Matrix Membranes for OSN	10751
2.4.2. Research Work on TFC Mixed Matrix Membranes for OSN	10752
2.5. Ceramic Membranes	10753
2.5.1. Research Work on Ceramic Membranes for OSN	10753
2.6. Commercial OSN Membranes	10754
2.6.1. Commercial Polymeric Membranes	10754
2.6.2. Commercial Ceramic Membranes	10758
2.7. Summary of Membrane Performance	10758
2.8. Membrane Physicochemical and Structural Characterization	10759
2.8.1. Physicochemical Characterization	10759
2.8.2. Microscopy	10760
2.8.3. Positron Annihilation Spectroscopy	10760
2.9. Membrane Configurations and Modules	10761
2.10. Future Perspectives	10762
3. Transport Models and Process Design	10763
3.1. Classification of Membrane-Scale Transport Models	10764
3.1.1. Irreversible Thermodynamics Models	10765
3.1.2. Models Based on Concentration and Pressure Gradients in the Membrane	10765
3.1.3. Solution-Diffusion Models	10766
3.1.4. Solution-Diffusion Model Based on the Maxwell–Stefan Equation	10766
3.1.5. Pore-Flow Models	10767
3.1.6. Solution-Diffusion with Imperfections Model	10769
3.2. Film Theory for Mass Transfer Limitations	10769
3.3. Application of Transport Models and Film Theory	10771
3.3.1. Application of Transport Models to Polymeric Membranes	10771
3.3.2. Application of Transport Models to Ceramic Membranes	10775
3.4. Model Parameters and the Effects of Solute–Solvent–Membrane Interactions	10776
3.4.1. Effective Solute and Solvent Diameters and Polarity Effects	10777
3.4.2. Charge Effects	10778
3.5. Modeling of OSN Processes	10778
3.5.1. Single-Stage Processes	10778
3.5.2. Multistage Processes	10779
3.5.3. Design of Experiments and Modeling	10780
3.5.4. Process Design	10780
3.6. Future Perspectives	10781
4. Membrane Applications in Organic Solvents	10782
4.1. Concentration	10782
4.1.1. Solute Enrichment	10782
4.1.2. Solvent Recovery	10783
4.2. Solvent Exchange	10785
4.2.1. Pharmaceuticals	10785
4.3. Purification	10786
4.3.1. Impurity Removal	10786
4.3.2. OSN-Assisted Chemical Synthesis	10791
4.3.3. Catalytic Processes	10792
4.3.4. OSN-Assisted Crystallization	10795
4.4. Future Perspectives	10795
5. Conclusions	10795
Author Information	10797
Corresponding Author	10797
Notes	10797
Biographies	10797
Acknowledgments	10798
Nomenclature	10798
Abbreviations	10798
References	10799

Received: January 4, 2014

Published: October 21, 2014

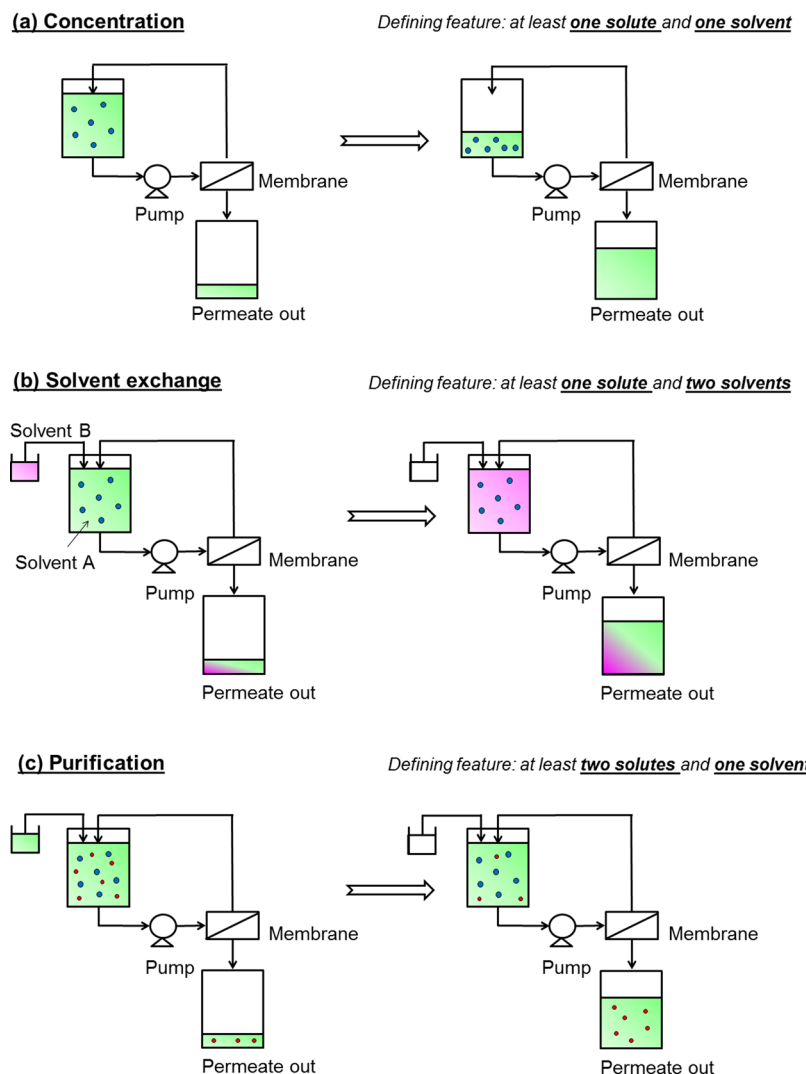


Figure 1. Membrane filtration processes for liquid applications: (a) concentration, (b) solvent exchange, and (c) purification processes.

1. INTRODUCTION

Separation processes play a remarkable role in the chemical and pharmaceutical industries, where they account for 40–70% of both capital and operating costs.¹ Organic syntheses in the chemical and pharmaceutical industry are frequently performed in organic solvents and consist of products with high added value that should be removed from the organic solvents. Additionally, organic solvents, used as raw materials, for chemical syntheses, and as cleaning agents, have to be recovered or discarded at the end of the process. The costs of processing these organic solvents for separation, recovery, or disposal are substantial and comprise a significant fraction of chemical process operating expenses. This Review considers a new paradigm technology for more efficient solvent operations, so-called organic solvent nanofiltration (OSN).

Starting in the late 1960s, membrane processes have been gradually used for industrial applications, and have provided feasible alternatives for, and have been combined with, more traditional purification and separation processes (such as distillation, evaporation, adsorption, extraction, and chromatography). This has been motivated by the benefits that membrane technology offers over conventional techniques, in terms of economy, environment, and safety,^{2–5} but has been largely

limited to aqueous applications. In this Review, we report on how OSN is advancing and how the technology is leading to the benefits of membrane processing being applied in organic solvents.

Hence, we classify all OSN operations as one of three conceptually simple operating modes for membrane processing of liquids, which are concentration, solvent exchange, and purification. These simple operating modes, shown in Figure 1, can be used in many different processes and arranged in different ways to develop a wide range of applications. The defining feature of each of concentration, solvent exchange, and purification is also shown in Figure 1.

Figure 1a shows concentration processes, which are based on a separation of the solute from the solvent, to either recover a high-value solute from a dilute solution (solute enrichment) or recover the solvent by removing an impurity dissolved in it (solvent recovery). In both cases, the defining feature is that the solute(s) is(are) rejected by the membrane, and so is(are) concentrated as the solvent passes through the membrane. Often conventional concentration processes are materials and energy demanding and difficult to perform at a large scale. As an example, to concentrate 1 m³ of a diluted solution of a solute in a solvent (e.g., methanol, enthalpy of vaporization $\Delta H_{ev} = 37.6 \text{ MJ kmol}^{-1}$, molecular weight MW = 32 g mol⁻¹, density ρ

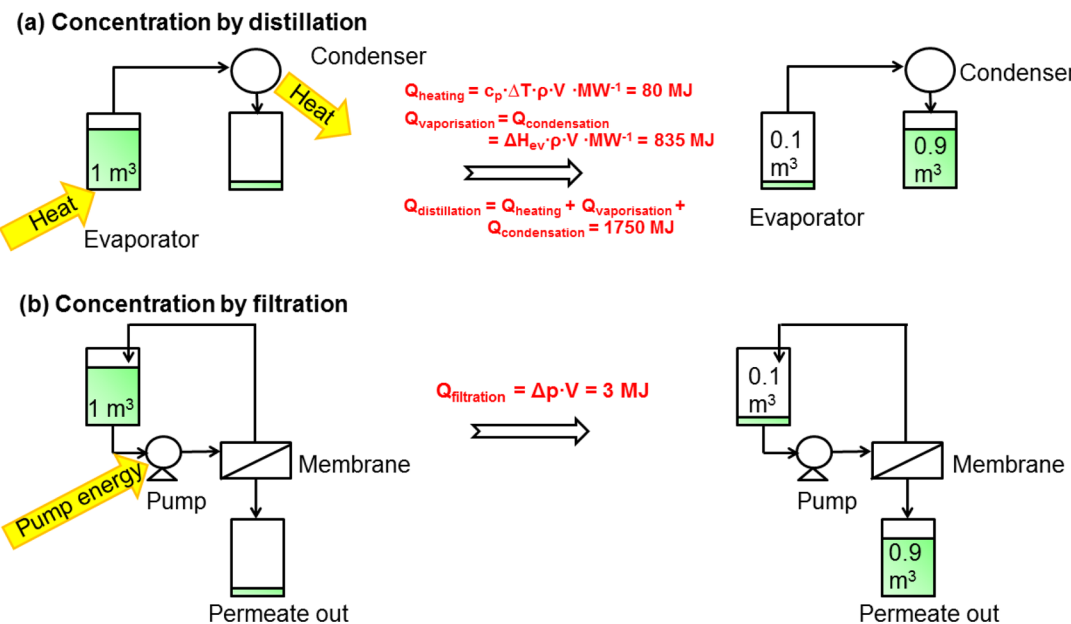


Figure 2. Energy consumption to concentrate 1 m³ of a dilute solution in methanol by a factor of 10, using (a) distillation and (b) membrane filtration.

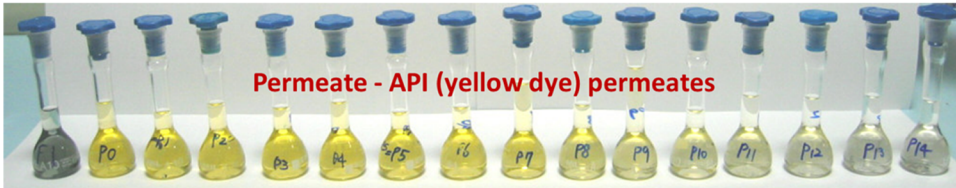


Figure 3. Photograph of the initial solution, permeate, and retentate samples at each diafiltration volume (with 14 times dilution of feed and retentate) for the separation of a blue dye (Brilliant Blue R, 826 g mol⁻¹, representative of a high molecular weight impurity) and a yellow dye (Basic Yellow K, 273.3 g mol⁻¹, representative of a main product, such as an active pharmaceutical ingredient, API).

= 790 kg m⁻³, heat capacity $c_p = 81.6 \text{ J mol}^{-1} \text{ K}^{-1}$, and boiling temperature $T_b = 337.7 \text{ K}$) by a factor of 10, distillation requires an energy consumption of 1750 MJ, while the pump energy required for performing membrane filtration at ambient temperature and 30 bar is only 3 MJ. This is schematically represented in Figure 2.

Additionally to low energy consumption, with respect to alternative unit operations such as distillation and evaporation, thermal damage of heat-sensitive molecules can be minimized during the separation, due to the low operating temperature.

Figure 1b shows a solvent swap carried out by diafiltration. A second solvent (solvent B, pink) is pumped into a solution of a solute in a first solvent (solvent A, green), and the solute is retained by the membrane. The solution changes from being rich in solvent A to being rich in solvent B; thereby the solvent is exchanged. The main advantage of applying membrane filtration to perform a solvent swap is that it is an athermal

process, allowing, for example, solvent exchange from a high-boiling to a low-boiling solvent. Both concentration and solvent exchange processes require tight membranes, which can efficiently retain the solute and permeate the solvent(s).

In purification processes, shown in Figure 1c, the goal is to separate two or more solutes contained in a solution, for example, the main product of a reaction from an impurity. The effect of membrane filtration on the separation of a blue dye (Brilliant Blue R, 826 g mol⁻¹, representative of a high molecular weight impurity) and a yellow dye (Basic Yellow K, 273.3 g mol⁻¹, representative of a main product, such as an active pharmaceutical ingredient, API) is shown in Figure 3. The blue dye is retained by the membrane, due to its larger size, while the yellow dye is collected in the permeate. As the yellow dye is removed by diafiltration, the retained solution becomes intensely blue and the permeate progressively intensely yellow.

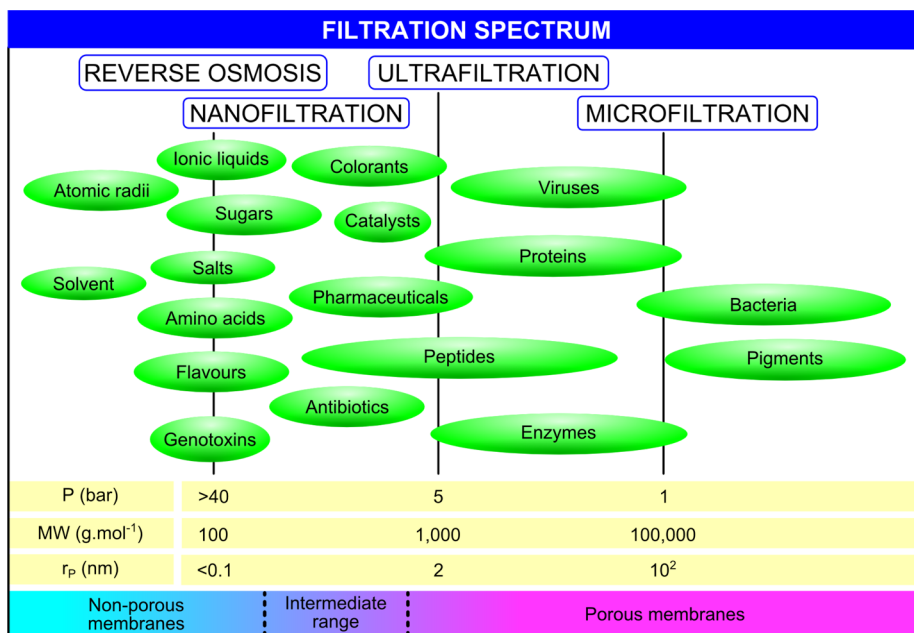


Figure 4. Classification of membrane processes according to operating pressure, retained solute/pore size [nm], molecular weight cutoff [g mol⁻¹], transport mechanism, and examples of applications.

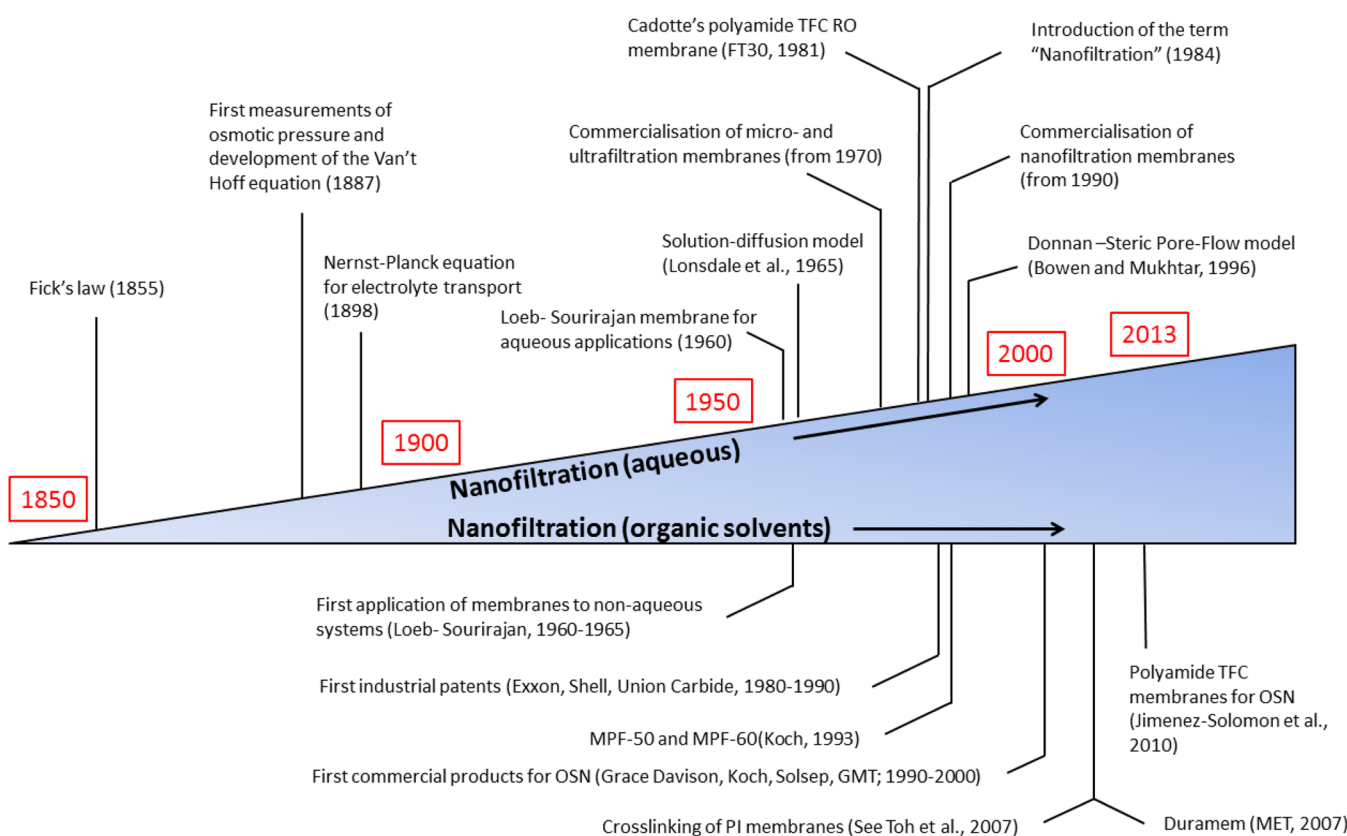


Figure 5. Summary of the most significant events, which have contributed to the development of NF, over time.

Purification processes require highly selective membranes, capable of discriminating between solutes of different molecular size and/or physicochemical properties.

Other incentives for applying membrane filtration, with respect to conventional separation techniques, are that membrane filtration can be easily installed in a continuous process or combined with existing processes into a hybrid

configuration, and upscaling is simpler than for other processes, such as crystallization or chromatography.² Remarkably, the potential of membrane filtration is still growing in terms of diversity of both applications and process scale.

Several membrane processes, such as microfiltration (MF), ultrafiltration (UF), nanofiltration (NF), reverse osmosis (RO), electrodialysis (ED), and pervaporation (PV), have been

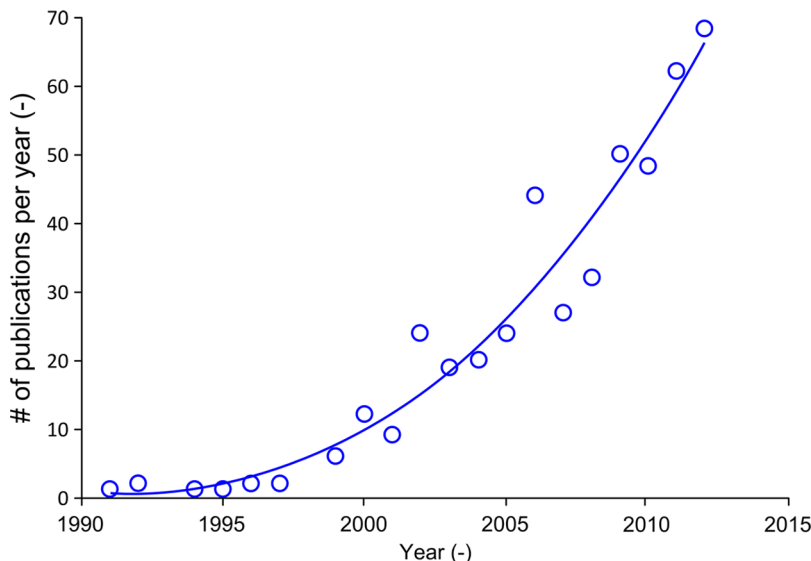


Figure 6. Growing interest in OSN, demonstrated by the increasing number of publications per year in the field. The research has been carried out in Web of Knowledge, using “organic solvent nanofiltration” or “solvent resistant nanofiltration” or “organophilic nanofiltration” as a keyword.

proposed to address different liquid and gas separations. The classification of membrane processes for liquid applications is represented schematically in Figure 4.

As shown in Figure 4, filtration processes have been classified, according to (i) the pressure required for the separation; (ii) the size of the rejected solute or, in turn, the size of the pore; (iii) the molecular weight cutoff (MWCO); and (iv) the transport mechanism governing the separation.

According to the classification based on the pressure required for the separation, Mulder⁶ classified UF as a process in which pressures from 1 to 5 bar are applied, NF as a process in which pressures from 5 to 20 bar are applied, and RO as a process with operating pressure higher than 10 bar. Because many recent NF membranes have been used up to higher pressure values, we propose to extend the pressure range for NF up to 40 bar.

According to the classification based on the size of the retained solute, UF is classified as a process in which molecules from 2 to 100 nm are retained, NF as a process in which particles up to 2 nm are retained, and RO as a process in which only solvent permeates.⁷

For commercial purposes, NF membranes are often characterized by their nominal MWCO, defined as the molecular weight of a reference compound, which is typically rejected by 90%.² Because the MWCO value is obtained from rejection experiments, this characterization is strongly dependent on the properties of the solute and solvent, and the operating conditions chosen for the test.

According to the transport mechanism, membrane separation is based on both size exclusion and additional effects, characteristic of the molecular level. Baker⁸ reported that UF and MF are characterized by a sieving transport mechanism through pores of significant dimension, therefore described by the pore-flow theory, while RO is characterized by the solution-diffusion transport mechanism, because the free volume is so small, that it is in the range of thermal motion of the polymer chains that form the membrane. NF is intermediate between the two, and characterized by both solution-diffusion and pore-flow transport mechanisms. In the NF range, characterized by a high specific surface, purification/separation processes are

usually based on a combination of separation methods, which exploit different physicochemical properties of the solute molecule: size, charge, hydrophilicity/hydrophobicity. At a molecular level, mutual interactions between solute and membrane play a key role, and can be sometimes even dominant.

NF broke through around the end of the previous century. A schematic summary of the most significant events, which have contributed to the development of the field, is shown in Figure 5.

The term “Nanofiltration” was proposed for the first time during a FilmTec meeting in 1984 to solve the terminology problem for a selective reverse osmosis process that allows ionic solutes in a feed water to permeate through a membrane.⁹ The extension of membrane processes to applications in organic solvents is more recent. It has been referred to as “organic solvent nanofiltration” (OSN),¹⁰ or alternatively as “solvent resistant nanofiltration” (SRNF) or “organophilic nanofiltration”.² The terminology “organic solvent nanofiltration” (or OSN) will be used throughout this Review. The first application of membranes to nonaqueous systems was reported in 1964 by Sourirajan¹¹ for the separation of hydrocarbon solvents using a cellulose acetate membrane, and Loeb mentioned pressure-driven solvent separations in 1965.¹² Sourirajan and co-workers continued the work on the separation of organic solvent mixtures using cellulose acetate membranes for almost two decades.^{13,14} Growing interest into applications in organic solvents has been demonstrated by the increasing number of patents about new materials and processes for applications in organic solvents, published from 1980 onward, by major oil companies, such as Exxon^{15–21} and Shell,^{22–24} and chemical companies, such as Union Carbide.²⁵ As reported by Peeva et al.,¹⁰ major potential applications were for oil recovery,^{15–17} enrichment of aromatics,^{19–21,24} and homogeneous catalyst recycle.²⁵ The first commercial products on the market appeared from the mid-1990s, by the membrane producers Grace Davison,^{26–28} Koch,²⁹ Solsep,³⁰ and GMT.³¹ The largest success at the industrial scale so far is the MAX-DEWAX process, installed at ExxonMobil Beaumont refinery and used for the recovery of dewaxing solvents from lube oil

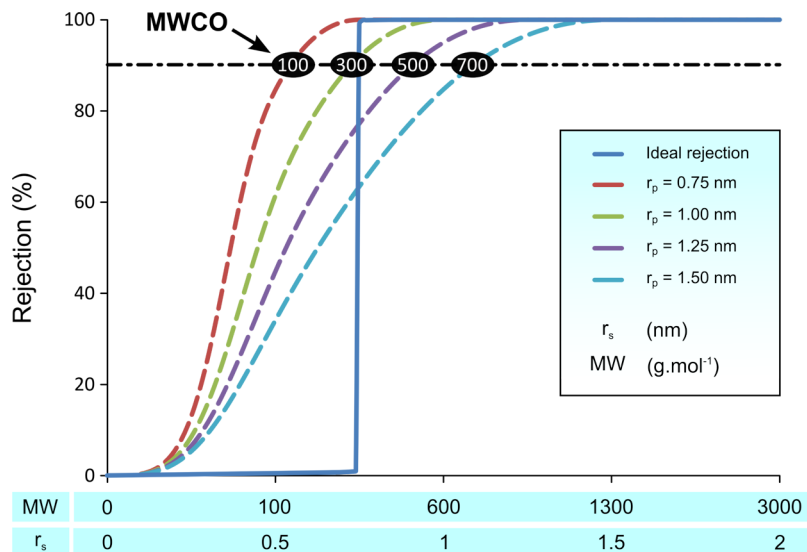


Figure 7. Schematic representation of rejection profile for uncharged solutes by a membrane with uniform pore sizes (r_p) between 0.75 and 1.5 nm by Donnan steric pore-flow model.³⁶ The dashed lines were obtained by simulation; the solid line represents the desired rejection profile. Adapted with permission from ref 37. Copyright 2013 Elsevier.

filtrates.²⁷ The increase of the number of publications per year in the last two decades, shown in Figure 6 for “organic solvent nanofiltration” or “solvent resistant nanofiltration” or “organophilic nanofiltration” as a keyword, represents the rising interest in this technology by both the scientific community and industrial producers and users.

Nowadays, the main issues related to the development of membrane processes for OSN are (i) the robustness of the membrane materials in organic solvents, in harsh acid and basic conditions, and during module preparation; (ii) the robustness of the membrane materials toward swelling and leaching; (iii) the lack of “multipurpose membranes”, which may be a prerequisite for many customers given the current membrane/module prices; (iv) the membrane selectivity for challenging molecular separations, as in the case of mixtures of main products and impurities with similar molecular size or for mixtures of isomers; (v) the capability to describe/predict NF performance by means of modelling tools and to carry out process design; and (vi) the need for capital investment to install new nanofiltration plants. From the point of view of material development, current research is directed toward the synthesis of new membranes, stable in organic solvents and more selective for solutes with similar size and physicochemical properties. Designing and synthesizing membranes with the ideal nanostructure to allow molecular scale separations has been also investigated; however, for these materials, it is still difficult to understand and precisely control the nanostructure. The integration of nanofiltration units with conventional separation techniques (i.e., chromatography or crystallization) in hybrid processes has been proposed,³² to overcome the selectivity issue. Finally, deeper understanding of basic transport phenomena by more efficient modelling tools has been addressed, to strengthen the fundamental understanding of the overall transport mechanism and carry out process simulation. In conclusion, the improvement of nanofiltration performance, in terms of membrane materials, fundamental understanding, and process development, allows the selection of the optimal working conditions, necessary to enhance the competitiveness of OSN technology and stimulate the chemical and pharmaceutical industries to invest in new filtration plants.

As a consequence of the clear advantages and potential of membrane technology over conventional separation techniques, some process scale installations have already taken place in recent years. VITO, for example, has recently acquired a large-scale mobile pilot installation for OSN, which can be equipped both with ceramic membranes (membrane surface: 0.7 m^2) and polymeric membranes (membrane surface: 6 m^2) and meets the requirements established by the pharmaceutical and fine chemical industries.³³ Furthermore, OSN membrane modules have been successfully applied in cGMP manufacturing processes in the pharmaceutical industry (GSK,^{34,35} Johnson and Johnson³⁵), and for larger scale chemicals processing including homogeneous catalyst retention at Evonik.³⁵

An excellent review on OSN was published by Vandezande et al.² in 2008. Vandezande et al. reviewed general OSN issues, such as the main membrane materials applicable for OSN, their properties and synthesis procedures, as well as the main commercial OSN membranes available on the market up to 2008. They dedicated a chapter to membrane transport mechanisms and transport modeling. Furthermore, they studied applications of membrane processes per industry branch, commented on upscaling and module design, and concluded with a general prospect of the field. Significant advances have been made in the last 6 years in the field of OSN. The majority of these advances are related to new membrane materials and synthesis techniques. As a consequence of the development of many new membranes, stable in organic solvents and under acidic/basic conditions, more OSN processes have become feasible, and more research has been dedicated to the design and development of new membrane applications at the industrial level. For all of these new developments, a new critical review on OSN is needed.

This Review revisits the development of OSN, from the synthesis of the first solvent stable membranes to the first industrial applications. It summarizes the significant recent advances in the field, and focuses particular attention on the recent developments, which have occurred since the previous OSN review by Vandezande et al.² Furthermore, it provides a critical insight into the state-of-the-art research, with special emphasis on process design and development. This Review is

divided into three parts, which will focus on the following aspects.

(i) Membrane and membrane characterization: The first section focuses on the development of new polymeric and ceramic OSN membranes, the engineering of membrane modules and scale-up, and the characterization procedures for membrane structural properties and performance.

(ii) Transport models and process design: The second section deals with the modeling studies on the transport mechanisms through OSN membranes, through a detailed review of the main models developed for OSN and their application in performing process design and prediction. The significance of solute–solvent–membrane interactions on the separation performance is discussed, and the integration of transport modeling with process modeling is introduced.

(iii) Membrane applications in organic solvents: The third section presents OSN applications, classified per industry branch and per process configuration. Advantages of membrane technology over conventional processes and benefits of integrating membrane technology in hybrid processes are discussed.

For each section, future perspectives are outlined, and finally conclusions on the state of the whole field are reached in the last section of this Review.

2. MEMBRANES AND MEMBRANE CHARACTERIZATION

2.1. Membrane Functional Characterization

Membrane performance is usually characterized by two parameters: flux (or permeance) and rejection (or selectivity). Flux is defined as the liquid volume flowing through the membrane per unit area and per unit time, and is usually expressed in terms of $\text{L m}^{-2} \text{ h}^{-1}$, while permeance is normalized to the applied pressure, and therefore expressed in terms of $\text{L m}^{-2} \text{ h}^{-1} \text{ bar}^{-1}$. Rejection is calculated as a function of the solute concentration in the permeate, $c_{i,l}$, and the solute concentration in the retentate (or feed) side, $c_{i,0}$:

$$\text{Rej}_i = 100 \left(1 - \frac{c_{i,l}}{c_{i,0}} \right) \quad (1)$$

As schematically shown in Figure 7, in the NF range a typical membrane rejection profile can exhibit a broad curve, with rejection rising slowly over a wide range of solute sizes (light blue line), or an ideal sharp separation curve, with an abrupt change in rejection (dark blue line). The sharp rejection profile is ideal, as it represents a neat separation between two solutes of different molecular size; that is, it represents a high separation selectivity. The dashed curves in Figure 7 were obtained by simulating the rejection of uncharged solutes by a membrane with uniform pore sizes (r_p) between 0.75 and 1.5 nm using the Donnan steric pore-flow model.³⁶

Membrane performance is also characterized by the membrane nominal molecular weight cutoff (MWCO), which is defined as the smallest solute molecular weight for which the membrane has 90% rejection ($\text{Rej}_i (\%) \geq 90$). However, it should be noted that the MWCO often does not give sufficient information on the separation performance, and about the quality of the separation. Comparing the two curves that intercept the 90% rejection line at MW = 300 (green and dark blue lines, respectively), it is clear that the $r_p = 1 \text{ nm}$ membrane

(green line) cannot give as sharp a cutoff as the ideal curve, even though it assumed uniformly sized pores.

Many authors in the literature chose different systems to characterize the MWCO of OSN membranes, and the most common markers for OSN are summarized in Table 1. The concentrations used depend on the solute solubility and are in the range of mg L^{-1} to g L^{-1} .

Table 1. Markers Used for OSN Membrane Characterization

marker	references
linear and branched <i>n</i> -alkanes	White et al. ³⁸
dyes	Bhanushali et al., ^{39,40} Vandezande et al., ⁴¹ and Gevers et al. ⁴²
hexaphenyl benzene (HPB)	Bhanushali et al. ³⁹ and Fritsch et al. ⁴³
Polyethylene glycol (PEG)	Kwiatkowski et al., ⁴⁴ Tsuru et al., ⁴⁵ and Rohani et al. ⁴⁶
Polyisobutylene	Stafie et al. ⁴⁷ and Van der Bruggen et al. ⁵²
Oligostyrenes	See Toh et al. ⁴⁸ and Dutczak et al. ⁴⁹

Branched and linear alkanes of increasing MW have been used to characterize the membrane performance,³⁸ allowing a more precise determination of the MWCO at a low range of $100\text{--}400 \text{ g mol}^{-1}$. However, the lack of commercially available pure species of $\text{MW} > 400 \text{ g mol}^{-1}$ and the difficulty of detecting these compounds are some of the drawbacks concerning alkanes. Furthermore, the limited solubility of these compounds in many polar organic solvents also makes it difficult to compare the MWCO of membranes across different solvents. The use of different compounds with increasing MW covering the NF range ($200\text{--}1000 \text{ g mol}^{-1}$) represents an alternative to the alkane system. The MW of the test compound gives an indication of the expected rejection; however, the variability in the structure and functionalities of the compounds can result in different solute–membrane interactions.^{50,51} Using different test compounds also implies that it is not possible to determine the MWCO of a membrane in a single filtration, because the detection of multiple compounds in a single test solution is not always achievable. The use of dyes has also been proposed by several authors^{39–42} to determinate the MWCO of membranes. However, as dyes absorb UV light over a wide range of wavelengths, the use of dyes of different sizes in a single test to determine the MWCO is not possible. Furthermore, many dyes are charged and could interact with the membrane, thus affecting the observed rejection. The limited solubility of dyes in a broad range of solvents also limits their further application. An alternative marker with UV absorbance for apolar solvents such as *n*-hexane or *n*-heptane is hexaphenyl benzene (HPB) with a MW of 543 g mol^{-1} .^{39,43} The use of polyethylene glycol (PEG)^{44–46} and polyisobutylene^{47,52} has also been proposed. Recently, See Toh et al.⁴⁸ developed a method to characterize the MWCO of OSN membranes, based on rejection of styrene oligomers in several organic solvents. The oligostyrenes cover a large range of MW and provide an extensive description of the membrane integrity and performance in the NF range. Oligostyrene molecules were used also by Dutczak et al.⁴⁹ to characterize poly(dimethylsiloxane) (PDMS) membranes.

The different solute and solvent properties (molecular shape, charge, solubility) and the experimental filtration conditions (pressure, temperature) applied in these studies make filtration data and MWCO values of different studies hardly comparable.

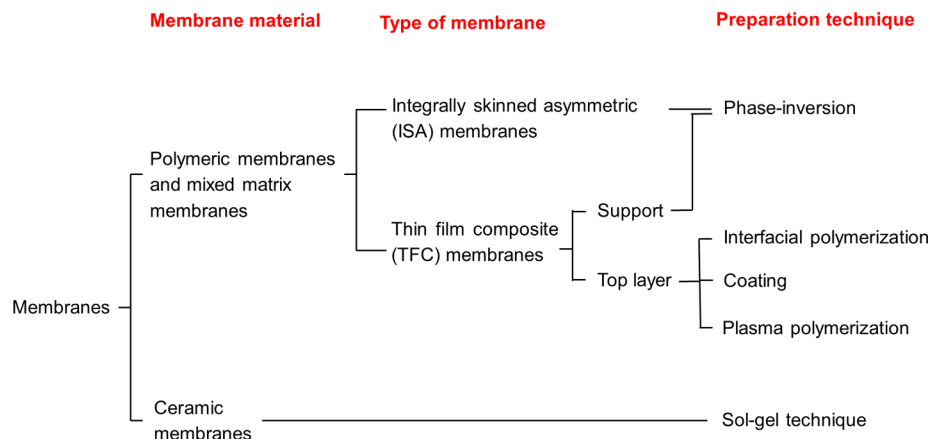


Figure 8. Membrane taxonomy chart.

For this reason, the selection of a suitable membrane for an application based on literature data or manufacturer specifications is often difficult and requires the screening of many membranes. A uniform method to characterize the performance of OSN membranes would be a significant advantage for membrane selection purposes.

2.2. Membrane Materials and Preparation

OSN membranes have been prepared from both polymeric and inorganic materials. To obtain excellent membranes, these materials must have mechanical, chemical, and thermal stability. One of the drawbacks of most polymeric membranes is that they suffer from flux decline due to aging or compaction. Ceramic membranes are superior considering mechanical, thermal, and chemical stability; they do not compact under pressure, do not swell in organic solvents, and can be easily cleaned. However, their up-scaling is more difficult, and they are more brittle than polymeric membranes. In contrast to polymeric membranes, ceramic membranes have no pore fillers, and hence there is no risk of these leaching. Also, ceramic membranes typically require lower pressures. Sealing is easy (glass, polytetrafluoroethylene), and there is no need for spacers and glues as in spiral elements. On the other hand, there is less variety in materials as compared to polymers, metal hydroxide membranes are inherently hydrophilic and therefore less suitable for more apolar solvents, and the lowest MWCO is at present significantly larger than that of polymeric membranes. Composite organic–inorganic membranes (known as mixed-matrix membranes) reduce polymer swelling and flux decline due to compaction, and improve the membrane mechanical stability (e.g., are less brittle than ceramic membranes). Mixed matrix membranes (MMMs) can combine the best properties of both polymeric and inorganic materials to tailor a membrane with desirable properties such as good solvent stability, high rejection and high flux, reduced flux decline, improved mechanical stability, and antifouling properties. This section will focus on the different types of membranes available for OSN (polymeric as well as ceramic and mixed matrix membranes), and on their synthesis techniques (cf., membrane taxonomy chart in Figure 8).

First, phase inversion for integrally skinned asymmetric (ISA) membranes, interfacial polymerization and dip-coating for thin film composite (TFC) membranes, and sol–gel techniques for ceramic membranes will be introduced. For each type of membrane, general aspects of support layers for composite membranes, cross-linking techniques, and post-

treatment procedures will be discussed. Advantages of TFC over ISA membranes will be also reported. Finally, the commercially available OSN membranes will be presented.

This Review focuses particular attention on the recent developments in membrane formation, which have occurred since the previous OSN review by Vandezande et al.² A more detailed review on OSN-membrane preparation for both aqueous and organic solvent applications can be found in Vandezande et al.² and in Vankelecom et al.⁵³

2.3. Polymeric Membranes

Most polymeric membranes are formed on a nonwoven backing material to provide mechanical stability. In OSN, the nonwoven backing material must be solvent resistant and should ideally behave the same way as the polymeric membrane (i.e., have a similar degree of swelling) to avoid the formation of creases, which could lead to membrane failure. Polymeric membranes must be solvent stable and preserve their separation characteristics in organic solvents. The two main types of polymeric membranes are the integrally skinned asymmetric (ISA) membrane and the thin film composite (TFC) membrane, which are shown in Figure 9.

The main features of these two types of membranes and the common polymers and synthesis procedures used to make them are described in this section.

2.3.1. Integrally Skinned Asymmetric (ISA) Membranes.

ISA membranes possess a skin layer on top of a

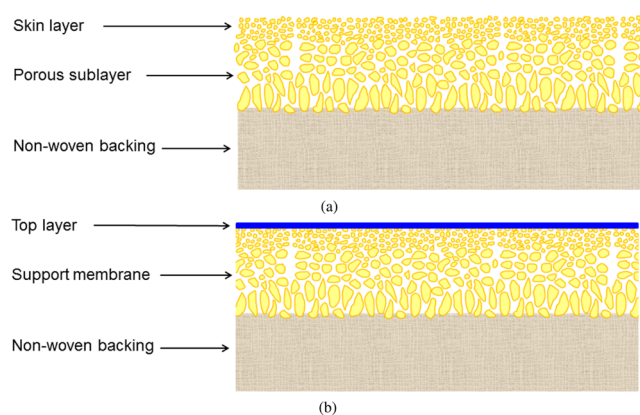


Figure 9. Schematic representation of (a) an integrally skinned asymmetric (ISA) membrane and (b) a thin film composite (TFC) membrane.

more porous sublayer with the same composition (cf., Figure 9a). The top skin layer is formed at the same time as the underlaying support layer. The thin skin layer affects the final membrane performance, that is, selectivity and permeance. ISA membranes are formed by the phase inversion technique, developed by Loeb and Sourirajan.⁵⁴ This technique consists of the precipitation of a casting solution by immersion in a nonsolvent (water) bath. Figure 10 is a representation of a membrane formation process by phase inversion.

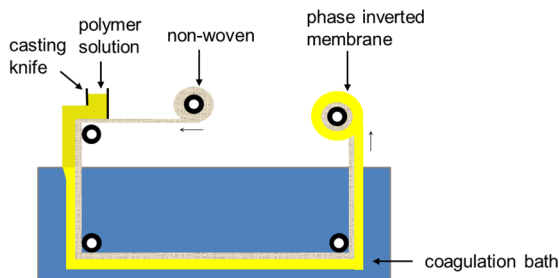


Figure 10. ISA membrane formation process by phase inversion.

The film rapidly precipitates from the top surface down, due to water absorption and loss of solvent. A casting solution consisting of only one phase is precipitated into two phases: a polymer-rich, solid phase that forms the matrix of the membrane and a polymer-poor, liquid phase that forms the membrane pores.⁸ Because of contact with water, the top surface of the cast film precipitates rapidly, forming the dense, selective layer. This layer slows the entry of water into the underlying polymer solution, which precipitates much more slowly and forms a more porous substrate. The thermodynamic properties of the system and the kinetics of the exchange of solvent and nonsolvent have a strong impact on the membrane morphology, as they affect its permeance and solute rejection.⁵⁵ More detailed information on NF membrane preparation was reported by Vankelecom et al.⁵³ and by Mulder.⁶ The key for high performance is the thin skin layer, which makes higher selectivity and permeance possible.

To prepare ISA membranes, the polymer must be soluble in a solvent to form a casting solution. This means that once the membrane is formed, it could redissolve in the solvent used for the casting solution, resulting in poor membrane stability. To overcome this problem, several postformation modifications are possible to make the membrane stable in such organic solvents, and will be discussed later in this section.

2.3.1.1. Research Work on ISA Membranes for OSN. Various chemically stable polymeric materials have been used to prepare OSN ISA membranes by phase inversion.^{53,56,57} ISA membranes have been used as both NF and UF membranes. Materials used to prepare OSN ISA membranes, reported in Table 2, include: (i) polyacrylonitrile (PAN), polyimide (PI) (Matrimid) and polyimide (PI) (P84), applicable as such (NF) or as UF supports;^{58,59} (ii) polyaniline (PANI),^{60,61} polybenzimidazole (PBI),⁶² and polysulfone (PSf)/sulfonated poly(ether ether ketone) (SPEEK) blends,⁶³ applicable as such (NF); and (iii) poly(ether ether ketone) (PEEK)⁵⁸ and polypropylene (PP),⁶⁴ applicable as UF supports. UF membranes by phase inversion can be used as supports for TFC NF membranes (cf., membrane taxonomy chart in Figure 8).^{65–67}

The different factors during and after the membrane formation process and their effect on the membrane performance have been largely studied. It has been shown, for example, that the polymer concentration in the dope solution has a significant effect on the structure of ISA membranes; in fact, membranes with thicker and denser skin layers were obtained with higher polymer concentrations, resulting in higher selectivities but lower permeabilities.^{68–72} The selectivities of ISA membranes were enhanced by the addition of volatile solvents in the dope, resulting in a defect-free ultrathin and dense skin layer on top of a highly porous sublayer with sponge-like structure.⁷³ This technique is used to prepare highly selective ISA membranes made from PI,^{68,74} poly(ether imide) (PEI),⁷¹ and sulfonated poly(phthalazine ether sulfoneketone) (SPPESK).⁷⁵ It has been also reported that increasing the evaporation time or the casting temperature induces lower permeances but higher selectivities for PI,^{68,76,77} PEI,⁷¹ polyamide (PA),⁷⁸ and PPESK.⁷⁹

The performance, microscale morphology, and formation mechanism of OSN ISA membranes made from P84, Matrimid, HT, and in-house synthesized polyimide have been reported in a series of studies.^{80–84} It has been found that MWCOs are in the range of 200–1200 g mol⁻¹, and permeance is in the range of 0.5–7 L m⁻² h⁻¹ bar⁻¹ in dimethylformamide (DMF).

Polysulfone (PSf) membranes have been used and explored to develop OSN membranes for mild organic solvents. Holda et al.⁸⁵ have developed PSf ISA membranes stable in isopropanol using commercial PSf Udel and N-methyl pyrrolidone (NMP) and tetrahydrofuran (THF) as solvent and volatile cosolvent, respectively, for the casting solution. The effect of polymer concentration and evaporation time on membrane performance was investigated. Increasing polymer concentration increased Rose Bengal rejections from 37% to 92%, considerably decreasing isopropanol permeance from 9.7 to 0.07 L m⁻² h⁻¹ bar⁻¹. An increase in rejection from 47% to 76% and a decrease in permeance from 2.4 to 0.08 L m⁻² h⁻¹ bar⁻¹ were observed when evaporation time was increased (i.e., increasing rejection of Rose Bengal compromised permeance significantly). In another publication,⁸⁶ PSf materials from 10 different origins were utilized, and the effects of PSf MW, purity, and polydispersity on the structure and performance of the prepared ISA membranes were investigated. A significant amount of contaminating compounds was found to be present in the commercial PSfs. When membranes were prepared from purified PSf, all permeances increased up to a factor of 5, accompanied by increased rejections of Rose Bengal up to 94%. Holda et al. have also studied the role of adding different high⁸⁷ and low⁸⁸ molecular weight additives in the casting solution on the performance of membranes made from commercial PSf Udel. Their influence on the phase inversion process was studied via viscosity and cloudpoint measurements. When using high MW additives, their highest Rose Bengal rejection in isopropanol was achieved when PEG 200 was used as additive with a concentration of 5 wt % but gave a very low permeance (lower than 0.1 L m⁻² h⁻¹ bar⁻¹).⁸⁷ On the basis of scanning electron microscopy analyses, the authors claimed that increasing the MW of PEG or increasing its concentration created a thicker layer with increased density on top of the macrovoid layer. In their publication on the effect of low MW additives,⁸⁸ to obtain a membrane with satisfactory performance, casting solutions containing NMP as the solvent and a relatively high concentration (e.g., 25 wt %) of low MW additive were used, achieving higher than 90% rejection of Rose

Table 2. List of Polymers Used To Prepare OSN Integrally Skinned Asymmetric (ISA) Membranes by Phase Inversion, Applicable as Such (NF) or as UF Supports

Polymer	Membrane type	Structure
Polyacrylonitrile (PAN)	NF, UF	
Polyimide (PI) Matrimid	NF, UF	
Polyimide (PI) P84	NF, UF	(80%) (20%)
Polyaniline (PANI)	NF	
Polybenzimidazole (PBI)	NF	
Polysulfone (PSf) + sulfonated poly (ether ether ketone) (SPEEK)	NF	
Poly (ether ether ketone) (PEEK)	UF	
Polypropylene (PP)	UF	

Bengal with a permeance of $4.5 \text{ L m}^{-2} \text{ h}^{-1} \text{ bar}^{-1}$. In conclusion, low MW additives gave higher rejection of Rose Bengal and higher isopropanol permeance.

Another class of ISA membranes from the PSf family promising for filtrations in mild organic solvents including lower alcohols and short chain alkanes has been developed by Darvishmanesh et al.⁸⁹ and is based on polyphenylsulfone (PPSf). They studied different polymer concentrations and dimethylacetamide (DMAc), NMP, or a mixture of DMF and NMP as solvents for the polymer. Their membranes showed good performance in methanol with up to 88% rejection of Rose Bengal and good stability in *n*-hexane. Methanol permeance decreased with increasing polymer concentration,

while rejection of Rose Bengal increased. Darvishmanesh et al.⁹⁰ developed also PPSf hollow fiber membranes varying the polymer concentration. The membranes with better rejection showed lower isopropanol permeance ($0.02 \text{ L m}^{-2} \text{ h}^{-1} \text{ bar}^{-1}$) with 98.6% rejection of Rose Bengal and 73.5% rejection of Bromothymol Blue. The solvent stability was assessed via permeation experiments; based on these experiments, membranes were stable in methanol, ethanol, isopropanol, *n*-hexane, and *n*-heptane and unstable in acetone and methyl ethyl ketone. However, to fully assess their stability in those solvents, membrane rejection should also be tested. Ideally, rejection tests should be carried out in each of the solvents. Immersing the membrane in another solvent and testing it in methanol

could be misleading as the membrane could swell when immersed in the solvent and deswell when again tested in methanol. To further improve the solvent stability of PPSf membranes in solvents such as acetone or methyl ethyl ketone (MEK), Jansen et al.⁹¹ blended PPSf with Matrimid PI to prepare OSN membranes from blends of different compositions in NMP. Fluxes of organic solvents through these membranes were dependent on the PPSf/Matrimid blend composition. The highest flux was achieved with a 50/50 wt % blend for alcohol and alkanes, with a 75/25 wt % blend for acetone and MEK, and with a 25/75 wt % blend for alkyl acetates. Solvent stability was tested measuring rejection of Sudan II before and after immersion in the chosen solvent for 2 days. All membranes were stable in acetone and MEK. Their best membrane showed a 95% and 96.9% rejection of Sudan II with a permeance of 2.1 and 1.8 L m⁻² h⁻¹ bar⁻¹ after exposure to MEK and acetone, respectively.

Another interesting and promising class of OSN membranes with superior chemical stability is the class of poly(ether ether ketone)-based membranes. Buonomenna et al.⁹² have developed phenolphthalein-based poly(ether ether ketone) (PEEKWC) ISA OSN membranes by phase inversion using commercial PEEKWC, a PEEK polymer that contains a cardo-group. These membranes showed a 99.8% rejection of Rose Bengal in isopropanol with a permeance of around 0.9 L m⁻² h⁻¹ bar⁻¹ and a 90% rejection of Rose Bengal in methanol with a permeance of around 1.7 L m⁻² h⁻¹ bar⁻¹. However, using commercially available polymers that were not developed explicitly as membrane materials has the disadvantage that these polymers may contain various additives such as stabilizers and flame retardants that can influence the phase inversion process.⁹³ To avoid this, Hendrix et al.⁹⁴ have synthesized for the first time a modified poly(ether ether ketone) with a *tert*-butyl group in its backbone (TBPEEK). The prepared polymer is soluble in NMP and THF, making it possible to prepare membranes via phase inversion. The developed OSN TBPEEK membranes were stable in a range of alcohols, *n*-hexane, and acetonitrile (ACN). The polymer length did not have a significant effect on membrane performance, but increasing the polydispersity had a negative effect on rejection of Rose Bengal. The role of the PEEK concentration in the casting solution on membrane performance and morphology was investigated. Membranes in the NF range were obtained by adding a volatile cosolvent to the casting solution, resulting in a 90% rejection of Rose Bengal in isopropanol with a permeance of almost 1 L m⁻² h⁻¹ bar⁻¹. Hendrix et al.⁹⁵ prepared also cross-linked PEEK membranes from lab-synthesized polymers via phase inversion. They introduced a carboxylic group into the PEEK polymer backbone (VAPEEK), which can be cross-linked using diamines. A high cross-linker concentration of 10% was required to achieve full cross-linking, but recycling of the coagulation bath by Buchner filtration proved possible. The cross-linking and the phase inversion were performed simultaneously, thus combining two steps. The highest rejections of around 90% for Rose Bengal in isopropanol and acetone were achieved for the membrane cross-linked with 1,6-hexamidine (HDA) with rather low permeances (around 0.1 and 0.2 L m⁻² h⁻¹ bar⁻¹ for isopropanol and acetone, respectively). PEEK polymer is solvent stable, exhibits high glass transition temperature, mechanical strength, and is hydrophobic, making it interesting as OSN membrane material. Recently, the phase inversion process to prepare NF membranes from lab-synthesized PEEK polymers (BPAPEEK

and TBPEEK) has been investigated. Hendrix et al.⁹³ studied the influence of polymer concentration on membrane performance, addition of a cosolvent, evaporation time, coagulation bath composition, and casting thickness. By optimizing the parameters mentioned before, they were able to produce NF membranes from these two polymers. Unfortunately, the prepared membranes showed poor stability in alkaline solutions. Their best TBPEEK and BPAPEEK membranes showed 90% and 87% rejection of Rose Bengal in isopropanol, respectively, with a permeance of 0.4 and 0.1 L m⁻² h⁻¹ bar⁻¹. Their more open membranes have potential as hydrophobic supports for TFC OSN membranes.

New work from da Silva Burgal et al.^{96,97} presented a nonmodified PEEK membrane specifically for OSN processing in polar aprotic solvents (such as DMF, THF) at high temperatures and both basic and acidic conditions. The effect of various grades of PEEK polymer on NF performance was assessed, and it was found that the postphase inversion drying process and the degree of sulphonation are crucial parameters. VESTAKEEP 4000P resulted in the tightest OSN membrane with an MWCO of 400/470 g mol⁻¹ and permeance of 0.22/0.07 L m⁻² h⁻¹ bar⁻¹ in THF/DMF, respectively. This is the first reported publication on a nonsulfonated and nonmodified PEEK membrane capable of separations in the NF range and resistant to DMF and THF and to basic and acidic aqueous solutions.

2.3.1.2. Post-Treatments. Various conditioning or post-treatment methods can be used to increase the long-term stability of ISA membranes, and to enhance their separation performance. These include cross-linking, wet or dry annealing, drying by solvent exchange, and treatment with conditioning agents.⁵³ Post-treatment is also crucial for polymeric UF supports prepared by phase inversion, used to prepare TFC membranes.⁵⁶

Cross-linking is used to enhance chemical stability and rejection properties of ISA membranes. Different cross-linking methods have been used for polymeric membranes, including thermal cross-linking, UV cross-linking, and chemical cross-linking. A recent review by Vanherck et al.⁹⁸ discusses in detail the work that has been published on cross-linking PI membranes for different applications. See Toh et al.⁸⁴ showed that cross-linking P84 PI ISA membranes made them stable in polar aprotic solvents such as DMF. Solvent stable Matrimid PI membranes were developed and chemically cross-linked with *p*-xylylenediamine.⁹⁹ The membranes were stable in DMAc, dimethyl sulfoxide (DMSO), NMP, THF, and DMF under filtration conditions. Vanherck et al.¹⁰⁰ have combined the phase inversion process and the cross-linking step for polyimide membranes in only one step. They added the cross-linker directly to the aqueous coagulation bath, thus eliminating an extra solvent-based production step. The newly proposed method is particularly efficient when xylylenediamine is used as the cross-linker, resulting in NF membranes with permeance in DMF and NMP of 0.4 and 0.2 L m⁻² h⁻¹ bar⁻¹ and a Rose Bengal rejection of 98%. Because no solvent is used, it can be regarded as a cheaper, less hazardous, and more environmentally friendly method.

P84 polyimide ISA membranes are usually prepared via a multistep process consisting of phase inversion, cross-linking, and pore preservation.¹⁰¹ Post-treatment of membranes with a pore preserving agent is very important and necessary to avoid pore collapse or aging of the membrane after drying. To avoid the conditioning pore preserving step, Siddique et al.¹⁰¹ have

combined cross-linking and pore preservation in one step. Using Jeffamine 400 as a cross-linker, no post-treatment with pore preserving agent was necessary. Membranes were stable in harsh solvents such as DMF at elevated temperature. Compaction resistance was improved with less than 10% decrease in permeance observed with negligible change in MWCO. Membranes were flexible and easy to handle, with no compaction after thermal annealing in solvents such as acetone and toluene. However, Jeffamine cross-linked membranes showed very low permeances as compared to the typically HDA cross-linked membranes.

Dutczak et al.¹⁰² have cross-linked commercial polyamide-imide (Torlon)-based membranes (provided by Solsep B.V.) for the first time using di-isocyanates. Prior to cross-linking, the membranes were dried at 150 °C for 12 h to remove water and then immersed in the cross-linking solution for 13 days at 50 °C. The cross-linked membranes possessed good mechanical properties. They showed a MWCO of 260 g mol⁻¹ in acetone/polystyrene mixtures with a permeance of 1.2 L m⁻² h⁻¹ bar⁻¹ and an 85% rejection of cholesterol (380 g mol⁻¹) in NMP after the membrane was in contact with NMP for 6 months. These cross-linked polyamide-imide Torlon membranes also possessed thermal stability; after being placed in a closed vessel with toluene at 120 °C for 48 h, their NMP permeance was unchanged. The authors suggested that it is possible to tailor the membrane MWCO by varying the cross-linking time. These membranes could have potential in high temperature OSN processes. However, from a production process perspective, the cross-linking time of 13 days should be optimized to a shorter time.

UV curing combined with well-selected cross-linker and photoinitiator systems can also be used to enhance the solvent stability of polymeric membranes. Solvent-stable PSf or PI membranes have recently been prepared via UV curing after phase inversion by Struzynska-Piron et al.¹⁰³ The effects of photoinitiator type, cross-linker functionality, and membrane thickness were investigated. UV modified polysulfone membranes showed good stability in ethyl acetate (91% rejection of Rose Bengal and permeance of 8.1 L m⁻² h⁻¹ bar⁻¹) and isopropanol (94% rejection of Rose Bengal and permeance of 0.2 L m⁻² h⁻¹ bar⁻¹). UV cured polyimide membranes were also stable in isopropanol (96% rejection of Rose Bengal and permeance of 1.4 L m⁻² h⁻¹ bar⁻¹). Struzynska-Piron et al.¹⁰⁴ showed also that acyl phosphine oxide-based photoinitiators in combination with a pentaacrylate cross-linker give a polysulfone UV-cross-linked membrane, which is stable in acetone, butyl acetate, ethyl acetate, toluene, and xylene. In another study, Struzynska-Piron et al.¹⁰⁵ prepared UV cross-linked PSf-based membranes containing additives with different number of acrylate groups. Reversing the process sequence from phase inversion/UV to UV/phase inversion gave membranes with higher isopropanol permeances (up to 1.2 L m⁻² h⁻¹ bar⁻¹) and 94% rejection of Rose Bengal.

Cross-linked PI membranes have also been used as UF support membranes for OSN TFC membranes made of two different polymers^{106–109} or the same polymer but two independent layers.¹¹⁰ Heating for a short period at high temperatures improved the rejection of PI OSN membranes, but on the other hand compromised permeance.⁶⁵ A drastic flux decline was observed upon heating a P84 polyimide membrane from 0 to 150 °C,⁶⁸ which was attributed due to reorganization of the polymer chains at elevated temperatures

to thermodynamically favored structures, accompanied by simultaneous densification of the membrane.

Membranes made from other polymeric materials, such as PAN⁵⁹ and PANI,^{60,61} have also been cross-linked to enhance their chemical and thermal stability. PANI cross-linked membranes were found to be stable at temperatures up to 70 °C and showed solvent stability in various organic solvents including acetone, THF, and DMF.⁶⁰

Polybenzimidazole (PBI) membranes are a new class of OSN membranes, which exhibit superior chemical stability as compared to other well-known polymeric membranes such as polyimide. Valtcheva et al.¹¹¹ have developed cross-linked PBI membranes using dibromoxylene (DBX) or dibromobutane (DBB) as cross-linkers, showing good tolerance toward extreme pH conditions. The membranes modified with DBX as the cross-linker were stable in DMF and exhibited superior stability and higher permeances to those cross-linked with DBB. Xing et al.¹¹² have used [EMIM]OAc ionic liquid as a greener solvent for the development of PBI OSN membranes. To further improve membrane stability, PBI was chemically cross-linked using one of two different cross-linking agents (glutaraldehyde (GA) in water, or 1,2,7,8-diepoxyoctane (DEO) in *n*-heptane). PBI membranes cross-linked with GA showed good stability in ethanol (3.7 L m⁻² h⁻¹ bar⁻¹) and ethyl acetate (5.2 L m⁻² h⁻¹ bar⁻¹) with good solute rejection but were not stable in more aggressive solvents like DMSO. PBI membranes cross-linked with DEO were stable in DMSO but showed lower permeances in ethanol and ethyl acetate. Recently, a novel class of OSN membranes featuring molecular recognition sites was fabricated by Szekely et al.¹¹³ via a phase inversion molecular imprinting technique employing PBI as functional polymer. The molecularly imprinted organic solvent nanofiltration (MI-OSN) membranes fabricated in this study showed both nanofiltration membrane performance and excellent molecular recognition ability. It was demonstrated that higher dope solution polymer concentration leads to lower flux, higher solute rejection and binding capacity, and more homogeneous binding site distribution. The addition of the template to the dope solution reduced the viscous hindrance forces and facilitated macrovoid formation leading to 4-fold higher flux. The investigation of the effect of pressure on molecular recognition revealed that increased pressure leads to polymer rearrangement eradicating the molecular recognition sites but leaving the solvent permeation unaffected. Such MI-OSN membranes could be applied for three-way separation of ternary systems in a single unit operation.

2.3.2. Thin Film Composite (TFC) Membranes. Another important class of membranes are thin film composite (TFC) membranes, which consist of an ultrathin “separating layer” cast on top of a chemically different porous support (cf., Figure 9b). These membranes are very flexible and are characterized by some freedom in their design for a specific application. Because of the membrane characteristic layered structure, the chemistry and performance of the barrier layer and the porous support can be independently optimized to maximize the overall membrane performance.^{6,67} The most common solvent-stable polymers used as UF supports for TFC membranes are asymmetric PSf, poly(ether sulfone) (PES), PAN, poly(vinylidene fluoride) (PVDF), PP, PI, and PBI (cf., Table 2), as well as inorganic membranes. The choice of the support layer for TFC membranes is important, as it must provide mechanical stability and allow the formation of defect-free top layers.

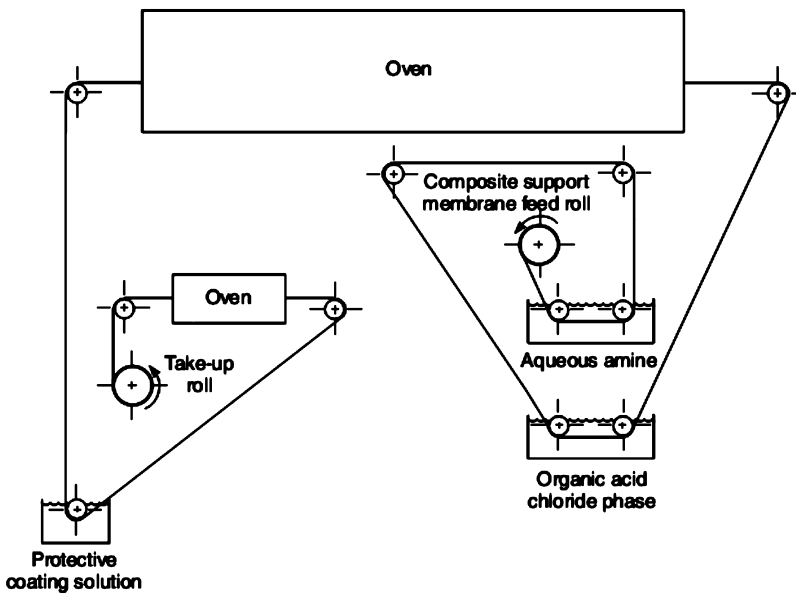


Figure 11. TFC membrane formation process by interfacial polymerization. Reprinted with permission from ref 8. Copyright 2012 John Wiley & Sons.

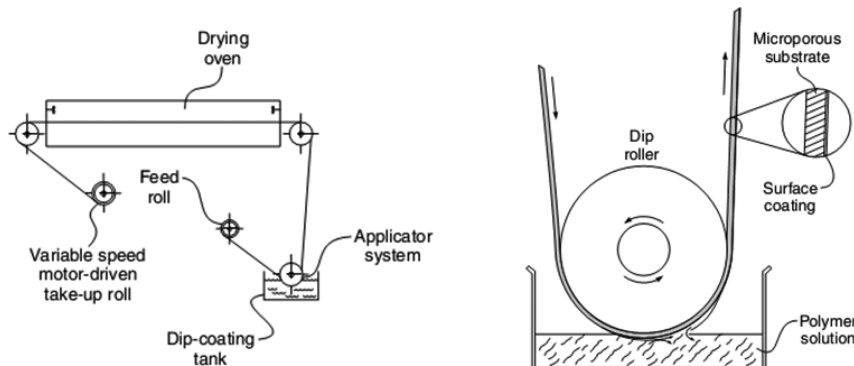


Figure 12. TFC membrane formation process by dip-coating. Reprinted with permission from ref 8. Copyright 2012 John Wiley & Sons.

The main methods for the formation of the top layer of TFC membranes on a porous UF support are⁶⁶ (a) casting an ultrathin film separately, then laminating it to a support; (b) interfacial polymerization at the surface of a support; (c) dip-coating/solvent casting a solution of a polymer onto a support; (d) dip-coating a solution of a reactive monomer or prepolymer onto a support, followed by a postcuring with heat or irradiation; and (e) depositing a barrier film directly from a gaseous phase monomer plasma. The most commonly used methods are interfacial polymerization and dip-coating on a support layer, usually prepared by phase inversion. The membrane formation processes using these two methods are shown in Figures 11 and 12 for interfacial polymerization and dip-coating, respectively.

Materials used to prepare OSN TFC membranes by interfacial polymerization or dip-coating are reported in Table 3.

2.3.2.1. Research Work on TFC Membranes via Interfacial Polymerization for OSN. The technique for interfacial polymerization (cf., Figure 11) consists of the formation of a thin film on top of an asymmetric, porous support layer by an *in situ* polymerization reaction occurring at the interface between two immiscible phases containing reactive monomers. The UF support is usually impregnated in an aqueous diamine

solution, then the excess water is removed and the saturated support is contacted with an organic phase containing acyl halides. A quick reaction between the two monomers forms a thin selective polyamide (PA) layer on the UF substrate. The top layer then acts as a barrier for further monomer transport, thus controlling the top-layer thickness.²

Cadotte⁶⁶ pioneered the work on interfacial polymerization. Although PA-based TFC membranes by interfacial polymerization have been mainly prepared for aqueous applications, the use of PA TFC membranes in organic solvents has been also recently reported. These TFC membranes were comprised of a thin film synthesized from piperazine/*m*-phenylenediamine and trimesoyl chloride on a PAN support membrane; they performed well in methanol ($6 \text{ L m}^{-2} \text{ h}^{-1} \text{ bar}^{-1}$), ethanol ($2 \text{ L m}^{-2} \text{ h}^{-1} \text{ bar}^{-1}$), and acetone ($6 \text{ L m}^{-2} \text{ h}^{-1} \text{ bar}^{-1}$), less well in isopropanol ($0.2 \text{ L m}^{-2} \text{ h}^{-1} \text{ bar}^{-1}$) and methyl–ethyl ketone (MEK, $0.8 \text{ L m}^{-2} \text{ h}^{-1} \text{ bar}^{-1}$), and gave no flux in *n*-hexane.¹¹⁴ These membranes were clearly not appropriate for filtrations in more apolar media. To permit hexane-based applications, nonreactive PDMS was added during the polymerization reaction.^{115,116} The resulting silicone-blended PA membrane showed high *n*-hexane permeance ($13 \text{ L m}^{-2} \text{ h}^{-1} \text{ bar}^{-1}$). The hydrophilicity change obtained upon blending thus broadened the applicability of PA membranes. PA-based TFC membranes

Table 3. List of Monomers and Polymers Used To Prepare OSN Thin Film Composite (TFC) Membranes by Interfacial Polymerization or Coating

Monomer / polymer	Method	Structure
Diamines	Interfacial Polymerisation	
Acyl chlorides	Interfacial Polymerisation	
Poly(ethylene imine) (PEI)	Interfacial Polymerisation	
Polydimethylsiloxane (PDMS)	Coating	
Poly(2,6-dimethyl-1,4-phenylene oxide) (PPO)	Coating	
Poly(vinyl alcohol) (PVA)	Coating	
Chitosan	Coating	
Polyacrylic acid (PAA)	Coating	
Polyphosphazene (PPz)	Coating	
Poly[1-(trimethylsilyl)-1-propyne] (PTMSP)	Coating	
Polyurethanes (PU)s)	Coating	
Polypyrrole (PPy)	Coating	
Polymers of intrinsic microporosity (PIM-1)	Coating	
Polystyrene- <i>b</i> -poly(ethylene oxide) diblock copolymer	Coating	
Poly(sodium styrene sulfonate) (PSS)	Coating	

Table 3. continued

Monomer / polymer	Method	Structure
Poly(diallyldimethylammonium chloride) (PDDA)	Coating	
Poly(vinyl sulfate) (PVS)	Coating	

were also applied as such for filtration in more apolar solvents. A method for the separation of lube oil from organic solvents (e.g., furfural, MEK/toluene, etc.) with a cross-linked PA membrane, using poly(ethylene imine) (PEi) and a diisocyanate on a solvent resistant nylon-6,6 support, was patented.²¹ Alternative to PA, Buch et al.¹¹⁷ reported that poly(amide imide) (PAI) is useful for the synthesis of thermally and chemically stable TFC membranes. Polypropylene support membranes have also been used as solvent stable supports for PA TFC membranes.^{118–121} These TFC membranes were prepared in both hollow fiber and flat sheets configurations. Minhas et al.¹²² used commercial hydrophilized polypropylene support (Celgard 2400) to prepare TFC membranes via interfacial polymerization with ethylene diamine and terephthaloyl chloride. Stability tests by soaking in ethanol and hexane for 30 days showed no change in permeation. Unfortunately, no rejection tests were performed after solvent exposure, making it therefore not possible to conclude whether these membranes are stable in organic solvents. Peyravi et al.¹²³ developed methanol resistant TFC membranes via interfacial polymerization with PEi and iso-phthaloyl dichloride on reinforced polysulfone supports; polysulfone was blended with sulfonated poly(ether sulfide sulfone) to improve stability in methanol. These TFC membranes showed good separation performance of Bromothymol Blue (624 g mol^{-1}) and Crystal Violet (407 g mol^{-1}) in methanol.

Recently, TFC membranes prepared by interfacial polymerization have been specifically designed for OSN applications for both polar and apolar solvents, and are stable in harsh solvents, such as DMF and THF.^{108,109} Jimenez Solomon et al.¹⁰⁸ developed OSN TFC membranes by interfacial polymerization on a cross-linked PI support. In order to enhance or activate solvent flux the authors post-treated the TFC membranes with an activating solvent. These membranes showed excellent stability in polar aprotic solvents (such as THF and DMF) and permeances much higher than and rejections comparable to those of commercial ISA membranes.

In another study, to increase apolar solvent flux the free acyl chloride groups on the PA TFC membrane surface were capped with different monomers containing hydrophobic groups.¹⁰⁹ Incorporation of fluorine and silicon to the polyamide top layer resulted in dramatically improved permeances for apolar solvents, suggesting that the chemistry of the membrane surface plays an important role in solvent permeation. These are the first reported hydrophobic TFC membranes which are stable in DMF. They exhibit significantly higher permeances for apolar solvents, including toluene and ethyl acetate, than commercial OSN hydrophobic integrally skinned asymmetric and rubber coated membranes and yet have comparable or better selectivity.

For the development of TFC OSN membranes, the choice of the UF support is as important as the selection of the separating layer. Jimenez Solomon et al.¹²⁴ studied the impact of the physicochemical properties of different solvent stable UF support membranes on the performance of OSN TFC membranes prepared via interfacial polymerization. Their work suggests that the hydrophilicity of the supports plays a significant role in solvent permeation. PA and modified hydrophobic PA TFC membranes were formed by interfacial polymerization on cross-linked PI and PEEK UF support membranes. They found that the optimal method to increase permeance without compromising rejection using these two different UF support membranes was achieved by (i) adding PEG into the pores of the support, and (ii) treating the TFC membranes with DMF as an “activating solvent”. These membranes exhibited up to 15 times higher solvent permeance without compromising solute rejection, when compared to commercial OSN ISA membranes.

2.3.2.2. Research Work on TFC Membranes via Coating for OSN. OSN TFC membranes can be prepared via coating a more porous sublayer with a different composition. Many parameters, including the mechanical strength and chemical stability of the polymer, its film forming properties, its solubility in different solvents, and its cross-linking capability, influence the polymer choice for preparing these membranes. Polymers studied as coating materials are PDMS, PEi, poly(2,6-dimethyl-1,4-phenylene oxide) (PPO), poly(vinyl alcohol) (PVA), chitosan and other cellulose derivatives, poly(ether-*b*-amide) (PEBAX), poly(acrylic acid) (PAA), polyphosphazene (PPz), poly(aliphatic terpenes), poly[1-(trimethylsilyl)-1-propyne] (PTMSP), and polyurethanes (PUs).²

PDMS is mostly used in apolar solvents, due to its low polarity, but is also chemically stable in some organic solvents when cross-linked. PDMS composite membranes were formed on cross-linked PI supports.^{106,107} Like most elastomers, PDMS tends to swell extensively in organic solvents, particularly in apolar solvents.

PTMSP is a hydrophobic glassy polymer with a high free-volume fraction (up to 25%). Highly permeable PTMSP/PAN composite membranes for OSN were developed by Volkov et al.¹²⁵ The optimized membrane with a top layer thickness of 1 μm showed an ethanol permeance of $4.8 \text{ L m}^{-2} \text{ h}^{-1} \text{ bar}^{-1}$ with a 90% rejection of the dye Remazol Brilliant Blue R (MW = 626 g mol^{-1}). The nanofiltration of dilute dye solutions in normal alcohols through self-standing PTMPS membranes was investigated,¹²⁶ suggesting that the selectivity of nanofiltration of dilute dye solutions through PTMSP membranes significantly depends not only on the nature of the solute, but also on the properties of the solvent.

Li et al.¹²⁷ developed an OSN membrane with a polypyrrole (PPy) modified top layer by in situ polymerization on different UF support membranes. The pyrrole monomer dissolved in ethanol was coated on the surface of the support membrane, and then polymerized to form a PPy top layer. The membrane showed stability in strong aprotic solvents, including DMF and THF, with a very high permeance of $67 \text{ L m}^{-2} \text{ h}^{-1} \text{ bar}^{-1}$ in THF and 98% rejection of Rose Bengal (MW = 1017 g mol⁻¹). Shao et al.¹²⁸ also developed a new OSN TFC membrane consisting of a top layer made of PPy polymer on hydrolyzed PAN (PAN-H) support. The composite membrane prepared under the optimal conditions has 99.2% Rose Bengal rejection in isopropanol, and methanol, ethanol and isopropanol permeances of 1.46, 1.30, and 0.79 $\text{L m}^{-2} \text{ h}^{-1} \text{ bar}^{-1}$, respectively. Graphene oxide (GO) was incorporated for the first time into the PPy/PAN-H composite OSN membrane by dispersing GO into the pyrrole ethanol solution before polymerization. Upon incorporation of GO into PPy/PAN-H composite membranes, the solvent permeance was significantly enhanced without compromising Rose Bengal rejection. With respect to pure PPy/PAN-H composite OSN membranes, the solvent permeances of the GO-PPy/PAN-H membrane were approximately 945% (methanol), 635% (ethanol), and 302% (isopropanol) higher, respectively. In a long-term experiment, the GO-PPy/PAN-H composite OSN membrane showed a constant isopropanol permeance of $1.2 \text{ L m}^{-2} \text{ h}^{-1} \text{ bar}^{-1}$ and a Rose Bengal rejection of approximately 99.0%.

Current polymeric OSN membranes have limitations for the separation of catalysts from Active Pharmaceutical Ingredient (APIs) due to the similarity in MW between the ligands on a catalyst and the product.¹²⁹ Long et al.¹²⁹ have developed the first dense high free volume nonsupported 100 μm thick membranes composed of polydicyclopentadiene (PDCPD) capable of separating many common ligands for metals from other molecules with MW lower and higher than those ligands. According to the authors, the separation is affected by the large cross-sectional area of ligands, which slows their diffusion through the heavily cross-linked PDCPD membrane. This material has a great potential for use as a separation layer in OSN TFC membranes, as it was shown capable of retaining key molecules with MW over 3 times as high as that of the permeate.

Novel polymeric materials characterized by ultrahigh free volume, capable of retaining their nanoporosity upon heating, have been developed and are known as polymers with intrinsic microporosity (PIMs).¹³⁰ The intrinsic microporosity of these materials is a direct consequence of the shape and rigidity of the macromolecular chain and does not allow the resulting polymers to pack closely.¹³⁰

These materials have potential in separation applications, due to their high free volume, which leads to high permeance. Up to date, the PIM polymer mostly used in membrane development for gas separation¹³¹ and pervaporation applications^{132,133} has been PIM-1, which has given high permeance and selectivity. Recently, TFC membranes using PIM-1 for OSN showing 30 times higher permeance than commercial Starmem 240, and no compaction at high pressure after 300 h, were produced by Fritsch et al.⁴³ Tsarkov et al.¹³⁴ tested PIM-1 for OSN with different dyes dissolved in ethanol and found significant sorption of the dye within the membrane. Ultrathin free-standing membranes with thickness down to 35 nm were fabricated from PIM-1 by Gorgojo et al.¹³⁵ via spin-coating and further floating and transfer of the films on a polymeric or

ceramic support. These membranes showed an HPB rejection of 90%. A maximum permeance for *n*-heptane of $18 \text{ L m}^{-2} \text{ h}^{-1} \text{ bar}^{-1}$ was obtained with the 140 nm thick membrane, which is about 2 orders of magnitude higher than Starmem240. Unexpectedly, an anomalous decrease in permeance was found when decreasing the film thickness below 140 nm, which was related to a packing enhancement of PIM-1, as measured by light interferometry. After thermal annealing up to temperatures in excess of 150 °C, PIM-1 membranes preserved their permeance, whereas the permeance of ISA PI Matrimid OSN membranes decreased significantly. The authors introduced the concept of membranes with intrinsic microporosity (MIMs) versus membranes with extrinsic microporosity (MEMs), to characterize this key difference in response to functional performance to annealing of the two materials.

Block copolymers, which self-assemble to form different ordered nanostructures, represent another promising novel class of polymeric materials for high permeance membranes. Li et al.¹³⁶ recently reported a new class of nanostructured TFC membranes for OSN applications, in which the top layer was obtained using blends of a polystyrene-*b*-poly(ethylene oxide) diblock copolymer and a poly(acrylic acid) homopolymer as template. The top layer was directly deposited on both inorganic and polymeric support membranes. These membranes showed promising performance in OSN, and their nanostructures can in principle be tuned for a desired application.

Using segmented polymer networks (SPN) is another way to make advanced architecture polymer top layers. Li et al.¹³⁷ developed multifunctional composite membranes with thin SPN toplayers by in situ polymerization on PAN supports. They used hydrophilic bis(acrylate)-terminated poly(ethylene oxide) as macromolecular cross-linker of different hydrophobic polyacrylates for the synthesis of amphiphilic SPNs. These membranes have high rejection of Rose Bengal in isopropanol (rejection of 99% Rose Bengal with permeance up to $0.4 \text{ L m}^{-2} \text{ h}^{-1} \text{ bar}^{-1}$) and in strong swelling solvents including THF (rejection of 99.3% Rose Bengal with permeance up to $1.3 \text{ L m}^{-2} \text{ h}^{-1} \text{ bar}^{-1}$) and DMF (rejection of 96% Rose Bengal with permeance up to $2.7 \text{ L m}^{-2} \text{ h}^{-1} \text{ bar}^{-1}$). Rejection of Rose Bengal was strongly affected by the composition or the ratio of the hydrophilic and hydrophobic phases of the SPN.

Another technique that can provide very accurate control over the film thickness on a nanometer scale is the layer-by-layer (LbL) assembly technique. With this method, very thin polyelectrolyte (PE) multilayers can be formed. A detailed review by Joseph et al.¹³⁸ on layer-by-layer preparation of PE multilayer membranes for separation has been recently published. Another review on polyelectrolyte complex membranes for nanofiltration applications describing different ways to prepare them was published by Zhao et al.¹³⁹ PEs are polymers with charged or chargeable groups within the monomer repeat units. The number of deposited layers determines the thickness of the PE membrane. Flux and selectivity can be finely tuned by the number of LbL cycles and by the chemical composition of the utilized PEs.¹³⁸ Li et al.¹⁴⁰ were the first ones to develop polyelectrolyte complex (PEC)-based membranes for filtration in organic solvents including aprotic solvents such as THF and DMF. They used a new combination of PEs to form supported membranes consisting of 5, 10, 15, and 20 bilayers via the LbL technique.⁶³ They observed rougher membrane surfaces with increasing bilayer number. These membranes showed high selectivity for charged

solutes due to Donnan exclusion and high flux in different solvents such as isopropanol (permeance of $0.50 \text{ L m}^{-2} \text{ h}^{-1} \text{ bar}^{-1}$ with 99% rejection of Rose Bengal), THF (permeance of $8.82 \text{ L m}^{-2} \text{ h}^{-1} \text{ bar}^{-1}$ with 98% rejection of Rose Bengal), and DMF (permeance of $0.05 \text{ L m}^{-2} \text{ h}^{-1} \text{ bar}^{-1}$ with 92% rejection of Rose Bengal). Multilayered PECs were further studied as OSN membranes by adding small ions (NaCl) to the PE dipping solutions. This permits one to control the charge and configuration of the PE.¹⁴⁰ Addition of salts had a direct effect on membrane morphology and performance, as it resulted in thicker and looser PEC topayers. With increasing NaCl concentration up to 0.5 M , the rejection of Rose Bengal increased to 95%. Ahmadiannamini et al.¹⁴¹ successfully prepared a new combination of multilayered PEC membranes by the LbL method from poly(diallyldimethylammonium chloride) (PDDA) as polycation and poly(sodium styrenesulfonate) (PSS) or poly(vinyl sulfate) (PVS) as polyanions, each either in Na- or in H-form. Interestingly, the membranes prepared from polyanions in the H-form showed higher permeabilities and higher rejections than the ones prepared from the Na-form. All membranes showed very good rejections for charged solutes in isopropanol (99% rejection of Rose Bengal and $1.6 \text{ L m}^{-2} \text{ h}^{-1} \text{ bar}^{-1}$) and in DMF (98% rejection of Rose Bengal and $0.2 \text{ L m}^{-2} \text{ h}^{-1} \text{ bar}^{-1}$). In another paper, Ahmadiannamini et al.¹⁴² used a new combination of PDDA with a weak polyacid (poly(acrylic acid), PAA). The effects of salt concentration during preparation and pH of the PE solutions were studied. It was observed that a thicker membrane surface was obtained by adding salt to the PE solutions during membrane preparation, and thinner layers were formed as the pH of PE solutions increases. Tylkowski et al.¹⁴³ used the LbL method to decrease swelling of polysulfone membranes. They successfully prepared layer-by-layer (LbL)-treated polysulfone membranes, using poly(acrylic acid) and branched poly(ethylene imine) (BPEi) layers. The swelling of the membranes in *n*-hexane, methanol, and isopropanol decreased with increasing the number of deposited bilayers. Anthracene ($\text{MW} = 178 \text{ g mol}^{-1}$) rejection evaluated on a membrane with 10 deposited bilayers increased up to 68%, as a consequence of the LbL treatment (with respect to 11% of the untreated PSf), and had a permeance of $29.6 \text{ L m}^{-2} \text{ h}^{-1} \text{ bar}^{-1}$.

The LbL method was also used to overcome the drawbacks of microcracks induced by adding inorganic fillers to the membranes.¹⁴⁴ Multiple bilayers of poly-(diallyldimethylammonium, chloride)/sulfonated poly(ether ether ketone) (PDDA/SPEEK) were deposited for the first time on charged silicon composite with hydrolyzed polyacrylonitrile support and evaluated as OSN membranes. These membranes showed high rejections of negatively charged solutes in isopropanol (permeance of $0.1 \text{ L m}^{-2} \text{ h}^{-1} \text{ bar}^{-1}$ and 99% rejection of Rose Bengal), THF (permeance of $10 \text{ L m}^{-2} \text{ h}^{-1} \text{ bar}^{-1}$ and 98% rejection of Rose Bengal), and DMF (permeance of $0.07 \text{ L m}^{-2} \text{ h}^{-1} \text{ bar}^{-1}$ and 89% rejection of Rose Bengal). In comparison with silicon composite membranes, the introduction of multilayered PDDA/SPEEK efficiently improved the membrane performance and overcame the drawback caused by inorganic fillers.

2.3.2.3. Research Work on TFC Membranes via Plasma Polymerization for OSN. Diamond-like carbon (DLC) nanosheets were used as ultrathin free-standing amorphous carbon membranes for OSN by Karan et al.¹⁴⁵ They prepared the uniform ultrathin DLC membrane on a sacrificial layer of cadmium hydroxide nanostrands by using a parallel-plate

plasma enhanced chemical vapor deposition reactor and dissolved afterward the sacrificial layer by treating it with an ethanolic solution of hydrochloric acid. The top layer of their TFC membranes deposited on porous alumina supports had 1 nm hydrophobic pores; these membranes were able to retain organic dyes better than commercially available membranes. The authors observed that the ultrafast permeation of organic solvents and the excellent separation performance for organic solutes of these DLC nanosheets vary widely with the preparation parameters (i.e., the precursor gas) and with the membrane thickness (from 10 to 40 nm in this study). Among all of the membranes prepared, the pure ethanol flux ranged between 21 and $201 \text{ L m}^{-2} \text{ h}^{-1}$ at 0.8 bar , the azobenzene rejection between 23% and 94.4%, the fluorescein-4-isothiocyanate rejection between 41.2% and 100%, and the protoporphyrin-IX rejection between 81.5% and 100%. A detailed review on ultrathin free-standing membranes from metal hydroxide nanostrands has been recently published by Karan et al.¹⁴⁶

2.3.2.4. Post-Treatments. The performance of TFC membranes can be further enhanced by applying an appropriate post-treatment method.² Several techniques used to enhance membrane performance of TFC membranes in water have been reported in the literature, such as curing, grafting, plasma, UV, and chemical treatment.² More details on the curing and chemical post-treatment methods for aqueous TFC membranes can be found elsewhere.^{147–153} Most of these techniques have not been intensively used to date for OSN membranes.

2.4. Mixed Matrix Membranes (MMM)

Organic–inorganic polymer hybrids allow tailoring new membranes combining properties of both inorganic and polymeric materials. MMMs can be ISA or TFC membranes.

The presence of nanostructures, such as nanotubes, zeolite nanoparticles, clay, and fullerenes, in the polymer matrix has been widely explored in the membrane separation field¹⁵⁴ and could be also applied to organic solvent nanofiltration. Nanocomposite membranes are comprised of nanoparticles in a polymer matrix. There are three different methods to use nanoparticles for membrane modification: (i) adding nanoparticles to the casting solution before the phase inversion process, (ii) depositing nanoparticles on the membrane surface, and (iii) filling the pores of the polymeric membrane with nanoparticles. When added to the casting solution before the phase inversion process, metal oxide nanoparticles have an important effect on the membrane performance as they change the structure and the properties of the nanocomposite membrane. Mechanical and thermal properties, crystallinity, and hydrophilicity of the membrane change when nanoparticles are incorporated into the polymeric matrix.¹⁵⁴ Deposition or pore filling methods may use presynthesized nanoparticles or nanoparticles formed *in situ*.

2.4.1. Research Work on ISA Mixed Matrix Membranes for OSN. Composite organic–inorganic polyimide mixed matrix membranes comprising TiO_2 nanoparticles for OSN have been successfully prepared by Soroko and Livingston.¹⁵⁵ The TiO_2 nanoparticles were incorporated inside the cross-linked PI membrane matrix by adding them to the casting solution before phase inversion. They report a dramatic change in membrane morphology; macrovoids were suppressed by increasing loading of TiO_2 nanoparticles. The presence of TiO_2 increased hydrophilicity and enhanced mechanical

strength by improving compaction resistance, while rejection and steady flux were unaltered.

Vanherck et al.¹⁵⁶ developed a novel approach to increase solvent fluxes in OSN membranes without compromising rejection, by incorporation of gold nanoparticles into a cellulose acetate membrane. No defects were introduced in the active separating layer. The membrane was heated by light irradiation during the separation process, resulting in increased fluxes for membranes containing as little as 2% weight ratio of nanoparticles. An increase of 15% in the water flux was observed, while pure solvent fluxes increased up to 400% for ethanol and isopropanol. No significant effect of the photothermal heating on rejection was found. The photothermal heating effect could increase fluxes more efficiently than increasing feed temperatures. The authors suggested that their method is most applicable for solvents with low thermal conductivity values, as energy loss by transfer to the medium occurs at a slow rate. This method has been further explored for well-known polymers used for solvent resistant nanofiltration membranes, including PDMS¹⁵⁷ and PI.¹⁵⁸ In the PI MMM, the gold nanoparticles had an effect on membrane structure: the membrane structure became more porous and macrovoids decreased at higher gold nanoparticles concentration. It was also shown that pure isopropanol fluxes could be increased up to 50% and even up to 168%, depending on the concentration of gold nanoparticles in the membrane. For denser membranes, improvements as high as 120% for ethanol and even 400% for isopropanol were observed. The authors suggest that the effect on permeance was higher for membranes with an intrinsically lower flux, due to a lower energy loss by convection in the membrane free volume. In a different publication, two different synthesis routes to obtain gold nanoparticles in polyimide membranes, *in situ* chemical reduction of a gold salt and the use of preformed poly(vinylpyrrolidone) protected gold nanoparticles, have been reported.¹⁵⁹ When the gold nanoparticles were synthesized *in situ*, they were very well dispersed, resulting in a stronger heating of the composite material upon laser irradiation.

One drawback of P84 PI-based OSN membranes is the decline in permeance over time and with pressure, which is affected by the compaction of the membrane separation layer. To overcome compaction, Siddique et al.¹⁶⁰ developed a novel compaction-free MMM in both flat sheets and spiral wound module configurations. An organic–inorganic hybrid network (3-aminopeoyl trimethoxysilane (APTMS)) was incorporated within the P84 polyimide membrane matrix after the membrane was formed. This inorganic organosiloxane network (Si–O–Si) was also a cross-linking agent for the polyimide membrane, making it stable in strong swelling solvents including acetone, DMF, and dichloromethane (DCM) and at temperatures up to 100 °C. Addition of maleic acid as pore forming additive in the dope helped increase the solvent flux. The MMMs developed were flexible and easy to handle, avoiding the need of conditioning with a pore preserving agent such as PEG.

Hybrid polymer/MOF membranes were prepared also by Campbell et al.¹⁶¹ using either a MMM or an *in-situ* growth (ISG) approach. MMMs were produced by dispersing preformed particles of the metal-organic framework (MOF) HKUST-1 in P84 PI dope solutions. MMMs demonstrated both (i) higher rejections of styrene oligomers and (ii) lower flux decline than the polymeric control membranes. Furthermore, an alternative hybrid membrane fabrication method-

ology, ISG of HKUST-1 in ISA polymer membrane supports, was successfully demonstrated. According to this technique, UF support membranes were submerged in HKUST-1 precursor solutions to promote the growth of MOF within the porous structure of the polymer membranes. X-ray powder diffraction and energy-dispersive X-ray spectroscopy were used to prove the presence and reveal the distribution of HKUST-1 in the membranes. Interestingly, the ISG membranes also had higher solute rejections and lower flux decline than the MMMs.

2.4.2. Research Work on TFC Mixed Matrix Membranes for OSN. To reduce PDMS swelling, addition of zeolites¹⁶² turned PDMS into highly useful OSN membranes that can be used in solvents that induce very high swelling and at temperatures as high as 80 °C. The problem of reduced permeance upon filler addition was overcome by using zeolites with porous structures that avoid polymer intrusion.¹¹⁶ Gevers et al.¹⁶³ suggested that the filler–polymer adhesion has an effect on the efficiency of the filler, reducing membrane swelling, which depends on the character and the availability of functional groups at the surface. The authors suggested also that zeolites induce an increased cross-linking density, which is explained by the interactions between the silanol groups of the filler and the PDMS chains. To increase permeance in PDMS-based MMM, Vanherck et al.¹⁰⁷ used micrometer-sized hollow spheres (HS) with silicalite-1 shell as inorganic fillers, enhancing solvent permeance as compared to traditional zeolite fillers, without compromising selectivity. As a control, silicalite-1 fillers were used. In each case, the HS-filled MMMs had higher average permeances than the silicalite-1-filled MMMs. Unfilled PDMS membranes swelled in toluene, ethyl acetate, and THF. However, the hollow spheres MMM showed no problems in such solvents, confirming that the PDMS matrix was reinforced by the fillers. Silicalite fillers have also shown reduced swelling for PDMS membranes,¹⁶⁴ resulting in increased rejection of Rose Bengal and Bromothymol Blue in *n*-propanol.

The photothermal heating effect has also been studied for PDMS-TFC MMMs containing gold nanoparticles.¹⁵⁷ These membranes were prepared by an *in situ* method. The photothermal heating improved PDMS membrane fluxes without significantly lowering their rejection. The authors conclude that the extent of permeance increase depends on the laser intensity, the amount of gold nanoparticles in PDMS, the heat capacity of the solvent, and the permeate flow rate.

MOFs have also been explored as fillers in PDMS-based mixed matrix membranes.¹⁶⁵ The introduction of MOFs ($[Cu_3(BTC)_2]$, MIL-47, MIL-53(Al), and Zif-8) showed that these had a poor adhesion with the polymer, resulting in poor performance. The polymer–filler adhesion was strongly improved by modifying the MOF surfaces with *N*-methyl-*N*-(trimethylsilyl)-trifluoroacetamide. The resulting membranes showed higher rejection of Rose Bengal in isopropanol due to good interaction with the fillers and decreased membrane swelling.

Recently, Sorribas et al.¹⁶⁶ synthesized thin film nanocomposite membranes containing a range of 50–150 nm MOF nanoparticles [ZIF-8, MIL-53(Al), NH₂-MIL-53(Al), and MIL-101(Cr)] in a PA thin film layer via *in situ* interfacial polymerization on top of cross-linked PI porous supports. Membranes were activated by a DMF treatment before usage, as previously reported by Jimenez Solomon et al.¹⁰⁸ Embedding of MOFs into the PA layer resulted in methanol and THF permeance increase, whereas the rejection remained higher

than 90% in all membranes. Moreover, permeance enhancement increased with increasing cage size and porosity of the MOF used as filler. The most exceptional increase in permeance for methanol/polystyrene and THF/polystyrene was obtained with the incorporation of nanosized MIL-101(Cr), with the largest cage size of 3.4 nm.

Peyravi et al.¹⁶⁷ have developed thin film nanocomposite NF membranes on PI supports, which were previously coated with poly(ethylene imine). They incorporated TiO₂ nanoparticles inside the PA layer during interfacial polymerization, resulting in higher methanol flux and good dye rejection when compared to their control TFC membrane without the nanoparticles.

Another research group has focused on making both the UF support and the top layer into MMMs. Namvar-Mahboub and Pakizeh¹⁶⁸ first developed a solvent resistant MMM support incorporating amino functionalized nanosilica in poly(ether imide) to improve its mechanical and thermal stability. They prepared a PA TFC membrane via interfacial polymerization on this support, showing a good separation performance of lube oil from MEK and toluene, achieving a lube oil rejection of 95%.

Another class of OSN MMMs was developed by Siddique et al.¹⁶⁹ by spin-coating polymer nanoparticles with methacrylate moieties of different diameters on a cross-linked polyimide UF support, followed by photo-cross-linking the nanoparticles with UV. The monomers for the nanoparticle synthesis were *N*-isopropylacrylamide (NIPAM) and 2-(hydroxy) ethyl methacrylate (HEMA), the cross-linker *N,N*-methylenebis(acrylamide) (BIS), and the stabilizer dodecyl sulfate sodium salt (SDS) and triethylamine (TEA). Membranes with different MWCO (from 200 to 1000 g mol⁻¹) in acetone and toluene were developed, and separation performance was tuned by simply varying the nanoparticles size and thickness of the nanoparticles layer. According to Siddique et al., membrane layers of these nanoparticles create a separation film functionally similar to the top layer of an asymmetric OSN membrane, where nanoscale interstitial spaces formed between the particles serve as permeation channels.

2.5. Ceramic Membranes

Ceramic materials such as silicon carbide and Zr-, Ti-, and Al-oxides^{6,53,73} are stable in organic solvents and can stand harsh temperature conditions. This makes them excellent materials for the development of ceramic membranes for OSN applications. Ceramic membranes usually possess an asymmetric structure composed of at least two porous layers.

A thin layer, which can have one or more intermediate layers, is applied by suspension coating to a porous ceramic support. The porous inorganic support has to provide sufficient mechanical stability and defines the external shape of the membrane. Membranes with pore sizes of around 30 nm (upper range UF) can be produced using the suspension coating technique, with the finest available powders (60–100 nm particle size).¹⁷⁰ To produce NF ceramic membranes with even smaller pore size, an additional defect free layer, usually prepared via the sol–gel process, is further applied. In this process, a colloidal or polymeric solution is converted into a gel. The process involves the hydrolysis and condensation of alkoxides or salts dissolved in water or organic solvents. Viscosity modifiers or binders are usually added to the sol before depositing a layer on the support by dip or spin coating, where the final gelation takes place. Finally, the gel is dried, and after controlled calcinations and/or sintering the NF ceramic

membrane is obtained. More details on the preparation of ceramic membranes can be found elsewhere.^{2,6,171}

The major challenge in developing OSN ceramic membranes was to lower their MWCO from the UF to the NF range. To achieve this for Zr- and Ti-based membranes, the particles in the sol–gel process were made smaller (2–3 nm diameter), resulting in 2–4 nm pore sizes and MWCO in the range of 1500–5000 g mol⁻¹. Tighter membranes were achieved with SiO₂ giving 1 nm pores.¹⁷² To date, the tightest hydrophilic NF ceramic membrane is made from TiO₂ with 0.9 nm pores, giving a MWCO of 450 g mol⁻¹ (obtained in water). This TiO₂-based NF ceramic membrane is commercially available under the name Inopor¹⁷¹ and has been used since 2001 for wastewater treatment in the textile industry.¹⁷² Because of the intrinsic hydrophilicity of the oxide pore surfaces, conventional ceramic NF membranes have poor permeance for apolar solvents. To render these membranes more hydrophobic, Dudziak et al.¹⁷⁰ modified the pore surface by coupling silylation. These membranes are commercially available from Inopor (Germany) and will be reviewed in more detail in section 2.6.2.

2.5.1. Research Work on Ceramic Membranes for OSN.

Most of the existing ceramic nanofiltration membranes are made of metal oxides such as alumina, zirconia, titania, or mixed oxides. The first works reporting the use of ceramic membranes for OSN were by Tsuru et al.^{45,173} They produced porous silica–zirconia membranes with pore diameters of 1–5 nm and tested them in alcohols (methanol, ethanol, and 1-propanol). Tsuru et al.¹⁷⁴ prepared also titania membranes by sol–gel technique, with pore sizes ranging from 1 to several nanometers, and applied them to permeation of *n*-hexane as a model nonaqueous solution system. These membranes showed a decrease in the *n*-hexane flux with an increase in water concentration, which was dissolved in *n*-hexane up to several hundred ppm. Interestingly, negative rejection of linoleic acid was observed during nanofiltration of linoleic acid/*n*-hexane solutions; that is, the linoleic acid was concentrated in permeate.

The existing oxide membranes have a hydrophilic nature and therefore an intrinsic high water flux.¹⁷⁵ In apolar organic solvents, they are less applicable due to the low solvent fluxes.¹⁷⁶ Better flux for apolar solvents can be achieved by grafting the top layer with hydrophobic groups (for example, by silanation). Tsuru et al.¹⁷⁶ modified the silica–zirconia membranes via a gas-phase reaction with trimethylchlorosilane at 200 °C to produce organic/inorganic hybrid membranes. The permeances of pure nonaqueous solvents and separation performance of alcohol and alkane solutes in ethanol were investigated. Their modified silica–zirconia membrane with an average pore size of 1 nm showed a MWCO of approximately 200 g mol⁻¹ and permeate flux of approximate 2 kg m⁻² h⁻¹ at 60 °C and 30 bar. Tsuru et al.¹⁷⁷ observed also that, in the presence of traces of water in *n*-hexane (10–100 ppm), an unmodified membrane showed a decrease in the permeance with increasing water concentration, while trimethylchlorosilane-modified membranes showed approximately the same *n*-hexane permeance, irrespective of water concentration. These results suggest that small amounts of water can adsorb to the inner surface of unmodified silica–zirconia membranes and block the permeation of *n*-hexane.

Recently, Tsuru et al.¹⁷⁸ prepared organic/inorganic hybrid membranes with pores of 2–4 nm from methylated SiO₂ colloidal sol solutions: the porous substrates were coated

with the methylated SiO_2 solutions and calcinated at 400–600 °C in an inert atmosphere. Methylated SiO_2 membranes were used for the nanofiltration of polyolefin oligomers in *n*-hexane solutions. They showed a *n*-hexane permeance of 7.2–27 $\text{L m}^{-2} \text{ h}^{-1} \text{ bar}^{-1}$, with MWCO of 1000–2000 g mol^{-1} .

Van Gestel et al.¹⁷⁹ modified the surface of hydrophilic $\gamma\text{-Al}_2\text{O}_3$ /anatase-TiO₂ multilayer membranes by a silane coupling treatment. *n*-hexane and water permeance were studied before and after silane treatment as an indication of the effect of the modification. No *n*-hexane permeance was obtained before modification, while the modified membranes were characterized by a MWCO of 410–650 g mol^{-1} and a *n*-hexane permeance of 3–5 $\text{L m}^{-2} \text{ h}^{-1} \text{ bar}^{-1}$.

Verrecht et al.¹⁸⁰ chemically modified the surface of a mesoporous $\gamma\text{-Al}_2\text{O}_3$ by reactions with different coupling agents (organochlorosilanes, fluoroalkylchlorosilanes, organophosphorus coupling agents). Difunctional and trifunctional silane reagents provided the best results, that is, an increase of the *n*-hexane permeance and only a slight decrease of the water permeance.

Rezaei Hosseiniabadi et al.¹⁷⁵ prepared functionalized ceramic nanofiltration membranes to be used for solvent filtration. The membranes were grafted using a novel method for surface modification based on Grignard chemistry. The result of this method is a direct, covalent bonding of the aimed functional group (R) to the metal (M, with M = Al, Zr, or Ti) of the metal oxide matrix, M–R. To generate a more hydrophobic membrane surface, commercially available 1 nm TiO₂ membranes were differently functionalized with a series of alkyl groups (methyl, pentyl, octyl, dodecyl). This occurred via partial replacement of the OH-groups on the membrane surface and the consequent amphiphilic character of the modified membrane surface. These new partially hydrophobic ceramic nanofiltration membranes were able to permeate both polar and apolar solvents, with high fluxes, and the rejection of polystyrene in acetone was significantly enhanced after modification (the performance was comparable to that of the DuraMem 300).

Recently, Ngamou et al.¹⁸¹ reported a proof of concept for applying an expanding thermal plasma to the synthesis of perm-selective hybrid silica films from an organically bridged monomer, 1,2-bis(triethoxysilyl)ethane. The authors showed that the organic bridging groups could be retained in the separating layer, by tuning the plasma and process parameters. A defect free film could be made this way. They tested the pervaporation performance only, but suggested that such membranes can be useful in OSN if they can be deposited on flexible, porous, and large area supports. An overview of recent development of hybrid silica membranes that contain organic bridges is reported by Agirre et al.¹⁸²

2.6. Commercial OSN Membranes

Excellent membranes are available at present for OSN applications. Commercial OSN membranes are made of both polymeric and inorganic materials. Apart from membranes specifically designed for OSN, membranes developed for water applications and used for OSN are also discussed in this section.

2.6.1. Commercial Polymeric Membranes. Commercial polymeric OSN membranes include the Starmem and the Koch SelRO membranes and the recently commercialized SolSep, DuraMem, and PuraMem membranes. Most of these membranes are ISA membranes. Membranes developed for

the water treatment market, such as Desal-5 and Desal-5-DK manufactured by Osmonics, are also effective for OSN applications in certain organic solvents.

2.6.1.1. Koch SelRO Membranes. Koch Membrane Systems, U.S.,¹⁸³ was the first company to enter the OSN market in the late 1990s. They produced OSN flat sheet hydrophobic composite membranes, MPF-60 and MPF-50 (now withdrawn from the market), consisting of a PDMS layer coated on top of a PAN support, which was cross-linked through reaction and heat treatment.^{184,185} According to the manufacturer, their hydrophilic MPF-50 and MPF-60 membranes were stable in methanol, ethanol, isopropanol, butanol, acetone, *n*-hexane, cyclohexane, MEK, dichloroethane, pentane, trichloroethane, methyl isobutyl ketone (MIBK), formaldehyde, ethylene glycol, propylene oxide, methylene chloride, nitrobenzene, THF, diethyl ether, ethyl acetate, acetonitrile (ACN), carbon tetrachloride, xylene, dioxane, and toluene, and had limited stability in DMF, NMP, and DMAc.¹⁸³ The MPF 50 and 60 membranes have been tested in many applications, including recovery of organometallic complexes from DCM, THF, and ethyl acetate, and of phase transfer catalysts from toluene, for solvent exchange in pharmaceutical manufacturing and separation of triglycerides from *n*-hexane.²

2.6.1.2. Starmem Membranes (W. R. Grace & Co.). These membranes were distributed by Membrane Extraction Technology (MET) but are no longer available in the market. This membrane series consisted of hydrophobic ISA membranes manufactured from polyimides by phase inversion.¹⁸⁶ The membranes were stable in alcohols (ethanol, isopropanol, and butanol), alkanes (*n*-heptane and *n*-hexane), ethers (MEK and MIBK), and other solvents such as butyl acetate and ethyl acetate. Starmem membranes have been tested in many applications, such as catalyst recycle and product separations, solvent exchange in pharmaceutical manufacturing, membrane bioreactors (MBRs) for biotransformations, ionic liquid-mediated reactions, and microfluidic purifications.² Starmem membranes were the first OSN membranes applied in the refining industry, at a large scale, for solvent recovery from lube oil dewaxing since 1998 (MAX-DEWAX).²⁸

2.6.1.3. SolSep Membranes. These membranes are distributed by the Dutch company SolSep BV³⁰ and consist of six NF-membranes with different chemical stabilities and MWCO values between 300 and 750 g mol^{-1} , and two UF-membranes with a MWCO around 10 000 g mol^{-1} . They are chemically stable in alcohols, esters, and ketones, and some membranes are also stable in aromatics and chlorinated solvents. It is believed that these membranes are TFC membranes, and that some of them possess a silicone top layer.¹⁸⁷ There are limited publications on the performance of these membranes.^{2,57,187–189} In 2006, AkzoNobel reported filtration data for SolSep 030306F in ethanol, isopropanol, *n*-hexane, *n*-heptane, cyclohexane, toluene, xylene, and butyl acetate.¹⁸⁹

2.6.1.4. DuraMem Membranes. These membranes are distributed by Evonik-MET Ltd.¹⁹⁰ They are ISA OSN membranes based on cross-linked polyimide¹⁹¹ prepared by phase inversion. These membranes are available in a wide range of MWCOs (150–900 g mol^{-1}) as flat sheets and spiral-wound elements (1.8 in. × 12 in., 2.5 in. × 12 in., 2.5 in. × 40 in., 4.0 in. × 20 in., 4.0 in. × 40 in., 8.0 in. × 40 in., with active membrane areas of 0.11, 0.17, 1.8, 2.0, 5.4, 24.0, respectively, and feed spacer of 31 mil).¹⁹⁰ They possess excellent chemical stability in a range of solvents, including polar aprotic solvents.⁸⁴ They are stable in solvents including ethanol,

Table 4. Summary of Polymeric, MMM, and Ceramic Membrane Performance

membrane type	membrane material	solvent	permeance (L m ⁻² h ⁻¹ bar ⁻¹)	marker	marker MW (g mol ⁻¹)	rejection (%)	ref
polymeric ISA	CA	ethanol	0.4	Bromothymol Blue	624	82	156
	cross-linked P84 PI	DMF	1.6	styrene oligomers	236–1200	95 (236 g mol ⁻¹)	80
	P84 PI	toluene	3.6	styrene oligomers	236–1200	95 (236 g mol ⁻¹)	80
	cross-linked P84 PI	DMF	0.5	styrene oligomers	236–1200	90 (236 g mol ⁻¹)	
	cross-linked HT PI	DMF	1.6	styrene oligomers	236–1200	92 (236 g mol ⁻¹)	81
	cross-linked Matrimid PI	DMF	1.0	styrene oligomers	236–1200	90 (500 g mol ⁻¹)	
	cross-linked PI	DMF	2.8	styrene oligomers	236–1200	92 (236 g mol ⁻¹)	83
		THF	0.1	styrene oligomers	236–1200	92 (236 g mol ⁻¹)	108
	DuraMem 150 (cross-linked PI)	acetone	0.3			99 (236 g mol ⁻¹)	
		ethanol	0.06	azobenzene	182	41	145
	Starmem 122 (PI)	toluene	0.6	styrene oligomers	236–1200	87 (236 g mol ⁻¹)	108
	Starmem 240 (PI)	isopropanol	1.1	Rose Bengal	1017	99.9	127
		<i>n</i> -heptane	0.1	styrene oligomers	236–1200	90 (400 g mol ⁻¹)	43
		toluene	0.7			90 (380 g mol ⁻¹)	
	cross-linked PANI	DMF	0.6	styrene oligomers	236–1200	95 (300 g mol ⁻¹)	61
		acetone	1.4			99 (236 g mol ⁻¹)	
		DCM	0.8			100 (236 g mol ⁻¹)	
		methanol	0.8			97 (236 g mol ⁻¹)	
		ethyl acetate	1.0			95 (236 g mol ⁻¹)	
cross-linked PBI	acetone	15.6	styrene oligomers	236–1200	80 (236 g mol ⁻¹)	62	
	THF	3.5				87 (236 g mol ⁻¹)	
	DCM	9.6				87 (236 g mol ⁻¹)	
	DMF	0.4				99 (236 g mol ⁻¹)	
PSf/SPEEK	isopropanol	0.47	Rose Bengal	1017		96	63
		0.9	Methyl Orange	327		59	
	2-butanol	0.05	Rose Bengal	1017		94	
		0.07	Methyl Orange	327		67	
PSf	isopropanol	0.07	Rose Bengal	1017		92	85
		<0.1				95	87
		4.5				>90	88
PPSf	methanol	0.4	Rose Bengal	1017		88	89
hollow fiber PPSf	isopropanol	0.02	Rose Bengal	1017		98.6	90
blend PPSf/PI	methanol	2	Sudan II	276		95	91
PEEKWC	isopropanol	0.9	Rose Bengal	1017		99.8	92
	methanol	1.7				90	
TBPEEK	isopropanol	0.4	Rose Bengal	1017		90	93
BPAPEEK		0.1				87	
TBPEEK	isopropanol	1	Rose Bengal	1017		90	94
VAPEEK	isopropanol	0.1	Rose Bengal	1017		90	95
	methanol	0.2				90	
cross-linked P84 PI	acetone	0.3	styrene oligomers	236–1200	90 (236 g mol ⁻¹)	101	
	toluene	0.2			90 (236 g mol ⁻¹)		
	DMF	0.2			90 (236 g mol ⁻¹)		
PAI	acetone	1.2	styrene oligomers	236–1200		>90	102
PSf	ethyl acetate	8.1	Rose Bengal	1017		91	103
	isopropanol	0.2				94	
cross-linked PI	isopropanol	1.4	Rose Bengal	1017		96	
PSf	isopropanol	1.2	Rose Bengal	1017		94	105
cross-linked PBI	acetonitrile	17–37	polyethylene glycols	400–8000	90 (2000 g mol ⁻¹)	111	
	DMF	1–7					
PBI	ethanol	3.7	Brilliant Blue R	826		99	112
	ethyl acetate	5.2				90	
molecularly imprinted PBI	acetonitrile	4	roxythromycin	837		99.3	113
polymeric TFCs via interfacial polymerization	PA/PAN	methanol	6.0	oleic acid	282	93	114
		acetone	6.0			92	
	(PA/PDMS)/PAN	<i>n</i> -hexane	9.0	oleic acid	282	93	115, 116

Table 4. continued

membrane type	membrane material	solvent	permeance (L m ⁻² h ⁻¹ bar ⁻¹)	marker	marker MW (g mol ⁻¹)	rejection (%)	ref
polymeric TFCs via coating	PA/PP	methanol	0.12	Safranin O	351	45	120
			0.15	Brilliant Blue R	826	88	
	PA/PSf	methanol	2	Bromothymol Blue	624	>90	123
				Crystal Violet	407	>90	
	PA/cross-linked P84 PI	methanol	1.5	styrene oligomers	236–1200	98 (236 g mol ⁻¹)	108,
		acetone	2.4			95 (236 g mol ⁻¹)	109
		DMF	1.5			91 (236 g mol ⁻¹)	
		THF	1.8			100 (236 g mol ⁻¹)	
		ethyl acetate	0.9			85 (236 g mol ⁻¹)	
		toluene	0.3			96 (236 g mol ⁻¹)	
polymeric TFCs via coating	hydrophobic PA/cross-linked P84 PI	THF	1.5	styrene oligomers	236–1200	100 (236 g mol ⁻¹)	109
		toluene	1.7			97 (236 g mol ⁻¹)	
		ethyl acetate	3.0			90 (400 g mol ⁻¹)	
	PA/PEEK	THF	0.9	styrene oligomers	236–1200	92 (236 g mol ⁻¹)	124
	hydrophobic PA/PEEK	toluene	2.0	styrene oligomers	236–1200	98 (236 g mol ⁻¹)	124
	cross-linked PI/cross-linked PI	DMF	0.7	Solvent Blue 35	350	46	110
		NMP	0.2			62	
	PDMS/PI	isopropanol	0.2	Rose Bengal	1017	100	107
			0.5			87	165
		toluene	1.2	Wilkinson catalyst	925	78	162
polymer TFCs via interfacial polymerization	PTMSP/PAN	ethanol	4.8	Remazol Brilliant Blue	626	90	125
		<i>n</i> -heptane	5.0	HPB	535	70	43
	polypyrrole/PAN-H	THF	67.1	Rose Bengal	1017	98	127
		DMF	0.05			91	
		isopropanol	2.7			99	
	polypyrrole/(PSf/SPEEK)	isopropanol	1.1	Rose Bengal	1017	98	
			0.8	Acid Fuchsin	586	83	
	polypyrrole/PI (acid treated)	isopropanol	0.03	Rose Bengal	1017	95	
	polypyrrole/PAN-H	isopropanol	0.79	Rose Bengal	1017	99.2	128
	PIM-1/PAN	ethanol	3.0	HPB	535	78	43
(PIM-1/PEi)/PAN		methanol	6.0			73	
		<i>n</i> -heptane	5.0			90	
			4.0	styrene oligomers	236–1200	90 (236 g mol ⁻¹)	
		ethanol	1.4	HPB	535	85	
		methanol	3.6			91	
		acetone	4.0			91	
		<i>n</i> -heptane	1.0			97	
		toluene	1.1			94	
			3.1	styrene oligomers	236–1200	90 (430 g mol ⁻¹)	
	PIM-1/cellophane	ethanol	0.06	Remazol Brilliant Blue	626	98	134
(PS-b-PEO/PAA)/alumina		methanol	0.1	Polyethylene glycols	200–900	80 (370 g mol ⁻¹)	136
		acetone	0.04			90 (370 g mol ⁻¹)	
		DMF	0.02			78 (370 g mol ⁻¹)	
		DCM	0.05			90 (370 g mol ⁻¹)	
	segmented polymer networks / PAN-H	isopropanol	0.4	Rose Bengal	1017	99	137
(SPEEK/PDDA)/PAN		THF	1.3			99.3	
		DMF	2.7			96	
		isopropanol	0.5	Rose Bengal	1017	99	140
		THF	8.82			98	
		DMF	0.05			92	
(PDDA/PSS)/PAN (PDDA/PVS)/PAN	isopropanol	1.6	Rose Bengal	1017		99	141
	DMF	0.2				98	
(PDDA/PAA)/PAN (PAA/BPEi/PSf)	acetonitrile	2	Rose Bengal	1017		90	142
	<i>n</i> -hexane	29.6	antracene	178		68	143
(PDDA/SPEEK)/PAN-H/Si	isopropanol	0.1	Rose Bengal	1017		99	144
	THF	10				98	
	DMF	0.07				89	

Table 4. continued

membrane type	membrane material	solvent	permeance (L m ⁻² h ⁻¹ bar ⁻¹)	marker	marker MW (g mol ⁻¹)	rejection (%)	ref
polymeric TFCs via plasma polymerization	PIM-1/alumina	<i>n</i> -heptane	18	HPB	535	90	135
	DLC/alumina	ethanol	64.4	azobenzene	182	94	145
			59.8	fluorescein-4-isothiocyanate	389	99	
			55.8	protoporphyrin IX	563	100	
MMM ISA	cross-linked P84 PI/ TiO ₂	DMF	2.1	styrene oligomers	236–1200	90 (236 g mol ⁻¹)	155
	CA/gold nanoparticles	ethanol	1.5	Bromothymol Blue	624	82	156
	P84 PI/gold nanoparticles	ethanol	0.2	Methyl Orange	324	82	158,
			2.9	Bromothymol Blue	624	58	159
		isopropanol	0.9	Rose Bengal	1017	55	
			0.9	Methyl Orange	324	95	
			0.1	stylene oligomers	236–1200	99	
	APTMS/PI	acetone	7.5			>95	160
		DCM	3			>90	
MMM TFCs via coating	MOF HKUST-1	acetone	15	styrene oligomers	236–1800	90 (1800 g mol ⁻¹)	161
	(PDMS/gold nanoparticles)/PI	isopropanol	0.04	Bromothymol Blue	624	97	157
	(PDMS/zeolites)/PI	toluene	0.6	Methyl Orange	324	99	
		ethyl acetate	0.6	Wilkinson catalyst	925	99	162,
		DCM	0.7			97	163
		THF	0.9			93	
	(PDMS/MOFs)/PI	isopropanol	0.6	Rose Bengal	1017	80	
	(PDMS/silicalite)/PI	isopropanol	0.3	Rose Bengal	1017	98	165
		THF	1.9	Bromothymol Blue	624	100	107
		toluene	0.9			79	
		ethyl acetate	1.0			80	
MMM TFCs via interfacial polymerization	(PDMS/silicalite hollow spheres)/PI	isopropanol	1.1	Rose Bengal	1017	100	
		THF	2.8	Bromothymol Blue	624	78	
		toluene	1.3			98	
		ethyl acetate	1.5			100	
	polymer nanoparticles/ PI	acetone	1.3	styrene oligomers	236–1200	90 (220 g mol ⁻¹)	
		toluene	0.6			90 (220 g mol ⁻¹)	
		methanol	3.9	styrene oligomers	236–1200	96 (236 g mol ⁻¹)	166
		THF	11.1			97 (236 g mol ⁻¹)	
	TiO ₂ nanoparticles + PA/PI	methanol	24	Bromothymol Blue	624	>90	167
	UZM-5/PA/(PEI/ modified SiO ₂)	MEK/ toluene	1	Crystal Violet	407	>90	
		methanol	0.4	lube oil		95	168
		acetone	0.4	Victoria Blue	506	99	
		70%v ACN/ water	6.0	Erythrosine B	880	97	
ceramic	Inopor TiO ₂ /alumina	methanol	0.4	3-nitro-2-pyridinethiol	156	38	196
		acetone	0.4			197	
	Inopor TiO ₂ /alumina	70%v ACN/ water	6.0	polyethylene glycols	200–2000	90 (2000 g mol ⁻¹)	173
	SiO ₂ /ZrO ₂ (9/1) /alumina	methanol	2.7				
	TiO ₂ /alumina	<i>n</i> -hexane	0.36	linoleic acid	280.5	−50	174
	SiO ₂ /ZrO ₂ + trimethylchlorosilane/ alumina	ethanol	0.003	<i>n</i> -hexane	86	40	176
	methylated SiO ₂ / alumina	<i>n</i> -hexane	7.2–72	olefin oligomers	500–2500	80–95 (1500 g mol ⁻¹)	178
	Grignard grafted TiO ₂ / alumina	acetone	10	styrene oligomers	236–1200	85 (580 g mol ⁻¹)	175

ethanol, isopropanol, acetone, THF, DMF, DMSO, DMAc, ACN, MEK, and ethyl acetate and are not recommended in the presence of chlorinated solvents and strong amines. Their applications at high temperatures are limited by possible reimidization and loss of cross-linking at elevated temperatures.

2.6.1.5. PuraMem Membranes. This new membrane is distributed by Evonik-MET Ltd.¹⁹⁰ According to the supplier, this membrane is an integrally skinned OSN membrane based on P84 polyimide, and is available in a wide range of MWCOs (280–600 g mol⁻¹) in both configurations, flat sheets and

spiral-wound elements (11.8 in. \times 12 in., 2.5 in. \times 12 in., 2.5 in. \times 40 in., 4.0 in. \times 20 in., 4.0 in. \times 40 in., 8.0 in. \times 40 in., with active membrane areas of 0.11, 0.17, 1.8, 2.0, 5.4, 24.0, respectively, and feed spacer of 31 mil).¹⁹⁰ It possesses excellent chemical stability in a range of solvents, including apolar hydrocarbon-based solvents. It is stable in solvents including *n*-hexane, *n*-heptane, toluene, MEK, MIBK, and ethyl acetate and is not recommended in most polar aprotic solvents, chlorinated solvents, and strong amines.

2.6.1.6. PuraMem S600 Membranes. This new membrane is distributed by Evonik-MET Ltd.¹⁹⁰ According to the supplier, this membrane is a rubber-coated polyimide membrane, and is available in a MWCO of 600 g mol⁻¹ in both configurations, flat sheets and spiral-wound elements (1.8 in. \times 12 in., 2.5 in. \times 12 in., 2.5 in. \times 40 in., 4.0 in. \times 20 in., 4.0 in. \times 40 in., 8.0 in. \times 40 in., with active membrane areas of 0.11, 0.17, 1.8, 2.0, 5.4, 24.0, respectively, and feed spacer of 31 mil).¹⁹⁰ It is stable in solvents including ethanol, isopropanol, butanol, *n*-hexane, *n*-heptane, toluene, MEK, MIBK, and ethyl acetate.

2.6.1.7. GMT Membranes. These membranes are distributed by GMT-GmbH, Germany.³¹ They are TFC OSN membranes based on a silicone separation layer. Their silicone separation layer is applied as a coating and then cross-linked by irradiation to avoid swelling in organic solvents; this cross-linking process has been patented.¹⁹¹ GMT has two membrane modules available: spiral wound modules for treatment of aqueous/organic liquids (size of 2.5 in., 4 in., 8 in. \times 40 in., feed flow of 2–30 m³ h⁻¹), and envelope-type module for OSN (feed flow of 0.5 m³ h⁻¹).

2.6.1.8. PoroGen Membranes. PoroGen manufactures PEEK hollow fiber membranes (PEEK-SEP) with tailored pore size and surface chemistry.¹⁹³ PEEK-SEP hollow fiber membranes are claimed to be able to operate at high temperature in aggressive environments and are designed to reject molecules with sizes in the order of nanometers, which are dissolved in organic solvent. These separations are enabled by the exceptional chemical and thermal durability of PEEK. PoroGen claims to be currently developing several industrial scale nanofiltration applications. No flux or rejection data are available for these membranes.

2.6.1.9. AMS Technologies Membranes. AMS Technologies offers an extensive line of innovative acid-resistant, alkaline-resistant, and solvent-stable nanofiltration and ultrafiltration membranes with elements for use in acid, alkaline, and organic solvent media.¹⁹⁴ They produce chemically and thermally stable NanoPro and UltraPro membranes, which are applicable to a wide range of industrial separations. All of their products are packaged in a spiral wound configuration of 2.5 in., 4 in., and 8 in. diameter with 31 and 46 mil spacers and a variety of components suitable for working in harsh environments. Other spacer sizes are available on request. No flux or rejection data are available for these membranes.

2.6.1.10. PolyAn Membranes. PolyAn is specialized in molecular surface engineering and molecular surface imprinting.¹⁹⁵ They offer a range of composite membranes for organophilic pervaporation and OSN. These membranes are claimed to be applicable for the separation of aromatics from aliphatics, olefins from aliphatics, and the separation of other organic mixtures. No flux or rejection data are however available for these membranes applied to OSN.

2.6.2. Commercial Ceramic Membranes. For a long time, the tightest ceramic membranes had a MWCO of around 1000 g mol⁻¹. NF membranes with pore sizes lower than 1 nm

were developed starting from the end of the last century. These membranes are based on silica membranes doped with zirconia and titania. An NF ceramic membrane based on TiO₂ with pore size of 0.9 nm and a MWCO of 450 g mol⁻¹ in water has been developed by a spin-off company of HITK (Germany), now known as Inopor, and commercialized under the name of Inopor.¹⁷¹ The Inopor company currently offers a range of ceramic UF and NF membranes in the form of mono- and multichannel tubes with lengths up to 1200 mm. The membranes are offered as a hydrophilic version; however, they can be made hydrophobic, on customer request. Although there is no specific information on the Web about the hydrophobic membranes, it is believed that the literature-cited HITK-T1 is a silylated TiO₂-based version of the hydrophilic membranes.¹⁰ The hydrophobic membranes showed a nominal MWCO of 220 g mol⁻¹ and methanol and acetone permeances of around 0.4 L m⁻² h⁻¹ bar⁻¹, with a 99% rejection of Victoria Blue (506 g mol⁻¹) in methanol, and a 97% rejection of Erythrosine B (880 g mol⁻¹) in acetone.¹⁹⁶ They also showed efficient catalyst recovery for Pd-2,2'-bis(diphenylphosphino)-1,1'-binaphthyl (BINAP) (849 g mol⁻¹) with rejections around 94.5%.²

2.7. Summary of Membrane Performance

In desalination, it has been shown that the manufacturing of TFC membranes is more expensive than the manufacturing of ISA membranes. However, the improved performance characteristics of the resulting membrane products counterbalance the extra cost of manufacturing TFC membranes.⁶⁶ In a similar way, TFC OSN membranes have the potential to achieve higher fluxes than ISA OSN membranes, without compromising selectivity.¹⁰⁸

A critical summary of nanofiltration performance for polymeric (ISA and TFC), MMM (ISA and TFC), and ceramic membranes is reported in Table 4. For each reference, when more than one membrane was tested, the tightest membrane was chosen and reported in the table. When more than one solute was tested, the rejection of the solute with the lowest MW or with a MW that is rejected close to 90% was selected.

In general, Table 4 shows that polymeric TFC membranes have higher permeances than ISA membranes in both polar and apolar solvents, suggesting that making the top layer in a separate step represents an advantage for solvent flux. In TFC membranes, the thin barrier layer can be optimized for the desired flux and solute rejection, while the porous support can be optimized to achieve maximum strength and compression resistance and minimum resistance to permeate flow. Moreover, a large variety of chemical compositions, including both linear and cross-linked polymers, can be used to form the thin barrier layer, whereas the asymmetric membrane formation process is limited to linear, soluble polymers. Only a few of such linear polymers have the right combination of flux and solute rejection characteristics to generate commercially attractive membranes.⁶⁷

High permeance and high rejection values were obtained with high-porosity nanostructured TFCs and with TFCs via plasma polymerization. Membranes made of PIM-1 showed high permeance for apolar solvents and alcohols, in comparison with commercial Starmem membranes. The free-standing DLC membranes on alumina supports prepared via plasma polymerization by Karan et al.¹⁴⁵ showed tremendously higher

permeance and rejection in ethanol, in comparison with the commercial DuraMem 150 membrane.

As shown in Table 4, addition of fillers to MMMs can improve permeance and in certain cases increase rejection. The addition of TiO_2 and gold nanoparticles to ISA and TFC membranes to obtain MMMs allowed the attainment of higher permeance, without compromising rejection,^{155,156,158,159} in aprotic solvents and alcohols. The addition of zeolites, MOFs, and silicalite to TFC membranes allowed the achievement of both higher permeance and higher rejection, in comparison with the corresponding polymeric TFC membranes^{107,162,163,165,166} in apolar and polar solvents. The presence of filler materials in PDMS MMMs also resulted in less membrane compaction and swelling.

The general trend suggests that the next generation high permeance OSN membranes should be TFC or free-standing membranes engineered at a nano level,^{43,145} and that nanomaterials will be added to the polymer matrix.

Commercial ceramic membranes have been used for OSN^{188,197} and showed fluxes in acetone and methanol similar to those of polymeric membranes, but they are looser (in comparison with the DuraMem 150,¹⁰⁸ for example). Ceramic membranes have been used in ACN/water mixtures¹⁹⁷ and showed high solvent permeance but also low rejection of a small organic solute (3-nitro-2-pyridinemethiol). Hybrid $\text{SiO}_2/\text{ZrO}_2$ and TiO_2 membranes were prepared by Tsuru et al.^{45,174} In methanol, hybrid $\text{SiO}_2/\text{ZrO}_2$ showed performance in the loose NF range.⁴⁵ In *n*-hexane, negative rejection of linoleic acid through TiO_2 membranes was observed.¹⁷⁴

From a general point of view, it is difficult to compare nanofiltration performance data from literature in more detail, due to the fact that many systems (both solutes and solvents) have been chosen by different authors to characterize the membrane MWCO (cf., Table 1), different concentrations of the solutes have been used, and different operating conditions were also adopted (cross-flow vs dead end, different operating pressure, flow rate, etc.). On the basis of this observation, we suggest that the use of standard testing systems and conditions would improve and accelerate the procedure for membrane comparison, characterization, and selection.

2.8. Membrane Physicochemical and Structural Characterization

Functional parameters, such as rejection and flux, determine the selection of a certain type of membrane for a specific application,¹⁹⁸ as described in section 2.1. Flux decline due to aging or compaction is an indication of poor stability, and a decrease in rejection in certain solvents can be a consequence of poor chemical stability (e.g., polymer swelling). Physicochemical parameters include hydrophobicity, hydrophilicity, swelling, pore size, pore size distribution, porosity, skin layer thickness, and charge. To date, the development of NF membranes to achieve a specific performance remains a challenge. Better understanding and characterization of their structure at a molecular level might allow better prediction of performance, and improvement in membrane design. The most important membrane physicochemical and structural descriptors and the corresponding characterization technique are discussed in the following paragraphs, and a summary of the parameters is shown in Table 5.

2.8.1. Physicochemical Characterization. The surface properties of the membrane have significant effects on the membrane performance. The contact angle technique is a

Table 5. Membrane Physicochemical and Structural Descriptors and the Corresponding Characterization Technique

membrane property	characterization technique
Physical Properties	
hydrophilicity/ hydrophobicity	contact angle
porosity	gas adsorption–desorption; mercury porosimetry
swelling	swelling test
Chemical Properties	
surface chemistry	attenuated total reflection Fourier transform infrared spectroscopy; X-ray photoelectron spectroscopy
Structural Properties	
cross-section	scanning electron microscopy; transmission electron microscopy; atomic force microscopy
surface roughness	scanning electron microscopy; atomic force microscopy
thickness of top layer	scanning electron microscopy; positron annihilation spectroscopy

captive bubble method suitable for the characterization of membrane surface properties, and capable of estimating differences in hydrophobicity between different membranes.¹⁹⁹ In membrane science, the contact angle is a measure of wettability of the membrane. A contact angle of zero degree (assuming water as the droplet) corresponds to an ideal hydrophilic surface.

Porosity is the fraction of accessible free volume of the membrane (defined as the volume of the pores divided by the total volume of the membrane). Two techniques are commonly used to determine membrane porosity: (a) gas adsorption–desorption; and (b) mercury porosimetry.²⁰⁰ Gas adsorption–desorption is used to determine the specific area, pore volume, and pore size distribution of porous materials.²⁰⁰ Frequently nitrogen is used as condensable gas at its boiling point. In this method, the volume of gas adsorbed at various vapor pressures is measured both for an adsorption and for an desorption step. A disadvantage is that this technique determines the porosity of the whole membrane and not only the porosity of the top layer, and that measurements are done dry so the pores of the polymeric membranes may collapse. Mercury intrusion porosimetry is used extensively for the characterization of porous materials, including membranes. It consists of measuring the volume of mercury, which is forced into the pores of an evacuated porous sample. By this technique, both pore size and pore size distribution can be determined.²⁰⁰ Some disadvantages of this technique are that it requires high pressure, which could damage the surface or the porous structure, and that it measures all of the pores present in the structure, including dead end pores.

Polymer swelling can have an effect on flux and rejection for OSN membranes.^{40,201,202} Several methods have been developed to quantify swelling of polymeric membranes. Ho and Sirkar's method²⁰³ is based on weight difference between solvent-impregnated and dry polymer samples. Piccinini et al.²⁰⁴ developed a technique in which a quartz spring microbalance was used to simultaneously measure solubility, diffusion coefficient, and swelling for a solvent/polymer combination of acetonitrile/polyetherurethane. Tarleton et al.²⁰⁵ used a new apparatus for *in situ* determination of swelling of TFC membranes, comprising a linear inductive

probe and electronic column gauge with an overall resolution of $0.1\text{ }\mu\text{m}$. Their approach has advantages over more conventional techniques including the ability to test membranes in their manufactured state. Tarleton et al.^{205,206} have reported that the extent of swelling is significantly related to the degree of polymer cross-linking and the affinity between polymer and solvent. However, it was not possible to correlate the results of the swelling experiments with the membrane performance in terms of solvent flux and solute rejection. In membrane science, Hildebrand solubility parameters indicate the ability of solvents to act as swelling agents for polymeric membranes. The Hildebrand solubility parameter is a measure of the intermolecular energy and can be calculated for liquids from the enthalpy of vaporization. Polymers degrade before vaporization, and their solubility parameters values are determined indirectly; they are assigned to the parameters of the solvent, causing the maximum swelling in a series of polymer swelling experiments.²⁰⁰

Attenuated total reflection (ATR) Fourier transform infrared (FTIR) spectroscopy is used to determine the functional chemistry of unknown materials. Functional groups in the material absorb energy at specific wavelengths, which results in an attenuated signal at the infrared detector.²⁰⁰ An interferometer is used to encode the detected signal, which is digitally Fourier transformed to produce an FTIR spectrum (absorbed intensity vs wavenumber). The resulting abruption spectrum is a unique fingerprint of a compound.²⁰⁰ ATR-FTIR is used in membrane science to characterize new structures after cross-linking and surface modification of existing membranes.²⁰⁷ The limitation of the technique for TFC membranes made of very thin top layers is that it penetrates further than the thickness of the top layer, so it is difficult to separate information on the UF support and the top layer in TFC membranes.

X-ray photoelectron spectroscopy (XPS) is used to perform chemical analysis of a sample. The sample surface is irradiated with X-rays, which produce photoelectrons in the sample, and the photoelectrons that escape into the vacuum are collected and counted as a function of their kinetic energy. A binding energy can be calculated from the kinetic energy. The binding energy is a characteristic of individual elements, which can be therefore identified. The limitation of the technique is that it can only characterize up to 12 nm in depth.²⁰⁰ However, this results in an advantage for the characterization of thin top layers for TFC membranes.

2.8.2. Microscopy. Microscopic techniques such as scanning electron microscopy (SEM),²⁰⁸ transmission electron microscopy (TEM),²⁰⁹ and atomic force microscopy (AFM)²¹⁰ made advances in the study of membrane structure possible. The imaging of nanoporous polymeric membranes at nanometer resolution is a long-standing goal of materials microscopy. The difficulty lies with the low electron contrast of polymers, which does not allow the acquisition of high magnification images.²¹¹ SEM applications are various and focus on membrane structure characterization.²¹² The major drawback of this technique is, however, that polymeric membranes are not conductive and need to be coated. AFM is a high-resolution type of scanning probe microscopy, used to profile surfaces in 3D, and makes it possible to represent nonconducting surfaces with a resolution of the order of nanometres, giving information about the membrane roughness.²¹³ The cross-section structures of NF membranes are usually characterized by SEM or TEM. Being able to image pores at the nanoscale would be greatly useful in elucidating the

functional performance of NF membranes. The interpretation of nanoscale features is challenging, as the nanostructures of NF membranes have dimensions that lie within the resolution of the microscope. AFM has been widely employed to characterize NF membranes for more than a decade to measure nodule size, pore size, and surface roughness.^{214–218} Surface roughness is an important structural property of OSN membranes and can be interpreted as the average roughness, root-mean-square (RMS) roughness, or peak-to-valley height. It is well-known that the average roughness increases with an increase of the scan size; hence, when comparing different membranes it is recommended to use the same scanning size. Recently, it has been shown that lack of resolution makes nanometer scale pore size measurements for polymeric membranes using AFM not very reliable,²¹¹ but very interesting information describing the internal polymer packing at the membrane surface can be obtained by phase imaging in AFM. It has also been demonstrated that the magnitudes of the phase lag and the dissipation energy have a correlation with the membrane functional performance (flux and selectivity).²¹¹

Recently, Stawikowska and Livingston²¹⁹ developed a technique to measure nanopores with dimensions in the $0.5\text{--}2\text{ nm}$ range for NF ISA polymeric membranes. With this nanoprobing technique, the size of the transport-active pores is measured. Nanopores in an ISA OSN polyimide membrane are filled with high contrast osmium dioxide (OsO_2) nanoparticles, whose spatial arrangement is mapped under TEM. Stawikowska and Livingston²¹⁹ found a correlation between the estimated pore size using their nanoprobing imaging technique and the membrane separation performance, suggesting that the molecular separation mechanism in P84 polyimide ISA membranes is due to size exclusion of the larger nanoparticles. This nanoprobe imaging technique has also been used to characterize TFC membranes used for OSN applications.²²⁰ The two membranes characterized were a PTMSP/cross-linked polyimide TFC membrane prepared via dip-coating, and a polyamide/cross-linked polyimide TFC membrane prepared via interfacial polymerization. Their pore size distributions were measured and correlated with the membrane functional performance, implying that their selectivity was significantly related to the pore size. The membrane cross-sectional images permitted detailed estimations of the thickness of the polyamide top layer. Nanoscale defects were detected for the PTMSP/cross-linked polyimide TFC membrane via imaging of excessive accumulations of high contrast nanoparticle in regions where the imperfections were present. The authors recommended this technique to characterize membranes under development and find causes responsible for poor reproducibility.

2.8.3. Positron Annihilation Spectroscopy. Positron annihilation spectroscopy (PAS) coupled with a slow positron beam has been used to characterize the layer structure and depth profile of the cavity size in ISA and TFC NF membranes.^{221,222} Tung et al.²²¹ were able to measure the thickness of the top layer of two different PA TFC membranes, using this nondestructive technique. Cano-Odena et al.²²² used PAS to correlate fundamental polymer properties to membrane performance for PI-based OSN membranes. They concluded that a correct membrane pretreatment was essential to enable PAS measurements. Furthermore, they observed that PAS revealed extra information with respect to SEM analysis. Thanks to PAS, they observed that the SEM skin layers consisted of three different regions: a surface layer with low

porosity, a transition layer with constantly increasing porosity, and a more porous sublayer. The porosity of the first two layers could be correlated with membrane permeance.

2.9. Membrane Configurations and Modules

Membranes can be produced in flat sheet or tubular shape, and this configuration determines the final module geometry. Polymeric membranes are usually produced as flat sheets, and the two most widely used lab-scale configurations are the dead-end and the cross-flow modes, shown in Figure 13.

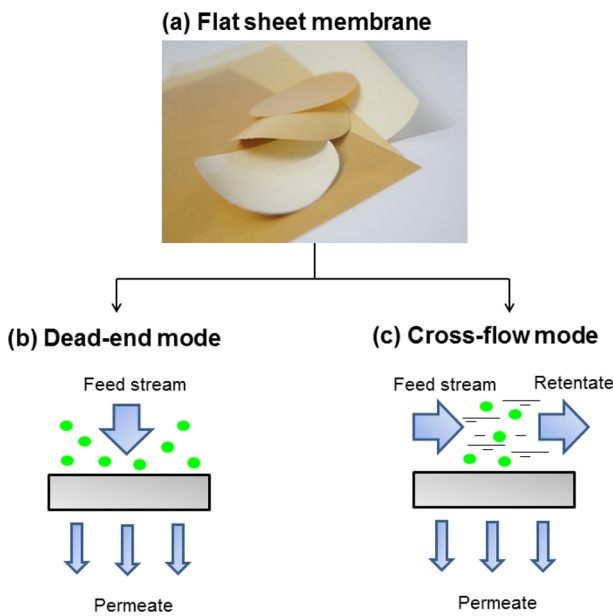


Figure 13. (a) Flat-sheet polymeric membrane. Reprinted with permission from ref 223. Copyright 2014 Evonik MET Ltd. (b) Dead-end configuration. (c) Cross-flow configuration.

The dead-end filtration mode (cf., Figure 13b) is characterized by feed flow in the same direction as the permeate flux; it is useful for membrane screening and proof of concept work. In cross-flow filtration mode (cf., Figure 13c), the feed flows tangentially over the membrane surface and perpendicularly to the permeate flux. In dead-end cells, concentration polarization can significantly affect the membrane performance even at low solute concentration values. Cross-flow mode allows better operating conditions, as it can reduce the extent of concentration polarization by increasing the shear rate over the membrane surface. In both configurations, however, osmotic pressure, gel layer formation, and other boundary layer related phenomena have to be taken into account, when working at significant solute concentrations.²²⁴

To perform separations at industrial scale, methods of efficient and economical packaging of large membrane areas are required. This is done by packing the membranes in modules. Three main factors contribute to the successful fabrication of a membrane module: the selection of the membrane material, for its appropriate chemical, mechanical, and permeation properties; the fabrication of the material into a defect-free, robust membrane; and the packaging of the membrane into a compact, high-surface-area module. The successful fabrication of efficient membrane modules is one of the reasons for the breakthrough of the membrane technology in the 1960s and 1970s.⁸ The earliest design was the plate-and-frame module, soon replaced by other more efficient and less expensive designs, the hollow fiber module, the tubular module, and the spiral-wound module. The different modules are shown in Figure 14. These modules are differentiated by compactness, fluid management, maintenance, ease of cleaning, and replacement.

In plate-and-frame modules, membrane, feed spacers, and permeate spacers are layered together between two end plates. The feed mixture is pumped across the surface of the

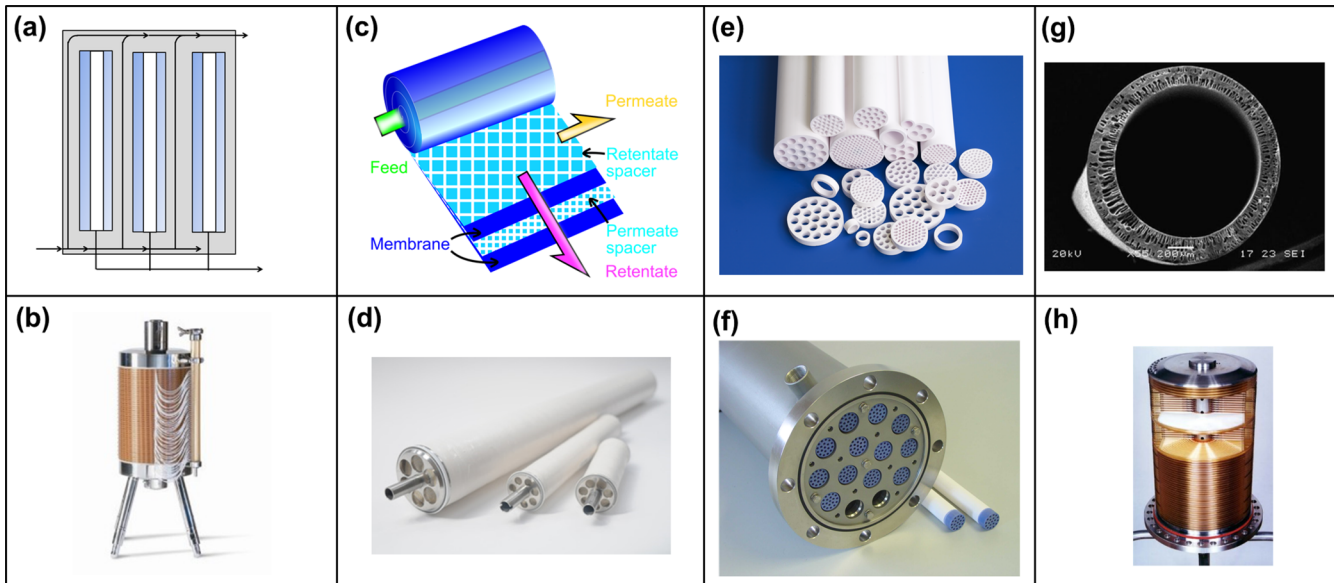


Figure 14. Membrane modules: (a) Schematic representation of plate-and-frame module; (b) plate-and-frame module (Reprinted with permission from ref 225. Copyright 2014 Alva Laval); (c) schematic representation of spiral-wound module; (d) spiral-wound module (Reprinted with permission from ref 223. Copyright 2014 Evonik MET Ltd.); (e) tubular membranes (Reprinted with permission from ref 171. Copyright 2014 Inopor); (f) housing of tubular membranes (Reprinted with permission from ref 171. Copyright 2014 Inopor); (g) SEM of hollow fiber membrane (Reprinted with permission from ref 226. Copyright 2008 Royal Society of Chemistry); and (g) envelope-type module (Reprinted with permission from ref 31. Copyright 2014 GMT Membrantechnik GmbH).

membrane. The part that passes through the membrane enters the permeate channel and is finally collected in a central permeate collection manifold.

For polymeric membranes, the spiral-wound module is the most attractive configuration at the industrial scale. In a spiral-wound module, flat membrane sheets are wound around a central collection pipe. The membrane sheets are glued along three sides and attached to the permeate channel along the unsealed edge of the leaf. To give mechanical resistance, avoid collapse due to pressure, and guide the permeate to the permeation tube, a permeate spacer is positioned between the internal sides of the leaves. A feed channel spacer separates the top layers of the membrane. The pressurized feed flows parallel to the permeation channel, while the permeate flows radially through the spiral-wound permeate spacer toward the central collection pipe. Finding adhesives that are stable in the organic solvents of interest is sometimes difficult, but this is fundamental for the implementation of such modules. Another challenge concerns when an elevated temperature is required for curing the adhesive; the membrane polymer has to be stable at the curing temperature and must not degrade or change in performance. Only a few papers report spiral-wound module performance. Among them, Sairam et al.⁶⁰ prepared a solvent stable ISA PANI membrane as a spiral-wound module. According to the authors, this membrane is suitable for solvent exchange application, due to its low MWCO. Sereewatthanawut et al.²²⁷ applied a 1.8 in. × 12 in. spiral-wound membrane module (DuraMem 200) to the separation of Solvent Yellow 7 (model product) from Brilliant Blue (model impurity) in DMF, and to separation of a real case-study API from its oligomeric impurities in THF. Silva et al.²²⁸ studied the performance of a spiral-wound membrane module (Starmem 122) over extended periods, with 0–20 wt % solutions of tetraoctylammonium bromide (TOABr) in toluene.

Inorganic membranes are usually on the market with a tubular shape, with one single channel or with complex multichannel geometries. The feed flows inside the channels, the permeate goes out in a radial direction through the porous support and the active layer, to be finally collected at the outside, as shown in Figure 14e. The module housing serves as a container for one or several filter elements. According to the needs of the application, the housing is made of stainless steel or other corrosion resistant materials. Darvishmanesh et al.,²²⁹ Marchetti et al.,^{197,230} and Buekenhoudt et al.²³¹ investigated the permeation of organic solvents through multichannel tubular ceramic membranes. Marchetti et al.²³² investigated the applicability of these membranes to peptide processes.

Hollow fiber modules consist of a bundle of fibers contained in a pressurized vessel. They can be fabricated in two geometries, shell-side feed design and bore-side feed design, depending on which side is pressurized (shell or bore side, respectively). The greatest advantage of this module is that they can pack a very large membrane area into a single module. Loh et al.²²⁶ fabricated ISA PANI hollow fibers, directly adding large organic acids to highly concentrated PANI solutions. These hollow fibers showed stability in a wide variety of organic solvents and had high rejections of most species in the nanofiltration range 200–1000 g mol⁻¹ in acetone (the MWCO was approximately 350 g mol⁻¹). The acetone permeance was around 9 L m⁻² h⁻¹ bar⁻¹.

Darvishmanesh et al.⁹⁰ developed PPSf hollow fiber membranes according to a dry-wet spinning method. The fiber dimensions could be controlled by the feed flow rate,

spinneret dimensions, air gap, and take-up speed. These membranes were already presented in section 2.3.1.1. Dutczak et al.²³³ explored a new technique called “chemistry in a spinneret”, to fabricate hollow fiber elements for organic solvent filtration. According to this technique, membrane formation and cross-linking reaction are combined into a single-step process. P84 PI was chosen as a membrane forming polymer and poly(ethylene imine) as a cross-linking agent. The authors systematically varied the composition of the bore liquid, including solvent/nonsolvent ratio and PEI concentration, to obtain a membrane with the best stability and low membrane MWCO. The final membranes had MWCO in the range of 2500–3500 g mol⁻¹ and toluene permeance in the range of 0.2–1.1 L m⁻² h⁻¹ bar⁻¹.

The envelope-type module from GMT (cf., Figure 14h) offers some advantages as compared to spiral wound modules; it has very short permeate distances, and it does not require the use of a feed spacer and a glue, which are sometimes not stable in certain solvents. It has some disadvantages as it operates at a maximum pressure of 40 bar and the membrane area covered by a spiral wound module of the same size is larger.

2.10. Future Perspectives

Nanotechnology has produced new classes of functional materials with application to desalination, water purification, and OSN processes, which need further exploration. For example, recent OSN and desalination membranes fabricated from rigid star amphiphiles,^{234,235} zeolite films,^{236,237} and carbon nanotubes^{238–240} offer exciting new possibilities. Mixed matrix or nanocomposite membranes also exhibit improved mechanical, chemical, and thermal stability as well as improved separation and permeance in OSN.

Polymeric membranes based on rigid star amphiphiles have been recently reported.^{234,235} They were prepared by direct percolation of solutions of rigid star amphiphiles in methanol, through ISA poly(ether sulfone) support membranes. The barrier layer in these membranes is 20 nm thick. These membranes exhibited very smooth surfaces with an average roughness in the range of 1–2 nm. They were able to control MWCO and obtained a narrower pore size distribution due to the composite multilayer dendrimer structure. According to Peng Lee et al.,²⁴¹ polymeric membranes fabricated by rigid star-shaped amphiphilic molecules are one of the breakthroughs since the interfacially polymerized RO/NF membrane as it offers the possibility of engineering membrane structure at a nano level. However, to date there is no reported research on the fabrication of OSN membranes using this technique.²⁴¹

UF membranes prepared by molecular imprinting of polymers with a predetermined affinity for a variety of molecules have been explored in organic solvents. These membranes are formed by adding templates into a polymer solution, and, depending on the phase separation conditions, different pore morphologies are obtained.²⁴² NF membranes made of molecular imprinted polymers are yet to be developed and could have potential in selective separations due to their high affinity to targeted molecules.

Recently, zeolite particles were employed as additives to form mixed matrix zeolite-polyamide TFC membranes by interfacial polymerization, which can increase the permeance of an RO membrane.²³⁶ The process involves a thin polyamide film periodically interrupted by NaA zeolite nanoparticles having hydrophilic and negatively charged three-dimensional molecular sieve pore network. While water diffusion through the

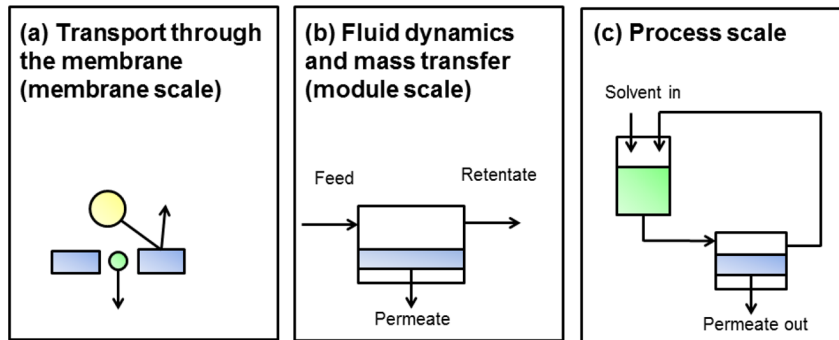


Figure 15. Modeling levels for the development of a membrane process: (a) membrane scale; (b) module scale; and (c) process scale. Adapted with permission from ref 247. Copyright 2013 Elsevier.

polyamide pores occurs only under high applied pressure, water penetrates through the nanoparticle pores with very little applied pressure. The fouling resistance is also enhanced by the hydrophilic nanoparticles, which make the overall membrane more hydrophilic. It is believed that these molecular sieve zeolite nanoparticles provide preferential water permeation paths while maintaining high solute rejection through both steric and Donnan exclusion effects.^{236,237} Pure water permeance was double ($1.4 \text{ L m}^{-2} \text{ h}^{-1} \text{ bar}^{-1}$) that of hand-cast polyamide membranes ($0.7 \text{ L m}^{-2} \text{ h}^{-1} \text{ bar}^{-1}$) with equivalent solute rejection.^{236,237} This approach has been mirrored for OSN by the MOF TFCs described by Sorribas et al.¹⁶⁶

Carbon nanotubes (CNTs) are another potential material for separation due to their fluid transport similarity with water transport channels in biological membranes.²⁴³ Membranes made from CNTs with a uniform pore distribution and a more permeable separation layer can potentially maintain or improve salt rejection while increasing permeance. Recently, it was demonstrated that the transport of water through hydrophobic double-walled carbon nanotubes was 3 orders of magnitude higher than that expected on the basis of viscous flow according to the Hagen–Poiseuille law through pores with that diameter.^{238,239} However, there are technological challenges for incorporating carbon nanotube materials, such as the development of efficient synthesis methods to align arrays of single-walled CNTs with subnanometer diameters and the functionalization of the pores to increase selectivity and potentially reduce hydrophobicity at the surface.²⁴⁴ A novel TFC polyamide membrane with embedded 0.8 nm single walled CNTs in the polyamide barrier has been patented.²⁴⁰ To blend the CNTs with the trimesoyl chloride organic solution, the CNTs were functionalized to increase their solubility in organic solvents. These novel membranes showed double the water flux and salt rejection coefficients that exceed those of TFC membranes prepared without CNTs.²⁴⁰ This novel technique to incorporate CNTs into a TFC membrane is promising and scalable, but the manufacturing costs of the suggested single walled CNTs for RO membranes can range from US \$1800 per gram and upward.²⁴¹ Unless savings from improved overall membrane performance are proven, the incorporation of CNTs into membranes for water desalination seems economically unfavorable.²⁴¹ Nonetheless, more dense and ordered packing of CNTs can further enhance the overall membrane performance. As suggested by Peng Lee et al.,²⁴¹ instead of blending CNTs with polymer solutions, in situ growth of CNTs by ceramic templating could offer a better method of engineering these novel membranes. CNTs

represent an advantage in terms of permeance and have a significant potential in OSN. However, to date no OSN membranes containing CNTs have been reported.

3. TRANSPORT MODELS AND PROCESS DESIGN

From the beginning of membrane development, a substantial amount of research has focused on the description and understanding of the transport mechanism through membranes. Mason and Lonsdale²⁴⁵ observed that, already in the 1900s, a lot of effort and time had been spent in trying to formulate general theories of membrane transport and wondered how the “experimentalists in the real world” can finally benefit from these “fancy” theories.²⁴⁵ The practical reason why understanding the basic mechanism is advantageous is that a well-founded theory (i) allows new situations to be approached with confidence; (ii) reduces the requirement for experiments; and (iii) is able to predict new phenomena.²⁴⁵

In OSN, a fundamental understanding of the basic separation mechanism is crucial to advance the field and wisely tuning materials to meet the growing needs and applications. Transport models are the tools used to understand membrane transport.²⁴⁶

The development of membrane processes involves several stages, from feasibility tests at laboratory scale, to pilot plant tests, and finally to large industrial scale processes. As illustrated in Figure 15, three levels can be distinguished within the modeling framework:²⁴⁷ (i) membrane transport mechanism; (ii) fluid dynamics and mass transfer in membrane modules; and (iii) process scale design.

From a general point of view, modeling can be applied for two purposes: design and prediction. At the membrane scale, design is performed when experimental data for standard solute + solvent systems are available, and the unknown parameters, characteristic of the model (solute, solvent, membrane, or interaction parameters), are obtained by analytical or numerical regression of the experimental data. Once the model parameters are available, modeling can be applied to perform prediction of the process performance at a different process scale (in this case, transport modeling at the membrane level has to be combined with modeling at module and process scales); and of the transport performance of a different solute + solvent system (in this case, fundamental or empirical correlations between model parameters and solute/solvent properties have to be available at the membrane scale).

Focusing now on OSN, many studies have been published in the past decade dealing with the modeling of transport at the membrane scale. On the other hand, there are only limited

studies on the fluid dynamics and mass transfer in modules, and few attempts to implement membrane transport models at process scale. According to Peshev and Livingston,²⁴⁷ by 2013 almost 50 papers deal with modeling at the membrane scale (which correspond to 91% of the studies published on OSN modeling), 2 papers deal with modeling at the module scale, and 3 papers deal with modeling at the process scale (4% and 5% of the studies published on modeling, respectively). This is shown in Figure 16.

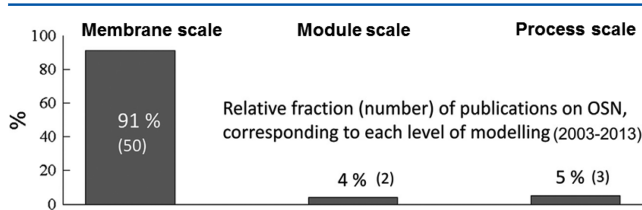


Figure 16. Numbers of relevant publications in the period 2003–2013. Reprinted with permission from ref 247. Copyright 2013 Elsevier.

In this section, the main transport models at the membrane scale, the mass transfer in the module, and the concepts of concentration polarization and osmotic pressure are introduced and critically discussed; the applications of the transport models, eventually combined with the film theory and extended to nonideal mixtures, are presented; other significant studies on solute–solvent–membrane affinity interactions, affecting transport in OSN, are discussed, and their importance for the further development of the modeling field is highlighted; and, finally, the modeling studies at the process level for process design are reviewed.

3.1. Classification of Membrane-Scale Transport Models

To describe, and possibly predict, fluxes and rejections through porous or dense membranes, the transport mechanism of solutes and solvents has to be understood. Steric and

electrostatic separation mechanisms, typical of aqueous environments, cannot be straightforwardly extended to non-aqueous systems, due to the significant differences in the structures and properties of the solvents.^{36,50,248,249} Often, it has been reported that the NF performance is much less predictable in the presence of organic solvents than in aqueous solutions,^{50,249,250} and that the separation capability of the membrane in organic solvents cannot be described by the MWCO only.⁵⁰

The transport through membranes has been described by three kinds of models. The first group is based on irreversible thermodynamics and considers the membrane as a black box, without accounting for any membrane property. The two other groups describe the transport of solutes as a function of structural and physicochemical parameters, and take into account membrane properties (they belong to the class of mechanistic models). These models are the solution-diffusion^{251,252} and pore-flow models,³⁶ respectively. Transport mechanisms with the characteristics of both pore-flow and solution-diffusion models have been also proposed, such as the solution-diffusion with imperfections model.²⁵³ Among the mechanistic models, the choice of the most suitable model class for a given type of membrane depends on the physical structure of the membrane (porous vs dense). The identification of a structure–performance relationship allows for a more fundamental understanding of membrane transport. Solution-diffusion, pore-flow, and solution-diffusion with imperfections models differ in the mathematical description of the permeation, that is, in the driving forces taken into account for the transport, and in the number of model parameters that have to be fitted or obtained from independent measurements.

A comparison of these models is reported in the following paragraphs and summarized in Table 6.

The model parameters that must be estimated for the models to be applied are reported in Table 6. Other considerations in choosing between the available models include: (i) whether it is

Table 6. Different Transport Models for OSN, Corresponding Transport Mechanism, and Model Parameters

model	transport mechanism	model parameters ($1 < i < n_{\text{solute}}$ and $1 < j < n_{\text{solvent}}$)
Irreversible Thermodynamics (IT) Models		
Kedem–Katchalsky ²⁵⁴	diffusion + convection	P_p, L_p, σ_i
Spiegler–Kedem ²⁵⁵	diffusion + convection	P_p, L_p, σ_i
Solution-Diffusion (SD) Models		
classical SD model ²⁵²	diffusion ($\Delta c + \Delta p$)	P_p, P_j
simplified SD model ²⁵²	diffusion (Δc)	P_p, L_V
Maxwell–Stefan equation ²⁵⁶	multicomponent diffusion	$D_{i,m}, D_{i,p}, D_{j,m}, K_{i(j)}^0, K_{i(j)}^l$
Pore-Flow (PF) Models		
Hagen–Poiseuille model ²⁵⁷	convection	$r_p, l, \varepsilon, \tau$
simple pore-flow models (Ferry, ²⁵⁸ Verniory, ²⁵⁹ steric hindrance pore (SHP), ²⁶⁰ and log-normal ²⁶¹)	convection	$P_p, L_p, \sigma_i(r_p, S_p)$
Donnan steric pore-flow model (DSPM) ³⁶	diffusion + convection + electrostatic interactions	$r_p, l, \varepsilon, \tau, \psi$
surface-force pore-flow model (SF-PF) ²⁶²	diffusion + convection + electrostatic/affinity interactions	$r_p, l, \varepsilon, \tau, \phi$
modified surface-force pore-flow model (MD-SF-PF) ²⁶³	diffusion + convection + electrostatic/affinity interactions	$r_p, l, \varepsilon, \tau, \phi$
space-charge pore-flow (SC-PF) model ²⁶⁴	diffusion + convection + electrostatic interactions	$r_p, l, \varepsilon, \tau, \bar{\psi}$
SD with imperfections model ^{253,265}	diffusion + convection	P_p, L_p, L_V

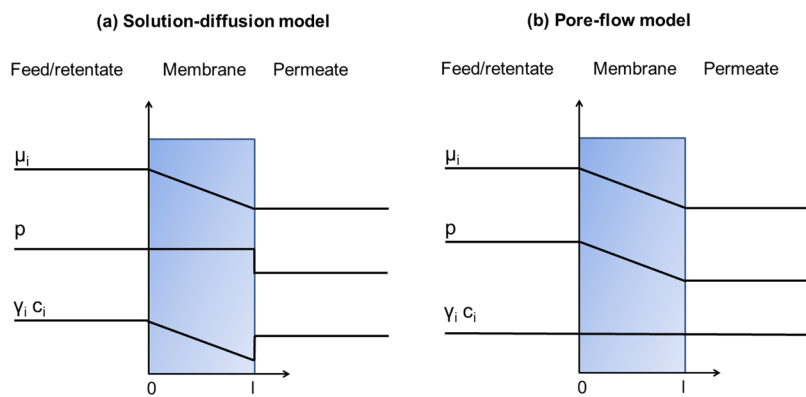


Figure 17. Profiles of chemical potential, pressure, and solvent activity characteristic of pressure-driven filtration of a one-component solution through a membrane according to (a) solution-diffusion and (b) pore-flow transport models. Adapted with permission from ref 252. Copyright 1995 Elsevier.

necessary to define a “solute” and a “solvent” for calculations to be made (in organic mixtures, in fact, it is not always clear which compound should be considered as the solute); and (ii) how easy it is for the solution thermodynamics, which impacts the driving force, to be taken into account. Non-ideality of the solution may in fact lead to significant effects.^{247,266}

3.1.1. Irreversible Thermodynamics Models. This class of models describes transport as an irreversible process that continuously dissipates free energy and produces entropy. The Kedem–Katchalsky²⁵⁴ and the Spiegler–Kedem²⁵⁵ models are the two first models based on irreversible thermodynamics, and are also the first models applied to ion transport through NF membranes.² According to irreversible thermodynamics, the process is described by means of phenomenological equations, which consider the membrane as a black box, with no characterization of membrane structural and electrical properties.

According to the Kedem–Katchalsky model, the solvent velocity, V , and the solute flux, J_i , are described by the following equations:

$$V = L_p(\Delta p - \sigma_i \Delta \pi) \quad (2)$$

$$J_i = P_i \Delta c_i + (1 - \sigma_i) V \bar{c}_i \quad (3)$$

L_p is the mechanical filtration coefficient of the membrane, or local permeability coefficient, σ_i is the reflection coefficient, corresponding to the solute fraction rejected by the membrane, and P_i is the permeability coefficient of the solute i . \bar{c}_i is the average solute concentration in the membrane.

According to the Spiegler–Kedem model, the solute flux is

$$J_i = -P_i \Delta x \left(\frac{dc_i}{dx} \right) + (1 - \sigma_i) V \bar{c}_i \quad (4)$$

The permeability coefficient of species i , P_i , and the reflection coefficient, σ_i , are obtained by fitting of experimental rejection versus flux, according to the following equation:

$$\text{Rej}_i = \frac{(1 - F)\sigma_i}{1 - \sigma_i F} \quad (5)$$

where

$$F = e^{[-V(1 - \sigma_i)/\bar{P}_i]} \quad (6)$$

$$\bar{P}_i = \frac{P_i}{l} \quad (7)$$

l is the membrane thickness along the radial coordinate x . In both eqs 3 and 4 for the Kedem–Katchalsky and Spiegler–Kedem models, respectively, the diffusion and convection contributions are represented by the first and second terms in the equations, which can be singularly quantified and compared. The model can be easily applied to all kinds of solute + solvent systems, by regressing σ_i and P_i from experimental data of solute and solvent fluxes, but requires the specification of which species is the solute (J_i) and which species is the solvent (V). In the case of n solutes in the mixture, irreversible thermodynamics models can be extended to calculate the local solute permeability coefficient for each solute (P_i , for $i = 1, 2, \dots, n$).²⁶⁷ However, it is not clear how to extend the model in the case of solvent mixtures, or how to use the model when it is not possible to distinguish a priori between solute and solvent. The model can be extended to nonideal mixtures by introducing the “rational osmotic coefficient”, defined as the ratio of the actual osmotic pressure to the osmotic pressure calculated by the van’t Hoff expression (cf, eq 8),²⁵⁵ and differentiating the osmotic pressure as in eq 9:

$$g = \frac{\pi}{\nu R T c_i} \quad (8)$$

$$\frac{d\pi}{dx} = \nu R T \left(g \frac{dc_i}{dx} + c_i \frac{dg}{dx} \right) \quad (9)$$

3.1.2. Models Based on Concentration and Pressure Gradients in the Membrane. This class of models accounts for membrane properties in the description of the chemical potential gradient, which represents the overall driving force producing movement of a permeant through the membrane.²⁵² The flux, J_i , of the component i , is

$$J_i = -L_i \frac{d\mu_i}{dx} \quad (10)$$

where μ_i is the total chemical potential of species i and L_i is the proportionality coefficient between flux and driving force. μ_i is comprised of a pressure-, temperature-, and concentration-dependent chemical potential and an electrochemical potential depending on electromotive force. In processes that involve more than one driving force, such as RO and NF, this unifying approach proves very useful. Considering only concentration and pressure gradients, the chemical potential reduces to

$$d\mu_i = RT d \ln(\gamma_i x_i) + v_i dp \quad (11)$$

where x_i and v_i are the molar fraction and the molar volume of species i , γ_i is the activity coefficient, and p is the pressure. The equation can be further simplified for incompressible phases:

$$\mu_i = \mu_i^0 + RT \ln(\gamma_i x_i) + v_i(p - p_{i,\text{sat}}) \quad (12)$$

where μ_i^0 is the chemical potential of pure species i at the saturation vapor pressure, $p_{i,\text{sat}}$.

A continuous gradient of chemical potential from one side of the membrane to the other is assumed as a consequence of equilibrium between fluids and solutes with the membrane materials at the interface. The solution-diffusion and pore-flow models describe the chemical potential in different ways (cf., Figure 17): the former is based on the assumption of concentration-dependent chemical potential gradient (cf., Figure 17a), while the latter assumes that the chemical potential across the membrane is a function of the pressure gradient (cf., Figure 17b).

The two classes of models are discussed in the following paragraphs.

3.1.3. Solution-Diffusion Models. The solution-diffusion model, introduced by the studies of Lonsdale et al.,²⁵¹ Meares et al.,²⁶⁸ Yasuda and Peterlin,²⁶⁹ and finally reviewed by Mason and Lonsdale²⁴⁵ and Wijmans and Baker²⁵² in the 1990s, describes the chemical potential gradient across the membrane as a concentration gradient only and has been largely used in the last 20 years to describe transport in reverse osmosis, dialysis, pervaporation, and gas permeation.²⁵² Significant studies were published by Rosenbaum²⁷⁰ and Rosenbaum and Skjens²⁷¹ on the water transport in cellulose acetate membranes during reverse osmosis, where the concentration gradient of water in the membrane was determined experimentally.

The solution-diffusion model, which assumes that the solute and solvent fluxes are independent from each other, is usually adopted to describe transport through dense membranes. In this kind of membrane, it is assumed that the motions of permeants through the membrane occur at about the same time scale as the statistical fluctuations of the free-volume elements. These free-volume elements should not be confounded with pores, which are conventionally assumed to be fixed in time and space. When no pressure gradient exists across the membrane, the solute flux is expressed as follows:

$$J_i = -\frac{RTL_i}{c_i} \frac{dc_i}{dx} = -D_i \frac{dc_i}{dx} \quad (13)$$

Equation 13 is similar to Fick's law, where the term RTL_i/c_i is represented by the diffusion coefficient D_i .

On the other hand, when a pressure gradient exists across the membrane, the final equation for the "classical solution-diffusion" model, after integration over the membrane thickness, is

$$J_i = \frac{D_i K_i}{l} (c_{i,0} - c_{i,l}) e^{-v_i(p_0 - p_l)/RT} \\ = P_i (c_{i,0} - c_{i,l}) e^{-v_i(p_0 - p_l)/RT} \quad (14)$$

K_i is the sorption coefficient of species i .

Equation 14 is valid for both solute (i) and solvent (V) fluxes across the membrane as a function of pressure and concentration. For diluted solutions, eq 14 can be simplified for the solvent flux:

$$J_V = \frac{D_V K_V c_{V,0}}{l} (1 - e^{-v_V(\Delta p - \Delta\pi)/RT}) \quad (15)$$

where $\Delta\pi = \pi_0 - \pi_l$ is the differential osmotic pressure, which can be calculated by the van't Hoff equation:²⁷²

$$\Delta\pi = \nu RT (c_{i,0} - c_{i,l}) \quad (16)$$

If $(v_V(\Delta p - \Delta\pi))/(RT)$ is small, the solvent and solute fluxes become:

$$J_V = \frac{D_V K_V c_{V,0}}{l} \frac{v_V(\Delta p - \Delta\pi)}{RT} = L_V (\Delta p - \Delta\pi) \quad (17)$$

$$J_i = \frac{D_i K_i}{l} (c_{i,0} - c_{i,l}) = P_i \Delta c_i \quad (18)$$

where L_V and P_i are the solvent and solute permeability coefficients, respectively.

Equations 17 and 18 are referred to as "simplified solution-diffusion" model in Table 6. Paul²⁵⁶ critically commented on the limitations of the simplified solution-diffusion model for NF. He explained that the original solution-diffusion theory fails in describing the separation of various types of organic systems, as not capable of accounting for any kind of coupling between solute and solvent fluxes. According to the simplified solution-diffusion model, flux is expected to increase linearly with pressure (cf., eq 17), but this disagrees with the experimental observations at high pressure; no permselectivity of the membrane is considered; finally, the simplified model cannot account for negative rejection, which has been observed to occur in some specific solute–solvent systems.²⁷³ Neglecting the effect of pressure on the solute transport is the reason for these limitations. This may be acceptable for desalination processes, but makes the model fail in the presence of some organic solutes or solvents.²⁵⁶

The "classical solution-diffusion" model (cf., eq 14) does not require a priori specification of which species is the solute and which is the solvent, and can be therefore easily extended to multicomponent mixtures. The "simplified solution-diffusion" model, on the other hand, differentiates between solute (J_i) and solvent (J_V), and its extension to solvent mixtures is not straightforward. Solution-diffusion models can be extended to nonideal mixtures by including the activity coefficient, as shown in eq 12.

3.1.4. Solution-Diffusion Model Based on the Maxwell–Stefan Equation. Paul and co-workers started investigating the role of pressure-driven diffusion of organic solvents through swollen polymer membranes back in 1970–1975.^{274–276} This research is summarized in a later paper by Paul.²⁷⁷ Later in 2004, Paul²⁵⁶ adapted the Maxwell–Stefan equation to consider potential frictional or convective coupling effects between solvent and solute within the membrane. The Maxwell–Stefan equation^{257,278,279} predicts a fully general diffusive coupling via composition-dependent multicomponent diffusion coefficients in systems of three or more components. The Maxwell–Stefan equation relies on force balances among the species. That is, the thermodynamical driving force df_i of species i is in local equilibrium with the total friction force. Under isothermal conditions, the driving force is

$$df_i = \frac{x_i}{RT} \nabla \mu_i^m \quad (19)$$

where the chemical potential in the membrane is $\nabla\mu_i^m = RT\nabla \ln a_i^m$ and the activity is $a_i = \gamma x_i$. The activity coefficient γ depends on the mixture composition (x_i).

The mutual friction force between species i and j is assumed to be proportional to the relative velocity ($\mathbf{u}_i - \mathbf{u}_j$) and to the molar mass. This leads to the relation:

$$d\mathbf{f}_i = - \sum_{j \neq i} f_{ij} x_j (\mathbf{u}_i - \mathbf{u}_j) \quad (20)$$

where f_{ij} are the drag coefficients ($f_{ji} = f_{ij}$).

Introducing the so-called Maxwell–Stefan diffusivities $D_{ij} = (1/f_{ij})$ yields

$$\sum_{j \neq i} \frac{x_j \mathbf{J}_i - x_i \mathbf{J}_j}{c_{\text{tot}} D_{ij}} = - \frac{x_i}{RT} \nabla \mu_i^m \quad (21)$$

By introducing $\mathbf{n}_i = w_i \rho \mathbf{J}_i$ and converting molar fractions (x_i) into mass fractions (w_i), the final set of equations to be solved for the case of a binary mixture is

$$\mathbf{n}_1 + \left(\frac{w_2 \mathbf{n}_1 - w_1 \mathbf{n}_2}{w_m} \right) \varepsilon_1 = - \frac{\rho D_{1m}}{w_m} \nabla w_1 \quad (22)$$

$$\mathbf{n}_2 + \left(\frac{w_1 \mathbf{n}_2 - w_2 \mathbf{n}_1}{w_m} \right) \varepsilon_2 = - \frac{\rho D_{2m}}{w_m} \nabla w_2 \quad (23)$$

n_i is the mass flux of species i , and ρ is the mass density of the solute–solvent–membrane mixture. The membrane mass fraction and the ε_i coefficients are defined as

$$w_m = 1 - w_1 - w_2 \quad (24)$$

$$\varepsilon_1 = \frac{D_{1m}}{D_{12}} \quad (25)$$

$$\varepsilon_2 = \frac{\text{MW}_2}{\text{MW}_1} \frac{D_{2m}}{D_{12}} \quad (26)$$

where MW_i is the molecular weight of species i . Equations 25 and 26 account for frictional coupling effects. It is expected that D_{12} is larger than either D_{1m} or D_{2m} , but little information is available in the literature about the relative magnitudes of these coefficients.²⁵⁶ The mass fractions w_i for solute and solvent can be expressed as a function of sorption coefficients at the retentate and permeate side ($K_{1(2)}^0$, $K_{1(2)}^1$), respectively. This model introduces nonlinearities that cannot be captured in the solution-diffusion model, and allows for solution nonidealities in all phases and for concentration dependence of the transport coefficients.²⁵⁶ The complexity of this model lies in the necessity for iterative calculations for solving the system of eqs 22 and 23. These equations reduce to the equations of classical solution-diffusion, when $\varepsilon_1 = \varepsilon_2 = 0$.

Similar to the classical solution-diffusion model, the Maxwell–Stefan equation (cf, eq 21) does not require a priori specification of which species is the solute and which species is the solvent, and can be therefore easily extended to multicomponent mixtures. This extension can be done by developing eq 21 analytically for n species and introducing binary diffusivities and ε_i coefficients for all of the species. The Maxwell–Stefan equation can be extended to nonideal mixtures by including the activity coefficient in the chemical potential term in eq 21.

3.1.5. Pore-Flow Models. Pore-flow models are based on the assumption that transport through the membrane is via

permeation pathways (pores), which are larger as compared to the solute and solvent molecular diameters, and that the concentrations of solute and solvent within a pore are uniform. These models describe the chemical potential gradient across the membrane as due to a pressure gradient.² In the absence of a concentration gradient, Darcy's law can be used to describe the transport through porous membranes:

$$J_i = k \frac{p_0 - p_l}{l} \quad (27)$$

k is the permeability coefficient and l is the membrane thickness. k is a function of structural factors, such as membrane pore size, surface porosity, and tortuosity.

Pure solvent flux through uniform cylindrical pores, where no significant concentration gradient is present across the membrane, is described by the well-known Hagen–Poiseuille model (which derives from Darcy's law):

$$V = \frac{\varepsilon r_p^2 \Delta p}{8l\tau \eta} = K_{HP} \frac{\Delta p}{\eta} \quad (28)$$

In eq 28, V is the solvent velocity through the membrane pores.

According to this simple model, the viscosity, η , is the only solvent parameter affecting permeation. The membrane is represented by the pore size, r_p , the porosity, ε , the tortuosity, τ , and the membrane thickness, l .

For the solute flux, several empirical pore-flow models have been developed. The simplest pore-flow models were developed to describe the reflection coefficient, introduced by the irreversible thermodynamics models, as a function of the pore radius, and are the steric hindrance pore model, the Ferry model, the Verniory model, and the log-normal model. According to the steric hindrance pore (SHP) model,²⁶⁰ the reflection coefficient is a function of the membrane pore size (assumed uniform) and the solute diameter. Solute transport is affected by both steric hindrance and interactions with the pore wall. The reflection coefficient is calculated as

$$\sigma_i = 1 - H_F S_F \quad (29)$$

where

$$H_F = 1 + \frac{16}{9} \lambda \quad (30)$$

$$S_F = (1 - \lambda)^2 [2 - (1 - \lambda)^2] \quad (31)$$

$$\lambda = \frac{d_i}{d_p} \quad (32)$$

H_F is defined as a “wall-correction parameter” and represents the effect of the pore wall, while S_F is representative for steric hindrance through the pores. d_i and d_p are the solute and pore diameters, respectively.

Ferry²⁵⁸ proposed a pore-flow model to describe the reflection coefficient, in which pores are considered to be uniform and cylindrical and the velocity has a parabolic profile in the pore. The reflection coefficient is calculated as

$$\sigma_i = 1 - 2(1 - \lambda)^2 - (1 - \lambda)^4 \quad (33)$$

The Verniory model²⁵⁹ incorporates frictional drag forces in the cylindrical membrane pores (taken into account in the factor $g(\lambda)$, cf, eq 35). The reflection coefficient is expressed by the following equation:

$$\sigma_i = 1 - g(\lambda)S_F \quad (34)$$

$$g(\lambda) = \frac{1 - (2/3)\lambda^2 - 0.2\lambda^5}{1 - 0.76\lambda^5} \quad (35)$$

Differently from the other models discussed so far, the pore size is considered not to be constant in the log-normal model.²⁶¹ This model assumes a log-normal pore size distribution and solute permeation through every pore that is larger than the diameter of the molecule. Negligible diffusion contribution does not affect the solute transport. The reflection curve is expressed as

$$\sigma_i = \int_0^{r_i} \frac{1}{S_p \sqrt{2\pi}} \frac{1}{r} \exp\left(-\frac{[\ln(r) - \ln(\bar{r}_p)]^2}{2S_p^2}\right) dr \quad (36)$$

with $r_i = d_i/2$, \bar{r}_p is a mean pore size (defined as the size of a molecule that is retained by 50%), and S_p is the standard deviation of the pore size distribution.

Pore-flow models originated from the Nernst–Planck equation correlate the diffusive and convective hindrance factors with the ratio of solute radius (r_i) to pore radius (r_p). The solute flux is affected by diffusion (driven by a concentration gradient) and convection (with the total volume flux). For aqueous solutions, the solute flux is further affected by electromigration (Donnan exclusion). On the basis of these considerations, Bowen and Mukhtar²⁸⁰ and Bowen and Welfoot³⁶ developed the Donnan steric pore-flow model (DSPM). The solute flux is described by eq 37.

$$J_i = -K_{i,d} D_i \frac{dc_i}{dx} + K_{i,c} c_i V - \frac{z_i c_i K_{i,q} D_i}{RT} F \frac{d\psi}{dx} \quad (37)$$

$K_{i,d}$ and $K_{i,c}$ are the diffusive and convective hindrance factors, respectively, z_i is the solute valence, ψ is the electrical potential, and x is the longitudinal direction. The electromigration driven by an electrical potential is normally negligible in organic solvents. The solvent flux, V , is described by the Hagen–Poiseuille model (cf., eq 28).

Two other pore-flow models, developed to account for solute–membrane interactions, are the surface force pore-flow (SF-PF) model²⁶² and the finely porous model.²⁸¹ In the former, interfacial forces between the solute and the membrane are used to describe the solute distribution at the membrane surface. In the latter, a kinetic effect, related to the mobility of the solute relative to that of solvent while permeating through the membrane pores, is considered. These two models are described by the same differential equation:

$$J_i = -\frac{RT}{\chi_{i,V} b} \frac{dc_i}{dx} + \frac{c_i V}{b} \quad (38)$$

b is a friction parameter, a function of the friction coefficients between solute and solvent, $\chi_{i,V}$, and between solute and membrane, $\chi_{i,m}$:

$$b = \frac{\chi_{i,V} + \chi_{i,m}}{\chi_{i,V}} \quad (39)$$

The friction coefficients are a function of the diffusion coefficients of the solute in the solvent, $D_{i,s}$, and in the membrane, $D_{i,m}$, respectively. The SF-PF and the finely porous model describe differently the solute distribution at the membrane–solution interface. A purely steric interaction affects the solute distribution in the finely porous model:

$$\begin{cases} x = 0: & c_{i,m}(0) = K_i c_{i,0} \\ x = l: & c_{i,m}(l) = K_i c_{i,l} \end{cases} \quad (40)$$

Subscript m refers to membrane, 0 to retentate, and 1 to permeate. The sorption coefficient K_i can be measured by sorption experiments.²⁰²

In the SF-PF model, the solute partitioning at the membrane–solution interface is influenced by interactions between the solute and the membrane and is a function of the radial position:

$$\begin{cases} x = 0: & c_{i,m}(0) = c_{i,0} e^{-\phi(r)/RT} \\ x = l: & c_{i,m}(l) = c_{i,l} e^{-\phi(r)/RT} \end{cases} \quad (41)$$

$\phi(r)$ is a potential function describing the force exerted on the solute molecule by the membrane surface (or pore wall). If $\phi(r)$ is positive, repulsion occurs between solute and membrane, while if $\phi(r)$ is negative, attraction occurs. $\phi(r)$ is assumed to be independent from axial position. The solute concentration in the pore follows a Boltzmann distribution:

$$c_i(r, x) = c_i(0, x) e^{-\phi(r)/RT} \quad (42)$$

The surface-force pore-flow model was further revised and the mass balance corrected. This led to the formulation of the modified surface force pore-flow (MD-SF-PF) model.²⁶³ The main differences between the original and the modified versions of the model lay in the formulation of the potential function to describe the solute distribution in the pore and in the description of the concentration at the pore outlet. The solvent flux, V , is described by the Hagen–Poiseuille model (cf., eq 28).

Space-charge (SC) models are the last class of pore-flow models developed from the extended Nernst–Planck equation.²⁶⁴ Pores are assumed to be straight capillaries having charge on their surface. The radial ion distribution in the pores is affected by the electrical potential, according to the Poisson–Boltzmann equation. The electrical potential, $\bar{\psi}$, is described as

$$\bar{\psi} = \psi_1(r, x) + \psi_2(x) \quad (43)$$

where $\psi_1(r, x)$ originates from the surface charge of capillaries, and $\psi_2(x)$ is a component due to a streaming potential in the axial direction. The potential function varies with both x and r , and thus the concentration in the capillary. The radial distribution of the solute has the typical Boltzmann distribution:

$$c_i(r, x) = c_i(0, x) e^{-z_i F \bar{\psi} / RT} \quad (44)$$

Equation 44 for the SC model has the same structure as eq 42 for the SF-PF model. The only difference is in the definition of the potential function. In SC models, the potential function considers electrostatic effects only, while in the SF-PF models, the potential function considers both electrostatic and affinity effects.

Pore-flow models require the specification of which species is the solute (J_i) and which species is the solvent (V). In the case of n solutes in the mixture, pore-flow models can be extended to calculate the local solute flux for each species (J_i , for $i = 1 - n$), but it is not clear how to extend the model in the case of solvent mixtures or how to use the model when it is not possible to a priori distinguish between solute and solvent. The models can be extended to nonideal mixtures by introducing

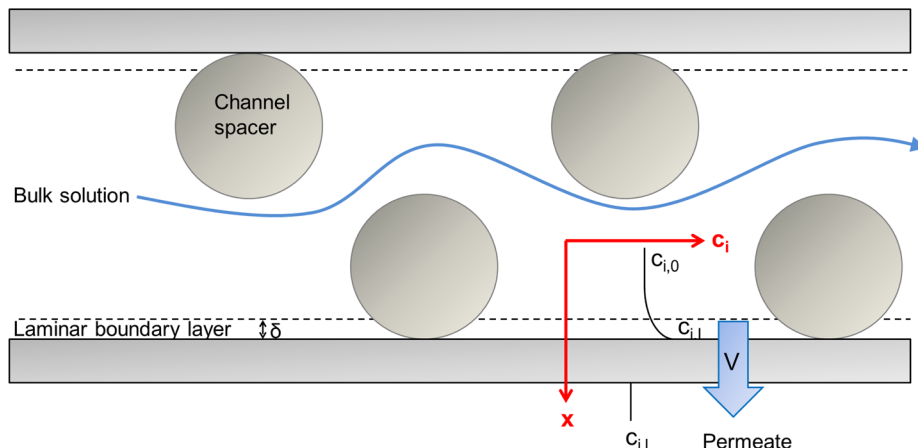


Figure 18. Schematic representation of a fluid flowing through the channel of a membrane module in the presence of zigzag spacers and concentration gradient adjacent to a membrane, in the laminar boundary layer.

the activity coefficient in the equations for the solute flux (cf., eqs 37 and 38).

3.1.6. Solution-Diffusion with Imperfections Model.

To account for the occurrence of viscous flow and interactions between the permeating species, the classical solution diffusion model has been extended to the solution diffusion with imperfections model.^{253,265} This model considers parallel transport paths through a matrix having the solution-diffusion mechanism of solute transport through dense material, with imperfections where solutes are convectively transported without change of concentration. According to the original formulation by Sherwood et al.,²⁶⁵ the transport equations for the solvent velocity and the solute flux are

$$V = L_V(\Delta p - \Delta\pi) + L_i\Delta p \quad (45)$$

$$J_i = P_i\Delta c_i + L_i c_0 \Delta p \quad (46)$$

where L_V and L_i are the partial mechanical permeability coefficients of the matrix and imperfections, and P_i is the partial diffusional permeability coefficient of the matrix (as in eqs 17 and 18 for the classical solution-diffusion model). Yaroshchuk²⁵³ modified this version of the solution-diffusion with imperfections model, considering the matrix as laterally inhomogeneous, and, therefore, allowing for diffusion through the imperfections. Because of simultaneous diffusion and convection in the pores, Yaroshchuk²⁵³ describes the solute flux as

$$J_i = -P_{i,\text{dif}} \frac{dc_i}{dx} + Vc_i \quad (47)$$

$P_{i,\text{dif}}$ is the diffusional permeability coefficient of imperfections. It is worth noting the similarity between eq 47 for the solution-diffusion with imperfections model and eq 37 for the DSPM model (when the electrostatic term is negligible).

Similarly to pore-flow models, solution-diffusion with imperfections models require the specification of which species is the solute (J_i) and which species is the solvent (V), as they consist of a convection transport term. The models can be extended to nonideal mixtures by introducing the activity coefficient in the equations for the solute flux (cf., eqs 46 and 47).

3.2. Film Theory for Mass Transfer Limitations

In addition to the transport mechanism through the membrane matrix, reviewed in the previous section, mass transfer limitations such as concentration polarization and osmotic pressure have to be taken into account as they make significant contributions to the overall membrane separation. The effect of the fluid dynamics in the module on the overall membrane separation is reviewed in this section. A schematic representation of a fluid flowing through a channel of a membrane module is shown in Figure 18.

The fluid velocity is reduced in the boundary layer next to the membrane, due to friction at the fluid–membrane surface. The fluid velocity in the middle of the channel is therefore higher and the fluid is well mixed, while in the boundary layer the flow is much lower, and mixing occurs by diffusion. Concentration polarization occurs when the convective flow of the solute toward the surface, caused by the applied pressure, cannot be balanced by the back diffusion of the solute toward the bulk of the retentate, caused by the difference in concentration between film layer and bulk.²⁶⁶ In processes such as RO, NF, and UF, concentration gradients form on the feed side of the membrane, as shown in Figure 18. The increase of the solute concentration at the interface increases the osmotic pressure difference, which in turn affects the driving force through the membrane. The effective differential pressure, Δp_e , across the membrane is therefore equal to the difference between the applied pressure, Δp , and the osmotic pressure, $\Delta\pi = \pi(c_{i,I}) - \pi(c_{i,P})$:

$$\Delta p_e = \Delta p - \Delta\pi \quad (48)$$

$c_{i,I}$ and $c_{i,P}$ are the concentrations of species i at the retentate–membrane interface and in the permeate, respectively.

$c_{i,I}$ is linked to the concentration in the retentate and in the permeate by the stagnant film theory.^{282,283} According to this theory, the solute flux through the membrane is given by the product of the permeate volume flux, V , and the permeate solute concentration, $c_{i,P}$. In the boundary layer, the convective solute flux toward the membrane, $(V \cdot c_i)$ minus the diffusive solute flux away from the membrane ($D_i \frac{dc_i}{dx}$) gives the net solute flux:

$$Vc_i - \frac{D_i \frac{dc_i}{dx}}{dx} = Vc_{i,I} \quad (49)$$

Table 7. Application of Transport models to Experimental Data for Polymeric and Ceramic Membranes and Coupling of Transport Models with Film Theory

reference	model used or recommended (regression (R)/prediction (P))	membrane	solute/solvent
Polymeric Membranes			
Silva et al. ²⁸⁵	solution-diffusion (R)	PI and composite PDMS	toluene, ethyl acetate, and methanol
Han et al. ²⁸⁶	solution-diffusion (R)	composite PDMS	phenol and toluene
White ³⁸	solution-diffusion (R/P)	PI	alkanes and aromatic compounds
Peeva et al. ²⁶⁶	solution-diffusion coupled with film theory (R)	PI	TOABr/toluene and docosane
Silva et al. ²⁸⁷	solution-diffusion coupled with film theory (R)	PI	DMMS/methanol
Silva et al. ²²⁸	solution-diffusion (R/P)	PI (spiral-wound module)	TOABr/toluene
Stafie et al. ²⁸⁸	solution-diffusion (R)	composite PDMS	oil/n-hexane and PIB/n-hexane
Ben Soltane et al. ²⁸⁹	solution-diffusion (R)	composite PDMS	ethanol, toluene, and n-heptane
Gevers et al. ⁵⁶	Maxwell–Stefan and Kedem–Katchalsky (R)	composite PDMS	dyes/alcohols
Hesse et al. ²⁹⁰	Maxwell–Stefan (P)	PI	ethyl acetate, alcohols, toluene
Bhanushali et al. ³⁹	surface-force pore-flow + Spiegler–Kedem (R)	PA and composite PDMS	dyes, tryglicerides/polar and apolar solvents
Gibbins et al. ²⁹¹	pore-flow (R)	composite PDMS, PI	quaternary alkyl ammonium bromide salts/methanol
Geens et al. ¹⁹⁶	pore-flow (R)	composite PDMS, PA, TiO ₂	different reference components/methanol, ethanol, acetone, ethyl acetate, and n-hexane
Robinson et al. ²⁹²	pore-flow (R)	composite PDMS	alkanes, aromatic solvents, alcohols
Leitner et al. ²⁹³	pore-flow (R)	swollen PDMS	alcohol, ethyl acetate, toluene, n-hexane, butanone, and their mixtures
Bhanushali et al. ⁴⁰	viscous-diffusion (R)	PA and composite PDMS	alcohols, alkanes
Geens et al. ¹⁸⁸	viscous-diffusion (R)	composite PDMS, PA, PES	water, methanol, ethanol
Tarleton et al. ⁵¹	viscous-diffusion (R)	composite PDMS	alkyl and aromatic solvents and low-polarity sulfur bearing, organometallic, and polynuclear aromatic solute compounds
Volkov et al. ²⁹⁴	viscous-diffusion (R)	PTMSP	ethanol/water
Dijkstra et al. ²⁹⁵	solution-diffusion with imperfections and Maxwell–Stefan equation (R)	composite PDMS	pentane-decane and pentane-dodecane
Fierro et al. ²⁹⁶	solution diffusion with imperfection (R/P)	composite PDMS	ketones and glycols
Miyagi et al. ²⁹⁷	regular solution combined with diffusion model (P)	composite PDMS	alcohol/n-hexane, alkane/n-hexane, lipid/n-hexane, and diesel fuel–kerosene systems
Schmidt et al. ²⁹⁸	combined model (R/P)	PI	organic solutes/toluene, n-hexane, and isopropanol
Machado et al. ²⁹⁹	resistance-in-series (R)	composite PDMS	alcohols, paraffins, acetone, and water
Robinson et al. ³⁰⁰	Spiegler–Kedem (R)	composite PDMS	xylenes and low-polarity solutes
Koops et al. ³⁰¹	Spiegler–Kedem (R)	CA	linear hydrocarbons and carboxylic acids/ethanol and n-hexane
Labanda et al. ²⁶⁷	Spiegler–Kedem (R)	PA	glucose, proline, tyramine, and tartaric acid/water–ethanol
Ceramic Membranes			
Tsuru et al. ¹⁷³	pore-flow (R)	SiO ₂ /ZrO ₂	methanol, ethanol, and 1-propanol
Tsuru et al. ³⁰²	Spiegler–Kedem (R)	SiO ₂ /ZrO ₂	sugars/alcohols
Darvishmanesh et al. ³⁰³	solution-diffusion with imperfections (R)	TiO ₂ and composite PDMS	different organic solvents
Marchetti et al. ²³⁰	semiempirical (R/P)	TiO ₂ and ZrO ₂	different organic solvents and water
Buekenhoudt et al. ²³¹	semiempirical (R/P)	TiO ₂ , ZrO ₂ , and SiO ₂	different organic solvents and water
Darvishmanesh et al. ²²⁹	resistance-in-series (R)	TiO ₂ and ZrO ₂	different organic solvents and water

The integration of the mass balance over the thickness of the boundary layer, δ , gives the equation for the concentration polarization:²⁸⁴

$$\frac{c_{i,1} - c_{i,0}}{c_{i,0} - c_{i,1}} = e^{V\delta/D_i} \quad (50)$$

where $(D_i/\delta) = k_L$ is the mass transport coefficient in the liquid phase. Rearranging eq 50, the concentration at the interface is calculated as follows:

$$c_{i,1} = c_{i,0} + (c_{i,0} - c_{i,1}) e^{V/k_L} \quad (51)$$

The determining factors for the concentration polarization are the boundary layer thickness, δ , the diffusion coefficient of the species, D_i (which, in turn, determines the mass transfer coefficient, k_L , in the channel), the volume flux through the membrane, V , and the concentration in the permeate and in the retentate, $c_{i,1}$ and $c_{i,0}$, respectively.

In eq 50, the balance between convective and diffusive transport in the membrane boundary layer is characterized by the term (V/k_L) , which is commonly called the Peclet number (Pe). Concentration polarization is significant when the Peclet number is high ($V \gg k_L$), meaning that the convective flux through the membrane cannot be balanced by the diffusive contribution. On the other hand, concentration polarization is not significant when the Peclet number is low ($V \ll k_L$), meaning that convection is balanced by diffusion in the boundary layer.

Almost all membrane processes are affected by concentration polarization. If membrane permeance and selectivity increase, concentration polarization effects become more significant. Turbulent mixing at the membrane surface can help in reducing the boundary layer thickness. A direct technique to increase the turbulence at the membrane surface is to increase the fluid flow velocity over the membrane surface (i.e., the flow rate). However, this has practical limitations at the industrial scale, because it also increases axial pressure drops. Another option is to improve the membrane module design, selecting the optimal channel spacer geometries.⁸

3.3. Application of Transport Models and Film Theory

Various attempts have been made to use the transport models based on irreversible thermodynamics, solution-diffusion, pore-flow, and solution-diffusion with imperfection mechanisms, eventually combined with the film theory, to describe the molecular permeation through NF membranes and account for concentration polarization. As shown in Table 6, transport models are characterized by model parameters, which are a function of solute, solvent, or membrane properties. Obtaining the model parameters by independent measurements is often difficult or impossible. Semiempirical models, based on mechanistic models (i.e., solution-diffusion or pore-flow models) or a combination of those, have been therefore proposed to describe the model parameters as a function of selected solute/solvent/membrane properties. Regression of experimental data is often used to quantify the unknown model parameters. Once the model parameters are known, the model can be used to carry out simulations, allowing the prediction of membrane performance at different operating conditions.

Applications of transport models and film theory to OSN processes reported in the literature are presented below for polymeric (CA, PA, PI, and PDMS) and ceramic (TiO_2 , ZrO_2 , and SiO_2) OSN membranes and summarized in Table 7 in terms of the type of model used (for regression and/or prediction), type of membrane, and testing system (solute/solvent).

3.3.1. Application of Transport Models to Polymeric Membranes. *3.3.1.1. Solution-Diffusion Model.* Silva et al.²⁸⁵ compared the solution-diffusion model with one and two-parameter pore-flow model approaches to describe the permeation of binary solvent mixtures of methanol, toluene, and ethyl acetate through Koch MPF-50 and Starmem 122 membranes. They observed that the solution-diffusion model predicts solvent fluxes for both toluene/ethyl acetate and methanol/toluene mixtures in Starmem 122, while the Hagen–Poiseuille models are not very successful for predictions in methanol/toluene.

Similarly, Han et al.²⁸⁶ and White³⁸ concluded that solution-diffusion type models describe the transport of aqueous solutions of phenol and toluene through the polymeric MPF-50 membrane²⁸⁶ and mixtures of alkanes and aromatic

compounds in toluene through PI (P84) membranes³⁸ better than pore-flow models. White³⁸ used the solution-diffusion model in the form of eq 18, while Han et al.²⁸⁶ used the simplified solution-diffusion equation eq 14. In both models, the fitting parameter is the permeability coefficient, P_i .

Peeva et al.²⁶⁶ investigated the permeation of highly concentrated solutions of docosane and tetraoctylammonium bromide (TOABr) in toluene (up to 20 wt %) through Starmem 122 by the solution-diffusion model. Because the data suggested that concentration polarization becomes significant at these high concentrations, the solution-diffusion model coupled with the film theory for mass transfer (cf., eq 52) was used to describe the data:

$$J_i = P_i \left(x_{i,I} - \frac{\gamma_{i,I}}{\gamma_{i,P}} x_{i,P} e^{(-\nu_i \Delta p / RT)} \right) \quad (52)$$

P_i is the permeability coefficient of species i , $x_{i,I}$ and $x_{i,P}$ are the molar fractions at the feed–membrane and permeate side, and $\gamma_{i,I}$ and $\gamma_{i,P}$ are the activity coefficients at the feed–membrane and permeate side. The film theory (cf., eq 50) was used to correlate the molar fractions at the feed–membrane interface with the molar fractions in the feed bulk.

In this work, the authors estimated the mass-transfer coefficients in a cross-flow cell dissolving a plate of benzoic acid into water at two different cross-flow rates. Specifically, a layer of molten benzoic acid was solidified in a cross-flow cell and then dissolved by circulation of water through the cell. The mass-transfer coefficient was calculated from the benzoic acid concentration in the water as a function of time. The modified UNIFAC method was used to calculate the activity coefficients of docosane and toluene,³⁰⁴ while the activity coefficient of toluene in the TOABr–toluene system was calculated using a model that combines the UNIFAC group contribution method for the short-range physical interactions with a modified Debye–Hückel term for the long-range electrostatic forces.³⁰⁵ Significant effects of solute concentration and flow rate were found on the membrane performance; flux reduction was observed at large solute concentration and low flow rate, as a consequence of concentration polarization effects.

Silva et al.²⁸⁷ also described the rejection profiles for the permeation of concentrated (5–30 wt %) dimethyl methylsuccinate (DMMS)–methanol solutions (5–30 wt %) through Starmem 122 and MPF-50 by the solution-diffusion model combined with the film theory for mass transfer. To use this approach for predictive purposes, three parameters have to be determined experimentally, solvent permeance, solute permeance, and solute mass transfer coefficients.

In another work, Silva et al.²²⁸ studied the performance of organic solvent NF membranes using a spiral-wound (Starmem 122) membrane element, with 0–20 wt % solutions of TOABr in toluene. Two modeling approaches were tested: a simple approach based on considering the element as a flat-sheet membrane and ignoring radial and axial pressure, velocity, and concentration gradients, and a more complex approach, where axial and radial distributions were taken into account. The solution-diffusion model was used as a membrane transport model, based on the results from Peeva et al.²⁶⁶ Interestingly, a reasonable description of the experimental results was obtained using both the complex and the simple approach. Furthermore, they could obtain the membrane transport parameters necessary for the modeling of the spiral-wound module from cross-flow experiments using flat-sheet membranes.

A peculiarity of polymeric membranes, as compared to ceramic materials, is that they can swell significantly in organic solvents. Swelling has been studied for PDMS membranes, and the permeation performance of various solvents through hydrophilic and hydrophobic PDMS-based composite membranes has been addressed.^{288,306,307} Stamatialis et al.³⁰⁷ studied the transport of oil/toluene and TOABr/toluene mixtures through PDMS/PAN composite membranes, while Stafie et al.²⁸⁸ studied the separation of oil/*n*-hexane and polyisobutylene/*n*-hexane solutions through similar membranes. They found that the pure solvent flux correlates very well with the swelling/viscosity ratio and used the solution-diffusion model to describe the transport of *n*-hexane through the membrane. Furthermore, Stamatialis et al.³⁰⁷ studied the mixture non-ideality, in terms of its effect on the osmotic pressure. In the case of ideal systems, such as oil/toluene, they could describe the observed osmotic phenomena with the van't Hoff osmotic model. On the other hand, for nonideal systems, such as TOABr/toluene, the osmotic pressure was significantly lower than expected on the basis of the van't Hoff model. Concentration polarization phenomena were observed in such a mixture, which resulted in low toluene flux and 100% rejection of TOABr by the PDMS/PAN composite membrane.

Ben Soltane et al.²⁸⁹ studied the effect of pressure on swelling of thick PDMS films under conditions that are analogous to those in steady-state nanofiltration and determined OSN fluxes through composite PDMS membranes. Three solvents were tested: ethanol, toluene, and *n*-heptane. The results obtained in this study indicate the suitability of the solution-diffusion theory to model this type of transport behavior. It was shown that a simple linear relationship exists versus either the applied solvent pressure or the swelling extent. The results show very good agreement with those from previous studies by Paul and co-workers,²⁷⁶ who were the first to investigate the role of pressure on swollen polymers and the effect of pressure on membrane transport.

3.3.1.2. Solution-Diffusion Model Based on the Maxwell–Stefan Equation. Because many studies have highlighted the importance of solute–solvent coupling during transport through membranes, Maxwell–Stefan equation and extended irreversible thermodynamics models were also applied. Gevers et al.⁴² studied the transport of dyes of different MW (300–1000 g mol⁻¹) dissolved in alcohols though composite silicone NF membranes. They used the Maxwell–Stefan equation and the Kedem–Katchalsky model²⁵⁴ to explain the solute and solvent fluxes. They reported a difference in the transport of solutes with low and high molar volume: for the former, the convective flux (interpreted as “solvent dragging”) had a more important contribution, especially in highly swollen systems, while, for the latter, the contribution of the diffusive flux was dominant. In general, the state of the solvent in the membrane and the solvent viscosity strongly influenced the solute mobility.

Hesse et al.²⁹⁰ characterized the PI-based Starmem 240 membrane by measuring fluxes of pure organic solvents (ethyl acetate, isopropanol, toluene, ethanol) and their solvent mixtures. Because they reported that Fickian diffusion cannot be used to model permeation through PI glassy polymers, they developed a new predictive model, based on the Maxwell–Stefan equation, for the description of the solvent flux. This model accounts for the diffusivity and the solubility of the organic solvents in the dense active separation layer, as well as the swelling degree. Model parameters were determined from

independent measurements to model solubility and diffusivity. The PC-SAFT equation of state³⁰⁸ was used to quantify the solubility of the organic solvents in the membrane on the feed side and membrane swelling. Good agreement was found for the predicted solvent fluxes with the experimental data.

3.3.1.3. Pore-Flow Models. Bhanushali et al.³⁹ studied the rejection of dyes and tryglycerides through a PDMS-based membrane and an aromatic PA-based membrane and investigated the extension of the existing transport models, mainly developed for water applications, to OSN. Interestingly, they found that the rejection of Sudan IV dye was about 25% in *n*-hexane and about -10% in methanol. On the basis of the results obtained with Sudan IV, they concluded that the solute rejection was strongly dependent on both type of solvent and membrane. Such negative rejection implies preferential transport of Sudan IV dye over methanol and can be attributed to the occurrence of strong solute–membrane interactions. In terms of transport modeling, the solution-diffusion model was considered inadequate, because it could not account for coupling effects. The Spiegler–Kedem and the surface-force pore-flow models both account for coupling effects and were thus used to describe the experimental data. By modeling with the Spiegler–Kedem model, the importance of the convective flow on the overall transport was demonstrated, and a reduction of the convective contribution with increase in the solute MW was observed. The surface-force pore-flow model, which accounts for solute–membrane interactions via a potential function, was also used to describe the data. This model was found capable of accounting for faster solute than solvent transport and, therefore, describing negative rejection.

Gibbins et al.²⁹¹ studied solvent flux decline and membrane separation properties of Starmem 122, MPF-50, and Desal DL membranes with quaternary alkyl ammonium bromide salts in methanol. The membranes were characterized using three simple pore flow models, to describe the reflection coefficient: the steric hindrance pore model, the Ferry model, and the Verniory model. Reasonable estimates for pore size (0.5–0.8 nm) were obtained.

Geens et al.¹⁹⁶ studied different reference solutes in methanol, ethanol, acetone, ethyl acetate, and *n*-hexane through different hydrophilic and hydrophobic membrane (PDMS, PA, and TiO₂) and used the simple pore-flow models as in Gibbins et al.²⁹¹ to describe the data and evaluate the pore diameter of the membrane. Additionally to the SHP, Ferry, and Verniory simple pore-flow models, they used the log-normal model, to account for pore nonuniformity. The experimental data were in good agreement with the model fits, and both pore dimension and model parameters could be quantified. The different models provided however different results for the pore diameter, for a given solvent–membrane combination. The best fit was found using the log-normal model, suggesting that the pore distribution of a NF membrane is nonuniform (in agreement with observations by Van Der Bruggen and Vandecasteele in a previous work³⁰⁹).

Robinson et al.²⁹² studied the permeation mechanism of alkanes, aromatic solvents, and alcohols through PDMS membranes and applied a Hagen–Poiseuille type of pore-flow model to their data. They found that the transport was governed by viscous flow for a feed pressure above 30 bar. This was justified by the nonseparation of binary solvent mixtures and the dependency of flux on viscosity and membrane thickness. Below this pressure value, they propose the presence of a second transport mechanism, additional to the viscous

flow, implying that, ultimately, the permeation can be interpreted as a combination of sorption and diffusion. Interestingly, they found a correlation between the Hagen–Poiseuille proportionality constant and the Hildebrand solubility parameter of the solvent and used this information as a proof of the importance of swelling (i.e., sorption) effects.

Recently, Leitner et al.²⁹³ reported that the Hagen–Poiseuille model better explained some of the tendencies of the solvent permeance through swollen 125 μm thick PDMS membranes (usually described in terms of solution-diffusion mechanism²⁸⁹). Several solvents and pressures (from 5 to 50 bar) were used, so that the degree of swelling varied according to the solvent and the pressure applied. By mimicking the thickness reduction of the membrane using uniaxial compression tests, the nonlinear flux profile as a function of pressure could be linearized, concluding that the hydraulic mechanism could well explain the experimental data.

3.3.1.4. Semiempirical and Combined Models. Bhanushali et al.⁴⁰ studied the permeation of alcohols and alkanes through a composite polyamide-based RO membrane (Osmonics), a composite dimethylsilicone membrane (Osmonics), and a silicone-based membrane (MPF 50, Koch). They developed a semiempirical model based on the solution-diffusion theory (cf, eq 53), which assumes the permeance of any species *i* to be proportional to the product of diffusivity and solubility of the species *i* in the membrane:

$$J_i = K_{\text{Bh}} \left(\frac{\nu_i}{\eta_i} \right) \left(\frac{1}{\phi^n \gamma_{\text{SV}}} \right) \quad (53)$$

This model accounts for the viscosity, η_i , the surface energy of the membrane, γ_{SV} , the molar volume, ν_i , and a solvent–membrane interaction parameter, ϕ^n , where ϕ is a sorption value and n is an empirical constant obtained from the best fitting of the experimental data. K_{Bh} is the proportionality constant of the model. Because of the presence of an interaction parameter specific to the solvent–membrane combination (ϕ^n), the predictive capability is limited.

Geens et al.¹⁸⁸ obtained experimental flux data for binary mixtures of water, methanol, and ethanol through seven different hydrophilic and hydrophobic commercially available NF membranes (N30F and NF-PES-010 from Nadir, Desal-5-DL and Desal-5-DK from Osmonics, MPF-44 and MPF-50 from Koch, and SolSep-030505 from SolSep). They developed a model for the permeation of solvents, introducing the difference in surface tension between membrane and solvent, $\Delta\gamma$, as a solvent–membrane interaction parameter:

$$J_i = K_G \frac{\nu_i}{\eta_i \Delta\gamma} \Delta p \quad (54)$$

where K_G is a constant for the membrane. The dependence on molar volume, ν_i , and viscosity, η_i , was inspired by Bhanushali's model,⁴⁰ and the dependence on the difference in surface tension between solvent and membrane, $\Delta\gamma$, was inspired by Machado's model.²⁹⁹

Tarleton et al.⁵¹ studied alkyl and aromatic solvents and low-polarity, sulfur bearing, organometallic, and poly nuclear aromatic solutes through PDMS membranes and, similarly to Robinson et al.,²⁹² used a viscous-diffusion mechanism to interpret the data. They found that three distinct regions were evident, as a function of the maximum length of the solute molecule. For small solutes, the membrane swelling caused sufficiently small solutes to permeate directly with the solvent

flow. Large solutes, on the other side, were mostly rejected by a size exclusion mechanism. In the intermediate region, they suggested that a mixture of viscous flow and diffusion exists, and they proposed a new viscous-diffusion model (cf, eq 55) to describe this region:

$$J_i = a \frac{c_{i,0} k \Delta p}{l} + (1 - a) \frac{D_i (c_{i,0} - c_{i,l})}{l} \quad (55)$$

a is the fraction of solute undergoing transport with the viscous flow.

Recently, a new semiempirical model was proposed by Volkov et al.²⁹⁴ for the permeation through PTMSP dense membranes. The model takes into account the polymer free volume, swelling degree, membrane compaction caused by pressure, and the physicochemical properties of the liquid and polymer phases, such as viscosity, surface tension, and molar volume.

$$J_i = a' \left(\frac{\phi_{S,P}^3}{(1 - \phi)^2 l_{S,P}} \right) \left(\frac{\nu_i}{\eta_i \Delta\gamma} \right) \Delta p \quad (56)$$

where a' is a model parameter. The thickness of the swollen membrane at the applied pressure, $l_{S,P}$, and the fractional void volume, $\phi_{S,P}$, are calculated from experimental data for swelling and membrane compaction. The model was capable of describing permeation of ethanol/water mixtures of different compositions and revealed that there is a threshold value for the pressure, below which permeation through PTMSP membranes does not occur, due to the absence of sorption and swelling.

Dijkstra et al.²⁹⁵ used the solution-diffusion with imperfections model, in the form of eq 57, for describing the permeation of pentane–decane and pentane–dodecane through PDMS/PAN membranes.

$$J_i = \frac{c_i D_i \nu_i}{R T l} (\Delta p - \Delta\pi) + \frac{c_i B_0}{\eta_i l} \Delta p \quad (57)$$

B_0 is the specific permeability coefficient of the membrane. They found more reliable results by using the Maxwell–Stefan transport equation than the solution-diffusion with imperfections model, but, surprisingly, they conclude that friction effects between both permeating components had only a small influence on the permeation.

Fierro et al.²⁹⁶ used the solution-diffusion with imperfections model combined with diffusion models (such as Vrentas and Duda diffusion theory and Wesselingh and Bollen multi-component diffusion) to successfully describe the permeation behavior of nonideal mixtures of ketones and glycols through PDMS composite membranes.

Miyagi et al.²⁹⁷ modeled the permeance of binary alcohol/*n*-hexane, alkane/*n*-hexane, lipid/*n*-hexane, and diesel fuel–kerosene systems through a PDMS membrane, using a model combining the regular solution model with the solution-diffusion model, represented by eq 58. The regular solution model³¹⁰ assumes that there is a correlation between membrane swelling degree, interaction between solvent and membrane, and solvent mole fraction present in the membrane:

$$J_i = \frac{D_i (\Delta p - \Delta\pi)}{l} \cdot e^{(-\phi_{\text{membrane}}^2 \nu_i (S_{\text{membrane}} - S_i)^2 / RT)} \quad (58)$$

S_i and S_{membrane} are the solubility parameters of solvent *i* and membrane, respectively, and ϕ_{membrane} is the volume fraction of

the membrane polymer in the solvent phase. No separation of alkane/*n*-hexane and diesel fuel/kerosene mixture was observed by the membranes, while preferential permeation of *n*-hexane was observed in the alcohol/*n*-hexane and lipid/*n*-hexane systems. The selectivity of the membrane in the presence of *n*-hexane was explained by the occurrence of significant interactions between *n*-hexane and the membrane.

Schmidt et al.²⁹⁸ investigated the permeation of different organic solutes in isopropanol, toluene, and *n*-hexane through Starmem 122 and developed a phenomenological permeation model, which includes solution-diffusion, pore-flow, and mutual ternary interaction terms. The model equations for the solvent are

$$J_{i,\text{solvent}} = J_{i,\text{solvent}}^{\text{SD}} + J_{i,\text{solvent}}^{\text{SD,coupling}} + J_{i,\text{solvent}}^{\text{PF}} + J_{i,\text{solvent}}^{\text{PF,coupling}} \quad (59)$$

$$\begin{aligned} J_{i,\text{solvent}}^{\text{SD}} &= C_{i,\text{solvent}}^{\text{SD}} \frac{1}{\exp\left(\frac{|S_{i,\text{solvent}} - S_{\text{membrane}}|}{S_{\text{membrane}}}\right)} \\ &\times \frac{1}{\exp\left(\frac{|\gamma_{i,\text{solvent}} - \gamma_{\text{membrane}}|}{\gamma_{\text{membrane}}}\right)} \left[a_{i,0} - a_{i,l} \exp\left(-\frac{v_i \Delta p}{RT}\right) \right] \end{aligned} \quad (60)$$

$$J_{i,\text{solvent}}^{\text{SD,coupling}} = \sum_{j=1, i \neq j}^{N_{\text{solvent}}} (J_{j,\text{solvent}}^{\text{SD}} + J_{j,\text{solvent}}^{\text{SD,coupling}}) \chi_{i,j} \quad (61)$$

$$\begin{aligned} J_{i,\text{solvent}}^{\text{PF}} &= C_{i,\text{solvent}}^{\text{PF}} \frac{1}{\eta_{i,\text{solvent}}} \left(\frac{d_p^{\text{eff}}}{d_{i,\text{solvent}}} \right)^2 \\ &\times \left[a_{i,0} - a_{i,l} \exp\left(-\frac{v_i \Delta p}{RT}\right) \right] \end{aligned} \quad (62)$$

$$J_{i,\text{solvent}}^{\text{PF,coupling}} = \sum_{j=1, i \neq j}^{N_{\text{solvent}}} (J_{j,\text{solvent}}^{\text{PF}} + J_{j,\text{solvent}}^{\text{PF,coupling}}) \chi_{i,j} \quad (63)$$

The model equations for the solute are

$$J_{i,\text{solute}} = J_{i,\text{solute}}^{\text{SD}} + J_{i,\text{solute}}^{\text{SD,coupling}} + J_{i,\text{solute}}^{\text{PF}} + J_{i,\text{solute}}^{\text{PF,coupling}} \quad (64)$$

$$\begin{aligned} J_{i,\text{solute}}^{\text{SD}} &= C_{i,\text{solute}}^{\text{SD}} \frac{1}{\exp\left(\frac{|S_{i,\text{solute}} - S_{\text{membrane}}|}{S_{\text{membrane}}}\right)} \\ &\times \left[a_{i,0} - a_{i,l} \exp\left(-\frac{v_i \Delta p}{RT}\right) \right] \end{aligned} \quad (65)$$

$$J_{i,\text{solute}}^{\text{SD,coupling}} = \sum_{j=1}^{N_{\text{solvent}}} (J_{j,\text{solute}}^{\text{SD}} + J_{j,\text{solute}}^{\text{SD,coupling}}) \chi_{i,j} \quad (66)$$

$$J_{i,\text{solute}}^{\text{PF}} = C_{i,\text{solute}}^{\text{PF}} \left(\frac{d_p^{\text{eff}}}{d_{i,\text{solute}}} \right)^2 \left[a_{i,0} - a_{i,l} \exp\left(-\frac{v_i \Delta p}{RT}\right) \right] \quad (67)$$

$$J_{i,\text{solute}}^{\text{PF,coupling}} = \sum_{j=1}^{N_{\text{solvent}}} (J_{j,\text{solute}}^{\text{PF}} + J_{j,\text{solute}}^{\text{PF,coupling}}) \chi_{i,j} \quad (68)$$

The effective pore diameter, d_p^{eff} , was calculated from the maximum pore diameter, d_p^{max} , according to the following equation:

$$d_p^{\text{eff}} = d_p^{\text{max}} \frac{1}{\exp\left(\frac{|S_{\text{solvent,mix}} - S_{\text{membrane}}|}{S_{\text{membrane}}}\right)} \quad (69)$$

$S_{\text{solvent,mix}}$ and S_{membrane} are the solubility parameters of solvent mixture and membrane, respectively. This model was integrated in process design via the generation of membrane modeling maps, membrane rejection maps, and membrane selectivity maps.^{298,311}

3.3.1.5. Resistance-in-Series Model. Machado et al.²⁹⁹ studied the permeation of pure solvents and solvent mixtures (alcohols, paraffins, acetone, and water) through PDMS-based MPF-50 membranes, and developed a resistance-in-series model to extend the predictability of the Hagen–Poiseuille model. According to the authors, a composite NF membrane is composed of three main layers: (i) a NF top skin, (ii) an intermediate UF layer, and (iii) a base support layer (cf., Figure 19), which in turn create three resistances, a surface resistance

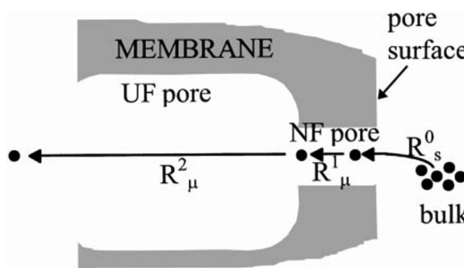


Figure 19. Representation of the three main layers and flow resistances encountered during filtration through a NF membrane. Reprinted with permission from ref 299. Copyright 2000 Elsevier.

R_s^0 , at the pore entrance, a viscous resistance R_η^1 during flow through the UF pore, and another different viscous resistance R_η^2 during flow through the UF pore.

The three resistances are described as a function of viscosity, surface tension, and solvent–membrane interactions, as shown in eq 70:

$$J_i = \frac{\Delta p}{R_s^0 + R_\eta^1 + R_\eta^2} = \frac{\Delta p}{\phi_M [(\gamma_{SV} - \gamma_{LV}) + f_1 \eta_i] + f_2 \eta_i} \quad (70)$$

f_1 and f_2 are model parameters characterizing the intrinsic properties of the NF and UF layers, the solid and liquid surface tensions, γ_{SV} and γ_{LV} , and a solvent parameter, ϕ_M . It was found that a single solvent parameter gave a good fit for a large number of different solutions, except for the acetone–water mixture (this was explained by the high surface tension difference between the two solvents).

3.3.1.6. Classical and Extended Irreversible Thermodynamics Approaches. Robinson et al.³⁰⁰ studied the permeation of low-polarity solutes in a mixture of xylene isomers and found that the degree of cross-linking affects the permeance and selectivity of PDMS membranes by changing the swelling degree. Large degrees of swelling corresponded to larger transport regions within the membrane, thus increasing solvent permeance and decreasing solute rejection. Likewise, higher solute rejection and lower solvent permeance were found for lower swelling degree. The Spiegler–Kedem model could be applied across the entire range of membranes studied, whereas the applicability of the solution-diffusion model was diminished when the degree of swelling was large, suggesting that a

potential transition between solution-diffusion and pore-flow mechanisms could occur as a function of the swelling degree.

Koops et al.³⁰¹ investigated the separation of linear hydrocarbons and carboxylic acids from ethanol and *n*-hexane solutions with CA membranes. They observed solvent dependent rejection of the hydrocarbons, and higher hydrocarbon rejection corresponding to higher solvent flux. This is in agreement with the observations by Bhanushali et al.³⁹ for Sudan IV in different alcohols. Koops et al.³⁰¹ described their data using the Spiegler–Kedem equation, according to which, in fact, higher solvent fluxes result in higher rejections.

Labanda et al.²⁶⁷ studied the permeation process of solutes of similar MW and different charge (glucose, proline, tyramine, and tartaric acid) in water/ethanol/0.01 M NaCl through PA-based NF and RO membranes. The extended Spiegler–Kedem model (cf., eqs 71 and 72) was used to characterize the multicomponent solutions considering the interaction between solutes:

$$V = \bar{L}_p \left[\frac{dp}{dx} - \sum_{s=1}^n \left(\sigma_s \frac{d\pi_s}{dx} \right) \right] \quad (71)$$

$$J_s = - \sum_{i=1}^n \left(\bar{P}_{si} \frac{d\pi}{dx} \right) + (1 - \sigma_s) c_s V \quad (72)$$

where \bar{L}_p is the specific hydraulic permeability coefficient, σ_s is the reflection coefficient, \bar{P}_{si} is the local solute permeability coefficient of solute s considering the interaction of solute i , and c_s is the average solute concentration across the membrane.

In analogy with the original Spiegler–Kedem model (cf., eqs 4–6), eqs 71 and eq 72 can be written as

$$V = L_p (\Delta p - \sum_s \sigma_s \Delta \pi_s) \quad (73)$$

$$\text{Rej}_s = \frac{(1 - F_s) \sigma_s}{1 - \sigma_s F_s} \quad (74)$$

where

$$F_s = \exp \left[- \frac{(1 - \sigma_s) V}{P_{ss}} (1 + \sum_{i=1(i \neq j)}^n A_i) \right] \quad (75)$$

$$A_i = \frac{P_{si} (c_{i,l} - c_{i,0})}{V [c_{s,l} - (1 - \sigma) c_s]} \quad (76)$$

where P_{si} is the solute permeability coefficient, determined by the ratio of the local solute permeability coefficient and membrane thickness ($P_{si} = (\bar{P}_{si}/l)$). They observed that low ethanol concentrations could change significantly the membrane performance. The rejection of organic solutes decreased from 94% without ethanol to 50% with 13% vol ethanol. This was attributed to a reduction of the dielectric constant of the aqueous solution in the presence of ethanol molecules, which modified the membrane swelling and increased the solute permeability coefficient.

3.3.2. Application of Transport Models to Ceramic Membranes. **3.3.2.1. Pore-Flow and Irreversible Thermodynamics Models.** For ceramic membranes, mainly pore-flow and irreversible thermodynamics models have been used to describe the permeation. Tsuru et al.^{45,173,174,176,177,302} investigated the permeation of nonaqueous solutions through ceramic NF and UF membranes. They prepared inorganic NF membranes using

silica–zirconia (Si/Zr) composite sols by the sol–gel method, and found that the permeation mechanism of methanol, ethanol, and 1-propanol through membranes with pores size of 70 nm obeys the viscous-flow mechanism (i.e., Hagen–Poiseuille model), irrespective of the types of alcohols,¹⁷³ while the permeance of alcohols through membranes with pore diameters of 1–5 nm is positively affected by the operating temperature (from 25 to 60 °C) and negatively affected by the solvent molecular size (methanol > ethanol > 1-propanol). In other words, the permeation through NF membranes required higher activation energies for large molecules and for membranes of smaller pore size.^{173,176}

In another study, Tsuru et al.³⁰² investigated the rejection of sugars and the permeate flux of alcohols through inorganic Si/Zr membranes with MWCOs of approximately 200, 600, and 2000 g mol⁻¹ at different temperatures. Using the Spiegler–Kedem model, they observed that the reflection coefficient (which corresponds to the fraction of solutes rejected by the membrane in convective flow) was almost constant, irrespective of experimental temperature, whereas solvent permeances increased with temperature. Again, the hindered diffusion of solutes through micropores was indicative of an activated process.

3.3.2.2. Semiempirical and Combined Models. Darvishmashesh et al.³⁰³ proposed a semiempirical model for the solvent permeation through organic (PDMS) and inorganic (TiO₂) nanofiltration membranes. This model is represented by eq 77:

$$J_i = \frac{a_0 \alpha}{\eta_i e^{(1-\beta)}} (\Delta p - \Delta \pi) + \frac{b_0}{\eta_i e^{(1-\beta)}} \Delta p \quad (77)$$

a_0 and b_0 are specific diffusivity and permeability coefficients, while α and β are defined as follows:

$$\alpha = \frac{\epsilon_L}{\epsilon_S} \quad (78)$$

$$\beta = \frac{\gamma_{LV}}{\gamma_{SV}} \quad (79)$$

For pure solvent, the osmotic pressure, $\Delta\pi$, is zero, and the equation reduces to eq 80.

$$J_i = \frac{a_0 \alpha + b_0}{\eta_i e^{(1-\beta)}} \Delta p \quad (80)$$

Marchetti et al.²³⁰ developed a semiempirical model for predicting organic solvent and water transport through TiO₂ and ZrO₂ NF and UF membranes. This model assumes the viscosity as the main influencing parameter for the permeation, and introduces several correction factors ($f_{C,\text{capillary}}$, $f_{C,\text{dipole}}$, and $f_{C,\text{steric}}$), to account for the surface phenomena that arise in a nanotube due to solvent–membrane surface interactions:

$$J_i = \frac{K_{HP} \Delta p}{\eta_i} (1 + f_C) \quad (81)$$

$$f_C = f_{C,\text{capillary}} + f_{C,\text{dipole}} + f_{C,\text{steric}} = C_1 \frac{2\gamma_{LV} \cos \theta}{r_p} + C_2 |\delta_i - k_{\text{pol}}| + C_3 \left(\frac{r_i}{r_p} \right)^2 \quad (82)$$

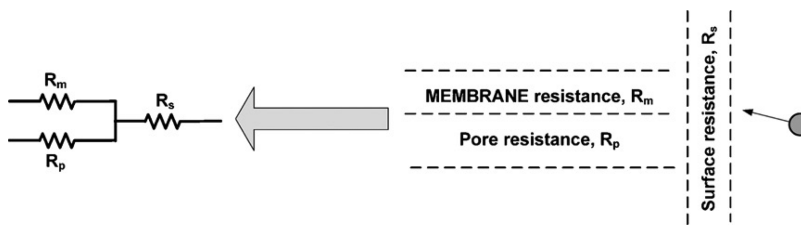


Figure 20. Representation of the resistances encountered by a solvent molecule through ceramic OSN membranes. Reprinted with permission from ref 229. Copyright 2009 Elsevier.

θ is the contact angle between solvent and membrane, δ_i is the dipole moment of solvent i , k_{pol} is the membrane polarizability, according to the theory of surface polarizability by Carré,³¹² and r_i and r_p are the radii of solvent i and pore, respectively. C_1 , C_2 , and C_3 are the three fitting parameters (or proportional factors) characteristic of the membrane. The model can be applied to both UF and NF membranes, because the correction terms in eq 82 are functions of the pore size. Furthermore, the model can be used to predict pure solvent and solvent mixture fluxes for a specific membrane by obtaining the necessary model parameters via regression of a limited number of experimental data for pure solvents. The model was also extended to describe solvent mixtures as in eq 83:

$$J_{ij,\text{mix}} = \frac{K_{\text{HP}}}{\eta_{\text{mix}}} (1 + f_{C,\text{mix}}) \Delta p \quad (83)$$

$$f_{C,\text{mix}} = x_i f_{C,i} + (1 - x_i) f_{C,j} \quad (84)$$

η_{mix} and $f_{C,\text{mix}}$ are the solvent viscosity and correction factor for the mixture $i + j$. $f_{C,\text{mix}}$ was calculated as a weighted average of the correction factors of the pure components (cf., eq 84).

Buekenhoudt et al.²³¹ developed an elegant linear relationship to describe the product of flux and viscosity for organic solvents and water through TiO_2 , ZrO_2 , and SiO_2 NF and UF membranes, as a function of the total Hansen solubility parameter of the solvent:

$$\frac{J_i \eta_i}{J_{\text{water}} \eta_{\text{water}}} = (1 - C) + C \frac{S_{\text{Hansen},i}}{S_{\text{Hansen},\text{water}}} \quad (85)$$

where J_i is the flux of the solvent i , and $S_{\text{Hansen},i}$ is the total Hansen solubility parameter. C is the only unknown model parameter to be found by fitting of experimental data. The linear relationship was validated for ceramic membranes of different pore size and material. This result emphasized the importance of viscosity and solvent–membrane affinity on the solvent transport.

The model developed by Marchetti et al.²³⁰ for ceramic membranes cannot be extended to polymeric membranes, because it is based on the assumption of constant pore radius. Polymeric membranes, in fact, swell to different extents in organic solvents, as discussed in section 3.3.1. The model developed by Buekenhoudt et al.²³¹ is not based on the hypothesis of constant pore radius, but has not yet been tested on permeability data for polymeric membranes.

3.3.2.3. Resistance-in-Series Model. Darvishmanesh et al.²²⁹ studied the permeation of different organic solvents and water through ceramic TiO_2 and ZrO_2 NF membranes. Following the studies of Machado et al.,²⁹⁹ the authors developed a semiempirical model based on resistances-in-series-and-parallel to describe the solvent transport. Transport was described as

consisting of three main resistances, surface resistance, R_s , pore resistance, R_p , and matrix resistance, R_m (cf., Figure 20).

The functional form of the model is represented by eq 86:

$$J_i = \frac{1}{R_{\text{overall}}} \Delta p \quad (86)$$

where the overall resistance, R_{overall} , is defined as in eq 87:

$$R_{\text{overall}} = R_s + \frac{R_m R_p}{R_m + R_p} \quad (87)$$

and the three single resistances are defined as

$$R_s = k_s \frac{r_i}{r_p} \exp(1 - \beta) \quad (88)$$

$$R_m = k_m \left(\frac{\eta_i}{\alpha} \right) \quad (89)$$

$$R_p = k_p \left(\frac{r_i}{r_p} \right)^2 \eta_i \quad (90)$$

with the coefficients α and β given by eqs 78 and 79.

Four solvent parameters are included in this model: viscosity, surface tension, dielectric constant, and effective molecular radius. The ratio of solvent to membrane dielectric constant, ϵ_L and ϵ_S , and the ratio of solvent to membrane surface tensions, γ_{LV} and γ_{SV} , accounts for polarity and surface effects, respectively.

3.4. Model Parameters and the Effects of Solute–Solvent–Membrane Interactions

It is clear from the previous paragraphs that, together with the main driving forces responsible for the transport through membranes, the different interactions between solute, solvent, and membrane play an important role in affecting the molecular sorption, rejection, and permeation. Furthermore, recent advances in the structural characterization techniques provided the capability to measure pore size, pore length, porosity, and tortuosity of both ISA and TFC membranes (cf., section 2.8). These membrane structural characteristics, together with the intermolecular interactions, should be included in the transport models to help explain the membrane transport and permit predictions of membrane performance. All of these parameters deserve an accurate analysis, which is presented in this paragraph.

The solute–solvent–membrane interactions, which affect the overall separation performance, can be classified according to the following effects: (i) effective solute diameter; (ii) pore wettability and effective pore diameter; (iii) solute and solvent polarity; and (iv) charge effects.

These interactions are schematically represented in Figure 21.

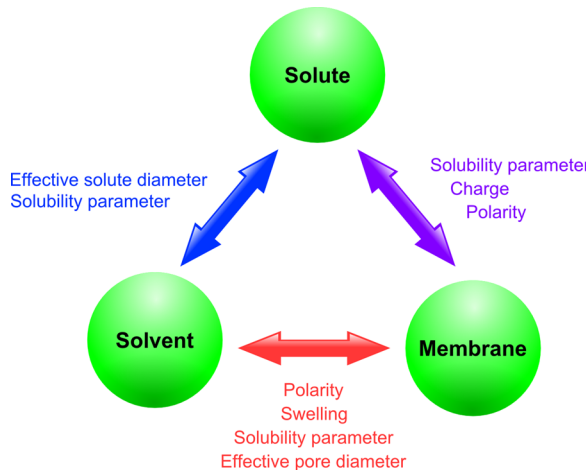


Figure 21. Solute–solvent–membrane interactions affecting the overall separation performance.

3.4.1. Effective Solute and Solvent Diameters and Polarity Effects. Significantly lower rejections of dyes (Orange II, Safranin O, and Solvent Blue) in organic solvents than in water were observed by Yang et al.²⁴⁹ for different commercial hydrophilic polymeric membranes. This was attributed to a complexation of water molecules with the solute molecules, which enlarged the effective solute size and increased the solute rejection in water with respect to that in methanol.

Van der Bruggen³¹³ studied the rejection of phenol in water, ethanol, and *n*-hexane through N30F, NF-PES-10, MPF-44, and MPF-50 membranes and observed that the properties of the solvent used largely affected both solvent flux and solute rejection. A major role was played by the solvent polarity, which affected negatively the solvent flux through hydrophobic membranes, and positively through hydrophilic membranes. They attributed the effect of the organic solvent to its interaction with the polymeric chains of the membrane, which in turn determines the membrane pore size.

Geens et al.²⁵⁰ investigated the rejection of raffinose in water–alcohol mixtures and observed that rejection is not always lower in organic solvents, as observed by Yang et al.²⁴⁹ and Van der Bruggen.³¹³ Raffinose rejection depended on the hydrophilic/hydrophobic character of the membrane. Membrane performance was explained by a “hydration/solvation” mechanism, which affected the relative solute–membrane versus solvent–membrane molecular affinity.

Geens et al.,³¹⁴ furthermore, carried out experiments with reference organic compounds of different MW and polarity dissolved in methanol and ethanol and emphasized the effect of solute diameter on the convective solute transport. The Stokes diameter was used as a solute size, d_s , according to eq 91.

$$d_s = \frac{kT}{3\pi\eta D_i} \quad (91)$$

D_i is the solute diffusivity in the solvent, calculated by the Wilke–Chang equation:

$$D_i = 7.4 \times 10^{-12} (\phi_s \text{MW}_s)^{0.5} \frac{T}{\eta v_i^{0.6}} \quad (92)$$

ϕ_s is the association parameter of the solvent, MW_s is the solvent molecular weight, and v_i is the solute molar volume.

In another work, Geens et al.¹⁹⁶ proposed to calculate the effective solute diameter in the solvent, d_i^s , based on an empirical correlation with the solute diameter in water, d_i^w :

$$d_i^s = d_i^w \left(\frac{\phi_w \text{MW}_w}{\phi_s \text{MW}_s} \right)^{1/2} \quad (93)$$

where ϕ_s and ϕ_w are the association parameters of the solvent s and of water. An empirical relationship for the solute diameter in water was developed by Van Der Bruggen and Vandecasteele:³⁰⁹

$$d_i^w = 0.065 \text{MW}_i^{0.438} \quad (94)$$

Geens et al.³¹⁴ also observed significantly lower rejection of the solutes with smaller effective diameter (Victoria Blue and Erythrosine B) than of larger solutes (Vitamin E or Bromothymol Blue); this was attributed to the higher polarity of the two former solutes. Furthermore, they proposed that charge effects might play a role as additional solute–membrane interactions, based on the observation of higher rejection for solutes that can dissociate in methanol (i.e., Victoria Blue, Bromothymol Blue, and Erythrosine B), as compared to neutral solutes.

The importance of the solubility parameter as a significant influencing factor for the permeation through OSN membranes has been investigated by different authors. Schmidt et al.³¹¹ studied flux and rejection performance of two commercial PI membranes, Starmem 122 and PuraMem 280, using multi-component mixtures, and they emphasized the importance of solute critical diameter, solubility parameter, and membrane swelling in affecting solute rejection.

Significant negative rejections were observed by Koops et al.³⁰¹ for docosanoic acid in *n*-hexane through cellulose acetate membranes; these were attributed to an accumulation of the solute at the membrane, due to a higher affinity of the solute with the membrane, with respect to the solvent. Sorption experiments supported this hypothesis. Darvishmanesh et al.³¹⁵ found significant negative rejection of Sudan II/Sudan Black/Sudan 408 in *n*-hexane through PI membranes. Because a higher rejection was observed with methanol as compared to ketones, these results did not support the “hydration/solvation” mechanism.²⁵⁰ Results were explained by lower solvent–membrane than solute–membrane affinity, and compared to the relative differential solubility parameters. A very low permeance of *n*-hexane was observed, which also demonstrated its low affinity.

Zeidler et al.³¹⁶ investigated the rejection of two, three, and four ring-type core substances with different functional groups and side chain lengths in ethanol, *n*-heptane, and THF using a PDMS/PAN composite membrane, to study the influence of functional groups in the solute molecules on the rejections in OSN. Different rejections were obtained in the three solvents: rejection varied between 55% and 95% in THF, between 20% and 80% in *n*-heptane, while significantly negative values were obtained in ethanol, in a range between –10% and –45%.

Postel et al.³¹⁷ investigated the permeation of four different solute classes, polyethylene glycol, linear carboxylic acid, polystyrene, and *n*-alkanes, dissolved in *n*-hexane, toluene, isopropanol, or methanol, through dense PDMS-based polymeric OSN membranes. Their investigation demonstrated that strong solute–membrane interactions can lead to a

solubility determined solute transport, resulting in surprisingly higher transport rates for the larger solute molecules. Similarly to Darvishmanesh et al.³¹⁵ and Zeidler et al.,³¹⁶ a comparison of the solubility parameter of the solute, the membrane, and the solvent was undertaken to explain these results.

Recently, the concept of negative rejection in OSN was proposed to enhance solute fractionation between pairs of dyes using membranes made of PTMSP and ethanol as a solvent.³¹⁸

Among the studies on nonswelling ceramic membranes, Tsuru et al.⁴⁵ observed significantly higher rejection of PEG₆₀₀ in methanol than in water. Again, these data suggest that the “hydration/solvation” mechanism²⁵⁰ did not hold for PEG through hydrophilic ceramic membranes. To understand the role of surface effects in ceramic membranes, Tsuru et al.^{174,177} investigated the permeation of *n*-hexane, with traces of water (from zero to several hundred ppm), as a model nonaqueous solution system through nanoporous TiO₂ membranes¹⁷⁴ and through organic/inorganic hybrid membranes, developed by modifying the surface of the Si/Zr porous membranes by a gas-phase reaction with trimethylchlorosilane (TMCS).¹⁷⁷ TiO₂ and unmodified Si/Zr membranes showed a decreased *n*-hexane flux with an increase in water concentration, which was pronounced at low permeation temperatures, while TMCS-modified membranes showed approximately the same permeance, irrespective of water concentration in *n*-hexane. Therefore, it was suggested that a layer of water adsorbed to the hydrophilic TiO₂ and unmodified Si/Zr membranes surfaces and reduced the effective pore size for *n*-hexane permeation. Negative rejection was observed in nanofiltration of linoleic acid in *n*-hexane solutions through TiO₂.¹⁷⁴

Significant effects of solute–membrane affinity on the NF performance through ceramic membranes, which result in negative rejection, were found also by Marchetti et al.¹⁹⁷ for the permeation of monovalent salts in organic solvent/water mixtures and explained by the preferential hydration of the ions.

3.4.2. Charge Effects. Zhukov³¹⁹ investigated the surface charge properties of metal oxides (SiO₂, TiO₂, and ZrO₂) in contact with organic solvents. He observed that surface charge may be present also in organic solvents, but the mechanism of charge formation is different from that in water. For example, in protic liquids, such as alcohols, charge is formed due to acid–base interactions, differently from dipolar aprotic liquids where it is determined by donor(base)–acceptor(acid) interactions. Zhang et al.³²⁰ explored the surface charge on polymeric membranes in aqueous solutions of methanol and ethanol by streaming potential measurements and observed a significant effect of the solvent dielectric constant on the streaming potential across the membrane.

The occurrence of charge interactions has been investigated also for OSN. Bhanushali et al.³⁹ explained the higher rejection of Orange II and Safranine O (charged solutes) over Solvent Blue 35 (neutral solute) in methanol through MPF-60 as due to charge effects. On the other hand, no charge effects during the NF of charged solutes in methanol through Desal-DK, MPF-44, and Starmem membranes were observed by Zhao and Yuan.²⁴⁸ They observed higher rejection of neutral molecules in water than in organic solvents for hydrophilic NF membranes and solvent- and membrane-dependent rejection for hydrophobic NF membranes. Furthermore, in their study, rejection of charged organic molecules was always higher than that of neutral molecules for both hydrophilic and hydrophobic membranes, and was higher in water than in organic solvents

(in agreement with what was observed by Yang et al.²⁴⁹). It is possible that the higher rejection of charged solutes by the hydrophobic MPF-60, observed by Bhanushali et al.,³⁹ was also due to hydrophilic–hydrophobic effects.

3.5. Modeling of OSN Processes

Modeling OSN at the process scale has an important role in successful industrial applications. Hence, this section gives an insight into the modeling of membrane processes, from single-stage configurations to membrane cascades.

3.5.1. Single-Stage Processes. The simple filtration processes for all membrane applications (i.e., concentration, diafiltration, and purification, cf., Figure 1) can be represented as shown in Figure 22. c_i^{in} and c_i^{out} are the concentrations of *i*

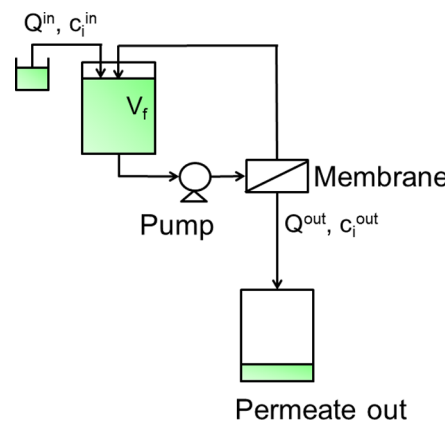


Figure 22. Schematic representation of the simple membrane filtration stage, which is applicable for concentration, solvent exchange, and purification processes.

entering and exiting the retentate loop, respectively. Q^{in} and Q^{out} are the inlet and outlet flows. Q^{out} represents the permeate flux, and V_f is the volume in the feed tank (cf., Figure 22). The mass balance for the species *i* is given by eq 95:

$$\frac{dm_i}{dt} = Q^{\text{in}} c_i^{\text{in}} - Q^{\text{out}} c_i^{\text{out}} \quad (95)$$

By introducing $c_i^{\text{out}} = (1 - \text{Rej}_i)c_i$, where c_i is the concentration inside the retentate loop, and developing the derivative for $m_i = c_i V_f$ eq 95 becomes

$$V \frac{dc_i}{dt} + c_i \frac{dV_f}{dt} = Q^{\text{in}} c_i^{\text{in}} - Q^{\text{out}} (1 - \text{Rej}_i) c_i \quad (96)$$

The mass balance for the volume, V_f is

$$\frac{dV_f}{dt} = Q^{\text{in}} - Q^{\text{out}} \quad (97)$$

The initial conditions for eqs 96 and 97 are $c_i(0) = c_i^0$ and $V_f(0) = V_f^0$. For a concentration process, $Q^{\text{in}} = 0$:

$$\frac{dc_i}{dt} = \frac{1}{V_f(t)} Q^{\text{out}} \text{Rej}_i c_i \quad (98)$$

For a constant volume diafiltration process, $V_f = \text{constant}$ and $Q^{\text{in}} = Q^{\text{out}} = Q$. Equation 96 becomes therefore

$$\frac{dc_i}{dt} = \frac{Q}{V_f} [c_i^{\text{in}} - (1 - \text{Rej}_i) c_i] \quad (99)$$

Sereewatthanawut et al.²²⁷ used OSN spiral-wound membrane modules to address a model separation challenge, such as

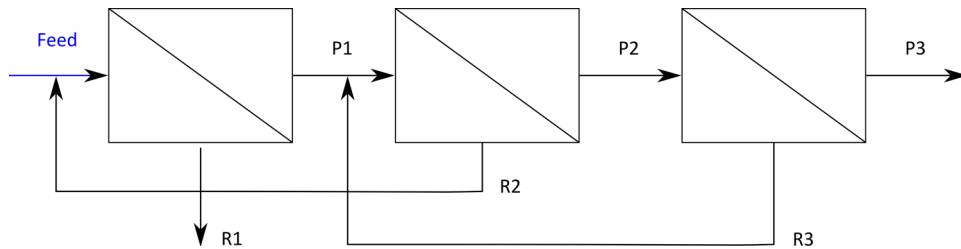


Figure 23. Schematic representation of three-stage membrane cascade with recycle of retentate. Adapted with permission from ref 322. Copyright 2013 John Wiley and Sons.

separation of Solvent Yellow 7 (model product) from Brilliant Blue R (model impurity) in DMF, as well as a typical separation challenge in the synthesis of APIs, such as the separation of an API from its oligomeric impurities in THF. They developed a mathematical model to calculate the concentration profiles of each solute in the system during the diafiltration. The model was based on mass balances at steady state and constant volume operation mode. Solute concentration effects, including concentration polarization and osmotic pressure, were neglected, and no selectivity for the solvent was assumed. As a result, solute rejections and fluxes were all assumed to be constant with respect to time (i.e., no transport model at the membrane scale was used), and the solvent rejection was equal to zero.

Whu et al.³²¹ generalized the mass balance reported in eq 98 including the reaction term, to model the coupling of a semibatch reactor with a nanofiltration membrane unit, as shown in eq 100.

$$\frac{dc_i}{dt} = \frac{1}{V_f(t)} Q^{\text{out}} \text{Rej}_i c_i + \nu_i r_r \quad (100)$$

They assumed the occurrence of a generic reaction $A + B \rightarrow C + D$, with reaction rate r_r , and modeled the evolution of the reaction over time for different batch and semibatch process arrangements and operating conditions. They assumed the observed rejection of species i to be independent of the concentration in the reaction mixture and the solvent flux to be constant with time. Provided that basic kinetic data are available, the authors suggested that the model can be extended to more complex reaction systems.

3.5.2. Multistage Processes. The simple filtration unit of Figure 22 can be arranged in multistage membrane cascades, to overcome the selectivity limit intrinsic to a single filtration stage. Caus et al.³²² studied the applicability of integrated countercurrent cascades for the separation of individual organic components (xylose and maltose) in aqueous solutions. They modeled the system of Figure 23 by means of overall material balances and recoveries of the modules, where the recovery of the module N , REC_N , was defined as the ratio of the permeate flux, P_N , to the feed flux, F_N , of the module.

$$\text{REC}_N = \frac{P_N}{F_N} \quad (101)$$

The modeling was done using Matlab software. Experimental rejections from single-stage filtration experiments were assumed to be constant, that is, independent of pressure and feed concentration. From the simulation, they compared the performance of single-stage filtration experiments, a three-module cascade with recycle of the retentate, a multistage filtration with recycle, and a multistage cascade without recycle.

They concluded that membranes with a low rejection for the desired component are preferred to obtain a high product recovery, whereas membranes with a much higher rejection for the undesired component are preferred to obtain a high product purity or a high selectivity.

Lin and Livingston⁴ estimated the solvent exchange performance of a membrane cascade for the solvent swap of TOABr from toluene to methanol through a series of algebraic calculations. The effects of number of stages in the cascade and the ratio of initial and replacing solvent flows were taken into account. As in the previous study, rejections and fluxes at each stage were assumed constant (and equal to zero solvent rejection). Good agreement was found between the experimental results employing single-stage, two-stage, and three-stage membrane cascades and the theoretical predictions.

Vanneste et al.³²³ investigated the application of membrane cascades to solvent-based pharmaceutical separations in methyl isopropyl ketone (MIK), DMAc, THF and methanol through DuraMem 150 and DuraMem 200. The goal of the cascade configuration was the enhancement of the product yield in the retentate while maintaining a purity of at least 90%. The results from the cascade modeling, assuming a simple transport model based on constant rejection, showed that the addition of two stages effectively increased the product yield in the retentate. Using smaller membrane modules can also help to increase the yield. Optimum number of stages and optimum module size were obtained via cost analysis.

Siew et al.³²⁴ demonstrated how the use of a membrane cascade can significantly improve the solute concentration and solvent recovery of a dilute API solution. They studied three different cascade configurations: (i) batch permeate multipass cascade, in which the permeate stream from stage j is sent for further filtration in stage $j + 1$; (ii) continuous permeate multipass cascade, in which the permeate stream from stage j is sent continuously for further filtration in stage $j + 1$; and (iii) multipass cascade, where a stripping section was introduced into the cascade to provide additional solute enrichment capacity with respect to the two other cascade systems. This is shown in Figure 24.

Material balances were written for both rectifying and stripping sections:

$$P_j - \nu_{i,j-1} = W_j x_{i,j} + P_j y_{i,p} \quad (102)$$

$$W_{j+1} x_{i,j+1} = P_j y_{i,j} + W_j x_{1,i} \quad (103)$$

W and P are the retentate and permeate fluxes, and x and y the retentate and permeate compositions, respectively. Solute i partitions across the membrane according to the relationship:

$$y_{i,j} = (1 - \text{Rej}_{i,j}) x_{i,j} \quad (104)$$

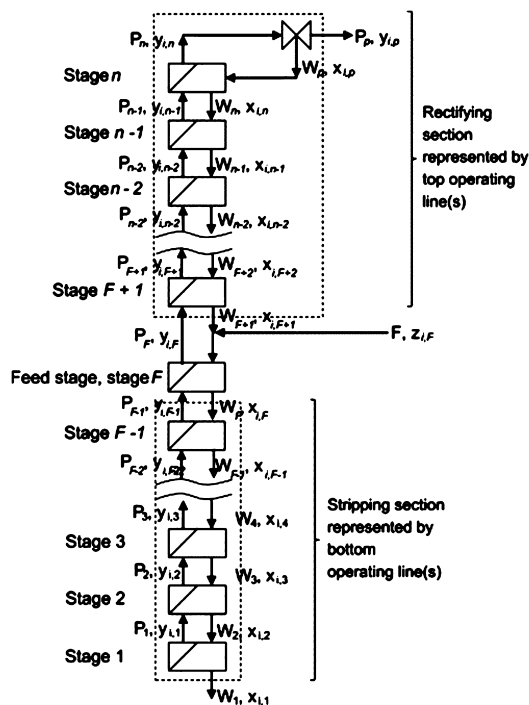


Figure 24. Schematic representation of a multipass membrane cascade. Cascade stages in the rectifying section decrease solute content in the recovered solvent, while stages in the stripping section enrich solute content in the concentrate stream. Reprinted with permission from ref 324. Copyright 2013 Elsevier.

and the overall rejection is expressed as

$$\text{Rej}_{i,o} = 1 - \frac{y_{i,p}}{x_{i,o}} \quad (105)$$

The three cascades were compared by assuming a constant single pass partitioning, $\text{Rej}_{i,j}$, of 55%.

Abejón et al.³²⁵ designed a continuous organic solvent nanofiltration systems based on a dual membrane cascade for the separation of an intermediate precursor of an anesthetic compound from an impurity. The dual membrane cascade consisted of a multistage retentate section, to purify the least permeable solute, and a multipass permeate section, to purify the most permeable solute. The Kedem–Katchalsky model was integrated to model the membrane transport, and four process parameters (product purity and yield, concentration factor, and total membrane area) were analyzed as a function of the applied

pressure and the recovery rate of the stage. A sensitivity analysis was performed on the effects of the operating parameters, and, from the possible set of solutions, the scenarios to maximize both the purity of the desired product and the process yield were identified.

3.5.3. Design of Experiments and Modeling. As is clear from the literature so far, the set of equations for process modeling is often solved by considering rejection and solvent flux as being constant. For a correct process modeling, however, the effect of the operating parameters on the membrane transport performance should be considered. This is not an easy task, because the mixtures often contain many components and differ widely in their properties, and the separation processes are often characterized by complicated matrixes of input parameters. One example of such integration, for process selection purposes, has been reported by Marchetti et al.²³² for the diafiltration of peptide solutions in ACN/water mixtures. In this work, concentration-dependent solute rejection and flux obtained by design of experiments were used to model the dynamics of different membrane filtration processes (constant volume and variable volume diafiltration processes for salt and solvent exchange) and select the most appropriate diafiltration technique. Model parameters were obtained by regression and statistical analysis of the experimental data.

3.5.4. Process Design. Attempts to implement fundamental transport models on a process level are few, and the reports that exist use simple, nonpredictive membrane transport models.^{227,323} Recently, Peshev and Livingston²⁴⁷ proposed to make OSN unit operations available in process modeling environments, such as Aspen Plus, HYSYS, ProSim Plus, to streamline OSN process design. Their so-called “OSN Designer” is schematically represented in Figure 25.

Matlab routines for the membrane transport models were interfaced to Aspen Plus by means of CAPE OPEN. Custom OSN unit operations for common membrane separation processes such as batch concentration, constant volume semi batch filtration, and steady-state filtration were used to describe the process. For solute and solvent properties of databank compounds, thermodynamic and physical property databases and engines were accessed. To have the possibility to use molecular structures in the simulations, the COSMO SAC method was used. They demonstrated the suitability of this technique by comparing the model simulation to the experimental data for ideal systems (rosmarinic acid in ethanol) and nonideal solutions (TOABr in toluene).

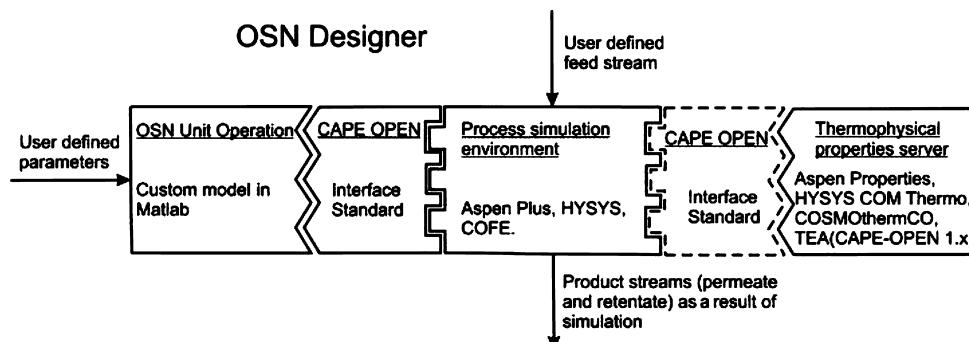


Figure 25. A schematic representation of the process simulation elements used in the OSN Designer and their interactions. Reprinted with permission from ref 247. Copyright 2013 Elsevier.

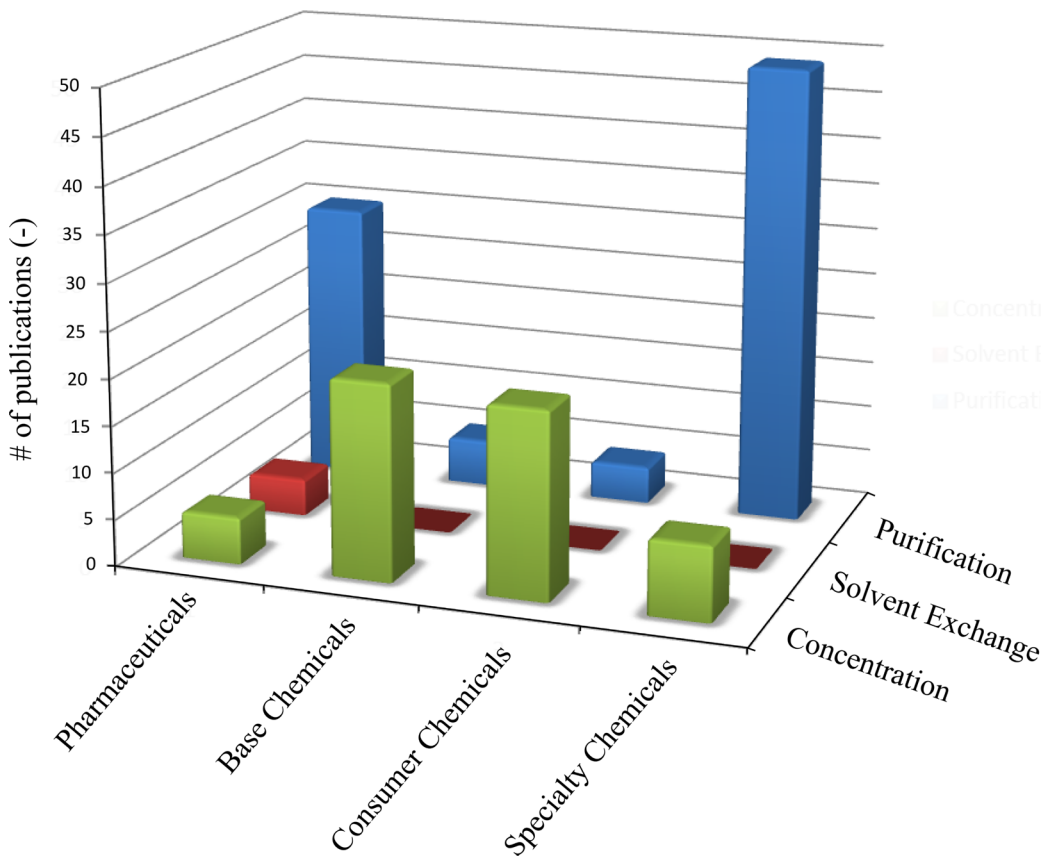


Figure 26. OSN publications focusing on applications: OSN processes versus industrial sectors.

3.6. Future Perspectives

Fundamental understanding of transport theories through OSN membranes has significantly improved in the last years. Kedem–Katchalsky and Spiegler–Kedem models can be used to describe solute and solvent transport of NF and RO membranes; however, these models treat the membrane as a “black box” and provide no information on the transport mechanism. Solution-diffusion models have been accepted and well-supported by experimental evidence for reverse osmosis and have been extended to OSN, by accounting for pressure-driven transport and allowing for the determination of sorption coefficient by solubility measurements. Multicomponent diffusion and solution-diffusion with imperfection models have been introduced to account for solute–solvent coupling. Pore-flow models, on the other hand, allow the description of the membrane structure and the correlation of the structure with the membrane performance. Uncertainties in using pore-flow models are due to the fact that the presence of pores in several nanofiltration membranes is questioned and the common hypothesis of uniform pores is often far from the reality. As it has been observed that transport at the nanoscale dimension is affected by molecular affinities between solute, solvent and membrane, different pore-flow models have been developed, which account for charge and molecular affinity effects, by potential functions. From the analysis of the different models, it can be concluded that solution-diffusion models are suitable for RO and dense NF membranes, while pore-flow models are suitable for membranes characterized by physically distinguishable pores. However, it is still challenging to establish which model provides the best description for some types of OSN membranes, when the membrane physicochem-

ical structure is not known. Furthermore, the generalization of the modelling strategy is complicated by the fact that the same membrane can behave differently in different solvents, when swelling comes into play. Finally, for thin film composite membranes, the effects of both support structure and chemistry on the overall membrane performance should be taken into account.

The use of mechanistic models based on structure–performance relationships can be supported by advanced structural characterization techniques, capable of measuring pore size, pore length, porosity, and tortuosity. On one hand, these membrane characteristics help mechanistically explain membrane transport and select the correct transport mechanism; on the other hand, they enable predictions of membrane performance and design of “customized” membranes for targeted applications. Contribution of computational simulations at the molecular level can also support the modelling tools. A priori methods for calculating sorption and diffusion coefficients, physicochemical solute and solvent properties, and accurate predictions of the molecular structure, thanks to computer-aided molecular dynamic simulations,^{326,327} could help in reducing the number of unknown model parameters and simplify the fitting procedure required to use the model. When the models contain unknown parameters that cannot be estimated a priori, empirical or semi-empirical correlations can be developed, characterized by fitted parameters. These permit the successful description of membrane transport, based on a limited number of experimental data. Such models are useful for experimentalists, because they allow saving of time and efforts, and allow one to make predictions from an initial dataset.

Furthermore, together with providing fundamental understanding, modeling at the membrane scale is also useful for supporting modeling at the process scale. Integration of transport modeling with process modeling should become a key point for efficient process development, thus promoting the implementation of NF processes at the large scale.

4. MEMBRANE APPLICATIONS IN ORGANIC SOLVENTS

Although OSN is a relatively new technology, it has already found applications in academic and industrial research. OSN applications range from the refining industry to fine chemicals and cover processes such as solvent recovery, enhanced organic synthesis, and pharmaceutical purifications. OSN has the potential to change the conventional way reactions, separations, and recycling are performed in the chemical industries. Besides stand-alone OSN, hybrid processes also offer great advantages. Process intensification by the combination of OSN with other purification technologies can lead to both greener processes and improved yields and purity.⁴⁸⁷

Figure 26 and Table 8 summarize the main areas of OSN applications based on OSN processes and industrial sectors. In

Table 8. Breakdown of the OSN Application References Based on Processes and Industrial Sectors, According to the CEFIC Report³²⁸

application	pharmaceuticals	base chemicals	consumer chemicals	specialty chemicals
Concentration				
solute enrichment	329–332	19	38, 333–338	186, 339
solvent recovery	340–343	20, 21, 24, 27, 28, 344–358	359–371	372–377
Solvent Exchange	4, 224, 378, 379			
Purification				
impurity removal	3, 32, 37, 119, 227, 322–324, 380–395	23, 396–399	400–404	405
OSN-assisted chemical synthesis	5, 321, 406–409			410–414
catalytic processes	415, 416		25, 416–459	
OSN-assisted crystallization	460, 461			

this section, we have attempted to categorize all of the reported applications of OSN from the literature according to whether the primary claimed use was for concentration, solvent exchange, or purification (cf., Figure 1). This is instructive when one considers the future needs for OSN membranes, because concentration and solvent exchange in general require a high solute rejection, whereas purification prizes better selectivity between two solutes over increased solute rejection. We have also assigned all reported applications according to the industrial sector to which they claim to be relevant. The European Chemical Industry Council (CEFIC)³²⁸ divides chemical utilizing industries into four broad sectors: (i) pharmaceuticals; (ii) base chemicals, which cover petrochemicals and derivatives and basic inorganics; (iii) consumer chemicals, which cover products sold to the final consumers;

and (iv) specialty chemicals, which cover the auxiliaries for industry, paints, inks, dyes, and pigments.

We have followed this classification scheme. Where an industrial sector was not stated by authors, we have nevertheless estimated the sector for which the work is most likely to be relevant. This analysis we believe gives some insight into which areas we might expect to see a more rapid accumulation of scaled up OSN applications.

4.1. Concentration

A schematic representation of a concentration process is shown in Figure 1a. This is based on separation of the solute from the solvent, to either recover a high-value solute from a diluted solution (solute enrichment) or recover the solvent, by removing an impurity dissolved in it (solvent recovery). In both cases, the defining feature is that the solute(s) is(are) retained by the membrane, and so is(are) concentrated as the solvent passes through the membrane. Distillation is the conventional process to perform solute concentration. However, distillation usually requires elevated temperature and phase change, which make the conventional process energy intensive and may induce degradation of the valued solute. Hence, OSN is an excellent alternative to distillation due to its mild operating conditions.

4.1.1. Solute Enrichment. **4.1.1.1. Pharmaceuticals.** A classical application of membrane technology in the pharmaceutical industry is the isolation and concentration of antibiotics, pharmaceutical intermediates, or peptides from organic solvents or aqueous solutions containing organic solvents. Cao et al.³²⁹ applied OSN to the postsynthesis recovery of 6-aminopenicillanic acid (6-Apa, 216 g mol⁻¹), an intermediate in the enzymatic manufacturing of synthetic penicillin, from its bioconversion solution using a MPS-44 membrane (Koch). Thanks to a high solute recovery (90–95%) and a low product loss, the payback time of the process was reduced to less than one year. Shi et al.³³⁰ developed a PI-based membrane for the concentration of the antibiotic spiramycin, which is conventionally extracted from bacterial broths with butyl acetate. The membrane showed a stable long-term separation performance with excellent solvent resistance and rejections around 99%. One of the current industrial OSN processes is an API recovery concentrating a 1 wt % API waste stream to 10 wt %, which is then fed to existing downstream processing units for further purification. The unit is small in size with the membrane area of only 15 m² (DuraMem 4 in. spiral modules), hence not very capital-intensive (<1 year payback period), but generates a profit of 1 million euros per year.³³¹

4.1.1.2. Consumer Chemicals. In recent years, the interest in the development of new separation techniques for natural compounds with biological activity and potential benefits for human health has increased. Such compounds are natural products found in aromatic herbs and other plants, vitamins, antioxidants, flavonoids, terpenoids, carotenoids, catechins, phytoestrogens, and minerals. Several separation processes have been developed for the extraction and concentration of such compounds. Peshev et al.³³³ used DuraMem 200 membrane to concentrate antioxidant extracts of rosemary in ethanol. They obtained good permeate fluxes and almost complete rejection of rosmarinic acid and other antioxidant constituents of the herb. Interestingly, no significant loss of antioxidant property was caused by the filtration process. In another investigation, OSN was applied to the enrichment of γ -oryzanol, a nutritionally valuable phytochemical with antiox-

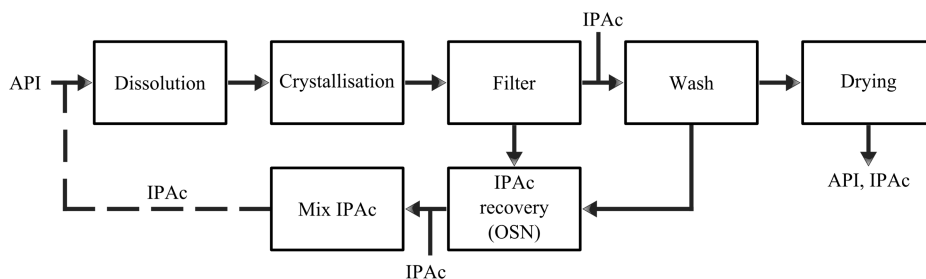


Figure 27. Process diagram of an API recrystallization combined with solvent recovery and recycle. Adapted with permission from ref 341. Copyright 2012 Royal Society of Chemistry.

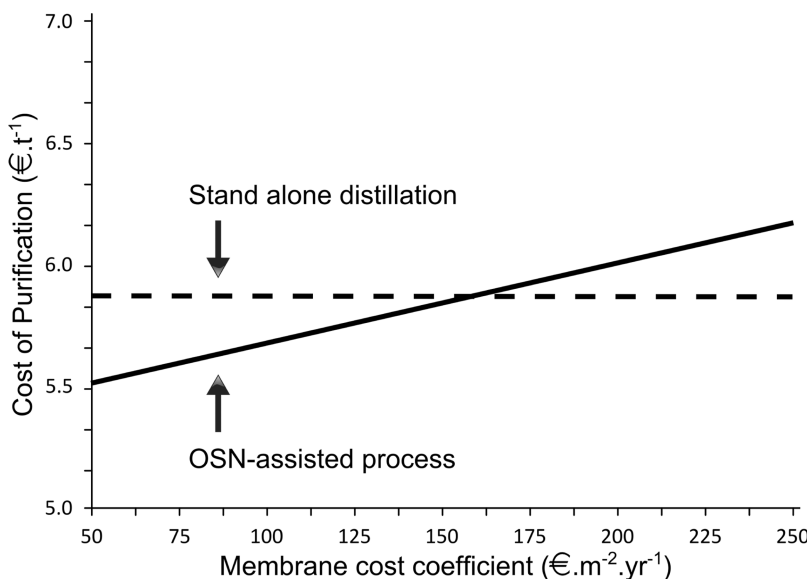


Figure 28. Economics of a hybrid OSN-distillation process based on the cost for the purification of one ton of product. Adapted with permission from ref 342. Copyright 2014 Elsevier.

idant properties, contained in crude rice bran oil.³³⁴ The increase in the oil antioxidant capacity was almost 2-fold. Several membranes were screened and applied in a two-step membrane cascade: (i) separation between glycerides and γ -oryzanol was performed in the first membrane stage, promoting oil enrichment in the phytochemical, and (ii) oil refining as well as further enhancing its γ -oryzanol content were performed in the second membrane stage.

4.1.1.3. Specialty Chemicals. Tsui and Cheryan³³⁹ reported a membrane-based method to purify and concentrate xanthophylls from ethanol extracts of corn. Xanthophylls are yellow-orange oxygenated pigments of the carotenoid family, valuable as natural colorants or as nutraceuticals. Different commercial UF- and NF-membranes were screened, and finally Desal-DK performed best in terms of flux, rejection, and stability.

4.1.2. Solvent Recovery. Industrial processes consume and discharge large volumes of organic solvents. Although new technologies are continuously being developed and evaluated to avoid use of organic solvents (e.g., solid-phase reactions), they are still the most widely used reaction media. In addition, purification technologies for industrial products are usually based on liquid–liquid, liquid–solid, or liquid–gas equilibria, requiring large quantities of organic solvents. Handling a large amount of organic solvents has a number of undesirable effects such as increased risks of cancer, mental diseases, air pollution, contamination of soil and groundwater, degradation of the

ozone layer, and greenhouse effect. Hence, reduction in the amount of solvent released from an industrial process is crucial. Current state-of-the-art OSN membranes allow the design of innovative configurations to drastically reduce solvent consumption and enhance sustainability of downstream processes which was assessed through a two-stage solvent recovery membrane cascade.⁴⁸⁸

4.1.2.1. Pharmaceuticals. In pharmaceutical processes, the use of OSN has been proposed to recover and reuse organic solvents, thus allowing reduction of the overall solvent consumption. Moreover, OSN-based solvent recovery features energy savings due to mild operating conditions, leading to increased safety and reduced environmental effects. Recent studies explored the use of Starmem 122 and DuraMem 150 membranes to recover methanol, ethanol, isopropanol, and ethyl acetate after the manufacturing process of Imatinib, Riluzole, Donepezil, Atenolol, and Alprazolam drug products and improve the sustainability of API production.³⁴⁰ Rundquist et al.³⁴¹ demonstrated the feasibility of using OSN as an alternative to solvent recovery using distillation. They showed that OSN was capable of recovering isopropyl acetate from crystallization mother liquors containing more than 40 different organic impurities, with sufficient purity for reuse in subsequent API crystallization. The process flow diagram for API recrystallization with solvent recovery and recycle is shown in Figure 27.

Regarding economics, energy-efficiency calculations confirmed that OSN uses 25 times less energy per liter of recovered solvent as compared to distillation. However, due to increasing solubility problems of the impurities during the filtration process, a hybrid approach combining OSN and distillation was also investigated, and the results demonstrate that the energy consumption remains 9 times lower than when distillation is used alone.

Furthermore, Micovic et al.³⁴² studied the separation of heavy boiler (hexacosane) from low and middle boiler (decane and dodecanal) in a wide boiling mixture from hydroformylation using a hybrid process combining OSN and distillation. It was concluded that at high temperatures, the OSN process can be more economical than stand-alone distillation as can be seen from Figure 28.

Nimmig and Kaspereit³⁴³ investigated a process combining single-column chromatography, racemization, and solvent recovery by membrane filtration to produce single enantiomers at high yields. The model substance used in this work is the racemic pharmaceutical ingredient chlorthalidone with a molecular weight of 339 g mol⁻¹. Thanks to the coupling of chromatography with nanofiltration, the process, shown in Figure 29, was capable of (i) increasing the yield of the production of single enantiomers and (ii) decreasing solvent consumption.

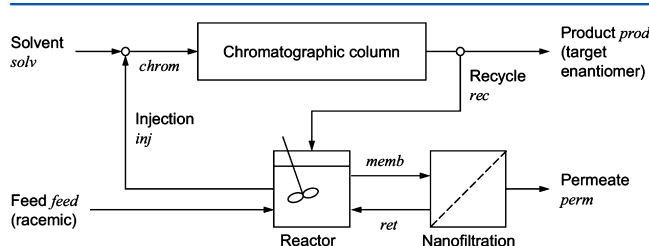


Figure 29. Schematic process setup for a direct coupling: chromatographic, racemization, and nanofiltration units. Reprinted with permission ref 343. Copyright 2013 Elsevier.

4.1.2.2. Base Chemicals. In recent years, increasing demand for more sustainable processing has led to the development of membrane-based concentration processes for chilled solvent recovery from lube oil filtrates.³⁴⁴ Solvent lube oil dewaxing processes are applied worldwide in refineries where a waxy oil stream is mixed with apolar solvents, such as toluene and methyl ethyl ketone. The wax component is precipitated by cooling the stream, followed by the filtration of the wax. Conventionally, the dewaxed solvent mixture is submitted to multistage flash and distillation operations to recover the solvent, which has to be cooled prior to recycling in the dewaxing process²⁸ (cf., Figure 30).

Different kinds of OSN membranes and processes have been developed to reduce the energy consumption of the recovery unit.³⁵⁵ Another advantage of such processes is that the recovery of solvent allows the use of a larger amount of washing solvent stream, leading to a higher purity wax product, while the overall solvent consumption is still kept low. The membrane-based solvent recovery unit of ExxonMobil's refinery allows the annual recovery of 300 000 m³ of clean solvent in the lube processing area.²⁷ Recently, Namvar-Mahboub et al.³⁴⁵ fabricated thin film nanocomposite membrane containing amino-functionalized UZM-5 nanoparticles by interfacial polymerization on poly(ether imide)/

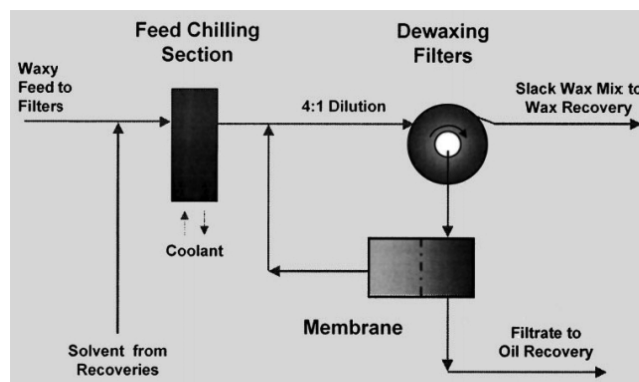


Figure 30. Process diagram of a dewaxing process with solvent recovery. Reprinted with permission from ref 28. Copyright 2000 Elsevier.

modified SiO₂ asymmetric substrate tailored for dewaxing solvent (MEK and toluene) recovery from lube oil.

4.1.2.3. Consumer Chemicals. The extraction stage of edible oil in the oil industry features toxic solvents, calling for efficient solvent removal and recycle. The conventional solvent recovery technology, distillation and evaporation, has high energy consumption, the solvent being around 70–75 wt % of the oil–solvent mixture. Hence, the possibility of a nanofiltration-based extraction methodology has been evaluated by Darvishmanesh et al.³⁶⁰ The study compared a wide range of membranes, from GE-osmonics, Nadir, Evonik MET, and SolSep, in a wide range of solvents: ethanol, isopropanol, acetone, cyclohexane, and *n*-hexane. The proposed OSN process allows the replacement of the latter two traditionally used solvents with the former solvents obtainable from renewable resources. Furthermore, deacidification and solvent recovery from soybean oil/*n*-hexane miscella using nanofiltration composite membranes present a high potential for application in the oil industry.³⁵⁹ Four tailor-made composite membranes of PVDF as a support and PDMS or CA as coating layer, and the commercially available SolSep 030306 composite membrane were used to remove *n*-hexane and free fatty acid from crude soybean oil/*n*-hexane mixture. Permeate flux of 20 L m⁻² h⁻¹ at 20 bar, 80% oil rejection, and 58% fatty acid removal were achieved by the best performing membrane, which was the PVDF containing 12 wt % Siloc paste.

4.1.2.4. Specialty Chemicals. Ionic liquids are salts in the liquid state, usually featuring low melting points, and they are immiscible both with many organic solvents and with water. Since the pioneering investigation of Wilkes et al.,³⁷² ionic liquids have shown growing popularity as synthesis and extraction media. Ionic liquids are considered designer solvents; the ease of tuning their physicochemical properties by carefully selecting the anion–cation pair extends their applicability. However, concerns about the sustainability of the synthetic routes to ionic liquids have been raised.³⁷³ Hence, the recovery and reuse of such high-value solvents could promote their industrial applicability. Heck, Suzuki, Stille, Sonogashira, and Ullmann carbon–carbon cross-coupling reactions are often performed in ionic liquids due to their ability to act as stabilizing agents for the monodispersed metal nanoparticles, thereby preventing agglomeration as well as forming a protective layer to reduce the oxidation rate of the active catalytic metal surface. Additionally, ionic liquids allow the immobilization of the catalyst and facilitate the extraction of the

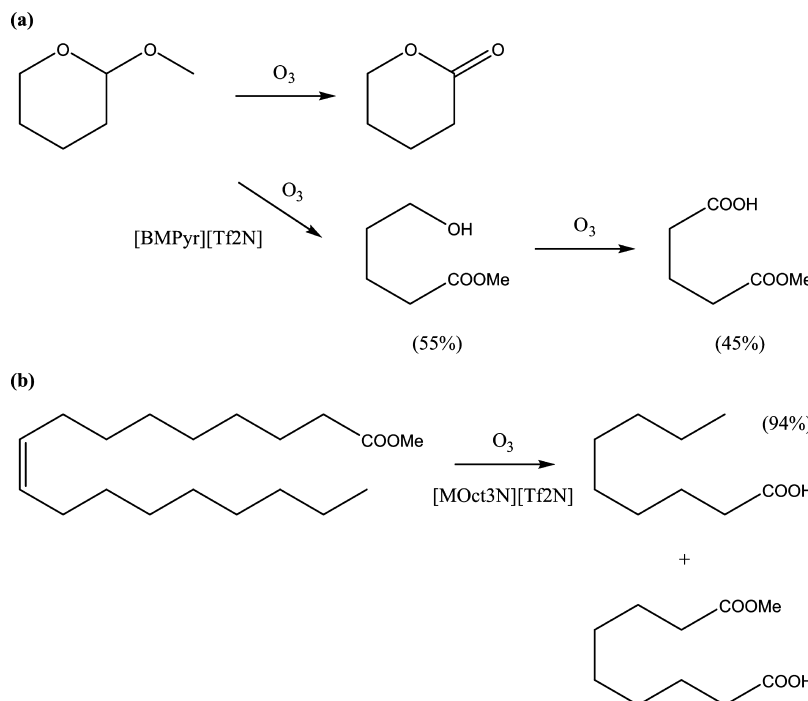


Figure 31. (a) Ozonation of 2-methoxytetrahydropyran, with formation of methyl 5-hydroxypentanoate or D-valerolactone. Methyl 5-hydroxypentanoate can be further oxidized to 5-methoxy-5-oxovaleric acid. (b) The oxidative splitting during the ozonolysis of methyl oleate yields pelargonic acid with high selectivity (94%).³⁷⁵

product to the organic layer, while the catalyst is retained in the ionic liquid phase and recycled.

An OSN-based process for carbon–carbon cross-coupling product purification and ionic liquid recycle was first proposed by Han et al.³⁷⁴ In this work, Cyphos 101 ionic liquid showed 95% rejection on Starmem 122 membrane in methanol and ethyl acetate. Using a single-stage OSN filtration, only 48% purity and 78% yield was achieved. However, a significant improvement (74% purity and 100% yield) in performance was possible with a two-stage membrane separation. Hence, OSN demonstrated to be a promising technique for postreaction separations following application of ionic liquids in organometallic catalysis. Moreover, the potential of OSN-assisted product separation from ionic liquids was tested with two ozone-mediated model reactions, the oxidation of acetals to esters, and the ozonation of methyl oleate to monomethyl azelate and pelargonic acid³⁷⁵ (cf., Figure 31).

The highest permeance was achieved with a PI-supported zeolite filled PDMS membrane, while the highest rejection (96%) among the studied ionic liquids was recorded for 1-butyl-1-methylpyrrolidinium bis(trifluoromethylsilyl) ether and methyltriocetyl ammonium bis(trifluoromethylsilyl) ether, using PI-based DuraMem membranes. Moreover, a single-stage nanofiltration unit was successfully employed in the downstream processing of the products using DuraMem membranes. Membranes were also proposed to be used in biofuel production for the recovery of ionic liquids. Ionic liquids are in general not applied in the biorefining industry due to recycling difficulties regarding economic and environmental considerations. However, ionic liquids are ideal solvents for lignocellulose. Hence, Abels et al.³⁷⁶ proposed OSN for the recovery of 1,3-dimethylimidazolium dimethylphosphate ionic liquid using Starmem 240, Desal DL, and DK membranes. Because of the high osmotic pressure and high ionic liquid viscosity, a strong flux decline was observed at higher concentrations. The attempt to overcome this issue by

gradually increasing the temperature to decrease the viscosity of the concentrated ionic liquid solutions (unexpectedly) did not enhance the permeation rate. Nevertheless, the OSN process achieved ionic liquid recovery with 80% purity through the effective fractionation of ionic liquids, water, glucose, cellobiose, and raffinose. A further example is the use of FilmTech NF270-44 membranes for the recovery of 1-butyl-3-methylpyridinium tetrafluoroborate ionic liquid, which was used to dissolve lignocellulose.³⁷⁷ The research reveals the effect of pressure gradient, investigates different feed concentrations, discusses the underlying kinetics, and also deals with membrane fouling and concentration polarization.

4.2. Solvent Exchange

A schematic representation of a solvent swap carried out by diafiltration is shown in Figure 1b. The solution changes from being rich in solvent A to being rich in solvent B. The main advantage of applying membrane filtration to perform a solvent swap is that it is an athermal process, allowing for solvent exchange from a high-boiling to a low-boiling solvent.

4.2.1. Pharmaceuticals. Chemical synthesis is mainly done in organic media and usually requires several reaction steps to obtain the final product. Furthermore, the purification and isolation of intermediates often require solvent exchange, elevated temperature, addition of chemicals, or vacuum. Athermal membrane separations offer a great alternative to these conventional downstream processes. Solvent resistant MPF-50 and MPF-60 nanofiltration membranes were successfully employed in a pharmaceutical solvent exchange from ethyl acetate with methanol.³⁷⁸ Such approach required solvent miscibility and can be carried out in batch or continuous constant volume diafiltration.

Lin and Livingston⁴ showed the feasibility of a counter-current membrane cascade applied to continuous solvent exchange (cf., Figure 32), which addresses the difficulties of

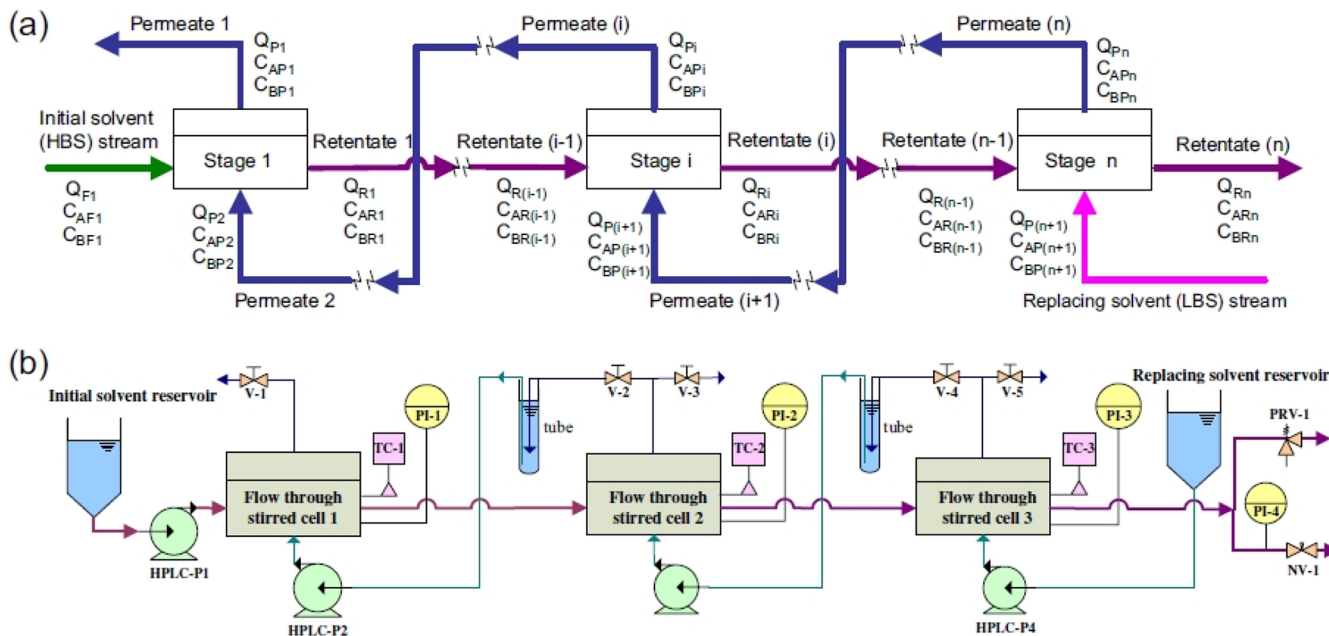


Figure 32. (a) Schematic representation of n -stage counter-current membrane cascade for solvent exchange from a high-boiling solvent (HBS) to a low-boiling solvent (LBS); (b) PID of a three-stage cascade, where PI, TC, PRV, and NV stand for pressure indicator, temperature controller, pressure release valve, and needle valve, respectively. Reprinted with permission from ref 4. Copyright 2007 Elsevier.

traditional distillation processes, such as the swap of target compounds from a high-boiling solvent (HBS) to a low-boiling solvent (LBS). A quaternary ammonium salt, TOABr, was used as a marker instead of an API intermediate. Theoretical and experimental investigations were carried out on the process parameters of the solvent exchange. It was shown that the cascade configuration allows continuous solvent exchange via counter-current approach and reduced solvent use.

Furthermore, Rundquist et al.³⁷⁹ demonstrated advantages of combining OSN with counter-current chromatography (CCC) for solvent exchange. The application of CCC was facilitated by the use of membrane assisted solvent exchange yielding a CCC feed with only traces of solvent used in the prior process.

4.3. Purification

The combined sales of the global top 50 largest chemical companies were as high as \$961.8 billion in 2012.⁴⁶² Purification processes can account for up to 90% of the total manufacturing costs,³ which indicates a significant market for OSN. The effectiveness of OSN purification processes can be described by product yield and purity as well as solvent consumption. Insufficient separation between solutes represents one of the major challenges of OSN purification, leading to low yield or purity and high solvent consumption, although these parameters are not always reported in each OSN application study. The sigmoidal rejection curves of OSN membranes, shown in Figure 7, call for large differences in rejection of product and impurity to achieve a feasible separation. This is summarized in Figure 33.

Insufficient discrimination between solutes to be separated limits the industrial application of OSN. To compete with conventional purification technologies, much better separation performance should be obtained by either the membranes themselves or the membrane processes. The improvement of membrane materials is revised in section 2, while the present section gives examples of membrane process development and intensification for the following applications: (i) impurity

removal; (ii) OSN-assisted chemical synthesis; and (iii) catalytic processes.

4.3.1. Impurity Removal. 4.3.1.1. Pharmaceuticals.

Because more than one-half of the capital investments of pharmaceutical processes are related to purification processes,³ improvement of separation strategies is of utmost importance for the pharmaceutical industry. Furthermore, synthesis of APIs is almost exclusively performed in organic solvents, which requires subsequent isolation of products with high added value from the solvent. The sustainability of API purification in organic solvent by means of membrane processes and the competitiveness of OSN processes with respect to conventional API purification methodologies such as chromatography and recrystallization were demonstrated by Szekely et al.³⁸¹ via environmental and economic analysis. Figure 34 illustrates the simplicity of OSN as compared to conventional API purification technologies. In general, low energy consumption, continuous operation mode, and straightforward scale-up are among the main advantages of membrane-based purification processes as compared to other separation processes.

Geens et al.³ showed that a single pass nanofiltration system has 200 times lower energy consumption than a throughput distillation unit (cf., Figure 2). Another advantage of using membranes in the pharmaceutical industry is the possibility of concentrating the API, intermediate, or end product at room temperature, avoiding its degradation. Martinez et al.³⁸⁶ developed a two-stage OSN system capable of recovering up to 99% drug product. Pharmaceutical regulatory authorities regularly issue guidelines lowering the limits of genotoxic impurities (GTI) in APIs, calling for GTI-specific purification steps.^{384,385,463} The main challenge associated with the degenotoxication of APIs by membranes lies in the fact that the majority of such impurities are highly reactive species and can thus attack the polymeric membrane framework at a molecular level.³⁸⁰ Alternative purification technologies for reaching ultralow genotoxin levels in drug products are based

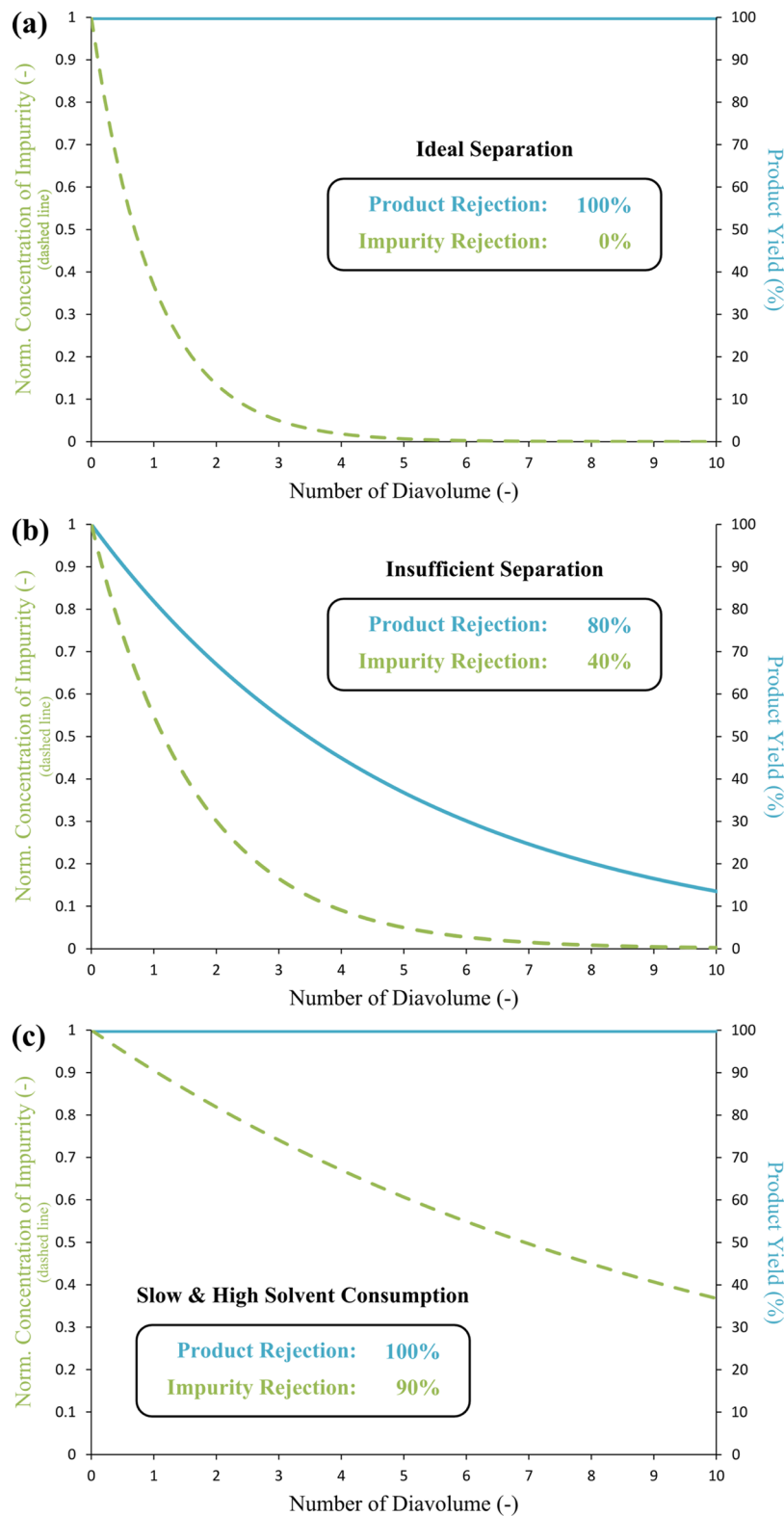


Figure 33. Case studies of purification via constant volume diafiltration: the product is retained and the impurity passes through the membrane. (a) Ideal separation; (b) insufficient separation; and (c) feasible but slow separation with high solvent consumption.

on the application of OSN alone or combined with scavengers. Successful API degenotoxication was demonstrated by Szekely et al.³⁸² by using OSN in diafiltration mode: the relatively small genotoxic molecules were pushed through the membrane by the continuous addition of fresh solvent to the retentate, while the relatively large API molecules were retained. The aim is

achieving high genotoxin removal and low API loss, which mainly depends on the molecular size gap between the impurity and the API, as well as the polarity of the impurity. Boundaries of OSN-assisted API downstream processing were identified, and three case studies were presented. The first case covered an example where the purification of an API postreaction stream is

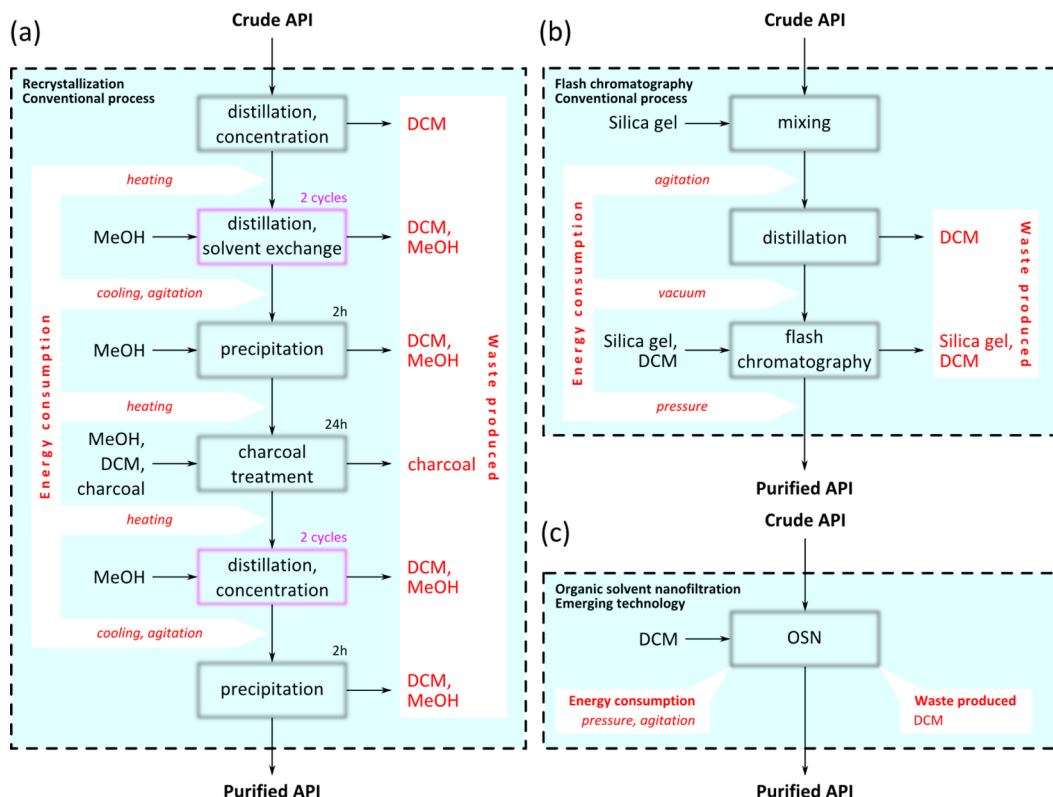


Figure 34. Comparison of purification processes for a steroid type API. The number of operation units, energy consumption, and the waste streams highlight the simplicity of OSN technology. Adapted with permission from ref 381. Copyright 2013 Royal Society of Chemistry.

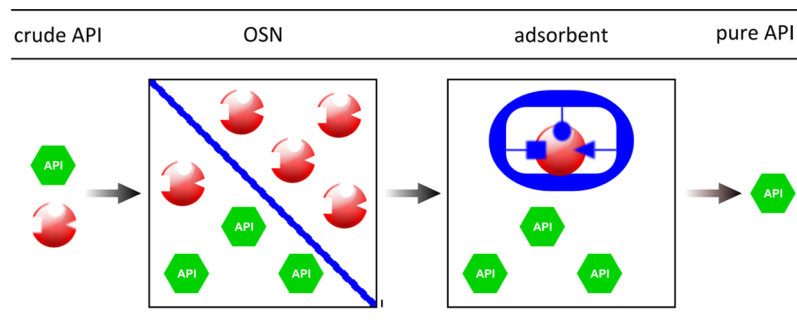


Figure 35. Schematic of hybrid purification process featuring nanofiltration coupled with adsorbents, where the latter was employed to remove trace level of impurities from the retentate stream.³²

straightforward, given the large molecular weight difference between the genotoxic impurity and the product. The molecular weight difference in the second case was much smaller but still allows reasonable purification efficiency via OSN. However, high number of diaulomes were required to obtain sufficient purity of the product, which eventually led to significant product loss. The third case was when OSN alone is not sufficient for API purification and other technologies, or improved OSN membranes are required. Molecularly imprinted OSN membranes have been fabricated for the three-way separation of ternary systems comprising an API, a potentially genotoxic building block, and catalyst.¹¹³

Furthermore, genotoxic bromoethane was successfully removed from an API despite the small molecular weight gap of only 33 g mol⁻¹.³²³ To achieve this separation, DuraMem 150 and 200 membranes were used in a cascade configuration. Further examples of hybrid separation processes featuring OSN include the removal of genotoxic palladium³⁸⁸ and *N,N*-

diisopropylurea^{32,464} from API postreaction streams (cf., Figure 35).

Interestingly, due to the small size of the API, the process by Pink et al.³⁸⁸ retained the Suzuki catalyst and allowed the permeation of the product through the membrane, followed by further polishing with commercial resins. On the other hand, the process by Szekely et al.³² retained the product and permeated the relatively small genotoxic impurity through the membrane. In this case, the API was further purified by impurity specific molecularly imprinted scavengers featuring methacrylic acid binding sites. Molecular imprinting has been recently suggested for genotoxin scavenging of acetamide,³⁸⁴ arylsulfonates,⁴⁶³ ureas,⁴⁶⁵ acrolein,⁴⁶⁶ and aminopyridines.⁴⁶⁷ It is worth noting that the latter filtration process is preferable, allowing the direct concentration of the product in the nanofiltration rig, while in the former process the API ends up in a large volume of solvent in the permeate stream after constant volume diafiltration. Constant volume diafiltration was

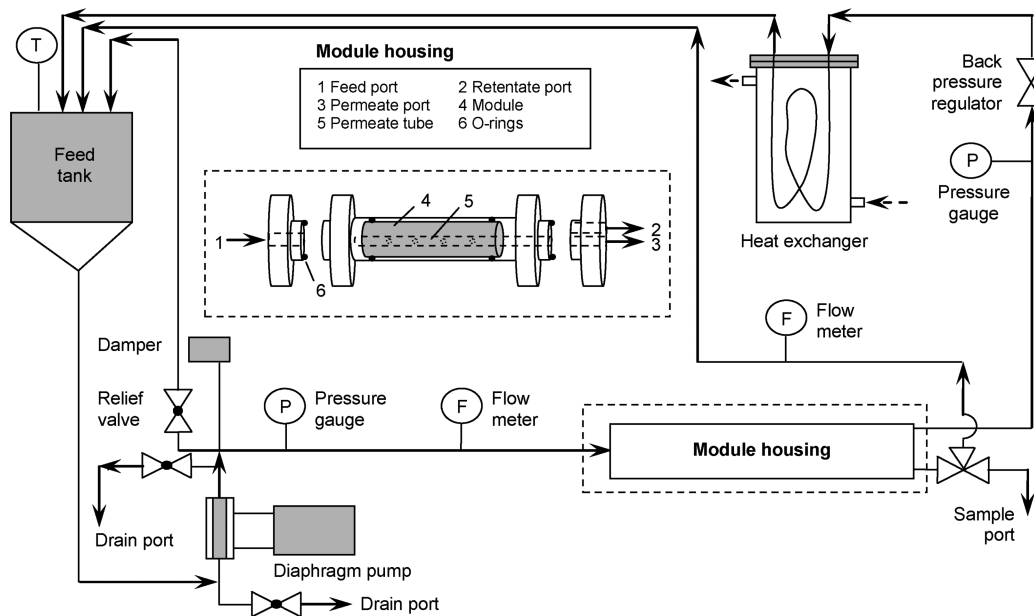


Figure 36. Pilot plant filtration system for API purification consisting of a 5 L capacity feed vessel and module housing equipped with 1.8-in. × 12-in. DuraMem spiral-wound module. Reprinted with permission from ref 227. Copyright 2010 American Chemical Society.

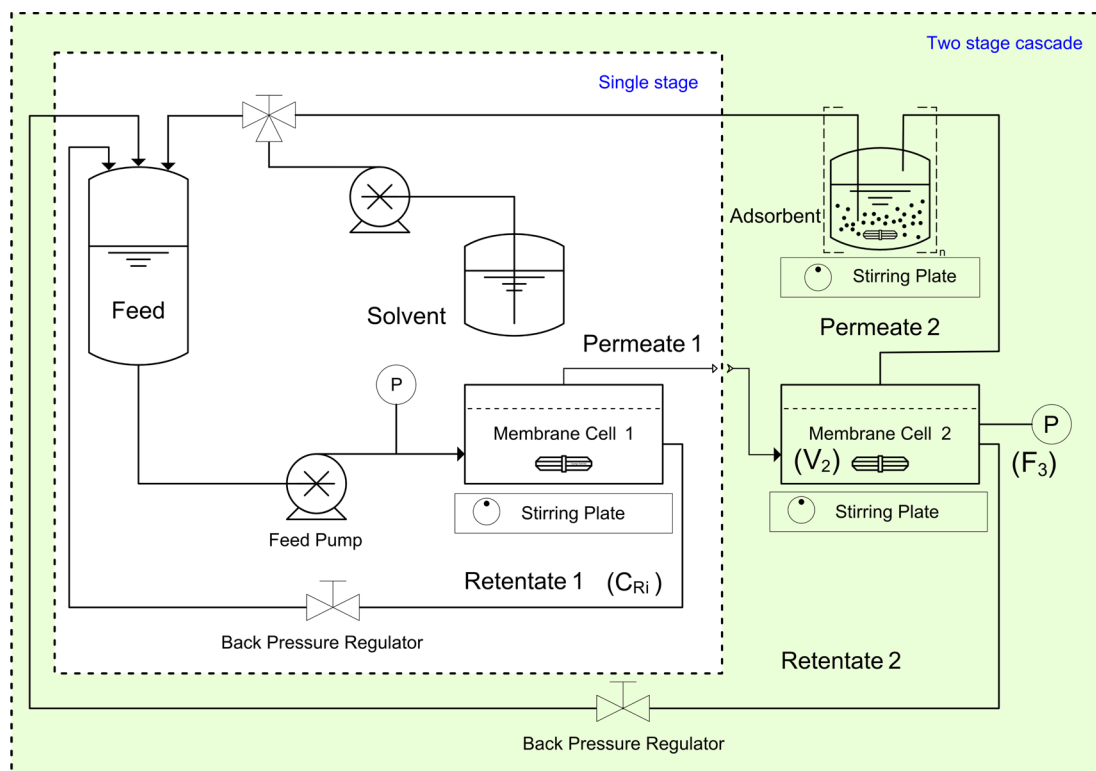


Figure 37. Schematic representation of a two-stage membrane cascade with recycle of retentate and an adsorption solvent recovery unit. Adapted with permission from ref 394. Copyright 2013 Royal Society of Chemistry.

carried out to purify APIs and remove trace genotoxic impurities from the class of aminopyridines and sulfonates.³⁸¹

Martinez et al.³⁸⁷ investigated the effect of impurities on API recovery. It has been demonstrated by Ormerod et al.³⁸⁹ that API purification can be facilitated through pH adjustment and addition of water to the feed solution. The protonation of the amine functionality of the API and the impurity increased the hydrophilicity and thus the rejection difference between the

two solutes. The stability of the DuraMem membrane was assessed, and it was concluded that mineral acids are more suitable for acidifying the API solution than organic acids.

Solute fractionation was also recently performed by employing a three-stage cascade.^{324,390} Stripping of a binary feed solution, containing an API and an excess reagent, was carried out to produce an API-rich product stream. The stream could

be further polished by crystallization (impossible with the original feed solution).³⁹⁰

The applications mentioned so far were performed at laboratory scale using flat sheet membranes. Examples of pilot and industrial scale application of OSN in the literature are scarce. A pharmaceutical separation challenge at Janssen Pharmaceutica NV has been overcome using OSN (cf., Figure 36).²²⁷ An intermediate of a drug candidate and its oligomeric impurities were successfully fractionated using spiral-wound membrane modules achieving 99.7% final purity and 90% API recovery. Operation of the DuraMem spiral-wound membrane modules in DMF and THF up to 10 days and 120 days, respectively, demonstrated stable flux and consistent separation performances over time.

Unfortunately, for a variety of processes, adequate separation of components with MW close to one another is impossible in a single-membrane separation process, due to the typical rejection–MW profile of NF membranes (cf., sigmoid rejection curve in Figure 7). Similar to the case of distillation, where counter-current cascades of several stages are used to obtain the desired separation, counter-current nanofiltration cascades can be applied to achieve better performance.^{322,391} The membrane cascade system is designed such as the permeate stream coming out from the one filtration unit is processed further in another filtration unit, while the retentate is recycled or collected. Although many cascade models have been proposed,^{392,393} several implementation and control challenges have posed difficulties for their widespread use. Recently, a simple cascade configuration has been proposed by Kim et al.^{37,394} that overcomes previous implementation limitations. A schematic representation of a two-stage cascade with recycle of permeate is given in Figure 37.

The process bypasses the use of buffer tanks between membrane units and pressure pumps, reducing capital expenditure and simplifying process control. The process has been demonstrated on separation of PEG compounds where the yield increased from 59% to 94% without compromising the product purity.

The most crucial limitation of OSN in API purification is the low product yield due to insufficient rejection of the product.³⁸² This is the reason why most of the OSN applications are limited to lab-scale or pilot-scale investigations and industrially implemented OSN processes are scarce. In other words, the high loss of product hinders the widespread application of OSN in the pharmaceutical and fine chemicals industries. Through an API purification case study, Kim et al.³⁹⁴ demonstrated that the proposed process significantly increases the API yield without compromising its purity (cf., Figure 38). Moreover, they reduced the membrane screening time. Peeva et al.³⁸³ demonstrated continuous purification of an API from a potentially genotoxic impurity in a two-stage membrane cascade: high purity of the API >99% could be achieved from a feed stream purity of 78%.

4.3.1.2. Base Chemicals. Werhan et al.³⁹⁸ applied OSN to the valorization of lignin as a renewable source of chemicals. Lignin is a biopolymer with a broad MW distribution and is currently a side product from pulping processes in the pulp and paper industry and is expected to be available in even larger amounts from biorefineries in the near future.³⁹⁷ High-value monomeric chemicals such as vanillin, methyl vanillate, 2-benzylphenol, and benzyl phenyl ether were separated from the high MW byproducts from the oxidation of lignin. DuraMem, Puramam, and Koch SelRo membranes were characterized by

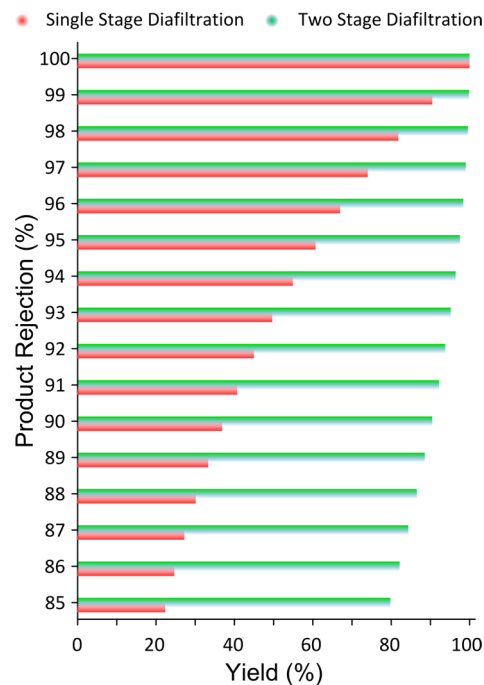


Figure 38. Improvement of the API yield after 10 diavolumes. The two-stage diafiltration configuration significantly improves the yield, overcoming the membrane limitation inherent in the conventional single-stage diafiltration for rejection less than 99%. The process achieves high product yield for APIs with rejection above 90%. Adapted with permission from ref 394. Copyright 2013 Royal Society of Chemistry.

ethyl acetate flux and monomer rejection, and PuraMem S600 (previously known as S380) was identified as the most appropriate membrane for the desired separation.

Othman et al.³⁹⁹ reported on the potential of incorporating OSN membranes for biodiesel separation processes. Commercially available Solsep, Starmem, Desal, and MPF membranes were compared in terms of their capabilities of separating the biodiesel from the mixture of the homogeneous catalyst, glycerin, and methanol after the transesterification process. The OSN process was enhanced by reducing the alkalinity value of the transesterification product from pH 12 to 9, as the membranes were found to be significantly damaged at pH 12.

4.3.1.3. Consumer Chemicals. The purification of mono- and oligosaccharides was proposed and successfully achieved by OSN membrane cascades.⁴⁰⁴ Because of the fact that single-stage membrane processes lead to insufficient purity or yield, conventionally simulated moving bed (SMB) chromatography is used for challenging industrial saccharide separations such as glucose–fructose. Hence, a membrane cascade designed with a derivative of the McCabe–Thiele method was proposed for three sugar separations, raffinose–sucrose, fructose–glucose, and xylose–glucose. It is worth mentioning that the same specifications as the reference SMB were reached by the nanofiltration approach as the fructose purity was increased from 50% to 94%. The techno-economic evaluation of OSN membrane cascades relative to SMB chromatography showed that, although a high number of OSN stages is required, the cost of the cascade is higher than the cost of the reference SMB only for the most difficult case (glucose–fructose). It was also concluded that the competitiveness of OSN cascades over SMB chromatography becomes significant as the production scale increases.

Nwuha et al.⁴⁰⁰ isolated biologically active catechins from green tea and removed caffeine from the extract by means of nanofiltration using Desalination Systems G-10 and G-20 membranes. A similar approach was carried out on Sideritis ssp. L to obtain valuable flavonoids using ethanol as a solvent and DuraMem 300 and 500 NF membranes.⁴⁰¹ The concentration and fractionation of polyphenols from plant extracts by nanofiltration and its combination with other separation techniques (adsorption, precipitation, crystallization) to increase the selectivity of the process have been investigated by Tsibranska and Saykova.⁴⁰² The separation of fatty acid mixtures by polydicyclopentadiene-based OSN membranes was explored envisaging large-scale industrial application.⁴⁰³ Although free fatty acids are not distinguished by the membranes, the addition of triisobutylamine led to the slower permeation of *cis*-fatty acids than saturated and *trans*-fatty acid salts. The formation of stable salt pairs between the amine and fatty acids in the toluene/*n*-hexane mixtures increased their cross-sectional areas being responsible for the difference in permeation. OSN-based separation of fatty acids addresses the challenge of limiting applications of fatty acid mixtures and opens new ways for their broader transformations into more valuable commercial products.

4.3.1.4. Specialty Chemicals. Having not only large molecular weights but branched, homostar-like structures radiating from a central hub, dendimeric macromolecules have sufficiently high rejections. Taking advantage of these properties, Rundel et al.⁴⁰⁵ isolated half-generation poly(amidoamine) dendrimers using Starmem 122 NF membranes. This particular example employed a microfluidic format for continuous-flow pressure-driven downstream processing.

4.3.2. OSN-Assisted Chemical Synthesis. OSN has been used to assist chemical syntheses for the production of pharmaceuticals and specialty chemicals, providing benefits in terms of process efficiency, costs, and solvent consumption.

4.3.2.1. Pharmaceuticals. Peptides are short oligomers of amino acid monomers linked by peptide bonds. Because of their large application in various areas of biomedical research, the interest in their production has increased in recent years, and peptide producers have tried to develop economically competitive methods for their large-scale manufacturing. The conventional method to synthesize peptide, based on solid-phase synthesis, has however some drawbacks, such as semiquantitative or incorrect coupling steps and need for an excess of reagents to overcome mass transfer limitations. Recently, OSN has been proposed as a new technology platform for peptide production, combined with solution-phase peptide synthesis (cf., Figure 39).^{406–408}

In the membrane enhanced peptide synthesis (MEPS), the initial amino acid was attached to a soluble polyethylene glycol anchor. Afterward, chain extension was performed via subsequent repeated coupling and deprotection steps, until the desired peptide length was reached. Diafiltration with a solvent-resistant NF membrane was done to remove residual byproducts and excess reagents after each reaction, while retaining the growing peptide. Similar levels of purity were obtained with this approach and with solid-phase synthesis, under the same operating conditions. Marchetti et al.⁵ performed a reactive peptide nanofiltration for peptide fragment condensation using ceramic membranes (Inopor 0.9 nm TiO₂). A solvent recycling unit was also incorporated, to increase the economic benefit of the membrane process. By

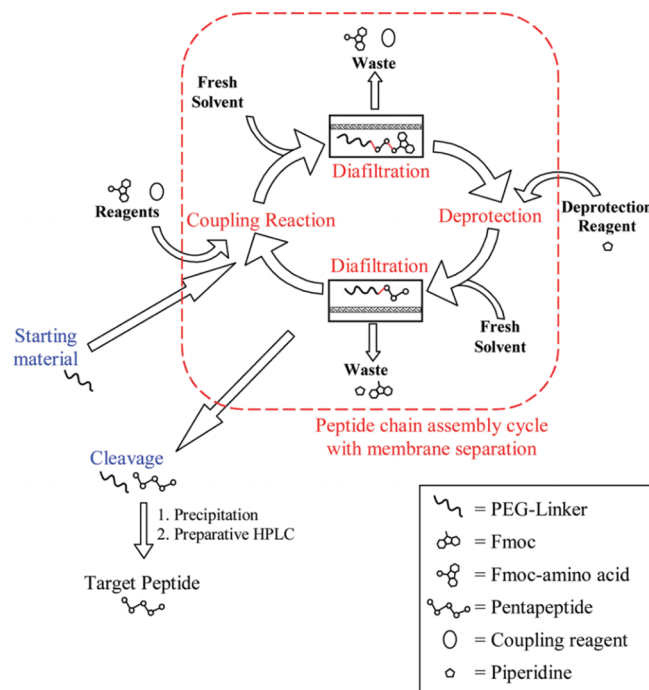


Figure 39. Schematic representation of membrane enhanced peptide synthesis (MEPS). Reprinted with permission from ref 406. Copyright 2010 American Chemical Society.

techno-economic comparison, the reactive peptide nanofiltration was competitive with the conventional batch process.

4.3.2.2. Specialty Chemicals. Stereochemistry is of great importance to the chemical industries due to the fact that physical or biological receptors are capable of distinguishing stereoisomers. Different isomers may have different physical or biological properties, and this affects the reactivity of the molecules in question.

Therefore, it is of utmost importance to form exclusively one enantiomer or isolate the desired enantiomer from the racemic mixture. OSN was identified as an effective solution to different stereochemical challenges including mechanism elucidation, resolution, and asymmetric synthesis. The mild operating conditions offered by OSN are ideal for the processing of nonvolatile and thermally labile enantiomers. For instance, OSN was proposed to understand the mechanism⁴¹⁰ of chiral selectivity in diastereomeric salt formation of α -phenylethylamine salt with various tartaric acid species.⁴¹¹ The investigation revealed that chiral interactions happen during the crystallization and not in solution. Another example is the use of Starmem 122 PI membrane in OSN-assisted chiral resolution where only one of the enantiomers pass through the membrane and the other enantiomer–catalyst complex is retained by the membrane.⁴¹² Furthermore, racemic phenethyl alcohol was resolved using OSN via inclusion complexation where the resolving agent formed complexes with the (*S*)-enantiomer, which precipitated, while the (*R*)-enantiomer permeates through the membrane during nanofiltration (cf., Figure 40).⁴¹³ The final step of the process is decomplexation via solvent exchange allowing the liberation of the free (*S*)-enantiomer, which can now also permeate through the membrane.

OSN-assisted recycling allowed for process intensification, as it resulted in 96% reduction in solvent usage. Wong et al.⁴⁵⁴ also showed an enhancement of both enantioselectivity and

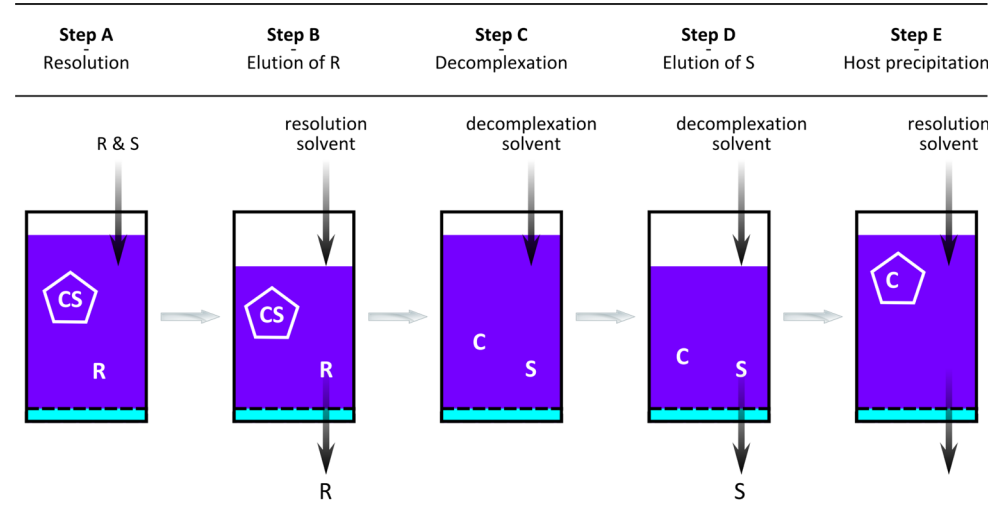


Figure 40. Hybrid process combining OSN and enantioselective inclusion complexation for the separation of phenethyl alcohol enantiomer pair. S = (S)-enantiomer, R = R-enantiomer, C = resolving agent. Adapted with permission from ref 413. Copyright 2006 Elsevier.

stability of Ru-BINAP catalyst with the CyPhos101 ionic liquid reaction medium through an asymmetric hydrogenation. Buekenhoudt et al.⁴¹⁴ patented an improved dilute chemical reaction process incorporating a membrane separation unit. The reaction mixture comprising product, solvent, and unreacted substrate is discharged to a filtration unit, which is permeable to the solvent while the substrate is retained. Process intensification is achieved by reusing the solvent from the permeate side to dilute the fresh and recycled, unreacted substrate.

4.3.3. Catalytic Processes. High value chemicals such as APIs are typically synthesized by multistep reactions, often involving homogeneous organometallic catalysts. The use of such complexes in high-value added organic synthesis promises higher atom economy than alternative routes based on stoichiometric reagents. However, the separation of the catalysts from the reaction products as well as their recycling is quite challenging. Metal-rich waste streams are generated by extensive downstream processing of catalytic postreaction mixtures, which have to be returned to catalyst suppliers for metal reclamation. Furthermore, disadvantages of such workup processes are the high energy and solvent consumption, as well as the loss of high-value stabilizing ligands of the metal catalyst centers. Soluble catalyst recycling by nanofiltration is an attractive approach.^{468,469} Despite the initial unsuccessful attempts reported by Wijkens et al.,⁴⁷⁰ this approach has demonstrated great potential in process intensification in enzyme, organo-, and homogeneous catalysis.^{468,471} Organometallic catalysts recycling can be performed by OSN technology as an alternative route.²²⁴ Among the main advantages, no phase transition or biphasic operation is required by OSN-assisted catalysts recovery. Hence, significant economic and process efficiency advantages are obtained by combining continuous catalytic process and catalyst recovery by OSN, in comparison with batch-based systems and biphasic operation units. However, in some cases, the catalysts are not large enough to be fully retained by the membranes requiring chemical modification,^{415,472,473} steric enlargement by means of polyethylene glycols,⁴⁷⁴ dendrimers,^{425,475} low dispersity poly-(*p*-methylstyrenes),⁴¹⁸ or polyaromatic benzyl bromide supports.⁴⁷⁶ The first enlarged catalyst to be recycled by

nanofiltration was proposed by Felder et al.⁴⁷⁷ in 1997 and validated by Giffels et al.⁴³⁰ in 1998. The polymer-enlarged chiral oxazaborolidine catalysts were applied for the enantioselective reduction of various ketones, and they were subsequently recycled using an MPF-50 membrane in methanol. Table 9 summarizes the application of OSN in the intensification of catalytic reaction. More information on the use of polymeric membranes in catalytic reactors for OSN until 2002 can be found also in a review by Vankelecom.⁴⁷⁸

4.3.3.1. Pharmaceuticals. The application of OSN in catalytic asymmetric synthesis of APIs has been effectively probed by Siew et al.⁴¹⁵ They tuned a quinidine-based organocatalyst to obtain both high enantioselectivity and high membrane rejection. Tsoukala et al.⁴¹⁶ applied OSN during the downstream processing of Idebenone pharmaceutical to separate the target molecule from the Pd catalyst that was used in a Heck coupling reaction. Commercially available PI membrane was applied in acetone allowing catalyst removal from the postreaction stream below the threshold level set by pharmaceutical regulatory agencies.

4.3.3.2. Specialty Chemicals. A continuous ring-closing metathesis reaction featuring a POSS enlarged Ru catalyst in continuous stirred tank and plug flow reactor was investigated by Peeva and Livingston⁴³³ using Starmem 228 and PuraMem 280 membranes in toluene. The catalyst was successfully retained by the OSN membranes, and its high reactivity was demonstrated by the 84% conversion. A contribution by Nair et al.⁴³⁴ demonstrates the feasibility of OSN catalyst recycle on the homogeneous, asymmetric hydrogenation of dimethyl itaconate (DMI) to dimethyl methylsuccinate (DMMS) with Ru-BINAP (Figure 41). The optimization of the process allowed 5 times higher substrate to catalyst ratio as well as 10 reaction cycles to be carried out with only 20% addition of the initial catalyst while still maintaining reaction rate, conversion, and enantiomeric excess.

Moreover, overcoming the challenge of separating and reusing homogeneous catalysts from postreaction streams by OSN was also demonstrated in the metathesis reaction of 1-octene to 7-tetradecene and ethene.⁴³⁵ Various Ru-type catalysts were successfully retained by the Starmem 228 membrane. In addition, the process of coupling reaction,

Table 9. Summary of the Application of Organic Solvent Nanofiltration in the Intensification of Catalytic Reactions

author	catalyst	MW (g mol ⁻¹)	membrane	solvent
1997–1998				
Giffels et al. ⁴³⁰ and Felder et al. ⁴⁷⁷	polymer enlarged oxazaborolidines	13 800	MPF-50	methanol
2001				
De Smet et al. ⁴²⁶	Ru-BINAP and Rh-DUPHOS	929, 723	MPF-50	methanol
2002				
Nair et al. ⁴⁵²	"Pd-phosphine", "Pd-imidazolylidene", "Pd-quat" palladium(II) acetate with $[PPh_3]Br$	643–856	Starmem 122	THF/H ₂ O
Nair et al. ⁴⁵²	Pd(OAc) ₂ + (PPh ₃) ₂ organocatalyst and TOABr phase transfer catalyst	749 (TMC) and 546 (PTC)	Starmem 122	50:50 ethyl acetate/acetone
2003				
Datta et al. ⁴¹⁸	polymer supported Pd(PhCN) ₂ Cl ₂ and Pd (OAc) ₂		PDMS/PAN	toluene
Dijkstra et al. ⁴⁴¹	multi(NCN-Pd and/or -Pt) pincer complexes	>700	MPF-50, MPF-60	methylene chloride
2005				
Chavan et al. ⁴²⁵	porphyrin-functionalized dendrimer-based photocatalysts	600–8700	MPF-50, PDMS, MMM	chloroform ($CHCl_3$), isopropanol (IPA), or IPA/ $CHCl_3$ mixtures
Mertens et al. ⁴³⁷	gold (Au) nanosols		PDMS/PAN, Desal-5 DK	alcohols
Witte et al. ⁴⁴⁰	Q ₁₂ POM catalysts		α -Al ₂ O ₃ / γ -Al ₂ O ₃	toluene
2006				
Aerts et al. ⁴³⁹	Jacobsen catalyst	700	VITO FS Ti 139c, N30F, MPF-44	diethyl ether, isopropanol
Roengpithya et al. ⁴¹²	Ru cymene, P ₁ -t-Oct		Starmem 122	toluene
Wong et al. ⁴⁵⁴	Ru-BINAP	795	Starmem 122	ionic liquids
Wong et al. ⁴³⁶	Pd ₂ (dba) ₃ –CHCl ₃ + PPh ₃	1035	Starmem 122 and ionic liquids	50:50 wt % ethyl acetate
Chowdhury et al. ⁴⁵³	polyoxometallate catalysts such as Q ₁₂ WZn ₃ (ZnW ₉ O ₃₄) ₂] (Q = [MeN(<i>n</i> -C ₈ H ₁₇) ₃] ⁺)	9325	ceramic γ -alumina membranes	toluene
2008				
Pink et al. ³⁸⁸	Pd(OAc) ₂ + PPh ₃	487	Starmem 122	toluene and ethyl acetate
Keraani et al. ⁴⁷²	Hoveyda II complex catalysts	627–2195	Starmem 228	toluene, dimethyl carbonate
2009				
Janssen et al. ⁴⁷⁵	"click" dendritic phosphines and (PdOAc) ₂	>1600	Inopor TiO ₂ 0.9 nm	THF
Nair et al. ⁴³⁴	Ru-BINAP	795	Starmem 122	methanol
Schoeps et al. ⁴⁴³	Nolan-type (NHC)Pd(allyl)Cl complexes	391–1081	PDMS/PAN	isopropanol
Schoeps et al. ⁴⁷⁹	Grubbs II and Grubbs–Hoveyda type complexes	1100	PDMS/PAN	toluene
Ronde et al. ⁴⁷⁶	PCP pincer ligand with [(allyl)PdCl] ₂ type catalyst	1200–1900	MPF-50	THF, DCM
2010				
Van der Gryp et al. ⁴³⁵	Grubbs catalyst	794	Starmem 120, 122, 228, 240	1-octene
Priske et al. ⁴⁸⁰	rhodium and cobalt hydroformylation catalyst	850	Starmem 122, 240	dodecene, octene
Cano-Odena et al. ⁴⁴²	copper(I) catalyst	317	PI	DMF
2011				
Long et al. ¹²⁹	Ru-BINAP	795	dicyclopentadiene	DCM
2012				
Tsoukala et al. ⁴¹⁶	[Pd ⁰ (PPh ₃)OAc] [–]	690	DuraMem	acetone
Peeva and Livingston ⁴³³	POSS enlarged Ru		Starmem 228, PuraMem 280	toluene
Shaharun et al. ⁴⁴⁸			DuraMem 200 and 500	

Table 9. continued

author	catalyst	MW (g mol ⁻¹)	membrane	solvent
2013				
Razak et al. ⁴⁴⁷	HRh(CO)(PPh ₃) ₃	>400	Starmem 122 and 240	ethyl acetate
Kajetanowicz et al. ⁴⁴⁹	POSS-tagged Grubbs catalysts	1577	Starmem 228, PuraMem 280	toluene
Fahrenwaldt et al. ⁴⁵⁰	quinine-based organocatalysts	310–428	DuraMem 150–500	THF
Ormerod et al. ⁴⁸¹	Hoveyda–Grubbs and Umicore M	600, 949	DuraMem 200 Inopor 0.9 nm TiO ₂	DCM, ACN, toluene
Siew et al. ⁴¹⁵	quinidine-based organocatalyst	1044–1332	DuraMem 300, DuraMem 500	THF
Peeva et al. ^{444,445}	Pd(OAc) ₂ + bis(diphenylphosphino)propane	225 + 412	PEEK, APTS cross-linked PI, DuraMem 300	DMF
Rabiller-Baudry et al. ⁴⁴⁶ and Nasser et al. ⁴⁷³	Grubbs–Hoveyda II catalyst	627–927	Starmem 122	toluene
2014				
Schmidt et al. ⁴⁸⁹	Rh-PPh ₃ type catalyst	365	PuraMem 280, GMT-oNF-2	<i>n</i> -hexanal, toluene

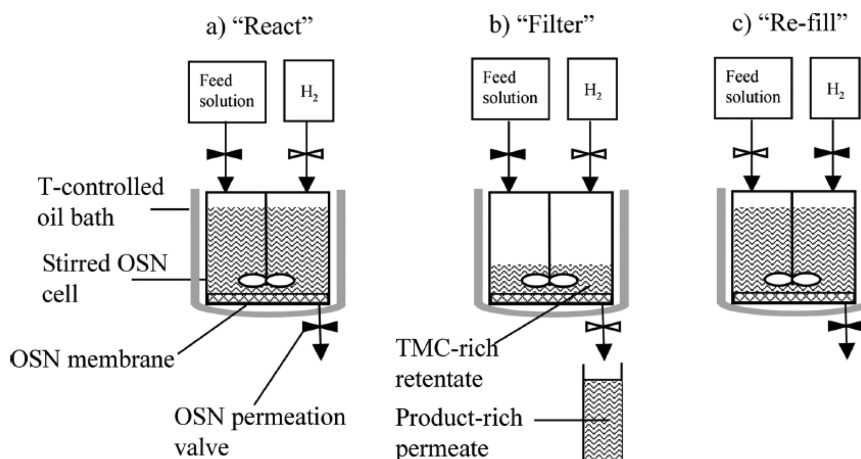


Figure 41. Homogeneous, asymmetric hydrogenation Ru-BINAP catalyst recycle sequence “react”—“filter”—“refill” using OSN; shaded valves are closed. Reprinted with permission from ref 434. Copyright 2009 American Chemical Society.

separation, and recycling also increased the turnover number 4 times for the overall consecutive reaction—separation steps of four cycles. Besides the Ru-type catalyst, Wong et al.⁴³⁶ successfully recovered and reused Pd-type catalysts in Suzuki coupling reactions. The Starmem 122 membrane was capable of retaining the ionic liquid and Pd catalyst, which were afterward recycled into subsequent consecutive reactions. However, the palladium per unit mass of product is unacceptable for pharmaceutical applications without further treatment. Although catalytic productivity can be increased by the recycle of homogeneous Heck catalysts by OSN, the increase in the number of catalyst recycles can cause catalyst deactivation, leading to lower reaction rates. Nair et al.⁴⁵¹ observed that six times recycle of a conventional Heck catalyst was possible at the cost of only 20% decrease in reaction rate as compared to the original value. Datta et al.⁴¹⁸ prepared PDMS NF membranes for the recycling of soluble polymer-supported palladium catalysts. Interestingly, they observed no significant change in the catalyst activity up to nine cycles of Sonogashira and Suzuki reactions. However, the use of polar aprotic solvents for the model Heck coupling led to rapid deterioration of the NF membranes. Mertens et al.⁴³⁷ successfully recycled gold metal colloids, used as homogeneous oxidation catalysts, by means of PDMS-based NF in alcoholic solvents. Through the

example of α -hydroxy-carboxylate synthesis, this hybrid oxidation process was demonstrated, as well as the preservation of catalytic activity in consecutive runs. The recycling of homogeneous Co-type Jacobsen catalysts, used for the hydrolytic kinetic resolution of epoxides,^{438,439} and sandwich-type polyoxometalate oxidation catalysts ($[WZn_3(ZnW_3O_{34})_2]^{12-}$ (POM¹²⁻), used as a multipurpose oxidation catalyst for transformations with aqueous H₂O₂, such as epoxidation, alcohol oxidation, and heteroatom oxidation,⁴⁴⁰ are two other examples of application of both commercially available and tailor-made OSN membranes. Furthermore, Dijkstra et al.⁴⁴¹ successfully prepared shape-persistent multi-(NCN-palladium and NCN-platinum) complexes having one-, two-, and three-dimensional geometries in nanofiltration membrane reactors. They proved that more efficient rejections of these multimetallic materials were obtained with NF membranes with a high degree of rigidity in the backbone of macromolecular complexes.

OSN technology for high-value product purification has been used also for the recovery of catalysts in the chemical and pharmaceutical industries. An easy and efficient nanofiltration technology was proposed by Cano-Odena et al.⁴⁴² for “click” chemistry product purification to reduce the potential health risks associated with the copper contaminants in the final

product. The use of solvent-stable cross-linked polyimide membranes in diafiltration mode allowed as high as 99% ligand-stabilized metal impurity removal, corresponding to an impurity level of 3 ppm, along with DMF solvent, while the polymer product is being almost completely retained. One of the industrial applications of OSN by Evonik Industries is the recycling of homogeneous catalysts, particularly a Rh-based hydroformylation catalyst used in production.⁴¹⁷ The significantly larger size of the homogeneous catalyst molecule (800 g mol^{-1}) as compared to the synthesized product (200 g mol^{-1}) allows the OSN membrane to recover the catalyst from the product. The recovered catalyst can be reused for subsequent reactions reducing the annual budget for homogeneous catalyst by as much as 80%.

4.3.4. OSN-Assisted Crystallization. As was discussed in section 4.1.2.1, OSN can intensify crystallization processes by allowing solvent recovery.³⁴¹ However, OSN can also enhance the yield and purity of crystallization processes. It was demonstrated by Ferguson et al.⁴⁶⁰ that integration of an OSN membrane into continuous mixed-suspension, mixed-product-removal (MSMPR) crystallization allows a dramatic increase in yield without compromising purity by preventing accumulation of impurities over time (cf., Figure 42). The

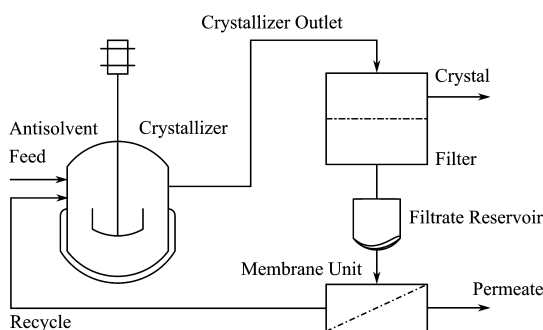


Figure 42. Flowchart of MSMPR crystallization coupled with membrane recycle.

continuous MSMPR crystallization coupled with membrane recycle in THF:ethanol:water mixture featuring PI, PBI, and PEEK membranes matched or exceeded the values of the batch equilibrium crystallizations.

Campbell et al.⁴⁶¹ proposed crystallization enhancement of the API compound griseofulvin employing OSN. The concentration of the API solution was controlled by OSN, and subsequently spontaneous nucleation of crystals was achieved. Manipulation of the solvent flux resulted in controlled crystallization: large crystals (1 mm) were obtained at high flux, while small crystals (2–25 μm) formed at low flux (cf., Figure 43). It is envisaged that fine-tuning crystallization conditions via OSN allows altering the nucleation mechanism toward the desired crystal morphology.

4.4. Future Perspectives

OSN-assisted repetitive synthesis is a relatively new field. On the basis of the success of its first application, peptide synthesis, the field is yet to be broadened with other high-value products requiring step-by-step synthetic approach. Possible applications include the synthesis of various monodisperse macromolecules for drug delivery and oligonucleotides.^{482–484} Although a lot of OSN applications have been reported in the literature, most of them are lab-scale studies. The literature on industrially implemented membrane processes in organic solvents is scarce.

This might be due to the fact that the first generation of OSN membranes (e.g., Starmem) were not stable in harsh solvents (e.g., DMF, DCM), and they showed fluctuating performance. However, the second generation of membranes (e.g., DuraMem, SolSep, GMT-oNF-2) are much more consistent in performance and reliability. Together with good knowledge transfer between academia and industry, the second generation membranes should encourage further implementation of OSN processes in industry.

Considering all of the reviewed applications, it can be concluded that 94% of OSN applications fall under purification (cf., Figure 26). Among purifications, pharmaceutical polishing and catalyst recovery are the fields in which OSN is most widely used. The key for efficient purification by OSN is the discrimination power of the membrane between the desired product and its impurities. Hence, higher selectivity is being sought, which can be achieved by improving either the membranes themselves or the membrane processes. The membrane materials are constantly being improved; however, it is unlikely that substantial breakthrough can be made only by improving the membrane performance (permeance, rejection, and selectivity).⁴⁸⁵ Parallel to material research, more attention should be directed to develop innovative process configurations, for instance, through membrane cascades or hybrid approaches.

In general, the industrial awareness of the existence and advantages of OSN needs to be increased. More techno-economic, life cycle, and process comparison analyses are needed to justify the place of OSN among conventional technologies. Moreover, new membrane process configurations (i.e., cascades, hybrid, and continuous processes) can offer process intensification benefits, which need further exploration.

5. CONCLUSIONS

Organic solvent nanofiltration is a versatile, energy-, waste-, and cost-efficient separation technique, with the potential to compete with established separation processes. Although there has been extensive research into OSN since the establishment of the field and the advantages of membrane filtration over conventional techniques in terms of safety, environment, and costs are always more attractive, the growth potential is still large, and there are many issues to be addressed to persuade industries to undertake significant modification of the established processes. Industries still hesitate to switch from well-established processes to membrane filtration, even if suitable membranes are available and the economical and technological advantages are obvious, due to the fact that the change is capital-intensive and the risk is high for installations that still perform well enough. The relation between capital costs and plant size is an important factor that can affect the establishment of the OSN technology at the industrial level; because the risk associated with the investments in small-scale plants is lower than the risk of investing in large-scale plants, it is more likely that industries will initially invest in small-scale plants (such as for pharmaceutical and specialty chemicals applications), and only after the establishment of the technology, investments will be done on a larger scale (such as for base and consumer chemicals applications). In some cases, the hesitancy of industries is related also to the competitiveness of membrane filtration with conventional processes to perform some challenging separations, as, for example, the separation of molecules with a difference in molecular weight of less than 200 g mol^{-1} . If membrane

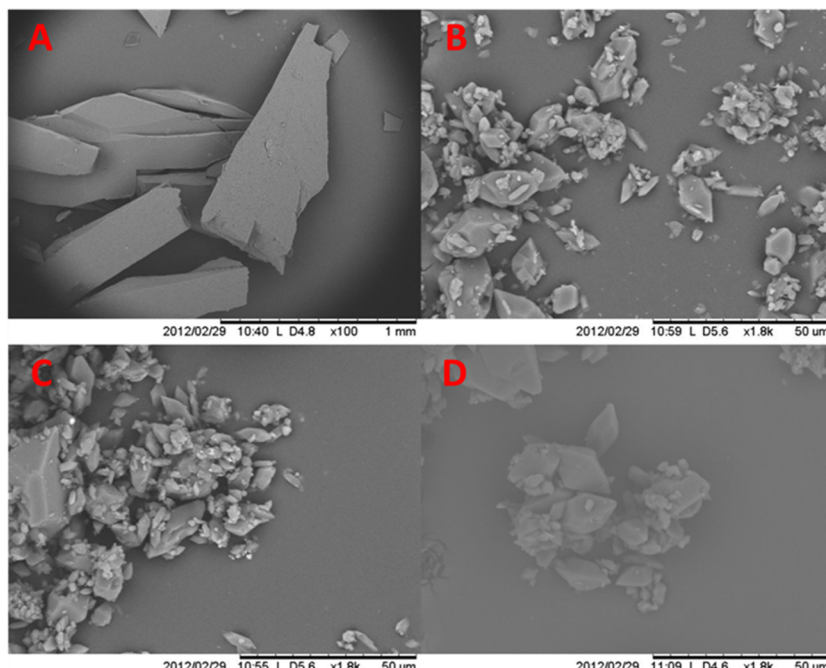


Figure 43. OSN-controlled API crystallization. SEM images of (A) crystals obtained at 24 bar, (B) crystals obtained at 12 bar, (C) crystals obtained at 6 bar, and (D) original griseofulvin crystals. Reprinted with permission from ref 461. Copyright 2014 American Chemical Society.

filtration is not selective enough to achieve the separation of interest, and therefore cannot substitute the conventional purification processes, membrane filtration can still be advantageous for concentration and/or diafiltration and integrate conventional purification processes in hybrid designs. On the other hand, there are cases where membrane filtration is the most practical alternative and helps processes to be more efficient or workable (for heat-sensitive molecules or solvent swap of nonvolatile solvents, for example).

One can expect to see a more widespread uptake of OSN technology in industry, along with the improvements in the fabrication methods and in characterization and modeling tools. Novel methodologies for both membrane fabrication and application are in continuous development. The challenge is to produce new materials with high selectivity, high flux, long-term stability, and nonsignificant physical aging in organic solvents and harsh pH conditions, which can finally overcome the trade-off between selectivity and permeability. Novel polymers, ceramic materials, and mixed matrix membranes have been therefore developed, which can well resist attack under reactive conditions and resist compaction and thermal degradation. Current research is also directed to the development of functionalized materials for molecule-sensitive separations, such as molecular imprinted polymeric membranes, to overcome selectivity issues; to the synthesis of functional nanoporous materials, from the assembly of preformed structures; and to the formation of chemically and mechanically robust ultrathin membranes (with a thickness of a few tens of nanometers), which can achieve ultrafast transport of solvent.

To support new initiatives and accelerate the industrial process development, high throughput membrane synthesis and screening are important.^{41,486} Advanced experimental design can help in the development of better performing tailor-made membranes and facilitate the upscaling from lab-scale to large-scale processes in an economic way, decreasing unit prices and allowing for more potential applications.

Advances in physicochemical characterization techniques could also help in capturing the membrane structure at the molecular scale, thus allowing a deeper fundamental insight of the membrane matrix. From the point of view of transport modeling, the understanding of the permeation mechanism through NF membranes has been largely investigated, and studies on solvent and solute permeation in OSN have been undertaken for commercially available membranes. Big improvements have been made in understanding the basics of the molecular transport; however, no general agreement has yet been reached about the actual transport mechanism and the most suitable mathematical model for its description. Modeling should be intended to support process development by reducing the experimental effort of obtaining flux and rejection to select the best membrane for an application. The characterization of membrane performance should be therefore uniform, because agreement on standard testing solute and solvent system could facilitate the direct comparison of the large number of available OSN membranes. Transport models are characterized by model parameters, which can be obtained by regression of experimental data. After regressing the model parameters, transport models should be used to make a prediction at different operating conditions. Further improvement of the simple models available so far could be reached by accounting for nonidealities, mass transfer limitations and fouling, compaction/aging, and scale-up. Implementation of the fundamental transport models on a process level in process modeling environments, such as Aspen Plus, HYSYS, and ProSim Plus, has been proposed to streamline OSN process design. This will allow process modeling that accounts for module and plant design and can help industries in overcoming the hesitancy to undertake significant modification of the established processes.

On the basis of the promising development of OSN in recent years, and the still significant growth potential, presented in this Review, OSN is a good candidate technology to make a

paradigm shift in molecular purification/separation processes in different industrial applications.

AUTHOR INFORMATION

Corresponding Author

*E-mail: a.livingston@imperial.ac.uk.

Notes

The authors declare no competing financial interest.

Biographies



Patrizia Marchetti received her B.Sc. (cum laude, 2007) and M.Sc. (cum laude, 2009) in Chemical Engineering from the Politecnico of Milan, Italy. She obtained her Ph.D. degree in Chemical Engineering under Marie Curie Actions from Imperial College London, UK, in 2013. During her Ph.D., she worked as an Early Stage Researcher in the Peptide Group at Lonza, Visp, Switzerland. She is currently a Postdoctoral Research Associate at Imperial College London, UK. Her research achievements have resulted in several research articles in international scientific journals, two book chapters, a patent application, and several oral and poster presentations in international conferences. Her research interests cover the fields of pharmaceutical downstream, peptide chemistry, membrane-based separation processes, functional and nanoscale materials, transport, and process modelling. During her postdoc at Imperial College, she has been active as Group Safety Officer. Furthermore, she is an Associate Member of the Institute of Chemical Engineers (IChemE).



Maria F. Jimenez Solomon obtained her B.Sc. (Hons) in Chemistry with distinction in 2007 at the National Autonomous University (UNAM) in Mexico City and spent 8 months at UC Berkeley as an exchange student. In 2008, she obtained her M.Res. in "Green Chemistry, Energy and the Environment" with distinction from Imperial College London and was awarded the Green Chemistry Prize for best overall achievement. She obtained her Ph.D. degree in

Chemical Engineering from Imperial College London as a Marie Curie fellow and was awarded the Weinberg Prize for original research, and the Armstrong Medal and Prize for best PhD thesis for outstanding research on the application of scientific methods to industrial problems. During her Ph.D. she was selected as one of the fellows in the Innovation, Entrepreneurship and Design one year prestigious course organized by Imperial College Business School and the Royal College of Arts. In 2012 she was a visiting researcher at GVS Filter Technology, in Italy. She is currently working as a Postdoctoral Research Associate at Imperial College London and was recently awarded the NAMS Young Membrane Scientist Award (2014), given by the North American Membrane Society for outstanding research in membrane science and technology. She also works as a scientific consultant for Imperial College Consultants. Her research achievements have resulted in two patent applications, both of which have been licensed, several peer-reviewed articles in international scientific journals, a book chapter, and participation in several international conferences. Her current interests are in polymeric membrane development, in particular thin film composite membranes via interfacial polymerization, thin coatings using nanostructured and smart materials, microfluidics, and microencapsulation.



Gyorgy Szekely received his M.Sc. degree in Chemical Engineering from the Technical University of Budapest, Hungary, and he earned his Ph.D. degree in Chemistry under Marie Curie Actions from the Technical University of Dortmund, Germany. He worked as an Early Stage Researcher in the pharmaceutical research and development center of Hovione PharmaScience Ltd. in Portugal and as an IAESTE fellow at the University of Tokyo, Japan. He was a visiting researcher at Biotage MIP Technologies AB in Sweden. Gyorgy was a Postdoctoral Research Associate in Imperial College London, UK and now he is a Lecturer in Chemical Engineering at The University of Manchester, UK. His multidisciplinary professional background covers supramolecular chemistry, organic and analytical chemistry, molecular recognition, molecular imprinting, process development, nanofiltration, and pharmaceutical impurity scavenging. Gyorgy has won several scientific prizes for his intellectual property activity, research proposal, graduate research, and thesis. In addition, he is a board member of the Marie Curie Fellows Association, serving as Secretary General, and is a member of the Royal Society of Chemistry.



Andrew Livingston studied Chemical Engineering in New Zealand. Following graduation, he worked for 3 years at an NZ food processing company doing general chemical engineering. In 1986, he started his Ph.D. at Trinity College, University of Cambridge. Upon finishing his Ph.D. in 1990, he joined the Department of Chemical Engineering at Imperial College. At Imperial, he has carried out research into membrane separations, biotransformations, chemical, and separations technology. He leads a research group of 20 Ph.D. students and Post-Docs, with current research interests in membranes and processes for molecular separations. Andrew was made full Professor in 1999, has published over 200 papers, and been granted 15 patents in chemical technology. His awards include Junior Moulton Medal, Cremer and Warner Medal of IChemE, and Silver Medal of Royal Academy of Engineering. He was elected a Fellow of the Royal Academy of Engineering in 2006, and became Head of the Department of Chemical Engineering at Imperial College in 2008. In 1993, Andrew graduated with an M.Sc. in Economics from London School of Economics (LSE) following part-time study. In 1996, he founded Membrane Extraction Technology, a spin-out company, which evolved to manufacture solvent stable nanofiltration membranes, and carry out process development and commercialization of OSN-based membrane separation processes. On 1 March 2010, MET was acquired by Evonik Industries of Essen, Germany, and continues in business as Evonik MET Ltd., a part of the Evonik Fibers and Membranes Business.

ACKNOWLEDGMENTS

We are grateful to EPSRC for funding under the project EP/J014974/1 entitled Molecular Builders: Constructing Nanoporous Materials.

NOMENCLATURE

a_i	activity of species i
b	friction parameter
c_i	concentration of species i [mol m^{-3}]
C_i	empirical fitting parameter
d_i	diameter of species i [m]
df_i	thermodynamic driving force of species i
d_p	pore diameter [m]
D_i	diffusion coefficient of species i [$\text{m}^2 \text{s}^{-1}$]
D_{ij}	Maxwell–Stefan diffusion coefficient of species i with respect to species j [$\text{m}^2 \text{s}^{-1}$]
F	Faraday constant [96 487 C mol $^{-1}$]
f_1	membrane parameter characteristic of the NF layer [m s^{-1}]
f_2	membrane parameter characteristic of the UF layer [m^{-1}]
$f_{C,i}$	correction factor for solvent i [-]
$f_{C,\text{mix}}$	correction factor for solvent mixtures [-]

f_{ij}	Maxwell–Stefan drag coefficient of species i with respect to species j
J_i	molar flux of species i [$\text{mol m}^{-2} \text{s}^{-1}$]
k_i	empirical fitting parameter
K_{HP}	Hagen–Poiseuille proportionality constant [m]
K_i	sorption coefficient of species i [-]
$K_{i,c}$	convective hindrance factor of species i [-]
$K_{i,d}$	diffusive hindrance factor of species i [-]
k_L	mass transport coefficient in the liquid phase [m s^{-1}]
l	membrane thickness [m]
$l_{S,P}$	thickness of swollen membrane [m]
L_p	mechanical filtration coefficient, or local permeability coefficient [$\text{L m}^{-2} \text{s}^{-1} \text{bar}^{-1}$]
m_i	quantity of species i [mol]
n_i	mass flux of species i [$\text{g m}^{-2} \text{s}^{-1}$]
MW_i	molecular weight of species i [g mol^{-1}]
$Q_{\text{in/out}}$	inlet/outlet volumetric flow rate [$\text{m}^3 \text{s}^{-1}$]
Re_i	rejection of species i [%]
r_i	radius of species i [m]
r_p	pore radius [m]
r_r	reaction rate [$\text{mol m}^{-3} \text{s}^{-1}$]
Δp	transmembrane pressure [bar]
P_i	permeation velocity, or permeability coefficient of species i [m s^{-1}]
$P_{i,\text{dif}}$	diffusional permeability coefficient of imperfections [m s^{-1}]
R	gas constant [$8.314 \text{ J mol}^{-1} \text{ K}^{-1}$]
S_i	solubility parameter of species i [$\text{J m}^{-3}]^{1/2}$
S_{membrane}	membrane solubility parameter [$\text{J m}^{-3}]^{1/2}$
T	temperature [K]
V	solvent velocity [m s $^{-1}$]
V_f	volume of feed tank [m^3]
v_i	molar volume of species i [$\text{m}^3 \text{ mol}^{-1}$]
x_i	mole fraction of species i [-]
w_i	mass fraction of species i [-]
X_{sm}	friction factor [-]
z_i	valence of species i
γ_i	activity coefficient of species i
γ_{SV}	solid surface tension [mN m^{-1}]
γ_{LV}	liquid surface tension [mN m^{-1}]
δ	laminar boundary layer [m]
δ_i	dipole moment of species i [D]
ε	volumetric porosity [-]
ε_L	solvent dielectric constant [-]
ε_S	membrane dielectric constant [-]
η_i	viscosity of species i [Pa s]
θ	contact angle [deg]
μ_i	chemical potential of species i [J mol^{-1}]
π	osmotic pressure [Pa]
ρ	mass density [kg m^{-3}]
σ_i	reflection coefficient of species i
τ	tortuosity [-]
$\phi(r)$	potential function of force exerted on solute by the pore wall [$\text{J g}^{-1} \text{ mol}^{-1}$]
$\phi_{S,P}$	fractional void volume [-]
χ_{ij}	friction coefficient of species i with respect to species j
ψ	electrical potential [V]

Abbreviations

ACN	acetonitrile
AFM	atomic force microscopy
API	active pharmaceutical ingredients
CNT	carbon nanotube

DCM	dichloromethane
DMAc	dimethylacetamide
DMF	dimethylformamide
DMSO	dimethyl sulfoxide
GTI	genotoxic impurity
HBP	hexaphenylbenzene
ISA	integrally skinned asymmetric
LbL	layer-by-layer
MEM	membrane with extrinsic microporosity
MF	microfiltration
MIM	membrane with intrinsic microporosity
MMM	mixed matrix membrane
MW	molecular weight
MWCO	molecular weight cutoff
NF	nanofiltration
NMP	<i>N</i> -methyl pyrrolidone
OSN	organic solvent nanofiltration
PA	polyamide
PAI	poly(amide imide)
PAN	polyacrylonitrile
PAN-H	hydrolyzed polyacrylonitrile
PANI	polyaniline
PAS	positron annihilation spectroscopy
PBI	polybenzimidazole
PDCPD	polydicyclopentadiene
PDMS	polydimethylsiloxane
PE	polyelectrolyte
PEEK	poly(ether ether ketone)
PEG	polyethylene glycol
PEI	poly(ether imide)
PEi	poly(ethylene imine)
PES	poly(ether sulfone)
PI	polyimide
PIM	polymer of intrinsic microporosity
PP	polypropylene
PPSf	polyphenylsulfone
Psf	polysulfone
PTMSP	poly[1-(trimethylsilyl)-1-propyne]
PVDF	poly(vinylidene fluoride)
RO	reverse osmosis
SEM	scanning electron microscopy
SPN	segmented polymer networks
SPPESK	sulfonated poly(phthalazinone ether sulfone ketone)
TOABr	tetraoctylammonium bromide
TEM	transmission electron microscopy
THF	tetrahydrofuran
TFC	thin film composite
UF	ultrafiltration

REFERENCES

- (1) Adler, S.; Beaver, E.; Bryan, P.; Robinson, S.; Watson, J. *Vision 2020:2000 Separations Roadmap*; Center for Waste Reduction Technologies of the AIChE and Dept. of Energy of the United States of America, 2000.
- (2) Vandezande, P.; Gevers, L. E. M.; Vankelecom, I. F. *J. Chem. Soc. Rev.* **2008**, 37, 365.
- (3) Geens, J.; De Witte, B.; Van der Bruggen, B. *Sep. Sci. Technol.* **2007**, 42, 2435.
- (4) Lin, J. C.; Livingston, A. G. *Chem. Eng. Sci.* **2007**, 62, 2728.
- (5) Marchetti, P.; Butté, A.; Livingston, A. In *Sustainable Nanotechnology and the Environment: Advances and Achievements*; Shamim, N., Virender, S., Eds.; ACS Symposium Series; American Chemical Society: Washington, DC, 2013.

- (6) Mulder, M. *Basic Principles of Membrane Technology*, 2nd ed.; Kluwer Academic Publisher: Dordrecht, 2004.
- (7) Koros, W. J.; Ma, Y. H.; Shimizu, T. *Pure Appl. Chem.* **1996**, 68, 1479.
- (8) Baker, R. B. *Membrane Technology and Applications*, 3rd ed.; John Wiley & Sons Ltd.: Chichester, England, 2012.
- (9) Petersen, R. J. In *Nanofiltration: Principles and Applications*; Schaefer, A., Fane, A. G., Waite, T. D., Eds.; Elsevier: Oxford, UK, 2005.
- (10) Peeva, L. G.; Malladi, S.; Livingston, A. G. In *Comprehensive Membrane Science and Engineering*; Drioli, E., Giorno, L., Eds.; Elsevier: Oxford, UK, 2010.
- (11) Sourirajan, S. *Nature* **1964**, 203, 1348.
- (12) Loeb, S. *Science* **1965**, 147, 1241.
- (13) Farnand, B. A.; Talbot, F. D. F.; Matsuura, T.; Sourirajan, S. *Ind. Eng. Chem. Proc. Des. Dev.* **1983**, 22, 179.
- (14) Sourirajan, S.; Matsuura, T. *Reverse Osmosis/Ultrafiltration Principles*; National Research Council of Canada: Ottawa, 1985.
- (15) Shuey, H. F.; Wan, W. U.S. Patent US4,532,041, 1985.
- (16) Anderson, B. P. U.S. Patent US4,963,303, 1990.
- (17) Gould, R. M.; Nitsch, A. R. U.S. Patent US5,494,566, 1996.
- (18) Gould, R. M.; Kloczewski, H. A.; Menon, K. S.; Sulpizio, T. E.; White, L. S. U.S. Patent US5,651,877, 1997.
- (19) Black, L. E.; Boucher, H. A. U.S. Patent US4,571,444, 1986.
- (20) Black, L. E.; Miasek, P. G.; Adriaens, G. U.S. Patent US4,532,029, 1985.
- (21) Black, L. E. U.S. Patent US5,173,191, 1992.
- (22) Bitter, J. G. A.; Haan, J. P.; Rijkens, H. C. U.S. Patent US4,748,288, 1988.
- (23) Cossee, R. P.; Geus, E. R.; Van Den Heuvel, E. J.; Weber, C. E. U.S. Patent US6,488,856, 2002.
- (24) Bitter, J. G. A.; Haan, J. P. U.S. Patent US4,810,366, 1989.
- (25) Miller, J. F.; Bryant, D. R.; Hoy, K. L.; Kinkade, N. E.; Zanapalidou, R. H. U.S. Patent US5,681,473, 1997.
- (26) White, L. S.; Wang, I. F.; Minhas, B. S. U.S. Patent US5,264,166, 1993.
- (27) Gould, R. M.; White, L. S.; Wildemuth, C. R. *Environ. Prog.* **2001**, 20, 12.
- (28) White, L. S.; Nitsch, A. R. *J. Membr. Sci.* **2000**, 179, 267.
- (29) Linder, C.; Nemas, M.; Perry, M.; Katraro, R. U.S. Patent US5,265,734, 1993.
- (30) Solsep, 2014; <http://www.solsep.com>.
- (31) GMT, 2014; <http://www.gmtmem.com>.
- (32) Szekely, G.; Bandarra, J.; Heggie, W.; Sellergren, B.; Ferreira, F. C. *Sep. Purif. Technol.* **2012**, 86, 79.
- (33) Buekenhoudt, A.; Beckers, H.; Ormerod, D.; Bulut, M.; Vandezande, P.; Vleeschouwers, R. *Chem. Ing. Tech.* **2013**, 85, 1243.
- (34) Pink, C.; Rundquist, E. *Organic Solvent Nanofiltration (OSN) in Pharmaceutical Processing*; Network Young Membranes (NYM), 2012.
- (35) Livingston, A. G.; Boam, A. T.; Meniconi, A.; Lim, F.; Makowski, M. Pilot Plant Development of Molecular Separations by Organic Solvent Nanofiltration (paper 71e). *AIChE Conf.* **2011**.
- (36) Bowen, W. R.; Welfoot, J. S. *Chem. Eng. Sci.* **2002**, 57, 1393.
- (37) Kim, J. F.; Freitas da Silva, A. M.; Valtcheva, I. B.; Livingston, A. G. *Sep. Purif. Technol.* **2013**, 116, 277.
- (38) White, L. S. *J. Membr. Sci.* **2002**, 205, 191.
- (39) Bhanushali, D.; Kloos, S.; Bhattacharayya, D. *J. Membr. Sci.* **2002**, 208, 343.
- (40) Bhanushali, D.; Kloos, S.; Kurth, C.; Bhattacharayya, D. *J. Membr. Sci.* **2001**, 189, 1.
- (41) Vandezande, P.; Gevers, L. E. M.; Paul, J. S.; Vankelecom, I. F. J.; Jacobs, P. A. *J. Membr. Sci.* **2005**, 250, 305.
- (42) Gevers, L. E. M.; Meyen, G.; De Smet, K.; Van De Velde, P.; Du Prez, F.; Vankelecom, I. F. J.; Jacobs, P. A. *J. Membr. Sci.* **2006**, 274, 173.
- (43) Fritsch, D.; Merten, P.; Heinrich, K.; Lazar, M.; Priske, M. *J. Membr. Sci.* **2012**, 401–402, 222.
- (44) Kwiatkowski, J.; Cheryan, M. *Sep. Sci. Technol.* **2005**, 40, 2651.

- (45) Tsuru, T.; Sudoh, T.; Yoshioka, T.; Asaeda, M. *J. Membr. Sci.* **2001**, *185*, 253.
- (46) Rohani, R.; Hyland, M.; Patterson, D. *J. Membr. Sci.* **2011**, *382*, 278.
- (47) Stafie, N.; Stamatialis, D. F.; Wessling, M. *Sep. Purif. Technol.* **2005**, *45*, 220.
- (48) See Toh, Y.; Loh, X.; Li, K.; Bismarck, A.; Livingston, A. G. *J. Membr. Sci.* **2007**, *291*, 120.
- (49) Dutczak, S. M.; Luiten-Olieman, M. W. J.; Zwijnenberg, H. J.; Bolhuis-Versteeg, L. A. M.; Winnubst, L.; Hempenius, M. A.; Benes, N. E.; Wessling, M.; Stamatialis, D. *J. Membr. Sci.* **2011**, *372*, 182.
- (50) Whu, J. A.; Baltzis, B. C.; Sirkar, K. K. *J. Membr. Sci.* **2000**, *170*, 159.
- (51) Tarleton, E. S.; Robinson, J. P.; Millington, C. R.; Nijmeijer, A. J. *Membr. Sci.* **2005**, *252*, 123.
- (52) Van der Bruggen, B.; Schaepe, J.; Wilms, D.; Vandecasteele, C. J. *Membr. Sci.* **1999**, *156*, 29.
- (53) Vankelecom, I. F. J.; De Smet, K.; Gevers, L. E. M.; Jacobs, P. A. In *Nanofiltration, Principles and Applications*; Schaefer, A. I., Fane, A. G., Waite, T. D., Eds.; Elsevier: Oxford, UK, 2005.
- (54) Loeb, S.; Sourirajan, S. *Sea Water Demineralization by Means of an Osmotic Membrane, in Saline Water Conversion-II, Advances in Chemistry Series Number 38*; American Chemical Society: Washington, DC, 1963; pp 117–132.
- (55) Park, J. S.; Kim, S. K.; Lee, K. H. *J. Ind. Eng. Chem.* **2000**, *6*, 93.
- (56) Gevers, L. E. M.; Aldea, S.; Vankelecom, I. F. J.; Jacobs, P. A. J. *Membr. Sci.* **2006**, *281*, 741.
- (57) Cuperus, F. P. *Chem. Ing. Tech.* **2005**, *77*, 1000.
- (58) Livingston, A. G.; Bhole, Y. S.; Jimenez Solomon, M. F. U.S. Patent Application US2013/0,112,619 A1, 2013.
- (59) Linder, C.; Nemas, M.; Perry, M.; Ketraro, R. U.S. Patent US5,032,282, 1991.
- (60) Sairam, M.; Loh, X. X.; Bhole, Y.; Sereewatthanawut, I.; Li, K.; Bismarck, A.; Steinke, J. H. G.; Livingston, A. G. *J. Membr. Sci.* **2010**, *349*, 123.
- (61) Loh, X. X.; Sairam, M.; Bismarck, A.; Steinke, J. H. G.; Livingston, A. G.; Li, K. *J. Membr. Sci.* **2009**, *326*, 635.
- (62) Livingston, A. G.; Bhole, Y. S. U.S. Patent Application US0,118,983, 2013.
- (63) Li, X.; De Feyter, S.; Chen, D.; Aldea, S.; Vandezande, P.; Du Prez, F.; Vankelecom, I. F. J. *Chem. Mater.* **2008**, *20*, 3876.
- (64) <http://www.celgard.com/specialty-membranes.aspx>.
- (65) White, L. S. U.S. Patent US6,180,008, 2001.
- (66) Cadotte, J. E.; Petersen, R. J. *Thin-Film Composite Reverse-Osmosis Membranes: Origin, Development, and Recent Advances; Desalination, ACS Symposium Series No. 153*; American Chemical Society: Washington, DC, 1981; p 305.
- (67) Petersen, R. J. *J. Membr. Sci.* **1993**, *83*, 81.
- (68) See Toh, Y. H.; Ferreira, F. C.; Livingston, A. G. *J. Membr. Sci.* **2007**, *299*, 236.
- (69) Boussu, K.; Vandecasteele, C.; Van der Bruggen, B. *Polymer* **2006**, *47*, 3464.
- (70) Ismail, A. F.; Lai, P. Y. *Sep. Purif. Technol.* **2003**, *33*, 127.
- (71) Kim, I.; Yoon, H.; Lee, K. *J. Appl. Polym. Sci.* **2002**, *84*, 1300.
- (72) Hicke, H.; Lehmann, I.; Malsch, G.; Ulbricht, M.; Becker, M. *J. Membr. Sci.* **2002**, *198*, 187.
- (73) Vankelecom, I. F. J.; Gevers, L. E. M. In *Green Separation Processes: Fundamentals and Applications*; Alfonso, C. A. M., Crespo, J. G., Eds.; Wiley-VCH: Weinheim, Germany, 2005.
- (74) Bulut, M.; Gevers, L. E. M.; Paul, J. S.; Vankelecom, I. F. J.; Jacobs, P. A. *J. Comb. Sci.* **2006**, *8*, 168.
- (75) Dai, Y.; Jian, X.; Zhang, S.; Guiver, M. D. *J. Membr. Sci.* **2001**, *188*, 195.
- (76) Leblanc, N.; Le Cerf, D.; Chappéy, C.; Langevin, D.; Metayer, M.; Muller, G. *J. Appl. Polym. Sci.* **2003**, *89*, 1838.
- (77) Ohya, H.; Okazaki, I.; Aihara, M.; Tanisho, S.; Negishi, Y. *J. Membr. Sci.* **1997**, *123*, 143.
- (78) Gupta, K. C. *J. Appl. Polym. Sci.* **1997**, *66*, 643.
- (79) Jian, X.; Dai, Y.; He, G.; Chen, G. *J. Membr. Sci.* **1999**, *161*, 185.
- (80) See Toh, Y. H.; Silva, M.; Livingston, A. G. *J. Membr. Sci.* **2008**, *324*, 220.
- (81) Soroko, I.; Lopes, M. P.; Livingston, A. G. *J. Membr. Sci.* **2011**, *381*, 152.
- (82) Soroko, I.; Makowski, M.; Spill, F.; Livingston, A. G. *J. Membr. Sci.* **2011**, *381*, 163.
- (83) Soroko, I.; Sairam, M.; Livingston, A. G. *J. Membr. Sci.* **2011**, *381*, 172.
- (84) See Toh, Y. H.; Lim, F. W.; Livingston, A. G. *J. Membr. Sci.* **2007**, *301*, 3.
- (85) Holda, A. K.; Aernouts, B.; Saeys, W.; Vankelecom, I. F. J. *J. Membr. Sci.* **2013**, *442*, 196.
- (86) Holda, A. K.; De Roeck, M.; Hendrix, K.; Vankelecom, I. F. J. *J. Membr. Sci.* **2013**, *446*, 113.
- (87) Holda, A. K.; Vankelecom, I. F. J. *J. Membr. Sci.* **2014**, *450*, 512.
- (88) Holda, A. K.; Vankelecom, I. F. J. *J. Membr. Sci.* **2014**, *450*, 499.
- (89) Darvishmanesh, S.; Jansen, J. C.; Tasselli, F.; Tocci, E.; Luis, P.; Degrève, J.; Drioli, E.; Van der Bruggen, B. *J. Membr. Sci.* **2011**, *379*, 60.
- (90) Darvishmanesh, S.; Tasselli, F.; Jansen, J. C.; Tocci, E.; Bazzarelli, F.; Bernardo, P.; Luis, P.; Degrève, J.; Drioli, E.; Van der Bruggen, B. *J. Membr. Sci.* **2011**, *384*, 89.
- (91) Jansen, J. C.; Darvishmanesh, S.; Tasselli, F.; Bazzarelli, F.; Bernardo, P.; Tocci, E.; Friess, K.; Randova, A.; Drioli, E.; Van der Bruggen, B. *J. Membr. Sci.* **2013**, *447*, 107.
- (92) Buonomenma, M. G.; Golemme, G.; Jansen, J. C.; Choi, S. H. *J. Membr. Sci.* **2011**, *368*, 144.
- (93) Hendrix, K.; Koeckelberghs, G.; Vankelecom, I. F. J. *J. Membr. Sci.* **2014**, *452*, 241.
- (94) Hendrix, K.; Van Eynde, M.; Koeckelberghs, G.; Vankelecom, I. F. J. *J. Membr. Sci.* **2013**, *447*, 96.
- (95) Hendrix, K.; Van Eynde, M.; Koeckelberghs, G.; Vankelecom, I. F. J. *J. Membr. Sci.* **2013**, *447*, 212.
- (96) Da Silva Burgal, J.; Ludmila, P.; Livingston, A. GB 1401392.4, 2014.
- (97) Da Silva Burgal, J.; Ludmila, P.; Livingston, A. *Organic Solvent Resistant Poly(ether ether) Ketone Nanofiltration Membranes*; 10th International Congress on Membranes and Membrane Processes, 2014.
- (98) Vanherck, K.; Koeckelberghs, G.; Vankelecom, I. F. J. *Prog. Polym. Sci.* **2013**, *38*, 874.
- (99) Vandezande, P.; Vanherck, K.; Vankelecom, I. F. J. U.S. Patent Application US2010181253, 2008.
- (100) Vanherck, K.; Cano-Odena, A.; Koeckelberghs, G.; Dedroog, T.; Vankelecom, I. F. J. *J. Membr. Sci.* **2010**, *353*, 135.
- (101) Siddique, H.; Bhole, Y.; Peeva, L. G.; Livingston, A. G. *J. Membr. Sci.* **2014**, *465*, 138.
- (102) Dutczak, S. M.; Cuperus, F. P.; Wessling, M.; Stamatialis, D. F. *Sep. Purif. Technol.* **2013**, *102*, 142.
- (103) Stružínska-Piron, I.; Loccufier, J.; Vanmaele, L.; Vankelecom, I. F. J. *Chem. Commun.* **2013**, *49*, 11494.
- (104) Stružínska-Piron, I.; Loccufier, J.; Vanmaele, L.; Vankelecom, I. F. J. *Macromol. Chem. Phys.* **2014**, *215*, 614.
- (105) Stružínska-Piron, I.; Bilad, M. R.; Loccufier, J.; Vanmaele, L.; Vankelecom, I. F. J. *J. Membr. Sci.* **2014**, *462*, 17.
- (106) Dobrak, A.; Figoli, A.; Chovau, S.; Galiano, F.; Simone, S.; Vankelecom, I. F. J.; Drioli, E.; van der Bruggen, B. *J. Colloid Interface Sci.* **2010**, *346*, 254.
- (107) Vanherck, K.; Aerts, A.; Martens, J.; Vankelecom, I. F. J. *Chem. Commun.* **2010**, *46*, 2492.
- (108) Jimenez Solomon, M. F.; Bhole, Y.; Livingston, A. G. *J. Membr. Sci.* **2012**, *423–424*, 371.
- (109) Jimenez Solomon, M. F.; Bhole, Y.; Livingston, A. G. *J. Membr. Sci.* **2013**, *434*, 193.
- (110) Fontananova, E.; Di Profio, G.; Artusa, F.; Drioli, E. *J. Appl. Polym. Sci.* **2013**, *129*, 1653.
- (111) Valtcheva, I. B.; Kumbharkar, S. C.; Kim, J. F.; Bhole, Y.; Livingston, A. G. *J. Membr. Sci.* **2014**, *457*, 62.

- (112) Xing, D. Y.; Chan, S. Y.; Chung, T. S. *Green Chem.* **2014**, *16*, 1383.
- (113) Szekely, G.; Valtcheva, I. B.; Kim, J. F.; Livingston, A. G. *React. Funct. Polym.* **2014**, <http://dx.doi.org/10.1016/j.reactfunctpolym.2014.03.008>.
- (114) Kim, I. C.; Jegal, J.; Lee, K. H. *J. Polym. Sci., Part B: Polym. Phys.* **2002**, *40*, 2151.
- (115) Kim, I. C.; Lee, K. H. *Ind. Eng. Chem. Res.* **2002**, *41*, 5523.
- (116) Lee, K. H.; Kim, I.; Yun, H. G. U.S. Patent US6,887,380, 2005.
- (117) Buch, P. R.; Mohan, D. J.; Reddy, A. V. *Polym. Int.* **2006**, *55*, 391.
- (118) Korikov, A. P.; Kosaraju, P. B.; Sirkar, K. K. *J. Membr. Sci.* **2006**, *279*, 588.
- (119) Kosaraju, P. B.; Sirkar, K. K. *J. Membr. Sci.* **2007**, *288*, 41.
- (120) Kosaraju, P. B.; Sirkar, K. K. *J. Membr. Sci.* **2008**, *321*, 155.
- (121) Sirkar, K. K.; Korikov, A. P.; Kosaraju, P. B. U.S. Patent US0,197,070, 2008.
- (122) Minhas, F. T.; Memon, S.; Bhanger, M. I.; Iqbal, N.; Mujahid, M. *Appl. Surf. Sci.* **2013**, *282*, 887.
- (123) Peyravi, M.; Rahimpour, A.; Jahanshahi, M. *J. Membr. Sci.* **2012**, *423–424*, 225.
- (124) Jimenez Solomon, M. F.; Gorgojo, P.; Munoz-Ibanez, M.; Livingston, A. G. *J. Membr. Sci.* **2013**, *448*, 102.
- (125) Volkov, A. V.; Parashchuk, V. V.; Stamatis, D. F.; Khotimsky, V. S.; Volkov, V. V.; Wessling, M. *J. Membr. Sci.* **2009**, *333*, 88.
- (126) Tsarkov, S.; Malakhov, A. O.; Litvinova, E. G.; Volkov, A. *Pet. Chem.* **2013**, *53*, 537.
- (127) Li, X.; Vandezande, P.; Vankelecom, I. F. *J. J. Membr. Sci.* **2008**, *320*, 143.
- (128) Shao, L.; Cheng, X.; Wang, Z.; Ma, J.; Guo, Z. *J. Membr. Sci.* **2014**, *452*, 82.
- (129) Long, T. R.; Gupta, A.; Miller, A. L.; Rethwisch, D. G.; Bowden, N. B. *J. Mater. Chem.* **2011**, *21*, 14265.
- (130) McKeown, N. B.; Budd, P. M. *Macromolecules* **2010**, *43*, 5163.
- (131) Budd, P. M.; Msayib, K. J.; Tattershall, C. E.; Ghanem, B. S.; Reynolds, K. J.; McKeown, N. B.; Fritsch, D. *J. Membr. Sci.* **2005**, *251*, 263.
- (132) Adymkanov, S. V.; Yampolskii, Y. P.; Polyakov, A. M.; Budd, P. M.; Reynolds, K. J.; McKeown, N. B.; Msayib, K. J. *J. Polym. Sci., Part A* **2008**, *50*, 444.
- (133) Budd, P. M.; Elabas, E. S.; Ghanem, B. S.; Makhseed, S.; McKeown, N. B.; Msayib, K. J.; Tattershall, C. E.; Wang, D. *Adv. Mater.* **2004**, *16*, 456.
- (134) Tsarkov, S.; Khotimskiy, V.; Budd, P. M.; Volkov, V.; Kukushkina, J.; Volkov, A. *J. Membr. Sci.* **2012**, *423–424*, 65.
- (135) Gorgojo, P.; Karan, S.; Wong, H. C.; Jimenez-Solomon, M. F.; Cabral, J. T.; Livingston, A. G. *Adv. Funct. Mater.* **2014**, *24*, 4729.
- (136) Li, X.; Fustin, C. A.; Lefevre, N.; Gohy, J. F.; De Feyter, S.; De Baerdemaeker, J.; Egger, W.; Vankelecom, I. F. *J. J. Mater. Chem.* **2010**, *20*, 4333.
- (137) Li, X.; Basko, M.; Du Prez, F.; Vankelecom, I. F. *J. Phys. Chem. B* **2008**, *112*, 16539.
- (138) Joseph, N.; Ahmadiannamini, P.; Hoogenboom, R.; Vankelecom, I. F. *J. Polym. Chem.* **2014**, *5*, 1817.
- (139) Zhao, Q.; An, Q. F.; Ji, Y.; Qian, J.; Gao, C. *J. Membr. Sci.* **2011**, *379*, 19.
- (140) Li, X.; Goyens, W.; Ahmadiannamini, P.; Vanderlinden, W.; De Feyter, S.; Vankelecom, I. F. *J. J. Membr. Sci.* **2010**, *358*, 150.
- (141) Ahmadiannamini, P.; Li, X.; Goyens, W.; Meesschaert, B.; Vanderlinden, W.; De Feyter, S.; Vankelecom, I. F. *J. J. Membr. Sci.* **2012**, *403–404*, 216.
- (142) Ahmadiannamini, P.; Li, X.; Goyens, W.; Joseph, N.; Meesschaert, B.; Vankelecom, I. F. *J. J. Membr. Sci.* **2012**, *394–395*, 98.
- (143) Tylkowski, B.; Carosio, F.; Castañeda, J.; Alongi, J.; García-Valls, R.; Malucelli, G.; Giamberini, M. *Ind. Eng. Chem. Res.* **2013**, *52*, 16406.
- (144) Chen, D. *J. Appl. Polym. Sci.* **2013**, *129*, 3156.
- (145) Karan, S.; Samitsu, S.; Peng, X.; Kurashima, K.; Ichinose, I. *Science* **2012**, *335*, 444.
- (146) Karan, S.; Wang, Q.; Samitsu, S.; Fujii, Y.; Ichinose, I. *J. Membr. Sci.* **2013**, *448*, 270.
- (147) Ghosh, A. K.; Jeong, B. H.; Huang, X.; Hoek, E. M. V. *J. Membr. Sci.* **2008**, *311*, 34.
- (148) Lind, M. L.; Suk, D. E.; Nguyen, T. V.; Hoek, E. M. V. *Environ. Sci. Technol.* **2010**, *44*, 8230.
- (149) Mukherjee, D.; Kulkarni, A.; Gill, W. N. *J. Membr. Sci.* **1994**, *97*, 231.
- (150) Kulkarni, A.; Mukherjee, D.; Gill, W. N. *J. Membr. Sci.* **1996**, *114*, 39.
- (151) Verissimo, S.; Peinemann, K. V.; Bordado, J. *J. Membr. Sci.* **2005**, *264*, 48.
- (152) Ramachandhran, V.; Ghosh, A. K.; Prabhakar, S.; Tewari, P. K. *Sep. Sci. Technol.* **2009**, *44*, 599.
- (153) Yu, S.; Liu, M.; Liu, X.; Gao, C. *J. Membr. Sci.* **2009**, *342*, 313.
- (154) Homayoonfal, M.; Mehrnia, M. R.; Mojtabaei, Y. M.; Ismail, A. F. *Desalin. Water Treat.* **2013**, *51*, 3295.
- (155) Soroko, I.; Livingston, A. G. *J. Membr. Sci.* **2009**, *343*, 189.
- (156) Vanherck, K.; Hermans, S.; Verbiest, T.; Vankelecom, I. J. *Mater. Chem.* **2011**, *21*, 6079.
- (157) Li, Y.; Verbiest, T.; Vankelecom, I. J. *Membr. Sci.* **2013**, *428*, 63.
- (158) Vanherck, K.; Vankelecom, I.; Verbiest, T. *J. Membr. Sci.* **2011**, *373*, 5.
- (159) Vanherck, K.; Verbiest, T.; Vankelecom, I. *J. Phys. Chem. C* **2012**, *116*, 115.
- (160) Siddique, H.; Rundquist, E.; Bhole, Y.; Peeva, L. G.; Livingston, A. G. *J. Membr. Sci.* **2014**, *452*, 354.
- (161) Campbell, J.; Szekely, G.; Davies, R. P.; Braddock, D. C.; Livingston, A. G. *J. Mater. Chem. A* **2014**, *2*, 9260.
- (162) Gevers, L. E. M.; Vankelecom, I. F. J.; Jacobs, P. A. *Chem. Commun.* **2005**, 2500.
- (163) Gevers, L. E. M.; Vankelecom, I. F. J.; Jacobs, P. A. *J. Membr. Sci.* **2006**, *278*, 199.
- (164) Dobrak-Van Berlo, A.; Vankelecom, I. F. J.; Van der Bruggen, B. *J. Membr. Sci.* **2011**, *374*, 138.
- (165) Basu, S.; Maes, M.; Cano-Odena, A.; Alaerts, L.; De Vos, D. E.; Vankelecom, I. F. *J. J. Membr. Sci.* **2009**, *344*, 190.
- (166) Sorribas, S.; Gorgojo, P.; Téllez, C.; Coronas, J.; Livingston, A. G. *J. Am. Chem. Soc.* **2013**, *135*, 15201.
- (167) Peyravi, M.; Jahanshahi, M.; Rahimpour, A.; Javadi, A.; Hajavi, S. *Chem. Eng. J.* **2014**, *241*, 155.
- (168) Namvar-Mahboub, M.; Pakizeh, M. *Sep. Purif. Technol.* **2013**, *119*, 35.
- (169) Siddique, H.; Peeva, L. G.; Stoikos, K.; Pasparakis, G.; Vamvakaki, M.; Livingston, A. G. *Ind. Eng. Chem. Res.* **2013**, *52*, 1109.
- (170) Dudziak, G.; Hoyer, T.; Nickel, A.; Puhlfuerss, P.; Voigt, I. Eur. Patent 1,603,663, 2004.
- (171) Inopor, 2014; <http://www.inopor.com>.
- (172) Voigt, I.; Stahn, M.; Woehner, S.; Junghans, A.; Rost, J.; Voigt, W. *Sep. Purif. Technol.* **2001**, *25*, 509.
- (173) Tsuru, T.; Sudou, T.; Kawahara, S.; Yoshioka, T.; Asaeda, M. *J. Colloid Interface Sci.* **2000**, *228*, 292.
- (174) Tsuru, T.; Narita, M.; Shinagawa, R.; Yoshioka, T. *Desalination* **2008**, *233*, 1.
- (175) Rezaei Hosseinabadi, S.; Wyns, K.; Meynen, V.; Carleer, R.; Adriaensens, P.; Buekenhoudt, A.; Van der Bruggen, B. *J. Membr. Sci.* **2014**, *454*, 496.
- (176) Tsuru, T.; Miyawaki, M.; Kondo, H.; Yoshioka, T.; Asaeda, M. *Sep. Purif. Technol.* **2003**, *32*, 105.
- (177) Tsuru, T.; Kondo, H.; Yoshioka, T.; Asaeda, M. *AIChE J.* **2004**, *50*, 1080.
- (178) Tsuru, T.; Nakasuji, T.; Oka, M.; Kanezashi, M.; Yoshioka, T. *J. Membr. Sci.* **2011**, *384*, 149.
- (179) Van Gestel, T.; Van der Bruggen, B.; Buekenhoudt, A.; Dotremont, C.; Luyten, J.; Vandecasteele, C.; Maes, G. *J. Membr. Sci.* **2003**, *224*, 3.
- (180) Verrecht, B.; Leysen, R.; Buekenhoudt, A.; Vandecasteele, C.; Van der Bruggen, B. *Desalination* **2006**, *200*, 385.

- (181) Ngamou, P. H. T.; Overbeek, J. P.; Kreiter, R.; van Veen, H. M.; Vente, J. F.; Wienk, I. M.; Cuperus, P. F.; Creatore, M. *J. Mater. Chem. A* **2013**, *1*, 5567.
- (182) Aguirre, I.; Arias, P. L.; Castricum, H. L.; Creatore, M.; ten Elshof, J. E.; Paradis, G. G.; Ngamou, P. H. T.; van Veen, H. M.; Vente, J. F. *Sep. Purif. Technol.* **2014**, *121*, 2.
- (183) Koch, 2014; www.kochmembrane.com.
- (184) Linder, C.; Nemas, M.; Perry, M.; Katraro, R. U.S. Patent US5,205,934, 1993.
- (185) Linder, C.; Nemas, M.; Perry, M.; Katraro, R. U.S. Patent US5,265,734, 1993.
- (186) Scarpello, J. T.; Nair, D.; Freitas dos Santos, L. M.; White, L. S.; Livingston, A. G. *J. Membr. Sci.* **2002**, *203*, 71.
- (187) Van der Bruggen, B.; Jansen, J. C.; Figoli, A.; Geens, J.; Boussu, K.; Drioli, E. *J. Phys. Chem. B* **2006**, *110*, 13799.
- (188) Geens, J.; Van der Bruggen, B.; Vandecasteele, C. *Sep. Purif. Technol.* **2006**, *48*, 255.
- (189) Bargeman, G.; Albers, J.; Westerlink, J. B.; Manahutu, C. F. H.; ten Kate, A. *Proceedings of the International Workshop on Membranes in Solvent Filtration*, Leuven, Belgium, 2006.
- (190) Evonik-MET, 2014; <http://duramem.evonik.com>.
- (191) Livingston, A. G.; See Toh, Y. H. GB Patent 2,437,519, 2007.
- (192) Schmidt, M.; Peinemann, K. V.; Scharnagl, N.; Friese, K.; Schubert, R. DE Patent 19,507,584 A1, 1996.
- (193) Porogen, 2014; <http://www.porogen.com>.
- (194) AMS Technologies, 2014; <http://www.amsmembrane.com>.
- (195) PolyAn, 2014; <http://www.poly-an.de>.
- (196) Geens, J.; Boussu, K.; Vandecasteele, C.; Van der Bruggen, B. *J. Membr. Sci.* **2006**, *281*, 139.
- (197) Marchetti, P.; Butté, A.; Livingston, A. G. *J. Membr. Sci.* **2013**, *444*, 101.
- (198) Cuperus, F. P.; Smolders, C. A. *Adv. Colloid Interface Sci.* **1991**, *34*, 135.
- (199) Zhang, W.; Hallstroem, B. *Desalination* **1990**, *79*, 1.
- (200) Mulder, M. H. V.; van Voorthuizen, E. M.; Peeters, J. M. M. In *Nanofiltration, Principles and Applications*; Schaefer, A. I., Fane, A. G., Waite, T. D., Eds.; Elsevier: Oxford, UK, 2005.
- (201) Bhanushali, D.; Bhattacharyya, D. *Ann. N. Y. Acad. Sci.* **2003**, *984*, 159.
- (202) Paul, D. R.; Garcin, M.; Garmon, W. E. *J. Appl. Polym. Sci.* **1976**, *20*, 609.
- (203) Ho, W. S. W.; Sirkar, K. K. *Membrane Handbook*; Springer Science - Business Media: New York, 1992.
- (204) Piccinini, E.; Giacinti Baschetti, M.; Sarti, G. C. *J. Membr. Sci.* **2004**, *234*, 95.
- (205) Tarleton, E. S.; Robinson, J. P.; Salman, M. *J. Membr. Sci.* **2006**, *280*, 442.
- (206) Tarleton, E. S.; Robinson, J. P.; Smith, S. J.; Na, J. J. W. *J. Membr. Sci.* **2005**, *261*, 129.
- (207) Song, Y.; Liu, F.; Sun, B. *J. Appl. Polym. Sci.* **2005**, *95*, 1251.
- (208) Wu, Q.; Wu, B. *J. Membr. Sci.* **1995**, *105*, 113.
- (209) Sheldon, J. M. *J. Membr. Sci.* **1991**, *62*, 75.
- (210) Bottino, A.; Capannelli, G.; Grossi, A.; Monticelli, O.; Cavalleri, O.; Rolandi, R.; Soria, R. *J. Membr. Sci.* **1994**, *95*, 289.
- (211) Stawikowska, J.; Livingston, A. G. *J. Membr. Sci.* **2013**, *425–426*, 58.
- (212) Zeman, L.; Denault, L. *J. Membr. Sci.* **1992**, *71*, 221.
- (213) Li, Q.; Elimelech, M. *Environ. Sci. Technol.* **2004**, *38*, 4683.
- (214) Otero, J. A.; Mazarrasa, O.; Villasante, J.; Silva, V.; Prádanos, P.; Calvo, J. I.; Hernández, A. *J. Membr. Sci.* **2008**, *309*, 17.
- (215) Hilal, N.; Mohammad, A. W.; Atkin, B.; Darwish, N. *Desalination* **2003**, *157*, 137.
- (216) Khulbe, K. C.; Feng, C. Y.; Matsuura, T. *Synthetic Polymeric Membranes. Characterization by Atomic Force Microscopy*; Springer: New York, 2008.
- (217) Boussu, K.; Van der Bruggen, B.; Volodin, A.; Snaauwaert, J.; Van Haesendonck, C.; Vandecasteele, C. *J. Colloid Interface Sci.* **2005**, *286*, 632.
- (218) Stamatialis, D. F.; Dias, C. R.; de Pinho, M. N. *J. Membr. Sci.* **1999**, *160*, 235.
- (219) Stawikowska, J.; Livingston, A. G. *J. Membr. Sci.* **2012**, *413–414*, 1.
- (220) Stawikowska, J.; Jimenez Solomon, M. F.; Bhole, Y.; Livingston, A. G. *J. Membr. Sci.* **2013**, *442*, 107.
- (221) Tung, K. L.; Jean, Y. C.; Nanda, D.; Lee, K. R.; Hung, W. S.; Lo, C. H.; Lai, J. Y. *J. Membr. Sci.* **2009**, *343*, 147.
- (222) Cano-Odena, A.; Vandecasteele, P.; Hendrix, K.; Zaman, R.; Mostafa, K.; Egger, W.; Sperr, P.; De Baerdemaeker, J.; Vankelecom, I. F. *J. Phys. Chem. B* **2009**, *113*, 10170.
- (223) <http://www.chemicalprocessing.com/articles/2013/membranes-target-organic-solvents/>.
- (224) Livingston, A. G.; Peeva, L. G.; Han, S.; Nair, D.; Luthra, S. S.; White, L. S.; Freitas dos Santos, L. M. *Ann. N. Y. Acad. Sci.* **2003**, *984*, 123.
- (225) Alfa Laval, 2014; <http://www.wassertech.net/content/view/34/29/lang,thai/>.
- (226) Loh, X. X.; Sairam, M.; Steinke, J. H. G.; Livingston, A. G.; Bismarck, A.; Li, K. *Chem. Commun.* **2008**, 6324.
- (227) Sereewatthanawut, I.; Lim, F. W.; Bhole, Y. S.; Ormerod, D.; Horvath, A.; Boam, A. T.; Livingston, A. G. *Org. Process Res. Dev.* **2010**, *14*, 600.
- (228) Silva, P.; Peeva, L. G.; Livingston, A. G. *J. Membr. Sci.* **2010**, *349*, 167.
- (229) Darvishmanesh, S.; Buekenhoudt, A.; Degrève, J.; Van der Bruggen, B. *Sep. Purif. Technol.* **2009**, *70*, 46.
- (230) Marchetti, P.; Butté, A.; Livingston, A. G. *J. Membr. Sci.* **2012**, *415–416*, 444.
- (231) Buekenhoudt, A.; Bisignano, F.; De Luca, G.; Vandecasteele, P.; Wouters, M.; Verhulst, K. *J. Membr. Sci.* **2013**, *439*, 36.
- (232) Marchetti, P.; Butté, A.; Livingston, A. G. *Chem. Eng. Sci.* **2013**, *101*, 200.
- (233) Dutczak, S. M.; Tanardi, C. R.; Kopeć, K. K.; Wessling, M.; Stamatialis, D. *Sep. Purif. Technol.* **2012**, *86*, 183.
- (234) Lu, Y.; Suzuki, T.; Zhang, W.; Moore, J. S.; Mariñas, B. *J. Chem. Mater.* **2007**, *19*, 3194.
- (235) Suzuki, T.; Lu, Y.; Zhang, W.; Moore, J. S.; Mariñas, B. *J. Environ. Sci. Technol.* **2007**, *41*, 6246.
- (236) Jeong, B. H.; Hoek, E. M. V.; Yan, Y.; Subramani, A.; Huang, X.; Hurwitz, G.; Ghosh, A. K.; Jawor, A. *J. Membr. Sci.* **2007**, *294*, 1.
- (237) Lind, M. L.; Ghosh, A. K.; Jawor, A.; Huang, X.; Hou, W.; Yang, Y.; Hoek, E. M. V. *Langmuir* **2009**, *25*, 10139.
- (238) Majumder, M.; Chopra, N.; Andrews, R.; Hinds, B. *J. Nature* **2005**, *438*, 44.
- (239) Holt, J. K.; Park, H. G.; Wang, Y.; Stadermann, M.; Artyukhin, A. B.; Grigoropoulos, C. P.; Noy, A.; Bakajin, O. *Science* **2006**, *312*, 1034.
- (240) Ratto, T. V.; Holt, J. K.; Szmodis, A. W. U.S. Patent US0,025,330, 2010.
- (241) Peng Lee, K.; Arnot, T. C.; Mattia, D. *J. Membr. Sci.* **2011**, *370*, 1.
- (242) Ulbricht, M. *Polymer* **2006**, *47*, 2217.
- (243) Noy, A.; Park, H. G.; Fornasiero, F.; Holt, J. K.; Grigoropoulos, C. P.; Bakajin, O. *Nano Today* **2007**, *2*, 22.
- (244) Mauter, M. S.; Elimelech, M. *Environ. Sci. Technol.* **2008**, *42*, 5843.
- (245) Mason, E. A.; Lonsdale, H. K. *J. Membr. Sci.* **1990**, *51*, 1.
- (246) Wang, J.; Dlamini, D. S.; Mishra, A. K.; Pendergast, M. T. M.; Wong, M. C. Y.; Mamba, B. B.; Freger, V.; Verliefde, A. R. D.; Hoek, E. M. V. *J. Membr. Sci.* **2014**, *454*, S16.
- (247) Peshev, D.; Livingston, A. G. *Chem. Eng. Sci.* **2013**, *104*, 975.
- (248) Zhao, Y.; Yuan, Q. *J. Membr. Sci.* **2006**, *279*, 453.
- (249) Yang, X. J.; Livingston, A. G.; Freitas dos Santos, L. *J. Membr. Sci.* **2001**, *190*, 45.
- (250) Geens, J.; Peeters, K.; Van der Bruggen, B.; Vandecasteele, C. *J. Membr. Sci.* **2005**, *255*, 255.
- (251) Lonsdale, H. K.; Merten, U.; Riley, R. L. *J. Appl. Polym. Sci.* **1965**, *9*, 1341.

- (252) Wijmans, J. G.; Baker, R. W. *J. Membr. Sci.* **1995**, *107*, 1.
 (253) Yaroshchuk, A. E. *J. Membr. Sci.* **1995**, *101*, 83.
 (254) Kedem, O.; Katchalsky, A. *Biochim. Biophys. Acta* **1958**, *27*, 229.
 (255) Spiegler, K. S.; Kedem, O. *Desalination* **1966**, *1*, 311.
 (256) Paul, D. R. *J. Membr. Sci.* **2004**, *241*, 371.
 (257) Bird, R. B.; Stewart, W. E.; Lightfoot, E. N. *Transport Phenomena*, 2nd ed.; John Wiley & Sons, Inc.: Hoboken, NJ, 2007.
 (258) Ferry, J. D. *Chem. Rev.* **1936**, *18*, 373.
 (259) Verniory, A.; Dubois, R.; Decoordt, P.; Gassee, J. P.; Lambert, P. P. *J. Gen. Physiol.* **1973**, *62*, 489.
 (260) Nakao, S. I.; Kimura, S. *J. Chem. Eng. Jpn.* **1982**, *15*, 200.
 (261) Van der Bruggen, B.; Schaep, J.; Wilms, D.; Vandecasteele, C. *Sep. Sci. Technol.* **2000**, *35*, 169.
 (262) Matsuura, T.; Sourirajan, S. *Ind. Eng. Chem. Process Des. Dev.* **1981**, *20*, 273.
 (263) Mehdizadeh, H.; Dickson, J. M. *J. Membr. Sci.* **1989**, *42*, 119.
 (264) Wang, X. L.; Tsuru, T.; Nakao, S. I.; Kimura, S. *J. Membr. Sci.* **1995**, *103*, 117.
 (265) Sherwood, T. K.; Brian, P. L. T.; Fisher, R. E. *Ind. Eng. Chem. Fundam.* **1967**, *6*, 2.
 (266) Peeva, L. G.; Gibbins, E.; Luthra, S. S.; White, L. S.; Stateva, R. P.; Livingston, A. G. *J. Membr. Sci.* **2004**, *236*, 121.
 (267) Labanda, J.; Sabaté, J.; Llorens, J. *Desalination* **2013**, *315*, 83.
 (268) Meares, P.; Craig, J. B.; Webster, J. In *Diffusion Processes*; Sherwood, J. N., Chadwick, A. V., Muir, W. M., Swinton, F. L., Eds.; Gordon and Breach: London, 1971; Vol. 2.
 (269) Yasuda, H.; Peterlin, A. *J. Appl. Polym. Sci.* **1973**, *17*, 433.
 (270) Rosenbaum, S. *J. Polym. Sci., Part B: Polym. Lett.* **1968**, *6*, 307.
 (271) Rosenbaum, S.; Skiens, W. E. *J. Appl. Polym. Sci.* **1968**, *12*, 2169.
 (272) Atkins, P.; De Paula, J. *Atkins' Physical Chemistry*, 8th ed.; Oxford University Press: New York, 2006.
 (273) Lonsdale, H. K.; Merten, U.; Tagami, M. *J. Appl. Polym. Sci.* **1967**, *11*, 1807.
 (274) Paul, D. R.; Ebra-Lima, O. M. *J. Appl. Polym. Sci.* **1970**, *14*, 2201.
 (275) Paul, D. R.; Ebra-Lima, O. M. *J. Appl. Polym. Sci.* **1971**, *15*, 2199.
 (276) Paul, D. R.; Paciotti, J. D. *J. Polym. Sci., Polym. Phys. Ed.* **1975**, *13*, 1201.
 (277) Paul, D. R. *Sep. Purif. Methods* **1976**, *5*, 33.
 (278) Maxwell, J. C. *Philos. Trans. R. Soc. London* **1867**, *157*, 49.
 (279) Stefan, J. *Sitzungsber. Kaiserlichen Akad. Wiss. Wien* **1871**, *63*, 63.
 (280) Bowen, W. R.; Mukhtar, H. *J. Membr. Sci.* **1996**, *112*, 263.
 (281) Niemi, H.; Palosaari, S. *J. Membr. Sci.* **1994**, *91*, 111.
 (282) Nagy, E.; Kulcsár, E.; Nagy, A. J. *Membr. Sci.* **2011**, *368*, 215.
 (283) Miranda, J. M.; Campos, J. B. L. M. *J. Membr. Sci.* **2002**, *202*, 137.
 (284) Brian, P. L. T. In *Desalination by Reverse Osmosis*; Merten, U., Ed.; MIT Press: Cambridge, MA, 1966.
 (285) Silva, P.; Han, S.; Livingston, A. J. *Membr. Sci.* **2005**, *262*, 49.
 (286) Han, S. J.; Luthra, S. S.; Peeva, L. G.; Yang, X. J.; Livingston, A. G. *Sep. Sci. Technol.* **2003**, *38*, 1899.
 (287) Silva, P.; Livingston, A. G. *J. Membr. Sci.* **2006**, *280*, 889.
 (288) Stafie, N.; Stamatialis, D. F.; Wessling, M. *J. Membr. Sci.* **2004**, *228*, 103.
 (289) Ben Soltane, H.; Roizard, D.; Favre, E. *J. Membr. Sci.* **2013**, *435*, 110.
 (290) Hesse, L.; Mićović, J.; Schmidt, P.; Górák, A.; Sadowski, G. J. *Membr. Sci.* **2013**, *428*, 554.
 (291) Gibbins, E.; D'Antonio, M.; Nail, D.; White, L. S.; Freitas dos Santos, L. M.; Vankelecom, I. F. J.; Livingston, A. G. *Desalination* **2002**, *147*, 307.
 (292) Robinson, J. P.; Tarleton, E. S.; Millington, C. R.; Nijmeijer, A. J. *Membr. Sci.* **2004**, *230*, 29.
 (293) Leitner, L.; Harscoat-Schiavo, C.; Vallières, C. *Polym. Test.* **2014**, *33*, 88.
 (294) Volkov, A. V.; Yushkin, A.; Grekhov, A.; Shutova, A.; Bazhenov, S.; Tsarkov, S.; Khotimsky, V.; Vlugt, T. J. H.; Volkov, V. *V. J. Membr. Sci.* **2013**, *440*, 98.
 (295) Dijkstra, M. F. J.; Bach, S.; Ebert, K. *J. Membr. Sci.* **2006**, *286*, 60.
 (296) Fierro, D.; Boschetti-de Fierro, A.; Abetz, V. *J. Membr. Sci.* **2012**, *413-414*, 91.
 (297) Miyagi, A.; Nabetani, H.; Nakajima, M. *Sep. Purif. Technol.* **2012**, *88*, 216.
 (298) Schmidt, P.; Lutze, P. *J. Membr. Sci.* **2013**, *445*, 183.
 (299) Machado, D.; Hasson, D.; Semiar, R. *J. Membr. Sci.* **2000**, *166*, 63.
 (300) Robinson, J. P.; Tarleton, E. S.; Ebert, K.; Millington, C. R.; Nijmeijer, A. *Ind. Eng. Chem. Res.* **2005**, *44*, 3238.
 (301) Koops, G. H.; Yamada, S.; Nakao, S. *J. Membr. Sci.* **2001**, *189*, 241.
 (302) Tsuru, T.; Izumi, S.; Yoshioka, T.; Asaeda, M. *AIChE J.* **2000**, *46*, 565.
 (303) Darvishmanesh, S.; Buekenhoudt, A.; Degrèvre, J.; Van der Bruggen, B. *J. Membr. Sci.* **2009**, *334*, 43.
 (304) Larsen, B. L.; Rasmussen, P.; Fredenslund, A. A. *Ind. Eng. Chem. Res.* **1987**, *26*, 2274.
 (305) Fredenslund, A.; Gmehling, J.; Rasmussen, P. *Vapor-Liquid Equilibria Using UNIFAC*; Elsevier: Amsterdam, The Netherlands, 1977.
 (306) Vankelecom, I. F. J.; De Smet, K.; Gevers, L. E. M.; Livingston, A. G.; Nair, D.; Aerts, S.; Kuypers, S.; Jacobs, P. A. *J. Membr. Sci.* **2004**, *231*, 99.
 (307) Stamatialis, D. F.; Stafie, N.; Buadu, K.; Hempenius, M.; Wessling, M. *J. Membr. Sci.* **2006**, *279*, 424.
 (308) Gross, J.; Sadowski, G. *Ind. Eng. Chem. Res.* **2002**, *41*, 5510.
 (309) Van der Bruggen, B.; Vandecasteele, C. *Water Res.* **2002**, *36*, 1360.
 (310) Shinoda, K. *Principles of Solution and Solubility*; Marcel Dekker: New York, 1978.
 (311) Schmidt, P.; Koese, T.; Lutze, P. *J. Membr. Sci.* **2013**, *429*, 103.
 (312) Carré, A. *J. Adhes. Sci. Technol.* **2007**, *21*, 961.
 (313) Van der Bruggen, B.; Geens, J.; Vandecasteele, C. *Chem. Eng. Sci.* **2002**, *57*, 2511.
 (314) Geens, J.; Hillen, A.; Bettens, B.; Van der Bruggen, B.; Vandecasteele, C. *J. Chem. Technol. Biotechnol.* **2005**, *80*, 1371.
 (315) Darvishmanesh, S.; Degrèvre, J.; Van der Bruggen, B. *Phys. Chem. Chem. Phys.* **2010**, *12*, 13333.
 (316) Zeidler, S.; Kaetzel, U.; Kreis, P. *J. Membr. Sci.* **2013**, *429*, 295.
 (317) Postel, S.; Spalding, G.; Chirnside, M.; Wessling, M. *J. Membr. Sci.* **2013**, *447*, 57.
 (318) Volkov, A.; Yushkin, A.; Kachula, Y.; Khotimsky, V.; Volkov, V. *Sep. Purif. Technol.* **2014**, *124*, 43.
 (319) Zhukov, A. N. *Adv. Colloid Interface Sci.* **2007**, *134-135*, 330.
 (320) Zhang, Y.; Xu, T.; Liu, Z. *Desalination* **2007**, *212*, 183.
 (321) Whu, J. A.; Baltzis, B. C.; Sirkar, K. K. *J. Membr. Sci.* **1999**, *163*, 319.
 (322) Caus, A.; Braeken, L.; Boussu, K.; Van der Bruggen, B. *J. Chem. Technol. Biotechnol.* **2009**, *84*, 391.
 (323) Vanneste, J.; Ormerod, D.; Theys, G.; Van Gool, D.; Van Camp, B.; Darvishmanesh, S.; Van der Bruggen, B. *J. Chem. Technol. Biotechnol.* **2013**, *88*, 98.
 (324) Siew, W. E.; Livingston, A. G.; Ates, C.; Merschaert, A. *Chem. Eng. Sci.* **2013**, *90*, 299.
 (325) Abejón, R.; Garea, A.; Irabien, A. *AIChE J.* **2014**, *60*, 931.
 (326) Goldsmith, J.; Martens, C. C. *J. Phys. Chem. Lett.* **2010**, *1*, 528.
 (327) Frentrup, H.; Avedaño, C.; Horsch, M.; Salih, A.; Mueller, E. A. *Mol. Simul.* **2012**, *38*, 540.
 (328) CEFIC, The European chemical industry, *Facts and Figures 2013*; <http://www.cefic.org/Facts-and-Figures/>.
 (329) Cao, X.; Wu, X. Y.; Wu, T.; Jin, K.; Hur, B. K. *Biotechnol. Bioprocess Eng.* **2001**, *6*, 200.
 (330) Shi, D.; Kong, Y.; Yu, J.; Wang, Y.; Yang, J. *Desalination* **2006**, *191*, 309.

- (331) Baumgarten, G. OSN at Evonik. 3rd International Conference on Organic Solvent Nanofiltration, 2010.
- (332) Katraro, R.; Linder, C.; Nemas, M. U.S. Patent US5,676,832, 1997.
- (333) Peshev, D.; Peeva, L. G.; Peev, G.; Baptista, I. I. R.; Boam, A. T. *Chem. Eng. Res. Des.* **2011**, *89*, 318.
- (334) Sereewatthanawut, I.; Baptista, I. I. R.; Boam, A. T.; Hodgson, A.; Livingston, A. G. *J. Food Eng.* **2011**, *102*, 16.
- (335) Köseoglu, S. S.; Engelgau, D. E. *J. Am. Oil Chem. Soc.* **1990**, *67*, 239.
- (336) Lin, L.; Rhee, K. C.; Köseoglu, S. S. *J. Membr. Sci.* **1997**, *134*, 101.
- (337) Subramanian, R.; Raghavarao, K. S. M. S.; Nabetani, H.; Nakajima, M.; Kimura, T.; Maekawa, T. *J. Membr. Sci.* **2001**, *187*, 57.
- (338) Darnoko, D.; Cheryan, M. *J. Am. Oil Chem. Soc.* **2006**, *83*, 365.
- (339) Tsui, E. M.; Cheryan, M. *J. Food Eng.* **2007**, *83*, 590.
- (340) Darvishmanesh, S.; Firoozpour, L.; Vanneste, J.; Luis, P.; Degrève, J.; Van der Bruggen, B. *Green Chem.* **2011**, *13*, 3476.
- (341) Rundquist, E. M.; Pink, C. J.; Livingston, A. G. *Green Chem.* **2012**, *14*, 2197.
- (342) Micovic, J.; Werth, K.; Lutze, P. *Chem. Eng. Res. Des.* **2014**, <http://dx.doi.org/10.1016/j.cherd.2014.02.012>.
- (343) Nimmig, S.; Kaspereit, M. *Chem. Eng. Process.* **2013**, *67*, 89.
- (344) Kong, Y.; Shi, D.; Yu, H.; Wang, Y.; Yang, J.; Zhang, Y. *Desalination* **2006**, *191*, 254.
- (345) Namvar-Mahboub, M.; Pakizeh, M.; Davari, S. *J. Membr. Sci.* **2014**, *459*, 22.
- (346) White, L. S. *J. Membr. Sci.* **2006**, *286*, 26.
- (347) White, L. S.; Wildemuth, C. R. *Ind. Eng. Chem. Res.* **2006**, *45*, 9136.
- (348) Bhore, N. A.; Gould, R. M.; Jacob, S. M.; Staffeld, P. O.; McNally, D.; Smiley, P. H.; Wildemuth, C. R. *Oil Gas J.* **1999**, *97*, 67.
- (349) Gould, R.; Kloczewski, H. A.; Menon, K. S.; Sulpizio, T. E.; White, L. S. U.S. Patent US5,651,877, 1997.
- (350) Gould, R.; Nitsch, A. R. U.S. Patent US5,494,566, 1996.
- (351) White, L. S.; Wang, I.; Minhas, B. S. U.S. Patent US5,264,166, 1993.
- (352) Wernick, D. L. U.S. Patent US4,678,555, 1987.
- (353) Anderson, B. P. U.S. Patent US4,963,303, 1990.
- (354) Shuey, H. F.; Wan, W. U.S. Patent US4,532,041, 1985.
- (355) Pasternak, M. U.S. Patent US5,238,567, 1993.
- (356) White, L. S.; Wormsbecher, R. F.; Lesemann, M. U.S. Patent US7,048,846, 2006.
- (357) Livingston, A. G.; Osborne, C. G. Eur. Patent WO 2002/050212 A3, 2003.
- (358) Chin, A. A.; Knickerbocker, B. M.; Trewella, J. C.; Waldron, T. R.; White, L. S. U.S. Patent US6,187,987, 2001.
- (359) Firman, L. R.; Ochoa, N. A.; Marchese, J.; Pagliero, C. L. *J. Membr. Sci.* **2013**, *431*, 187.
- (360) Darvishmanesh, S.; Robberecht, T.; Luis, P.; Degrève, J.; Van der Bruggen, B. *J. Am. Oil Chem. Soc.* **2011**, *88*, 1255.
- (361) Zwijnenberg, H. J.; Krosse, A. M.; Ebert, K.; Peinemann, K.; Cuperus, F. P. *J. Am. Oil Chem. Soc.* **1999**, *76*, 83.
- (362) Kale, V.; Katikateni, S. P. R.; Cheryan, M. *J. Am. Oil Chem. Soc.* **1999**, *76*, 723.
- (363) Wu, J. C.; Lee, E. *J. Membr. Sci.* **1999**, *154*, 251.
- (364) Kim, I.; Kim, J.; Lee, K.; Tak, T. *J. Membr. Sci.* **2002**, *205*, 113.
- (365) Gupta, A. K. S. U.S. Patent US4,533,501, 1985.
- (366) Ochoa, N.; Pagliero, C.; Marchese, J.; Mattea, M. *Sep. Purif. Technol.* **2001**, *22–23*, 417.
- (367) Tanahashi, S.; Nagano, K.; Kasai, M.; Tsubone, F.; Iwama, A.; Kazuse, Y.; Tasaka, K.; Isooka, Y. U.S. Patent US4,787,981, 1988.
- (368) Ebert, K.; Cuperus, F. P. *Membr. Technol.* **1999**, *107*, 5.
- (369) Friese, K.; Peinemann, K. V.; Scharnagl, N.; Schmidt, M.; Schubert, R. Eur. Patent WO 1996/027430 A1, 1996.
- (370) Bhosle, B. M.; Subramanian, R. *J. Food Sci.* **2005**, *69*, 481.
- (371) Bhosle, B. M.; Subramanian, R.; Ebert, K. *Eur. J. Lipid Sci. Technol.* **2005**, *107*, 746.
- (372) Wilkes, J.; Levisky, J.; Wilson, R.; Hussey, C. *Inorg. Chem.* **1982**, *21*, 1263.
- (373) Ranke, J.; Stolte, S.; Störmann, R.; Arning, J.; Jastorff, B. *Chem. Rev.* **2007**, *107*, 2183.
- (374) Han, S.; Wong, H. T.; Livingston, A. G. *Chem. Eng. Res. Des.* **2005**, *83*, 309.
- (375) Van Doorslaer, C.; Glas, D.; Peeters, A.; Cano-Odena, A.; Vankelecom, I.; Binnemans, K.; Mertens, P.; De Vos, D. *Green Chem.* **2010**, *12*, 1726.
- (376) Abels, C.; Redepenning, C.; Moll, A.; Melin, T.; Wessling, M. *J. Membr. Sci.* **2012**, *405–406*, 1.
- (377) Hazarika, S.; Dutta, N. N.; Rao, P. G. *Sep. Purif. Technol.* **2012**, *97*, 123.
- (378) Sheth, J. P.; Qin, Y.; Sirkar, K. K.; Baltzis, B. C. *J. Membr. Sci.* **2003**, *211*, 251.
- (379) Rundquist, E.; Pink, C. J.; Vilminot, E.; Livingston, A. G. *J. Chromatogr., A* **2012**, *1229*, 156.
- (380) Bandarra, J.; Heggie, W.; Szekely, G. PT105601(A), 2012.
- (381) Szekely, G.; Gil, M.; Sellergren, B.; Heggie, W.; Ferreira, F. C. *Green Chem.* **2013**, *15*, 210.
- (382) Szekely, G.; Bandarra, J.; Heggie, W.; Sellergren, B.; Ferreira, F. C. *J. Membr. Sci.* **2011**, *381*, 21.
- (383) Peeva, L.; da Silva Burgal, J.; Valtcheva, I.; Livingston, A. G. *Chem. Eng. Sci.* **2014**, *116*, 183.
- (384) Szekely, G.; Fritz, E.; Bandarra, J.; Heggie, W.; Sellergren, B. *J. Chromatogr., A* **2012**, *1240*, 52.
- (385) Szekely, G.; Henriques, B.; Gil, M.; Ramos, A.; Alvarez, C. J. *Pharm. Biomed. Anal.* **2012**, *70*, 251.
- (386) Brito Martínez, M.; Van der Bruggen, B.; Rodriguez Negrin, Z.; Luis Alconero, P. *J. Ind. Eng. Chem.* **2012**, *18*, 1635.
- (387) Brito Martínez, M.; Jullok, N.; Rodriguez Negrin, Z.; Van der Bruggen, B.; Luis, P. *Chem. Eng. Process.* **2013**, *70*, 241.
- (388) Pink, C. J.; Wong, H.; Ferreira, F. C.; Livingston, A. G. *Org. Process Res. Dev.* **2008**, *12*, 589.
- (389) Ormerod, D.; Sledsens, B.; Vercammen, G.; Van Gool, D.; Linsen, T.; Buekenhoudt, A.; Bongers, B. *Sep. Purif. Technol.* **2013**, *115*, 158.
- (390) Siew, W. E.; Livingston, A. G.; Ates, C.; Merschaert, A. *Sep. Purif. Technol.* **2013**, *102*, 1.
- (391) Peng, H.; Tremblay, A. Y. *Desalination* **2008**, *229*, 318.
- (392) Ghosh, R. *J. Membr. Sci.* **2003**, *226*, 85.
- (393) Lightfoot, E. N.; Root, T. W.; O'Dell, J. L. *Biotechnol. Prog.* **2008**, *24*, 599.
- (394) Kim, J. F.; Szekely, G.; Valtcheva, I. B.; Livingston, A. G. *Green Chem.* **2014**, *16*, 133.
- (395) Kröckel, J.; Kragl, U. *Chem. Eng. Technol.* **2003**, *26*, 1166.
- (396) Boam, A.; Nozari, A. *PharmaChem* **2005**, *4*, 57.
- (397) Zakzeski, J.; Bruijninckx, P. C. A.; Jongerius, A. L.; Weckhuysen, B. M. *Chem. Rev.* **2010**, *110*, 3552.
- (398) Werhan, H.; Farshori, A.; von Rohr, P. R. *J. Membr. Sci.* **2012**, *423–424*, 404.
- (399) Othman, R.; Mohammad, A. W.; Ismail, M.; Salimon, J. *J. Membr. Sci.* **2010**, *348*, 287.
- (400) Nwuha, V. *J. Food Eng.* **2000**, *44*, 233.
- (401) Tsibranska, I. H.; Tylkowski, B. *Food Bioprod. Process.* **2013**, *91*, 169.
- (402) Tsibranska, I.; Saykova, I. *J. Chem. Technol. Metall.* **2013**, *48*, 333.
- (403) Gupta, A.; Bowden, N. B. *ACS Appl. Mater. Interfaces* **2013**, *5*, 924.
- (404) Vanneste, J.; De Ron, S.; Vandecruys, S.; Soare, S. A.; Darvishmanesh, S.; Van der Bruggen, B. *Sep. Purif. Technol.* **2011**, *80*, 600.
- (405) Rundel, J. T.; Paul, B. K.; Remcho, V. T. *J. Chromatogr., A* **2007**, *1162*, 167.
- (406) So, S.; Peeva, L. G.; Tate, E. W.; Leatherbarrow, R. J.; Livingston, A. G. *Org. Process Res. Dev.* **2010**, *14*, 1313.
- (407) So, S.; Peeva, L. G.; Tate, E. W.; Leatherbarrow, R. J.; Livingston, A. G. *Chem. Commun.* **2010**, *46*, 2808.

- (408) Chen, W. Q.; Cristau, M.; Giraud, M.; Livingston, A. G. *J. Pept. Sci.* **2012**, *18*, S133.
- (409) Ferreira, F. C.; Macedo, H.; Cocchini, U.; Livingston, A. G. *Org. Process Res. Dev.* **2006**, *10*, 784.
- (410) Kozma, D.; Simon, H.; Kassai, C.; Madarász, Z.; Fogassy, E. *Chirality* **2001**, *13*, 29.
- (411) Ghazali, N. F.; Patterson, D. A.; Livingston, A. G. *Chem. Commun.* **2004**, 962.
- (412) Roengpithaya, C.; Patterson, D. A.; Taylor, P. C.; Livingston, A. G. *Desalination* **2006**, *199*, 195.
- (413) Ghazali, N. F.; Ferreira, F. C.; White, A. J. P.; Livingston, A. G. *Tetrahedron: Asymmetry* **2006**, *17*, 1846.
- (414) Buekenhoudt, A.; Vandezande, P.; Ormerod, D. Patent WO 2013/156600 A1, 2013.
- (415) Siew, W. E.; Ates, C.; Merschaert, A.; Livingston, A. G. *Green Chem.* **2013**, *15*, 663.
- (416) Tsoukala, A.; Peeva, L.; Livingston, A. G.; Bjorsvik, H. R. *ChemSusChem* **2012**, *5*, 188.
- (417) Evonik, 2014; <http://www.design-meets-polymers.com/sites/dc/Downloadcenter/Evonik/Product/DuraMem-PuraMem/brochures/duramem-and-puramem---general-brochure.pdf>.
- (418) Datta, A.; Ebert, K.; Plenio, H. *Organometallics* **2003**, *22*, 4685.
- (419) Luthra, S. S.; Yang, X.; Freitas dos Santos, L. M.; White, L. S.; Livingston, A. G. *Chem. Commun.* **2001**, 1468.
- (420) De Groot, D.; Reek, J. N. H.; Kamer, P. C. J.; van Leeuwen, P. W. N. M. *Eur. J. Org. Chem.* **2002**, *6*, 1085.
- (421) Goetheer, E. L. V.; Verkerk, A. W.; van den Broeke, L. J. P.; de Wolf, E.; Deelman, B.; van Koten, G.; Keurentjes, J. T. F. *J. Catal.* **2003**, *219*, 126.
- (422) Van den Broeke, L. J. P.; Goetheer, E. L. V.; Verkerk, A. W.; de Wolf, E.; Deelman, B.; van Koten, G.; Keurentjes, J. T. F. *Angew. Chem., Int. Ed.* **2001**, *40*, 4473.
- (423) Albrecht, M.; Hovestad, N. J.; Boersma, J.; van Koten, G. *Chem.—Eur. J.* **2001**, *7*, 1289.
- (424) Eggeling, E. B.; Hovestad, N. J.; Jastrzebski, J. T. B. H.; Vogt, D.; van Koten, G. *J. Org. Chem.* **2000**, *65*, 8857.
- (425) Chavan, S.; Maes, W.; Gevers, L. E. M.; Wahnen, J.; Vankelecom, I. F. J.; Jacobs, P. A.; Dehaen, W.; De Vos, D. E. *Chem.—Eur. J.* **2005**, *11*, 6754.
- (426) De Smet, K.; Aerts, S.; Ceulemans, E.; Vankelecom, I. F. J.; Jacobs, P. A. *Chem. Commun.* **2001**, *7*, 597.
- (427) Turlan, D.; Urriolabeitia, E. P.; Navarro, R.; Royo, C.; Ménendez, M.; Santamaría, J. *Chem. Commun.* **2001**, *24*, 2608.
- (428) Dwars, T.; Haberland, J.; Grassert, I.; Oehme, G.; Kragl, U. *J. Mol. Catal. A: Chem.* **2001**, *168*, 81.
- (429) Rissom, S.; Beliczy, J.; Giffels, G.; Kragl, U.; Wandrey, C. *Tetrahedron: Asymmetry* **1999**, *10*, 923.
- (430) Giffels, G.; Beliczy, J.; Felder, M.; Kragl, U. *Tetrahedron: Asymmetry* **1998**, *9*, 691.
- (431) De Groot, D.; Eggeling, E. B.; De Wilde, J. C.; Kooijman, H.; van Haaren, R. J.; van der Made, A. W.; Spek, A. L.; Vogt, D.; Reek, J. N. H.; Kamer, P. C. J.; van Leeuwen, P. W. N. M. *Chem. Commun.* **1999**, *17*, 1623.
- (432) Sablong, R.; Schlotterbeck, U.; Vogt, D.; Mecking, S. *Adv. Synth. Catal.* **2003**, *345*, 333.
- (433) Peeva, L.; Livingston, A. G. *Procedia Eng.* **2012**, *44*, 307.
- (434) Nair, D.; Wong, H. T.; Han, S.; Vankelecom, I. F. J.; White, L. S.; Livingston, A. G.; Boam, A. T. *Org. Process Res. Dev.* **2009**, *13*, 863.
- (435) Van der Gryp, P.; Barnard, A.; Cronje, J. P.; De Vlieger, D.; Marx, S.; Vosloo, H. C. M. *J. Membr. Sci.* **2010**, *353*, 70.
- (436) Wong, H.; Pink, C. J.; Ferreira, F. C.; Livingston, A. G. *Green Chem.* **2006**, *8*, 373.
- (437) Mertens, P. G. N.; Bulut, M.; Gevers, L. E. M.; Vankelecom, I. F. J.; Jacobs, P. A.; de Vos, D. E. *Catal. Lett.* **2005**, *102*, 57.
- (438) Aerts, S.; Weyten, H.; Buekenhoudt, A.; Gevers, L. E. M.; Vankelecom, I. F. J.; Jacobs, P. A. *Chem. Commun.* **2004**, 710.
- (439) Aerts, S.; Buekenhoudt, A.; Weyten, H.; Gevers, L. E. M.; Vankelecom, I. F. J.; Jacobs, P. A. *J. Membr. Sci.* **2006**, *280*, 245.
- (440) Witte, P. T.; Chowdhury, S. R.; ten Elshof, J. E.; Sloboda-Rozner, D.; Neumann, R.; Alsters, P. *Chem. Commun.* **2005**, 1206.
- (441) Dijkstra, H. P.; Kruithof, C. A.; Ronde, N.; van de Coevering, R.; Ramón, D. J.; Vogt, D.; van Klink, G. P. M.; van Koten, G. *J. Org. Chem.* **2003**, *68*, 675.
- (442) Cano-Odena, A.; Vandezande, P.; Fournier, D.; Van Camp, W.; Du Prez, F. E.; Vankelecom, I. F. *J. Chem.—Eur. J.* **2010**, *16*, 1061.
- (443) Schoeps, D.; Sashuk, V.; Ebert, K.; Plenio, H. *Organometallics* **2009**, *28*, 3922.
- (444) Peeva, L. G.; da Silva Burgal, J.; Vartak, S.; Livingston, A. G. *J. Catal.* **2013**, *306*, 190.
- (445) Peeva, L. G.; Arbour, J.; Livingston, A. G. *Org. Process Res. Dev.* **2013**, *17*, 967.
- (446) Rabiller-Baudry, M.; Nasser, G.; Renouard, T.; Delaunay, D.; Camus, M. *Sep. Purif. Technol.* **2013**, *116*, 46.
- (447) Razak, N. S. A.; Shaharun, M. S.; Mukhtar, H.; Taha, M. F. *Sains Malays.* **2013**, *42*, 515.
- (448) Shaharun, M. S.; Mustafa, A. K.; Taha, M. F. *AIP Conf. Proc.* **2012**, *1482*, 279.
- (449) Kajetanowicz, A.; Czaban, J.; Krishnan, G. R.; Malinska, M.; Wozniak, K.; Siddique, H.; Peeva, L. G.; Livingston, A. G.; Grela, K. *ChemSusChem* **2013**, *6*, 182.
- (450) Fahrenwaldt, T.; Grosseheilmann, J.; Erben, F.; Kragl, U. *Org. Process Res. Dev.* **2013**, *17*, 1131.
- (451) Nair, D.; Scarpello, J. T.; Vankelecom, I. F. J.; Freitas Dos Santos, L. M.; White, L. S.; Kloetzing, R. J.; Welton, T.; Livingston, A. G. *Green Chem.* **2002**, *4*, 319.
- (452) Nair, D.; Luthra, S. S.; Scarpello, J. T.; White, L. S.; Freitas dos Santos, L. M.; Livingston, A. G. *Desalination* **2002**, *147*, 301.
- (453) Chowdhury, S. R.; Witte, P. T.; Blank, D. H. A.; Alsters, P. L.; ten Elshof, J. E. *Chem.—Eur. J.* **2006**, *12*, 3061.
- (454) Wong, H.; See-Toh, Y. H.; Ferreira, F. C.; Crook, R.; Livingston, A. G. *Chem. Commun.* **2006**, 2063.
- (455) Nair, D.; Scarpello, J. T.; White, L. S.; Freitas Dos Santos, L. M.; Vankelecom, I. F. J.; Livingston, A. G. *Tetrahedron Lett.* **2001**, *42*, 8219.
- (456) Miller, J. F. U.S. Patent US7,084,284, 2006.
- (457) Mertens, P. G. N.; Vankelecom, I. F. J.; Jacobs, P. A.; de Vos, D. E. *Gold Bull.* **2005**, *38*, 157.
- (458) Mertens, P. G. N.; Cuypers, F.; Vandezande, P.; Ye, X.; Verpoort, F.; Vankelecom, I. F. J.; de Vos, D. E. *Appl. Catal., A* **2007**, *325*, 130.
- (459) Brinkmann, N.; Giebel, D.; Lohmer, G.; Reetz, M. T.; Kragl, U. *J. Catal.* **1999**, *183*, 163.
- (460) Ferguson, S.; Ortner, F.; Quon, J.; Peeva, L.; Livingston, A.; Trout, B. L.; Myerson, A. S. *Cryst. Growth Des.* **2014**, *14*, 617.
- (461) Campbell, J.; Peeva, L. G.; Livingston, A. G. *Cryst. Growth Des.* **2014**, *14*, 2192.
- (462) Tullo, A. H. *Chem. Eng. News* **2013**, *91*, 13.
- (463) Kecili, R.; Billing, J.; Leeman, M.; Nivhede, D.; Sellergren, B.; Rees, A.; Yilmaz, E. *Sep. Purif. Technol.* **2013**, *103*, 173.
- (464) Szekely, G.; Henrique, B.; Gil, M.; Alvarez, C. *Drug Test. Anal.* **2014**, *6* (9), 898.
- (465) Szekely, G.; Bandarra, J.; Heggie, W.; Ferreira, F. C.; Sellergren, B. *Sep. Purif. Technol.* **2012**, *86*, 190.
- (466) Kecili, R.; Nivhede, D.; Billing, J.; Leeman, M.; Sellergren, B.; Yilmaz, E. *Org. Process Res. Dev.* **2012**, *16*, 1225.
- (467) Kecili, R.; Billing, J.; Nivhede, D.; Sellergren, B.; Rees, A.; Yilmaz, E. *J. Chromatogr., A* **2014**, *1339*, 65.
- (468) Vougioukalakis, G. C. *Chem.—Eur. J.* **2012**, *18*, 8868.
- (469) Baumgarten, G.; Borgmann, C.; Büschken, W.; Kuppinger, F. F.; Möller, O.; Ortmann, D.; Wiese, K. D. DE Patent 102005046250 A1, 2007.
- (470) Wijkens, P.; Jastrzebski, J. T. B. H.; Van der Schaaf, P. A.; Kolly, R.; Hafner, A.; Van Koten, G. *Org. Lett.* **2000**, *2*, 1621.
- (471) Janssen, M.; Müller, C.; Vogt, D. *Green Chem.* **2011**, *13*, 2247.
- (472) Keraani, A.; Renouard, T.; Fischmeister, C.; Bruneau, C.; Rabiller-Baudry, M. *ChemSusChem* **2008**, *1*, 927.

- (473) Nasser, G.; Renouard, T.; Shahane, S.; Fischmeister, C.; Bruneau, C.; Rabiller-Baudry, M. *ChemPlusChem*. **2013**, *78*, 728.
- (474) Shahane, S.; Toupet, L.; Fischmeister, C.; Bruneau, C. *Eur. J. Inorg. Chem.* **2013**, *2013*, 54.
- (475) Janssen, M.; Müller, C.; Vogt, D. *Adv. Synth. Catal.* **2009**, *351*, 313.
- (476) Ronde, N. J.; Totev, D.; Müller, C.; Lutz, M.; Spek, A. L.; Vogt, D. *ChemSusChem* **2009**, *2*, 558.
- (477) Felder, M.; Giffels, G.; Wandrey, C. *Tetrahedron: Asymmetry* **1997**, *8*, 1975.
- (478) Vankelecom, I. F. J. *Chem. Rev.* **2002**, *102*, 3779.
- (479) Schoeps, D.; Buhr, K.; Dijkstra, M.; Ebert, K.; Plenio, H. *Chem.—Eur. J.* **2009**, *15*, 2960.
- (480) Priske, M.; Wiese, K. D.; Drews, A.; Kraume, M.; Baumgarten, G. J. *Membr. Sci.* **2010**, *360*, 77.
- (481) Ormerod, D.; Bongers, B.; Porto-Carrero, W.; Giegas, S.; Vlijt, G.; Lefevre, N.; Lauwers, D.; Bursten, W.; Buekenhoudt, A. *RSC Adv.* **2013**, *3*, 21501.
- (482) Szekely, G.; Schaeperoens, M.; Gaffney, P. R. J.; Livingston, A. G. *Polym. Chem.* **2014**, *5*, 694.
- (483) Livingston, A. G.; Gaffney, P. R. J.; Vasconcelos, R. C. Patent WO 2011/148177 A2, 2011.
- (484) Szekely, G.; Schaeperoens, M.; Gaffney, P. R. J.; Livingston, A. G. *Chem.—Eur. J.* **2014**, *20* (32), 10038.
- (485) Robeson, L. M. *J. Membr. Sci.* **2008**, *320*, 390.
- (486) Vandezande, P.; Gevers, L. E. M.; Vankelecom, I. F. J.; Jacobs, P. A. *Desalination* **2006**, *199*, 395.
- (487) Szekely, G.; Jimenez-Solomon, M. F.; Marchetti, P.; Kim, J. F.; Livingston, A. G. *Green Chem.* **2014**, *16*, 4440.
- (488) Kim, J. F.; Szekely, G.; Schaeperoens, M.; Valtcheva, I. B.; Jimenez-Solomon, M. F.; Livingston, A. G. *ACS Sustainable Chem. Eng.* **2014**, *2*, 2371.
- (489) Schmidt, P.; Bednarz, E. L.; Lutze, P.; Górkak, A. *Chem. Eng. Sci.* **2014**, *115*, 115.